ORDER HARDENING OF PLATINUM ALLOYS

by

Nicholas Richard Towle

A thesis submitted to the faculty of Engineering and the Built Environment, University of Cape Town, in fulfilment of the degree of Master of Science in Engineering.

Department of Materials Engineering
University of Cape Town
March 1999

ABSTRACT

The hardening behaviour of three cold-worked platinum alloys, Pt 5 at% Mo, Pt 5 wt% Ru and Pt 5 wt% Cu, has been investigated through a systematic series of heat treatments. All three of the experimental alloys showed a hardness increase during annealing within a specific temperature range. The hardness of the Pt-Mo and Pt-Ru alloys was found to increase rapidly at annealing temperatures above the recrystallisation temperature, with the final hardness similar to the original cold-worked hardness. The hardness of Pt-Cu showed an increase of up to 30% at low annealing temperatures of between 200°C and 500°C. In addition, the Pt-Cu alloy also showed the increased hardness found in Pt-Mo and Pt-Ru at high annealing temperatures, but the hardness increase was not to the same extent.

Specimens subjected to the annealing treatments were studied by means of optical, scanning electron and transmission electron microscopy, in order to determine the effect of annealing on microstructure and structural order. Resistivity, XRD and DTA techniques were employed in order to study the mechanisms of ordering with temperature, but these techniques did not produce any significant results.

It was concluded that the most likely cause for the hardness increase observed in all three experimental alloys was due to a change in structural order upon annealing. The Pt-Mo and Pt-Ru alloys hardened through an increase in short-range order at annealing temperatures above the recrystallisation temperature. The Pt-Cu alloy hardened through the development of long-range order on annealing between 200°C and 500°C. This increase in hardness was in addition to the high dislocation density in the alloy specimen due to prior cold-work.

ACKNOWLEDGEMENTS

I would like to express my sincere thanks to the following people:

To Dr. Duncan Miller and Dr. Candy Lang, my supervisors, for their continued support and guidance.

Dr. Mike Witcomb for the TEM specimens which he prepared for this investigation and for his unparalleled knowledge and expertise of TEM and specimen preparation.

Mr. Dane Gerneke and the staff of the Electron Microscope Unit for technical support.

Mr. Glen Newins for his enthusiasm and technical expertise.

Mr. Nick Dreze , Mr. Reggie Hendricks, Mrs. Doreen Young and Mr. Dave Dean for their many years of support and advice in and around the Materials Department.

Mira Topic for her assistance in the laboratory.

Mr. James Peterson, Mr. Bernard Greeves and Mr. Adriaan Loedolff for their photographic expertise.

Miss Julie Henry and Mrs. Anthea Williams for administrative support.

Miss Taryn Biggs of MINTEK for advice and encouragement.

And the staff and students of the Materials Engineering Department for all their support and encouragement.

The financial support of the FRD (Foundation for Research Development) is gratefully acknowledged.

CONTENTS

ABBREVIATIONS

PGM	-	Platinum Group Metals
wt%	-	weight percent
at%	-	atomic percent
f.c.c.	-	face centred cubic
b.c.c	-	body centred cubic
h.c.p.	-	hexagonal close packed
SRO	-	short-range order
LRO	-	long-range order
T_c	-	critical ordering temperature
p	-	probability of an atom site being filled
r	-	fraction of total sites occupied
n	-	total sites
APD	-	antiphase domains
APB	-	antiphase boundary
q	-	number of AB pairs
q_r	-	average number of AB pairs
q_m	-	maximum possible number of AB pairs
S	-	long-range order parameter
τ	-	stress required to move dislocation
γ	-	force to overcome by dislocation
b	-	Burgers vector
ρ	-	total resistivity
ρ_o	-	residual resistivity
$\rho(T)$	-	ideal resistivity
ρ_b	-	resistivity of individual band
σ_b	-	conductivity of individual band
x	-	fractional atomic composition
λ	-	wavelength
I_D	-	intensity of diffuse scattering
k	-	constant for one composition
f	-	atomic scattering factor

DTA	-	differential thermal analysis
DSC	-	differential scanning calorimetry
SEM	-	scanning electron microscopy/microscope
TEM	-	transmission electron microscopy/microscope
XRD	-	x-ray diffraction
EDS	-	energy dispersive spectroscopy

1 INTRODUCTION

The increasing demand for platinum in the international jewellery industry, accounting for nearly half of the Western worlds annual consumption, coupled to the fact that South Africa produces over 50% of the worlds platinum, means that the South African economy can only benefit from a developed, local, platinum jewellery industry. Important to this development is a thorough scientific knowledge and understanding of the properties and characteristic of platinum and its alloys. The objective of this study is to investigate the hardening characteristics of three low solute content platinum jewellery alloys concentrating on hardening of fully worked or shaped materials. Any increase in hardness of the final material will result in improved wear resistance, improved scratch resistance and more durability for every day use. In addition the study will provide a base for further scientific investigation into the hardening and hardening behaviour of platinum alloys that could be used directly in jewellery manufacture and possibly in other industries as well.

The ease with which pure platinum can be worked, together with its strength and oxidation resistance properties, render it attractive to both jewellery manufacturers and the consuming public. As with all pure metals, however, the properties of pure platinum can be enhanced by the addition of alloying elements, which can be used to impart different jewellery requirements that are lacking in the pure metal. Alloying with other metals influences not only platinum's hardness and other mechanical properties, but also its corrosion resistance, colour and general workability. The alloying of platinum with other platinum group metals (PGM) has been shown to offer a good compromise in properties due to their similar physical and chemical properties.

In the present work, the hardening behaviour of three alloys has been investigated. Platinum-copper, which is a commonly used jewellery alloy in South Africa, was chosen owing to the good mechanical properties shown by platinum when alloyed with certain base metals[1]. Ruthenium is also known to be a very suitable alloying element[1], as platinum-ruthenium alloys can be cast as well as worked and ruthenium is

used as an alloying element in the South African jewellery industry. The alloying contents have both been limited to 5 wt % as most countries specify that for an item to be described as "platinum" it must comprise not less than 95 wt% platinum[1]. An additional, novel alloy, platinum 5 at% molybdenum, has been added to the selection, as previous research into palladium alloys with the same solute content has shown interesting hardening characteristics[2]. It was hoped that these hardness effects might also occur in platinum 5 at% molybdenum alloys due to the very similar chemical and physical nature of platinum and palladium[2].

The project follows a systematic structure with the literature review, Chapter 2, following this introduction. The literature review is a comprehensive study of the scientific research on platinum and the three alloy systems in Section 2.1, ordering transformations in Section 2.2 and mechanical properties in Section 2.3. The final three sections of the literature review concentrate on the electrical resistivity, x-ray diffraction and differential thermal analysis of metals and alloys. Chapter 3, the experimental procedure, follows with Sections 3.1, 3.2 and 3.3 detailing material selection, specimen preparation and the annealing experiments respectively. The final four sections contain descriptions of the experimental techniques. Chapter 4 documents the results of the experimental investigation with Section 4.1 concentrating on the hardness results, Section 4.2 to 4.4 on the microscopy results and Sections 4.5 to 4.7 on resistivity, x-ray diffraction and differential thermal analysis. Prior to the conclusion in Chapter 6, Chapter 5 discusses and interprets the results of Chapter 4. Section 5.1 discusses the hardness results, Section 5.2 phase equilibria in the experimental alloys and Section 5.3 the effect of order on microhardness. The final three sections offer interpretations into the resistivity, x-ray diffraction and differential thermal analysis results respectively.

2 LITERATURE REVIEW

2.1 PLATINUM AND PLATINUM ALLOYS

The platinum group metals (PGM) are a group of six chemically and physically similar metals. The six metals are platinum, palladium, ruthenium, rhodium, iridium and osmium, with platinum being by far the most abundant of the PGM. They all belong to the transition metal elements which are characterised by very strong interatomic bonds. It is the nature of these bonds and the energy state of the electrons in the crystal lattice which determine the crystalline and physical properties of metals and alloys[3].

2.1.1 PLATINUM

Platinum is a silvery white metal and when pure, is malleable and ductile. The metal does not oxidise in air at any temperature but can be corroded by halogens, cyanides, sulphur and caustic alkalis. It is insoluble in nitric and sulphuric acid but dissolves when mixed as aqua regia. It has a face centred cubic (f.c.c.) lattice structure, lattice constant at 20°C of 3.9229 Å and is a group VIIIC transition metal. The electronic structure is 5d96s1, the atomic weight is 195.08 and the atomic number is 78. It has a melting point of 1772°C4. Details of the crystal structure and physical and mechanical properties can be seen in Table 2.1.1 and Table 2.1.2 respectively.

Table 2.1.1 Parameters of crystal structures of platinum group metals[3].

Metal	Crystal Structure	Type of Structure	Lattice Spacing A	Lattice Spacing c	c/a
Ruthenium	h.c.p.	Mg (A3)	2.7003	4.2730	1.5824
Rhodium	f.c.c	Cu (A1)	3.7967	-	-
Palladium	f.c.c.	Cu (A1)	3.8830	-	-
Osmium	h.c.p	Mg (A3)	2.7298	4.3104	1.5790
Iridium	f.c.c.	Cu (A1)	3.8312	-	-
Platinum	f.c.c.	Cu (A1)	3.9160	-	-

Table 2.1.2 Physical and mechanical properties of the platinum metals[5].

	Pt	Ir	Os	Pd	Rh	Ru
Density kg/m^3	21450	22650	22610	12020	12410	12450
Melting Point °C	1768	2443	3050	1552	1960	2310
Thermal conductivity W/mK	73	148	87	76	150	105
Specific heat J/kg.K	131.2	128.4	129.3	244.3	246.4	230.5
Resistivity μΩcm	9.85	4.71	8.12	9.93	4.33	6.80
Thermal emf mV	0.0039	0.0043	0.0042	0.0038	0.0046	0.0042
Tensile strength MPa	124	1100	-	172	688	496
Elastic Modulus GPa	172	516	556	117	316	417
Hardness HV	40-42	200-240	300-670	40-42	100-102	200-350

2.1.2 PLATINUM ALLOYS

Platinum is a very reactive metal and is compatible with a wide range of metals forming solid solutions with alloying elements of more than 1%. It is known readily to dissolve refractory metals such as tungsten and molybdenum, medium-melting metals such as zirconium and vanadium, some rare earth metals and the low-melting point metals aluminium, magnesium and gallium[5]. Even though the solubility of these metals can be as much as 50%, platinum is far less soluble in most elements of the periodic table. Platinum is known to form a large number of chemical compounds, the number increasing with the distance from the second component of the periodic system. Although platinum, and its very close neighbour palladium, exhibit similar chemical and physical properties, the constitutional diagrams of platinum are more complicated than those of palladium when alloyed with the same elements[5].

Platinum and palladium have other characteristics in common which include forming a large number of ordered phases as well as exhibiting short-range ordering (see Section 2.2.5) at both high and low temperatures. The platinum-copper alloy system, at medium to high copper composition, has been explored thoroughly by Irani & Cahn[6] and is the system most well understood and well documented and provides the basis on which to study ordering systems.

The solid solutions formed between binary alloys of the four f.c.c. platinum metals are very broad at high temperatures and often extend across the entire phase diagram. It

has been established that this is not so at lower temperatures and that several alloys will no longer form solid solutions. The result of this is that wide miscibility gaps, where the homogeneous alloy separates into two mutually saturated solid solutions, are formed at lower temperatures in many PGM alloys[5]. These miscibility gaps have been correlated by Raub[7] with the difference between the melting points of the two constituent metals. The critical temperature of the miscibility gap is higher the greater the difference in the melting point of the two alloys. Although gold and silver are not part of the PGMs they are often included informally with the platinum group metals as the generalisation of the above miscibility gap also applies to gold and silver alloys[5].

Very wide miscibility gaps have been found in the palladium-iridium, platinum-iridium and the platinum-rhodium systems. The exact limits of these miscibility gaps are very uncertain, since at temperatures around 600°C structural changes are extremely slow and annealing periods of years are necessary to reach equilibrium. Raub[7] advocated that these miscibility gaps also exist in the platinum-rhodium, platinum-palladium and rhodium-iridium alloy systems at low temperatures, although this has not been observed.

Alloys between f.c.c. (platinum, palladium, rhodium and iridium) and h.c.p. (ruthenium and osmium) platinum group metals are not very well studied, and the exact limits of solubility are again not very well known. This is due to the sluggishness shown by the alloys in reaching equilibrium. It is known that, of the platinum group metals, osmium and ruthenium form the simplest constitutional phase diagrams with the least number of chemical compounds[5]. They form continuous solid solutions only with each other and the metals of Group VII and are highly soluble in transition metals of Group IV through VI. These metals have a b.c.c. type crystal structure. Ruthenium and osmium form alloys with most metals but not the gold and silver systems and show wide areas of miscibility in the liquid state[5].

2.1.3 THE PLATINUM-MOLYBDENUM ALLOY SYSTEM

Although Driebholtz[8] did mention the platinum-molybdenum system in his paper of 1924, the first systematic investigation of this alloy was carried out by Raub[9] in 1954. By examining the products of melted mixtures of platinum and molybdenum he observed that the solid solubility of molybdenum in platinum was appreciable, but that of platinum in molybdenum was very small. At relatively low concentrations of molybdenum in platinum, Raub[9] found that the f.c.c. platinum solid solution suffered a tetragonal distortion to give an axial ratio of just above 1.0. This tetragonal phase was named α_1 and given the composition Pt_3Mo. He also observed superstructure lines in the X-ray diffraction pattern but did not discuss their origin. A second phase was also found, a hexagonal close-packed ε phase with a composition of Pt_3Mo_2. This phase was found to have a wide composition range extending towards compositions richer in molybdenum than PtMo. Greenfeld and Beck[10] made reference to the existence of the hexagonal phase in their paper of 1956. A decade later Rooksby and Lewis[11] investigated the system and found two additional phases. The first was a phase with an orthorhomic crystal structure with a composition between that of the tetragonally-distorted phase and the hexagonal phase described by Raub[9].

The latest study of this system seems to be that of Ocken and van Vucht[12] who investigated the crystal structure changes effected by heat treatment of platinum-coated molybdenum wire. Their work fully documents all seven single-phase regions, five intermetallics and two solid solutions, in the platinum-molybdenum system.

The first of the intermediate phases is that of the orthorhombic $MoPt_2$ phase with the approximate range shown on the phase diagram (Figure 2.1.1). This phase appears to be an ordered form of the terminal platinum solid solution with the critical ordering temperature at about 1800°C. Above this temperature the terminal f.c.c. phase was observed. Although the diagram indicates a dual phase region it is considered tentative due to difficulties in distinguishing between single phase $MoPt_2$ and two-phase $MoPt_2$ + f.c.c. platinum solid solution. This is due to X-ray reflections of the f.c.c. phase coinciding with those of the orthorhombic phase.

In addition to the orthorhombic $MoPt_2$ phase, there is an orthorhombic MoPt phase between 45 at.% and 53 at.% molybdenum. The experiments conducted by Ocken and van Vucht[12] indicated that at the Mo-rich side of this region, a temperature increase causes a transition from a MgCd-type order to the Mg_3Cd-type order before total disorder occurs.

The ordered and disordered hexagonal phases have been indicated on the phase diagram showing their position and shape. The shape of the two phase region and the peritectoid composition of the reaction $\beta + \varepsilon \Leftrightarrow \varepsilon'$ is rather uncertain and are only indicated as dashed lines due to their tentative nature. The ordered phase displays Mg_3Cd-type superlattice lines in the hexagonal X-ray pattern of the ε phase at temperatures below 1600°C.

Other than the solid solution of platinum in b.c.c. molybdenum, which has a maximum solubility of 12 at.% at 2000°C, the only other known phase is that of the A15-type Mo_6Pt. This phase was found in alloys containing between 5 and 37.5 at.% Pt which had been annealed at temperatures between 1300°C and 1800°C. The phase forms via a peritectoid reaction between the b.c.c. Mo solid solution and the h.c.p. solid solution, while it decomposes via an eutectic reaction to form a b.c.c. Mo solid solution and an ordered Mg_3Cd-type hexagonal phase with an approximate composition of Mo_3Pt_2. A single phase specimen of this phase was not found, but was always found in the presence of the b.c.c. phase and either the ordered or disordered hexagonal phase.

Ocken and van Vucht[12] found that at temperatures above 1800°C the solid solution phase extends to approximately 55 at.%. At temperatures lower than 1200°C the region only extends to about 20 at.% molybdenum. Although not dealt with in the paper by Ocken and van Vucht[12], but still considered important in that it is contrary to what is widely expected, the lattice parameter in the terminal f.c.c. solid solution initially decreases with increasing molybdenum content[9]. The lattice parameter decreases and reaches a minimum at between 9.6 at.% and 18.4 at.% Mo. The lattice parameter then increases again up to about 73 at.% which is consistent with the

molybdenum rich boundary of the ordered hexagonal ε' phase shown in the diagram of the Mo-Pt phase diagram.

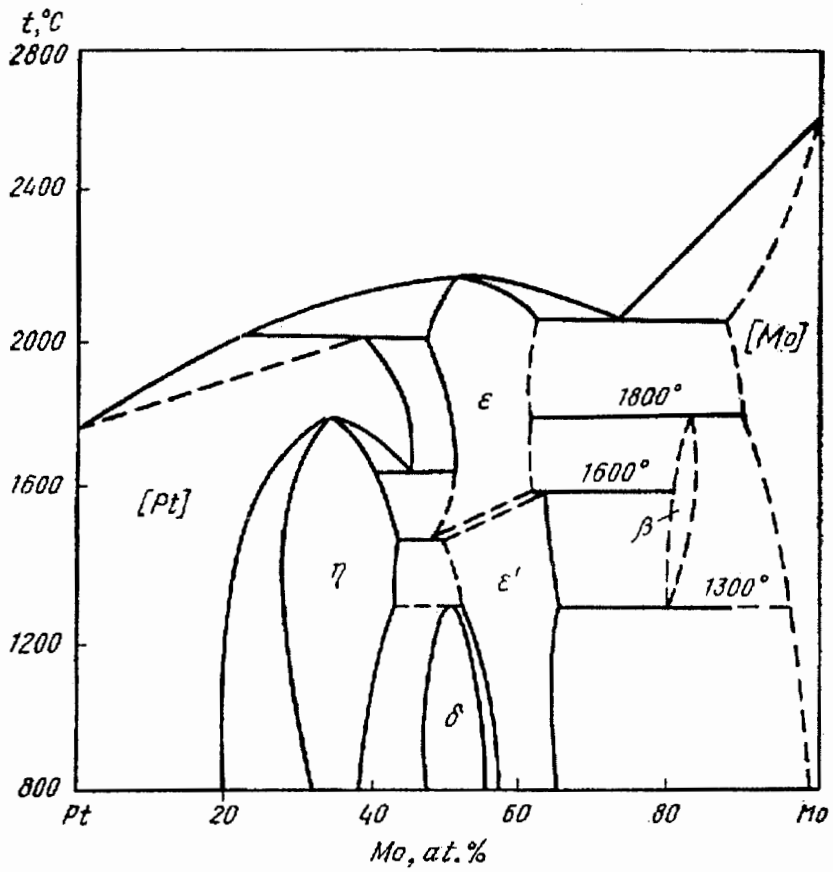

Figure 2.1.1 Equilibrium phase diagram of the platinum-molybdenum alloy system (after Savitskii[13]).

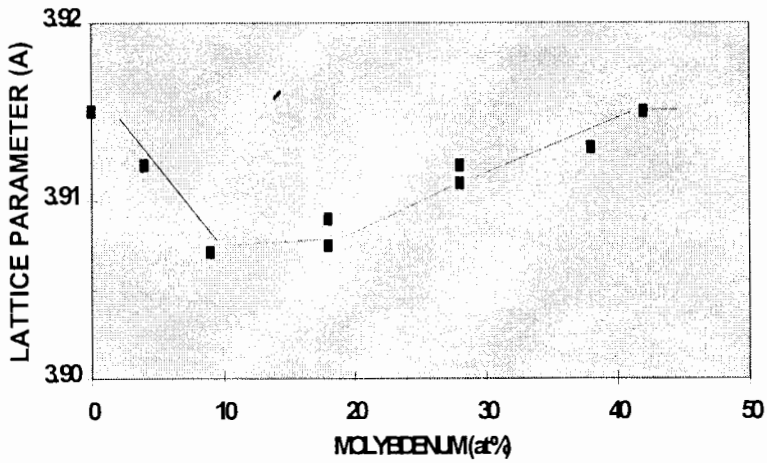

Figure 2.1.2 Graph of lattice parameter vs. concentration for platinum\ molybdenum (after Raub[9]).

2.1.4 THE PLATINUM-RUTHENIUM ALLOY SYSTEM

The platinum-ruthenium system is a simple peritectic with wide areas of solid solutions but no intermediate phases and has an equilibrium phase diagram as seen in Figure 2.1.3. Hutchinson[14], the only author to have investigated this system, established the limits of solubility using micro-probe analysis and showed very little inconsistency. She shows the solubility of ruthenium in platinum to be 62 at.% at 1000°C, increasing to 70 at.% at 1900°C, whereas the solubility of platinum in ruthenium averages 20 at.% and changes very little with temperature[14].

The solubility of platinum in ruthenium increases very slowly with temperature and little precipitation occurs from these solutions on quenching[14]. On the other hand, the solubility of ruthenium in platinum occurs rapidly with increasing temperature. As a result, it was found that the high temperature structure of the saturated platinum solutions could not be fully retained with quenching. Precipitation was therefore considerable, influencing the composition of the retained phases and resulting in high hardness values of the quenched duplex alloys. The hardness curve in Figure 2.1.4 shows the well defined hardness peak associated with the precipitation across the duplex region. The gently ascending line at low ruthenium contents is as a result of normal solution hardening.

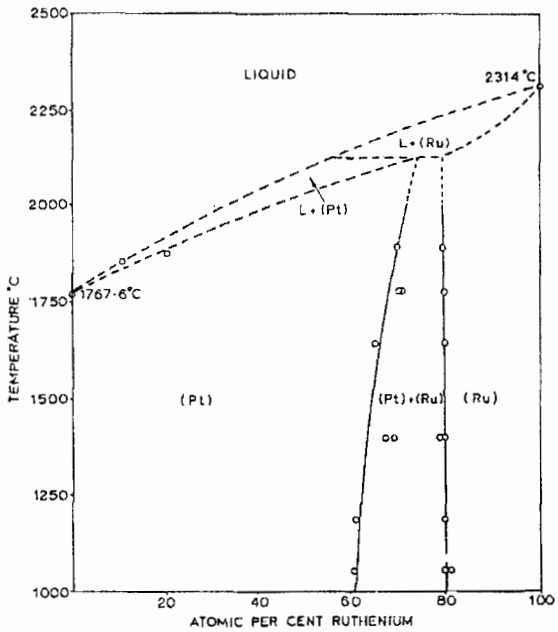

Figure 2.1.3 Equilibrium phase diagram of the platinum ruthenium system (after Hutchinson[14]).

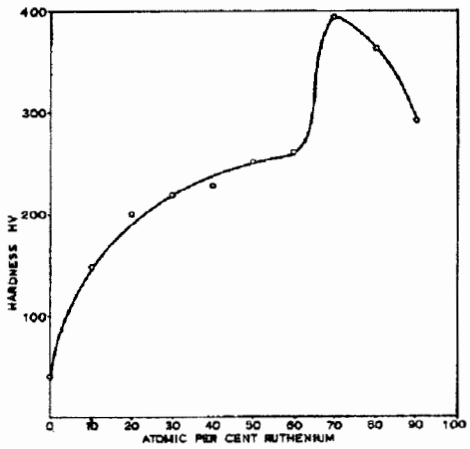

Figure 2.1.4 Hardness vs. composition for platinum ruthenium alloys quenched from 1800°C (after Hutchinson[14]).

2.1.5 *THE PLATINUM-COPPER ALLOY SYSTEM*

Figure 2.1.5 shows that the platinum-copper alloy solidifies in a continuous series of solid solutions with two Kurnakov type compounds, PtCu and $PtCu_3$, known to form at lower temperatures. Of these two ordered Pt-Cu phases, the equiatomic PtCu has been very well researched due to the unusual superlattice structure that forms during ordering. Although the ordered phases are centred around the stoichiometric values of PtCu and $PtCu_3$, the equiatomic PtCu section of the phase diagram (by Savitsky et al[3] seen in Figure 2.1.5 and by Irani & Cahn[6] seen in Figure 2.1.6) predicts that the ordered phase can extend down to very low copper contents.

The equiatomic alloy PtCu has a random f.c.c. solid solution structure at high temperatures but acquires an ordered configuration when cooled below 815°C[6] as shown in Figure 2.1.6. The long-range ordered rhombohedral superlattice consists of alternate layers of pure copper and pure platinum atoms arranged parallel to the (111) planes (Figure 2.1.7). The rhombohedral unit cell is related to the disordered cubic state by a slight compression along one body-diagonal[6]. The ordered superlattice is unusual in that each atom effectively still has 12 nearest neighbours, 6 like and 6 unlike, before and after ordering and there is no increase in the number of like neighbours on ordering. The CuPt superlattice is the only system known to date in which this type of ordering takes place[15].

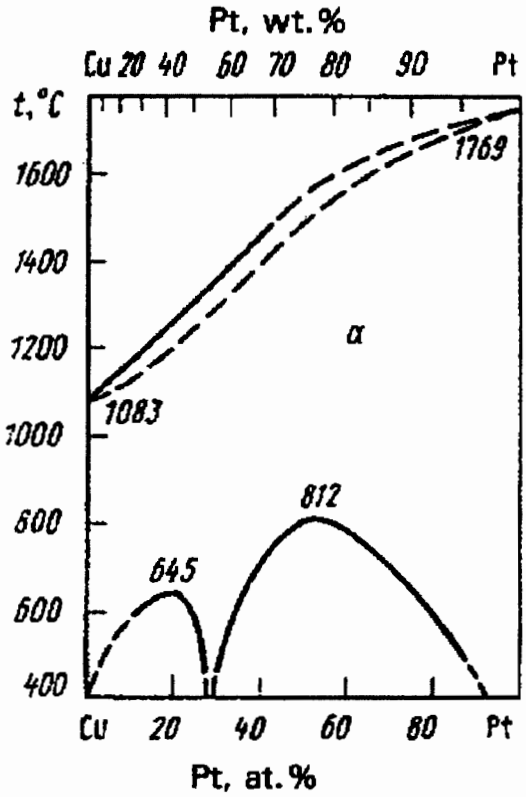

Figure 2.1.5 Equilibrium phase diagram of the platinum-copper system (after Savitskii[3]).

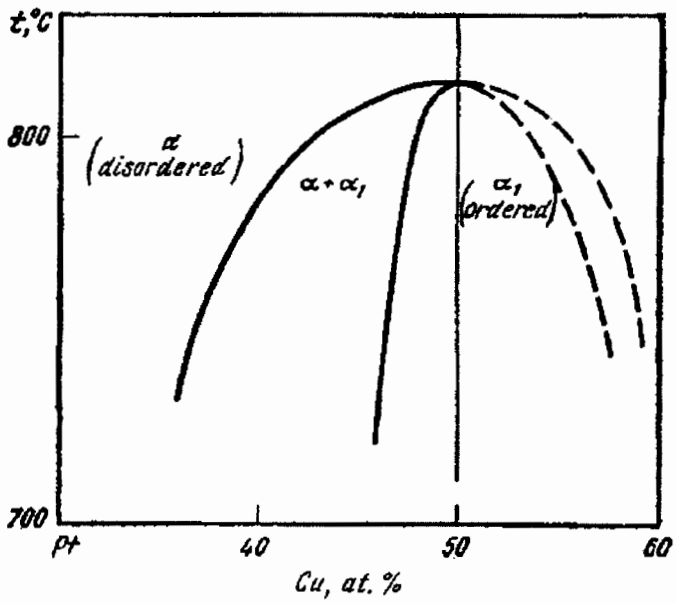

Figure 2.1.6 Part of the platinum-copper equilibrium phase diagram (after Irani & Cahn[6]).

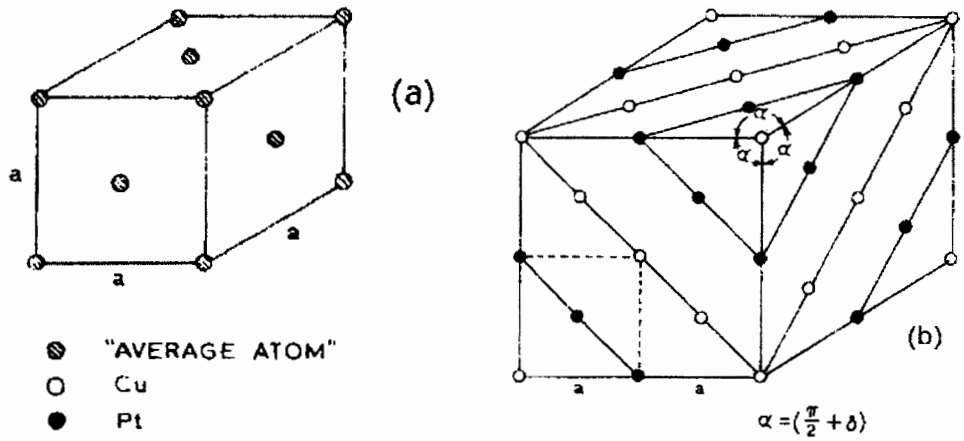

Figure 2.1.7 a) Disordered f.c.c. cell of equiatomic platinum-copper. b) Ordered cell of equiatomic platinum-copper showing segregation along (111) planes (after Irani and Cahn[6]).

The type of ordering mechanism of PtCu (whether it is first or second order) was under dispute until Irani & Cahn[6] showed x-ray evidence that both ordered and unordered phases can coexist transiently or in equilibrium. When a cubic alloy changes symmetry (eg. to tetragonal) on ordering then the fundamental diffraction lines split into pairs or multiplets with substantially different Bragg angles. If a second order, nucleation and growth mechanism (Type I: see Section 2.2.3) is in progress then peaks common to both fully ordered and fully disordered structures should be detectable. If the ordering mechanism is homogenous (Type II), the disordered peaks gradually broaden and then decompose into the new peak and the ordered and disordered peaks will not be simultaneously detectable. If there is no change of symmetry on ordering then the fundamental peaks of the ordered and disordered forms would be superimposed and therefore are not distinguishable[6] (for more detail see Section 2.5.2.).

Even given the comprehensive work undertaken by Irani & Cahn[6], there has been mention of additional phases in other works which have not been considered by the two authors. Existence of other superlattice structures has also been reported in the platinum rich region. Although the original papers could not be sourced, Miida & Watanabe[16] have stated the possibility of these additional ordered phases due to the work of Linde[17], Schneider & Esch[18] and Wu et al[19]. The ordered superlattice Cu_3Pt_5, with rhombohedral symmetry, has been proposed by Linde[17] and $CuPt_7$ by Schneider

& Esch[18]. The ordered Cu_3Pt_5, however, was not confirmed by x-ray diffraction studies performed by Schneider & Esch[18] or Wu et al[19]. Hirone & Adachi[20], also mentioned in the paper by Miida & Watanabe[16], discussed the stability of various types of superlattices in the Cu-Pt system by taking account of the influence of the second-neighbour interactions. They concluded that the superlattices of Cu_3Pt_5, $CuPt_3$ and $CuPt_7$ are stable at low temperatures in the composition range above 50 at% Pt, while the rhombohedral CuPt superlattice is stable at high temperatures. Miida & Watanabe[16] have published a partial phase diagram around the composition $CuPt_3$ as shown in Figure 2.1.8. It is interesting to see that past 70 at% Pt the PtCu phase changes from being rhombodedral to cubic with the $CuPt_3$ phase having an orthorombic type structure.

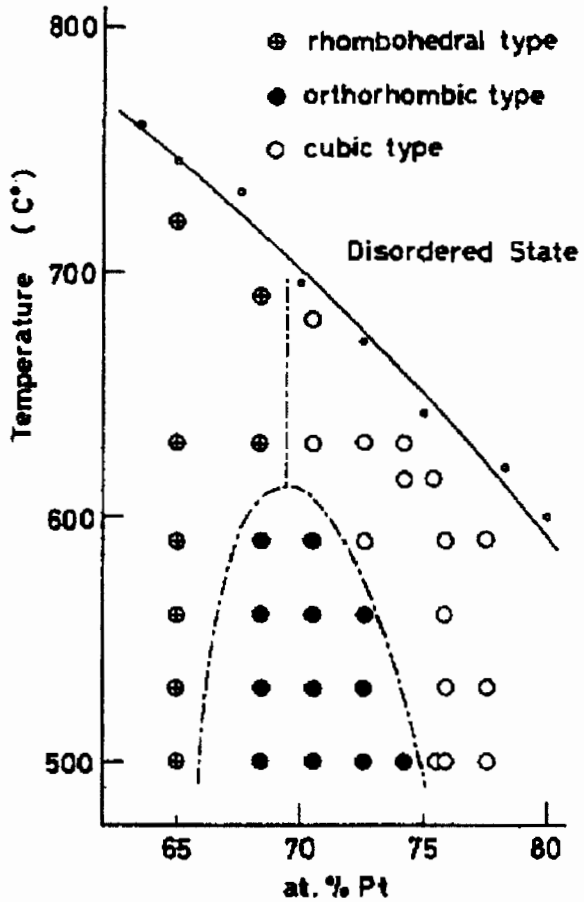

Figure 2.1.8 Partial phase diagram around the composition $CuPt_3$ (after Miida and Watanabe[16]).

This particular alloy system is one of the very few binary platinum alloy systems that has been investigated specifically for its hardening behaviour. Both Irani & Cahn[21] and Mitchell et al[22] have investigated the order hardening behaviour of equiatomic PtCu or just off the stoichiometric PtCu composition. By isothermally annealing previously quenched specimens at various temperatures below the critical ordering temperature, they found an interesting hardness profile. The hardness passed through a maximum value, which depended on the temperature, and for a given temperature was highest for the stoichiometric alloy. Both authors state that the maximum hardness occurred at an intermediate degree of long-range order and stated that domain size and internal stresses resulting from mismatch between neighbouring domains played a major part in the peak hardness. Figure 2.1.9 shows an example of the hardening behaviour that is seen in PtCu alloys at or near the equiatomic composition. The profile is characteristic of an age or precipitation hardened alloy although the precipitation of a second ordered phase does not occur.

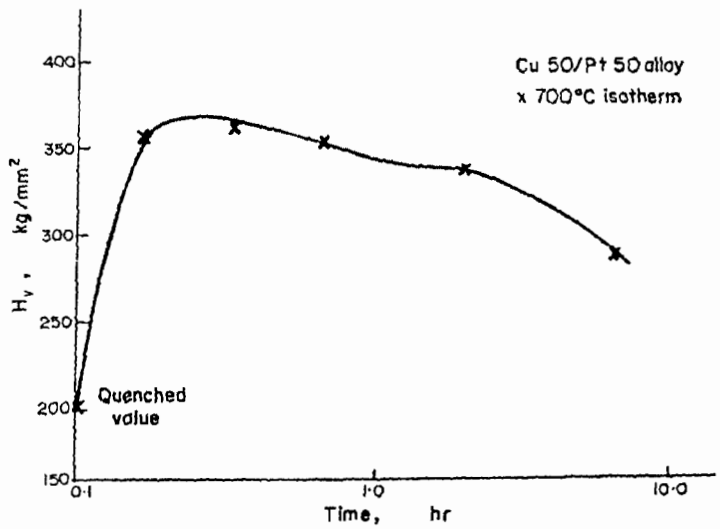

Figure 2.1.9 Microhardness isotherm for annealing at 700°C (after Irani and Cahn[21]).

2.2 ORDERING TRANSFORMATIONS

In a binary solid solution there are a number of different ways in which the two atomic species can arrange themselves. The arrangement of atoms can be broadly separated into ordered and random configurations. Almost all metals show some type of order, however small, and a truly random arrangement of atoms is very rarely found. The ordering that does occur in solid metals can be divided into three main types, two of which are associated with solid solutions and the third with compounds. The sections on ordering that follow, introduce two very important concepts, those of long-range and short-range order.

2.2.1 *ORDERING IN SOLID SOLUTIONS*

A large number of solid solutions become ordered at low temperatures. The process of ordering involves a change from a statistically random arrangement of atoms on the crystal lattice, to that of more regular arrangement. In the regular or ordered arrangement, any atomic site is occupied predominantly by one or other kind of atom[23]. In a disordered alloy of A and B atoms with a composition of AB, any given lattice site could be occupied by either an A or B atom. On ordering, the A and B atoms segregate to designated atomic sites. The resulting structure can be described as a lattice of A atoms interpenetrating a lattice of B atoms[23]. Figure 2.2.1 shows the disordered lattice where copper and gold atoms can occupy any of the atomic sites as long as the ratio of gold to copper remains at 1:3 according to the stoichiometric formula of $CuAu_3$. The ordered structure shows an example of the two interpenetrating lattices of the copper and gold atoms[24]. The arrangement described above, of interpenetrating lattices is described as a superlattice or superstructure.

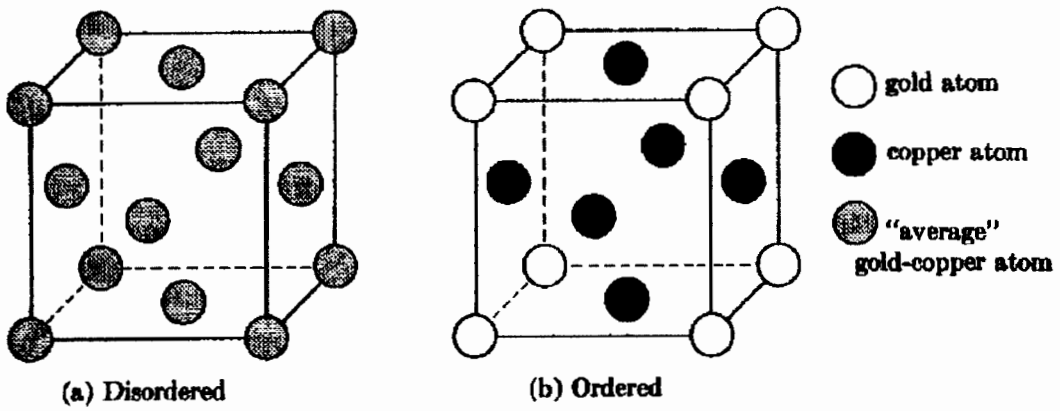

Figure 2.2.1 Unit cell of disordered and ordered Cu_3Au (after Irani[24]).

The formation of superlattices is commonly referred to as long-range ordering (LRO). Long-range order takes place at low temperatures and usually at or near stoichiometric compositions where the compositions can be expressed as a simple formula such as AB or AB_3[23]. At temperatures above a certain critical temperature (T_c), randomness will appear as thermal vibrations break down the very structured superlattice. When the temperature is cooled below T_c, ordering of the lattice will start to occur and the amount of order will increase as the temperature decreases. It is possible to achieve near perfect structures as very low temperatures are approached[23].

It is possible in some concentrated solid solutions, usually those that exhibit some type of superlattice structure, to have neither a perfectly random nor a perfectly ordered structure[25] above T_c. Even in the disordered state there is a certain correlation or statistical preferences for like or unlike nearest neighbours between neighbouring atoms. Even though the LRO structure breaks down at high temperatures, the atoms still have an affinity for one another. If the atoms have a greater preference for like nearest neighbours the ordering phenomenon is termed short-range clustering (SRC). If the atoms prefer unlike nearest neighbours, which is the more common case, the ordering arrangement is called short-range ordering (SRO)[24]. The alloy systems that show both LRO and SRO are simply termed ordered alloys. There are also alloys where only SRO persists with no corresponding LRO. The alloys with this statistical ordering in concentrated solid solutions occurs are often termed statistical alloys[24].

2.2.2 *INTERMETALLIC COMPOUNDS*

In addition to the two types of ordered alloys mentioned at the end of the previous section, there is a third type of ordered alloy. In certain alloy systems, at or near stoichiometric compositions, the superlattice is retained right up until melting point and is not destroyed at T_c as in ordered alloys. The phases in the alloy systems where this occurs are termed intermetallic compounds, although the word compound is not used in the true sense of a chemical compound. The intermetallic compounds, unlike the ordered alloys, have no corresponding disordered structure and always retain their order.

2.2.3 *ORDERED SUPPERLATTICE STRUCTURES*

The majority of typical superlattices are related to three principal metallic structures, f.c.c., b.c.c. and h.c.p.. They are commonly referred to by their Strukturbericht designations e.g. $D0_3$ or $L2_1$, both of which are based upon the b.c.c. lattice structure. The Strukturbericht designations are only available for the most common types of superlattices[23]. The most widely studied and understood superlattices are the ones that do not undergo a change in Bravais lattice or symmetry upon ordering (Figure 2.2.2). The most useful ones though, are those in which a change in Bravais lattice occurs below T_c[25]. This is because hardness increases are associated with this change and will be discussed in Section 2.3.2.

Figure 2.2.2 shows the superlattice structures that do not undergo a change in lattice with their respective Structurbericht. The most frequently observed ordered lattice is the $L2_o$ type which is b.c.c. in the disordered state as shown in Figure 2.2.2 a). It may be described as two interpenetrating cubic lattices with A atoms on one sublattice and B atoms on the other[25]. β-Brass is a good example of an alloy that exhibits this type of ordered structure. The remaining three superlattices, b, c and d in Figure 2.2.2, are represented by f.c.c. Cu_3Au, h.c.p. Mg_3Cd and b.c.c. Fe_3Al respectively. They are made up of four interpenetrating sublattices with B atoms on one sublattice and A atoms on the other three due to their A_3B formula[25]. In the f.c.c. $L1_2$ structure there is no change in the size of the unit cell on ordering but for the h.c.p. $D0_{19}$ structures the

ordered unit cell may be compared to four unit cells of the disordered h.c.p. structures such that the axial ratio is halved. This is achieved by the c parameter remaining the same while the a parameter doubles in length. The DO_3 type with eight b.c.c. unit cells is the most complex and is thought to be composed of four interpenetrating f.c.c. lattices.

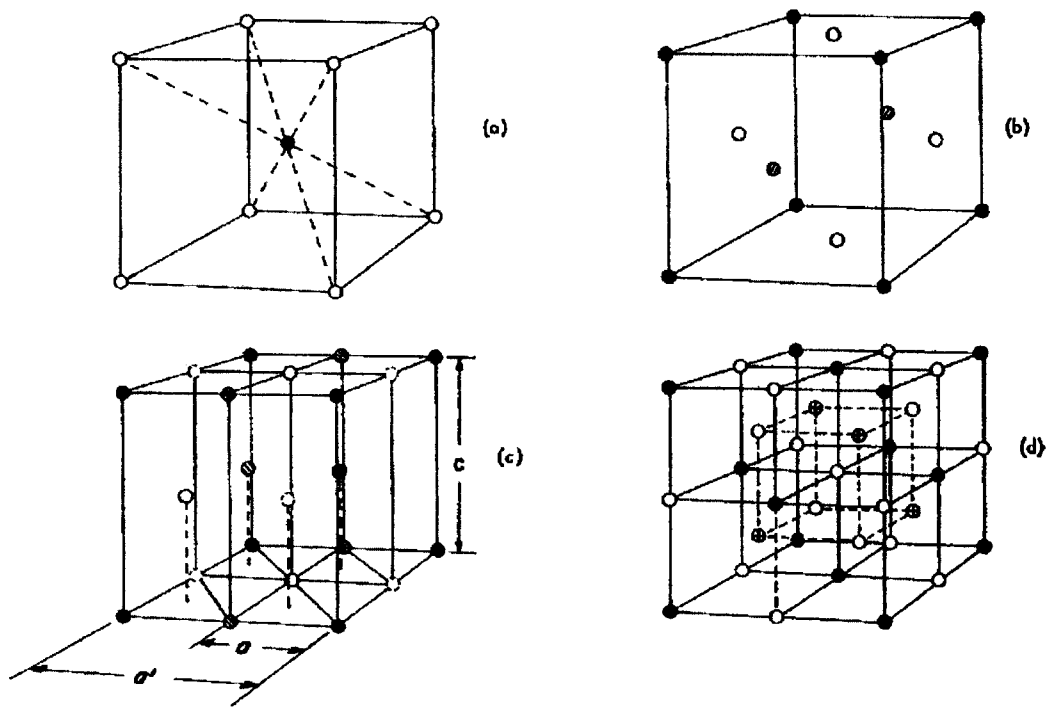

Figure 2.2.2 Common types of superlattices in which the crystal structure does not change upon the formation of long range order. a) $L2_0$, b) $L1_2$, c) DO_{19}, d) DO_3 (after Stoloff & Davies[25]).

Of the superlattices that undergo a change in symmetry upon ordering, the $L1_0$ ordered structure is the most common and is shown in Figure 2.2.3. CuAu is the best example of this group and transforms from disordered f.c.c. to ordered face centred tetragonal (f.c.t.) with an axial ratio that is usually between 0.9 and 1[25]. The CuPt alloy, which will be discussed in more detail later, undergoes a change from disordered f.c.c. to the $L1_1$ superstructure. It is the only alloy known to exhibit this change[23].

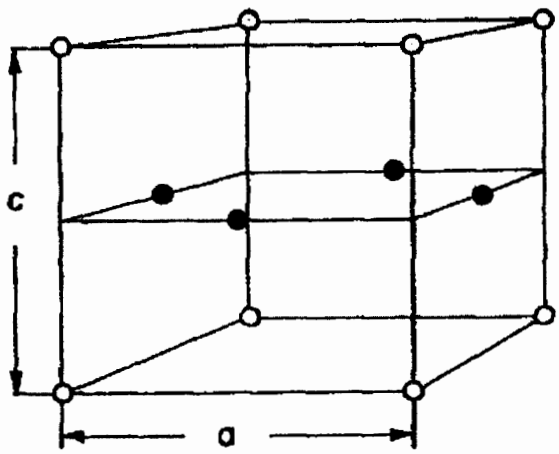

Figure 2.2.3 $L1_0$ superlattice which changes crystal structure from f.c.c. to f.c.t. upon ordering (after Stoloff and Davies[25]).

2.2.4 *LONG-RANGE ORDER*

The degree of long-range order, discussed in the previous sections, can be expressed by means of the Bragg-Williams parameter S, defined as

$$S = (p-r)/(1-n). \qquad \textbf{Equation 2.1}$$

Where p is the probability that an atom site is filled by an A atom, and r is the fraction of the total sites, n, that are occupied by A atoms for perfect order[25]. S will, therefore, vary from 0 for disorder to 1 for fully ordered. The transition from 0 to 1 may be either continuous or discontinuous, depending on the crystal structure of the alloy. Figure 2.2.4 shows the variation in degree of order with temperature for two different alloys. When heated, S, for fully ordered specimens of $L1_2$ or DO_{19} type structure, will decrease slowly from 1 to 0.8, then decrease discontinuously from 0.8 to 0. At temperatures above T_c, S will be zero. The figure also shows that for $L2_0$ and DO_2 structures that S decreases continuously from 1 to 0 as the temperature approaches T_c[25].

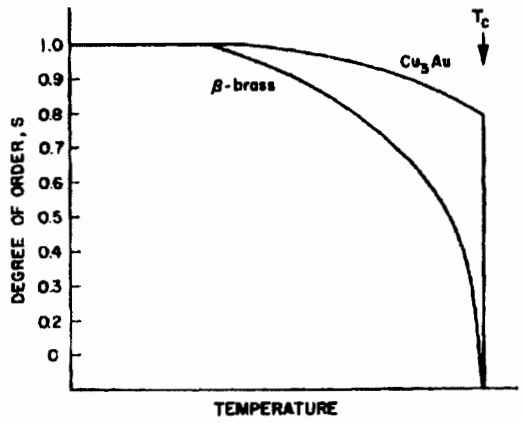

Figure 2.2.4 Variation in degree of order with temperature for β-brass ($L2_0$ structure) and Cu_3Au ($L1_2$ structure) (after Stoloff & Davies[25]).

During transformation from a disordered to an ordered structure, two mechanisms, nucleation and growth ordering and continuous (or homogeneous) ordering, are predicted by currently accepted theory. The nucleation and growth processes can be divided into two modes depending on whether homogeneous nucleation or heterogeneous nucleation is involved[26]. There has been some confusion from using equilibrium thermodynamic terms for mechanisms. There has been an attempt by Irani[24] to use notation adopted by Gibbs to avoid any confusion but it has not been adopted by many other authors. The suggested notation was to generalise transformations into different categories, governed by the atomic configurations present. Drastic atomic rearrangements within very small localised volumes he termed as a Type I transformation, while those corresponding to very small rearrangements spread over large volumes are termed Type II. It is difficult to rigidly categorise the ordering reaction in alloys as some alloys have been shown to exhibit both processes. There has been recent speculation that all superlattice alloys may transform isothermally by a nucleation and growth process but as of yet no definitive evidence has been reported[25].

The nucleation and growth process takes place by the nucleation, growth and ultimately coalescence of ordered regions in a disordered matrix. In a long-range ordered AB alloy, A atoms in some nuclei can occupy atomic sites on sublattice 1 and in another nuclei with the A atoms on sublattice 2. In this alloy there will be an approximately equal numbers of regions, domains or more correctly antiphase

domains (APD), in which A atoms are on different sublattices[25]. When the domains come into contact an antiphase boundary (APB) is formed at the plane of contact of the two domains. The APB indicates a change in sublattice occupancy across the boundary. During annealing of the ordered alloy, some APBs will grow at the expense of others until each grain encloses a single domain[25]. Antiphase boundaries can also arise during plastic deformation but will be discussed in the superdislocation section to follow.

The rate of ordering varies greatly with the type of the alloy. There are alloys such as the β(CuZn) where ordering is so rapid that it is impossible to quench in the disordered b.c.c. structure. This is due to a second order, ordering transformation and can occur by a rapid continuous ordering process. Ordering in Cu_3Au is very slow by comparison and takes several hours for complete ordering to occur. This is despite the fact that atomic mobilities ought to be the same as those in the CuZn transformation. Ordering of Cu_3Au proceeds by nucleation and growth and is further hindered by the formation of metastable APB networks.

2.2.5 SHORT-RANGE ORDER

Long-range order is a very well understood and very well-established phenomenon, but it is thought that short-range order, though less well known and understood, is an even more commonly occurring type of ordering transformation. This type of ordering is best understood in terms of one atom's chemical affinity for another or the difference in electronegativity between different atoms[27]. The discussion on LRO pointed out that certain sites are appropriate to atoms of a particular kind, the resulting arrangement being that an atom has more unlike nearest neighbours than it would do in a purely random arrangement. It is thought that this type of arrangement of atoms can exist, although not to the same extent, when no LRO is present. All atoms, of different chemical elements, have differing electronegativities which leads to an attraction of one atom to another and it is consequently thought that some degree of SRO should be expected in all solid solutions[27]. The difference in size between different atoms in a solid solution has also been thought to contribute to some time of ordering[28].

It is also thought that those alloys which form superlattices are particularly likely to exhibit SRO at temperatures just above T_c[32]. The attraction or electronegativity that resulted in the LRO still persists above T_c even though thermal agitation has destroyed the superlattice[27]. This SRO can also be retained at low temperatures by rapid quenching from temperatures above T_c. The transformation from disorder to order has been discussed from two points of view: a statistical treatment and a particle, nucleation and growth concept[29]. The latter treatment, of a first order, heterogeneous, nucleation and growth process, has received more interest in the literature but the homogenous, second order, statistical treatment has not been discarded. The homogeneous type transformation is concerned with the average deviation of the numbers of like and unlike atom pairs from a random distribution. The heterogenous, nucleation and growth process is based upon the presence of small ordered regions in a random matrix or a nonrandom distribution of like and unlike atom pairs[29].

The formation of SRO at temperatures just above T_c is to be discussed below using only the nucleation and growth process, as no literature on the exact formation through a statistical manner has been located. The nucleation and growth formation of SRO occurs at high temperatures, just above T_c where there are more than the random number of AB atom pairs. With the lowering of the temperature towards T_c, small nuclei or regions of SRO continually form and disperse in an otherwise disordered matrix[30]. The nuclei, which exist only as fluctuations, increase in size, degree of internal order and mean life time as T_c is approached[31]. As the temperature and thermal agitation decrease, these regions of order become more extensive, until at T_c they coalesce and the alloy consists of an interlocking mesh of small ordered regions. At temperatures below T_c, these domains absorb each other as a result of antiphase domain boundary mobility until LRO is established.

While S, the LRO order parameter discussed previously expresses the fraction of correct atoms upon precise sublattices, averaged over the entire lattice, the SRO parameter σ is slightly different. σ measures the extent to which an atom is surrounded by unlike neighbours, with no mention being made to sub- or superlattices[32]. σ is defined as;

$$\sigma = (q-q_r)/(q_m-q_r) \qquad \textbf{Equation 2.2}$$

where q is the number of AB pairs, and q_m is the maximum possible number of AB pairs; q_r is the average number of AB pairs for a random arrangement[32]. The short-range order parameter is usually measured above T_c and it decreases with increasing temperature. Below T_c the parameter σ and S are related because when S=1 so must σ, and σ is always greater or equal to (S^2) [32].

2.3 MECHANICAL PROPERTIES OF ORDERED ALLOYS

The study of mechanical properties of ordered alloys is devoted mainly to that of the intermetallic compounds, with little work carried out on the solid solution regions. The most detailed and current coverage of mechanical properties of locally ordered solid solutions has been undertaken by Stoloff & Davies[25] and Cahn[33]

2.3.1 DISLOCATION STRUCTURE IN ORDERED ALLOYS

When an alloy orders (long-range order), what was a unit dislocation in a disordered alloy, may be considered as a partial-dislocation with its attached anti-phase boundary interface in a superlattice[30]. The movement of a dislocation through a superlattice will not recreate the ordered structure in its wake and as a result will leave a disordered region across its slip plane in the form of an anti-phase boundary (APB). The resultant deformation APB is similar to the thermal APBs discussed above but formed in a different manner[30]. This process would, however, require a very high stress as any given atom in an ordered lattice prefers to have unlike atoms as its neighbours. Fisher's[30,34] equation for the stress required to move a dislocation against the force γ, exerted on it by the fault is

$$\tau = \gamma/b \qquad \textbf{Equation 2.3}$$

where b is the Burgers vector. If this equation is used for β-Brass, where γ is about 0.07 N/m, the shear stress is about 300 MN/m^2 which is an order of magnitude more than the practical critical shear stress for β-brass. Using this knowledge it was concluded that slip must occur by an easier process than the movement of unit dislocations[30]. It is consequently believed, using the analogy of the slip process in f.c.c. crystals, where the leading dislocation trails a stacking fault, that dislocations that cause slip in ordered lattices are not single dislocations but coupled pairs of dislocations. The first dislocation of the pair disorders the atoms across the slip plane; order is restored, however, if a second identical dislocation follows the first

dislocation on the same plane. Order will once again be disrupted as a third dislocation moves along the slip plane and so on[25]. This group, which consists of two or more unit dislocations of like sign, is called a superlattice dislocation or a superdislocation.

The equilibrium distance between the two dislocations comprising a superdislocation is determined by an energy balance between the mutual elastic repulsive forces between the two dislocations and the opposing force due to the APB energy[25,33]. In f.c.c. type alloys it must be also taken into account that each unit dislocation may itself dissociate into partial dislocations, separated by a stacking fault with its own equilibrium spacing. The superdislocation would then consist of two extended dislocations connected by an APB, as illustrated in Figure 2.3.1. The requirement that dislocations in superlattices must travel in pairs provides a strengthening mechanism in alloys containing ordered "precipitates"[35].

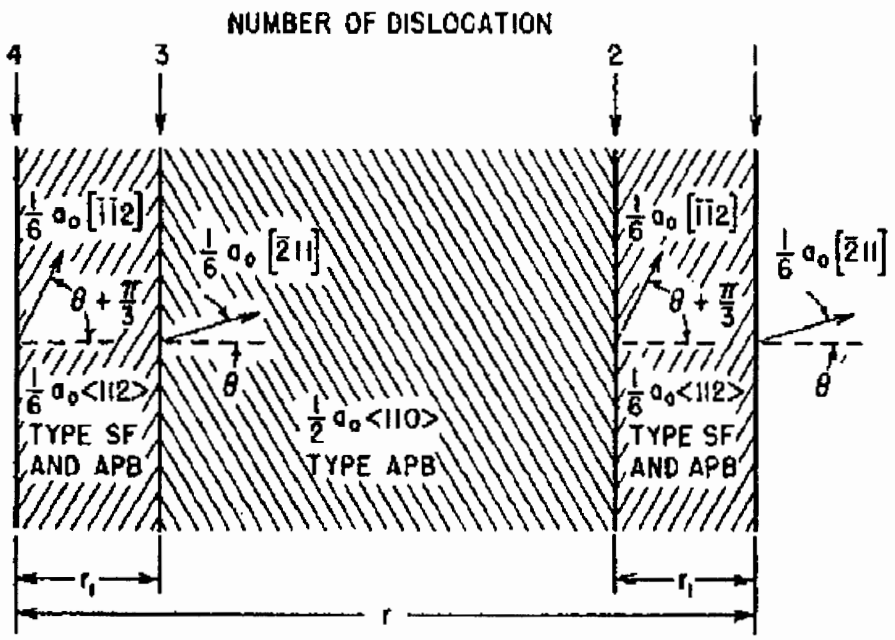

Figure 2.3.1 A [011] superlattice dislocation in an AB_3 superlattice (after Hull & Bacon[35]).

In short-range ordered alloys slip does not occur by the movement of superdislocations since there are no long-range faults to couple dislocations together in pairs. Fisher[34], however, recognised that statistical SRO could still affect the flow stress of moving dislocations. He advocated that SRO would influence the flow

stress of solid solution by increasing their frictional drag. He stated, with not much proof, that the movement of a number of successive dislocation across a slip plane would totally destroy the order across that plane. This reduction in the number of like nearest-neighbours bonds, or the equilibrium short range order, would consume energy, which is provided by the increased stress required to move the dislocations. This particular model implies that the stress required to move successive dislocations drops as the amount of order on the plane decreases. Cohen & Fine[36], using Fisher's earlier work, suggested that even though the superdislocation mechanism used to describe slip in superlattices does not apply to SRO alloys, that dislocation groups are present in alloys containing SRO. The rationale is that because order does not decrease monotonically during slip, that a stress sufficiently large to move the leading dislocation will move the following dislocation as well. Since the first dislocation destroys a significant fraction of the order along the slip plane, the second dislocation will move at a considerably higher velocity than the first under the same stress. The dislocations will move together until a steady state of separation is set up and then they will move as a group with the trailing dislocations "pushing" the lead dislocation.

2.3.2 *HARDENING DUE TO LONG RANGE ORDER*

EFFECT OF VARIATION OF DEGREE OF ORDER ON HARDNESS

Given the diversity of the superlattice structures that were discussed in Section 2.2.3, there are still many features of deformation that are common to all LRO alloys. The most characteristic of these features is the peak in flow stress at the critical temperature, T_c, or below. These peaks in flow stress have been seen in all ordered systems in which T_c occurs below the melting point, independent of whether there is a change in Bravais lattice upon ordering or not[32].

Cu_3Au, an $L1_2$ type superlattice, which shows a discontinuous degree of order from S= 0.8 - 0 (Figure 2.2.4), shows a peak hardness at T_c while for most other f.c.c., b.c.c. and h.c.p. superlattices the peak is observed at temperatures slightly lower than T_c. These hardness peaks occur both when testing is carried out at temperature to obtain different degrees of order, or when differing degrees of order have been

trapped by quenching from specific temperatures. An example of the variation of flow stress with LRO in FeCo-2% V at both elevated temperatures and room temperature can be seen in Figure 2.3.2. The data for FeCo-2% V has been used as an example as there is no stable anti-phase domain which can interfere with the interpretation of the data (see later section). The graphs in Figure 2.3.2 show that the peak flow stress occurs at approximately the same intermediate degree of order, S = 0.2-0.3, whether testing was carried out at elevated or room temperature[37].

a)

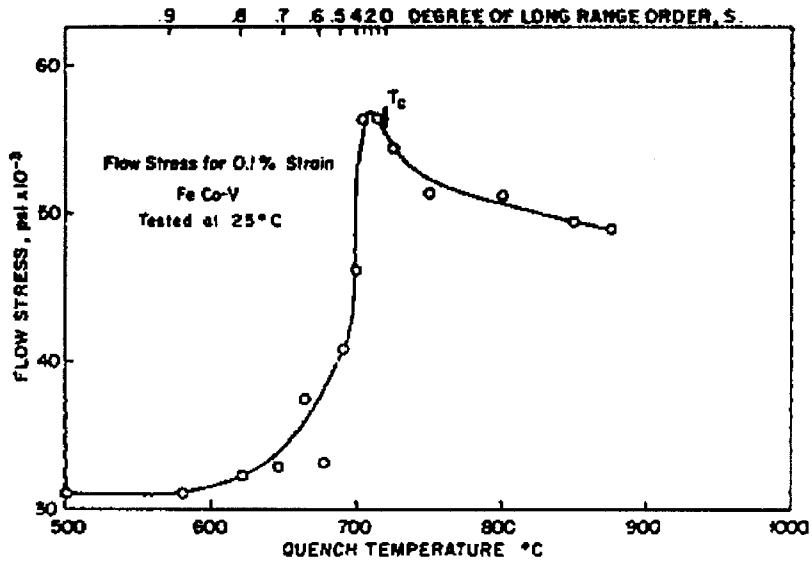

b)

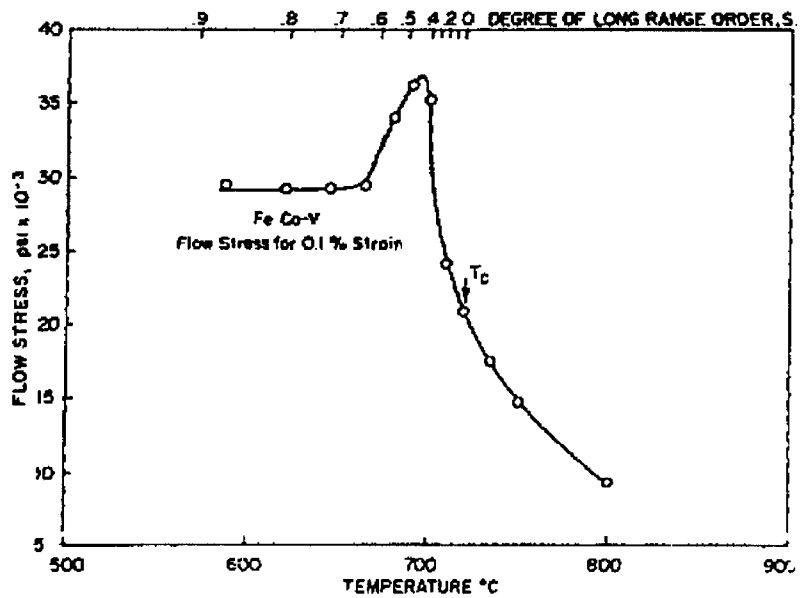

Figure 2.3.2 Variation in flow-stress with long-range order in FeCo-2% V: (a) elevated temperature; (b) room temperature (after Cahn[32]).

Attempts to explain the peak in flow stress have been offered by many investigators but have only concentrated on specific aspects of order hardening due to variations in degree of order in particular alloy systems. Ardley[38], considering the variation in yield strength with degree of order for Cu_3Au, said hardening was due to two processes: 1) as T_c is approached from higher temperatures the degree of SRO increases giving rise to increased strength by the bond cutting mechanism, which was proposed by Fisher[34]; 2) As T_c is approached from lower temperatures and the degree of order changes from 1 - 0.8, a restraining force is exerted on a superlattice dislocation which creates wrong bonds in its wake in a not perfectly LRO lattice. Ardley[38] added that at T_c there a discontinuous change in the degree of order, characteristic of first order transformations, and the peak is expected there. Rudman[39] discussed a similar mechanism using data for Fe_3Al but the Ardley-Rudman model has unexplained problems. The idea of a restraining force on a gliding superlattice dislocation due to imperfect LRO is not clear, as a superlattice dislocation should always restore the lattice on gliding, leaving an equal number of wrong bonds. There is also the added problem that this mechanism can not be applied to homogeneously ordered systems such as Fe_3Al since there is no abrupt change in the dislocation structure at T_c.

Flinn[40] proposed a mechanism whereby a temperature rise leads to a geometrical inhibition of slip. This is due to an increased rate of diffusion at the higher temperatures allowing dislocations to climb and drag domain boundaries with them. As the temperature increases even more, diffusion is so rapid that atomic rearrangements can keep place with dislocation motion. This enables the domain boundaries to migrate more easily through the lattice and there is, therefore, a peak in flow stress at some intermediate temperature and, therefore, degree of order. However, since there is no or very little diffusion in quenched specimens at 25°, this peak should not occur.

Two mechanisms that involve SRO have been suggested by Brown[41] and Marcinkowski & Miller[42]. The first, by Brown, suggests that the stress field of an edge dislocation can induce the alignment of short-range ordered regions. He considered that LRO could restrict the development of stress-oriented SRO so that a maximum in the dislocation locking force is to be anticipated at T_c. The mechanism

does not explain why a peak in alloys such as FeCo-V, Fe_3Al or Mg_3Cd does not occur at T_c, but at some intermediate temperature. The second mechanism[42] involving SRO, suggests that the peak in flow stress in Ni_3Mn is due to the interaction of superlattice dislocations with SRO. Some homogeneous ordered alloys, however, do not have distinct regions of SRO and the suggested mechanism does not apply. Marcinkowski et al[42] also pointed out that the separation of the two partials constituting each unit dislocation in a superlattice dislocation changes with changes in S, the long-range order parameter. This change in S will in turn affect the ease at which cross-slip occurs and through this the flow stress. Cross slip, they suggest, will become easier in a critical range of order and in this range the peak in flow stress will occur.

The theories documented above are not applicable to a wide range of experimental alloys that have been considered. Stoloff and Davies[37] have attempted, using their own work on FeCo and Fe_3Al alloys, to explain the position of the flow stress peaks in a way that that will account for the differences in the alloys that have been considered to date. Their attempt to explain the position of the flow stress peaks also attempts to explain the diversity of alloy structures exhibiting the peak, the similar peaks for elevated and room temperature tests, the higher relative strength of ordered alloys when tested at elevated temperatures and that Cu_3Au exhibits the peak at T_c while other systems always show a peak below T_c. They have retained the concept of SRO hardening and the dislocation spacing theory first proposed by Marcinkowski et al[42].

The spacing between associated unit dislocations in a superlattice dislocation is inversely proportional to S^2. It has been proposed, therefore, that when S is low the energy of the connecting boundary is so small that the superlattice dislocations will disassociate into their constituent unit dislocations, which then glide independently of one another[37]. When there is a very low degree of order, $S = 0.1$, the distinct, unit dislocations create APB trails when they glide. This creates wrong bonds which increases the flow stress, similar to the mechanism which occurs above T_c due to SRO. As S increases the unit dislocations will associate into pairs as superlattice dislocations. A gliding superlattice dislocation in an ordered matrix creates no wrong bonds and the flow stress will begin to decrease as the proportion of superlattice

dislocations increases. Therefore, a large drop in flow stress occurs when a large proportion of dislocations are gliding as superlattice dislocations. The flow stress will continue to drop as the order increases with only superlattice dislocations gliding in fully ordered structures and, therefore, fully ordered materials will be the weakest.

It is expected then, that when the degree of order of a material can be varied continuously from S = 0 to 1 that a peak in flow stress will occur at some intermediate degree of order. Cu_3Au, where order changes discontinuously from S = 0 to 0.8 at T_c, will have the peak stress at T_c as Ardley predicted. This alloy, as with other similar ones, is a special case as T_c represents the position of the transition from unit dislocations to superlattice dislocations.

Stoloff and Davies[37] constructed a schematic diagram (Figure 2.3.3) summarising the predicted variation in room temperature flow stress with changing degree of quenched in order. At quench temperatures above or just below T_c, the flow stress is due to the stress required to move a unit dislocation and this decreases with increasing temperature. At quench temperatures below T_c, the stress required to move a superlattice dislocation is considered to be constant. The increased flow stress is due to the increase in proportion of superlattice dislocations with decreasing quench temperatures. This theory will also apply to Cu_3Au since the proportion of superlattice dislocations disassociated into two unit dislocations is greater for S = 0.8 than if S = 1. Therefore, in conclusion, the change in flow stress with degree of order can be explained in terms of the transition from unit dislocations in the disordered state to superlattice dislocations in the order state.

Stoloff and Davies[37] have gone slightly further and considered Ni_3Mn and Mg_3Cd which order by nucleation and growth upon cooling, but with an equilibrium two phase field region (ordered and disordered) existing at temperatures above the fully ordered region. For this type of material, the experimentally determined changes in flow stress with order is slightly different. The mechanism involves the cutting of ordered domains by unit dislocations which arise from the surrounding SRO matrix. Ni_3Mn has shown the transition from superlattice dislocation to unit dislocations at some intermediate degree of order, but this was not considered conclusive proof that

the proposed mechanism contributes significantly to the behaviour of two phase ordered alloys.

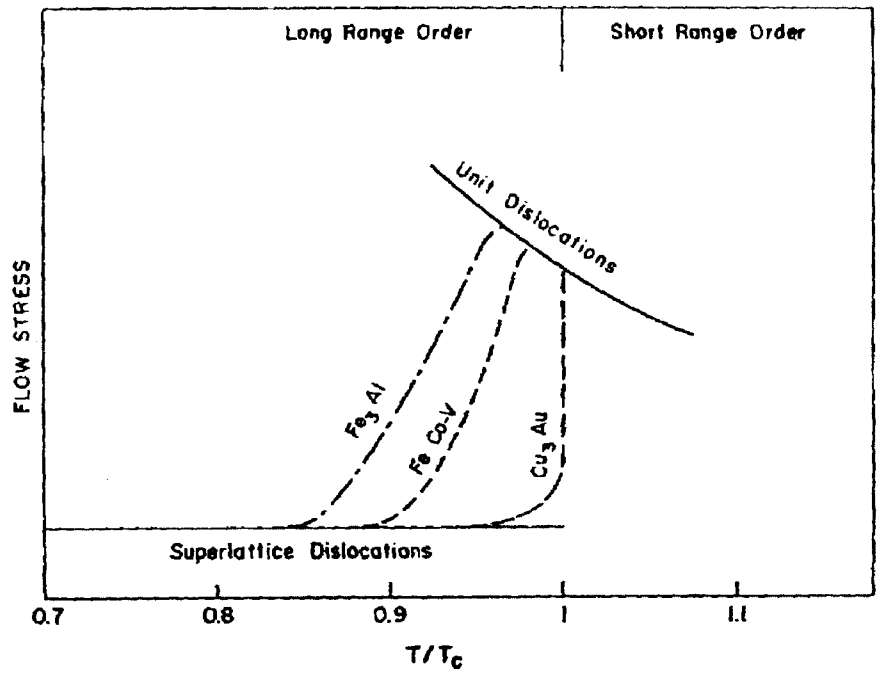

Figure 2.3.3 Flow stress variation (schematic) with quenched-in order for several supelattice alloys (after Stoloff &Davies[37]).

HARDENING DUE TO COHERENT STRESSES

To date, only alloys that keep their lattice symmetry upon ordering have been considered. Alloys such as CuAu I and CoPt, which transform from cubic disordered to an f.c.c. tetragonal ordered structure, show prolonged hardening when quenched from above T_c and annealed below T_c[32]. The change in symmetry will lead to large misfit stresses which vary from point to point in the specimen. Figure 2.3.4 shows results of a 20 hour anneal at 250°C leading to a 90% increase in yield strength in CuAu. The curve is characteristic of age hardening phenomena but does not show a distinct peak with over ageing at longer annealing times. At higher temperatures there is a marked initial increase in strength followed by a softening at longer annealing times[43].

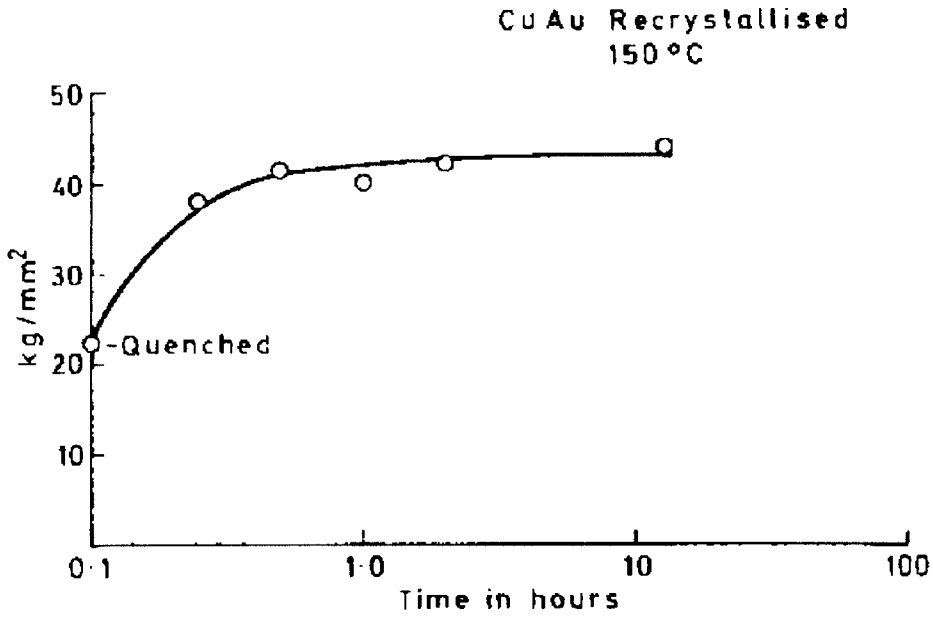

Figure 2.3.4 Order hardening in CuAu annealed at 150°C (after Arunachalam & Miller[43]).

Similar changes with annealing time have been found for CuPt[44] and Cu_4Pd[45]. In all these alloys, CuAu[6] CoPt[46] and the two just mentioned, the fully ordered condition is stronger than the disordered or partially ordered structure. This is different to the alloys already discussed as the peak hardness would occur in fully ordered materials and not at some intermediate degree of order.

ANTI-PHASE DOMAIN SIZE AND DOMAIN HARDENING

The previous section dealt with the changes in dislocation and domain structure during isothermal ordering and the manner in which strengthening arises mainly from the interaction of unit dislocations with a partially ordered structure. The peak in flow stress and hardness was a result of the transition from unit dislocation deformation to deformation by superlattice dislocations[25]. This theory, however, assumed a condition of constant and large antiphase domain size, as it is not always possible to vary the degree of order independently of the anti-phase domain size, particularly in the early stage of ordering[25]. It is during these early stages of ordering that domain size contributes significantly to strength and flow-stress. Hardening which has been attributed to anti-phase domains has been noted in many ordered systems e.g. Cu_3Au, Ni_3Fe and Ni_3Mn. The graph in Figure 2.3.5, typical for most alloys, shows a

hardness vs. isothermal annealing time curve for Mg_3Cd which shows that a peak hardness occurs at a domain size of approximately 60-80 Angstroms diameter. The graph in Figure 2.3.6 showing the changes in degree of order and domain size upon isothermal ordering at 68°C, indicates that complete order is attained at a domain size of 60-80 Angstroms. There is, therefore, a correlation between when complete order is reached, which results in a certain domain size, and when the maximum hardness occurs.

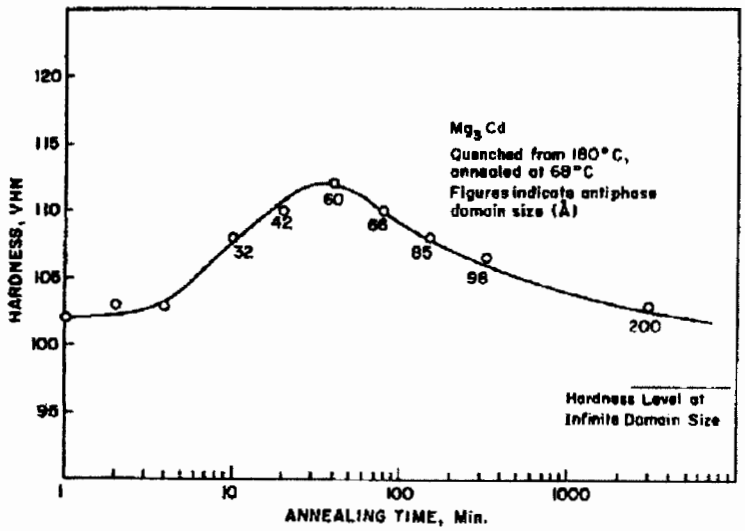

Figure 2.3.5 The change in hardness of Mg_3Cd with annealing times at 68°C (after Stoloff & Davies[25]).

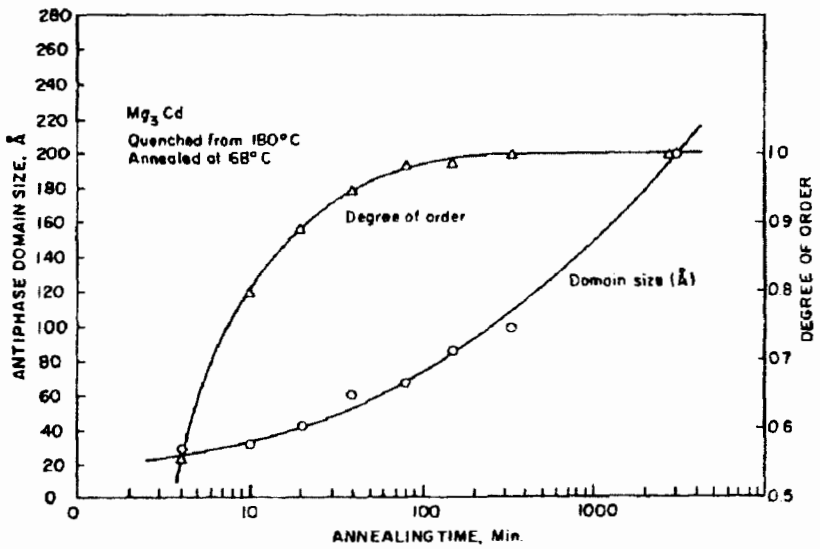

Figure 2.3.6 The change in degree of order and domain size upon isothermal ordering at 68°C (after Stoloff & Davies[25]).

The peak in hardness of many ordered alloys does not occur exactly when equilibrium order is reached but at some domain size just before complete order. Since most alloys order by the process of nucleation and growth of nearly perfectly ordered domains, any degree of order less than the equilibrium amount will indicate the coexistence of ordered and disordered regions[25]. This coexistence of an ordered and disordered structure will result in an increase in hardness during isothermal ordering. As the amount of ordered and disordered areas change so will the deformation mode due to changes in dislocation movement i.e. unit or super dislocations[25].

The growth of the ordered phase, through the nucleation and growth of highly ordered domains, will produce a non-equilibrium structure of two coexisting coherent phases as mentioned in the above paragraph. The disordered phase however is more likely to be of a SRO structure than a totally disordered one. Marcinkowski & Miller[47] and Copley & Kear[48] have proposed two similar mechanisms for the movement of dislocations through this ordered and SRO structure. Marcinkowski & Miller proposed that the movement of dislocations through the ordered regions of the two-phase structure will be easy, but more stress will be needed to move dislocations through the SRO regions. Copely & Kear[48] suggested a much more potent strengthening mechanism whereby a unit dislocation moves through the two-phase structure. In this case the interaction of unit dislocations with APD walls acts as an additional barrier to slip over and above the influence of SRO. For a unit dislocation to move through an ordered domain, it must leave a sheet of APB along the slip plane, whereas a superdislocation would only have created a small amount of APB.

As the amount of order increases at the expense of the SRO regions it becomes more energetically favourable for the dislocations to move in pairs[25]. It has been thought that the mechanism proposed by Macinkowski & Miller[47] might contribute to the strength and flow stress of the material at this stage, but the overall tendency is for the material to soften[25]. The amount of order increases as the domain size increases with the critical domain size for maximum strength and hardness occurring just as domains come into contact with each other. Once the domains come into contact with each other, the larger the grain size, the less extra APB energy has to be created by the superdislocations and the softer the material will be[25]. It is, therefore, believed that

hardening during isothermal ordering is due to the extra energy needed to create APBs by unit dislocations. The peak in hardness, usually at some intermediate degree of order, is due to the transition from unit dislocations to superdislocations as the amount of the ordered domains increase in size and volume.

DEVIATIONS FROM STOICHIOMETRY

The previous section shows that departures from perfect order lead to strengthening or increased flow stress through the disassociation of superlattice dislocations into unit dislocations. It is not only possible to change the degree of order by thermal treatment but also by lowering the degree of order and/or producing a two phase structure by preparing alloys which deviate in composition from the stoichiometric composition. At the stoichiometric composition, a minimum strength as a function of solute content is observed and this corresponds to a minimum superlattice dislocation spacing. Higher strengths are obtained if the composition is slightly off stoichiometric as unit dislocations will result in enhanced properties through creation of anti-phase material[32]. As an example, Cu-Au alloys in the ordered condition are shown in Figure 2.3.7. Minima in strength of slow cooled alloys were observed at compositions corresponding to the formation of the $L1_2$ superlattices.

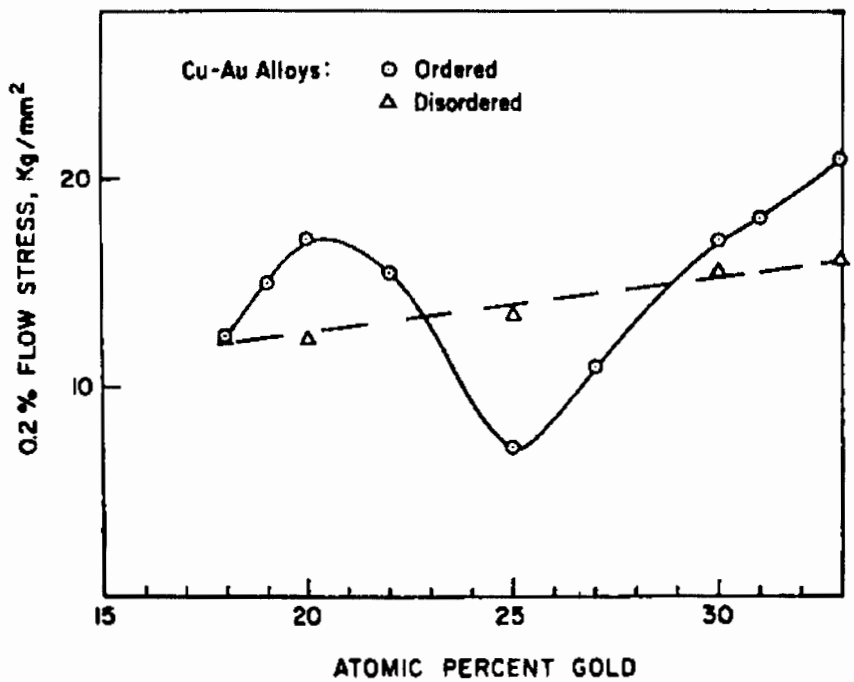

Figure 2.3.7 Effect of composition on flow-stress of Cu-Au alloys (after Kelley & Nicholson[32]).

2.3.3 *HARDENING DUE TO SHORT RANGE ORDER*

Strain-ageing, a process whereby cold rolled, heavily deformed specimens are annealed at specific times and temperatures, is thought to produce hardening in dilute alloys by increasing the flow stress. The exact mechanism by which the flow stress is increased has not been established, and at present there are two rival interpretations. The two most well studied alloy systems that exhibit this hardening effect are Cu-Al and brass[33].

Hasiguti[49], using his own work on brass, and that of other Japanese researchers on the same subject, suggested the first of the two rival interpretations on strain-ageing. Although the process he used was the same as strain-ageing, he termed it "anneal hardening" and attributed it to the "Suzuki effect". This effect involves the segregation of solute atoms to the stacking faults connecting partial dislocations in f.c.c. crystals. He found that the strain-ageing effect is greatest for fine grain materials and largest amounts of prestrain[49]. Although inconclusive, evidence was found by Davies and Cahn[50], using diffuse X-ray scattering experiments, as well as by Otte[51], from very precise lattice parameter measurements on brass. Otte showed evidence that prolonged, low temperature strain-ageing of cold worked brass causes a slight change in lattice parameter. He attributed this to the movement of solute from the lattice and its collection at stacking faults.

Chinowsky, working with Cahn[33], carried out experiments on the strain ageing of Cu-15 at% Al in a study of the second interpretation of strain ageing. They found that the increase in flow stress is a function of prestrain. Ageing after small prestrains produced a very small increase of flow stress or even produced strain-softening. The best results were obtained on long, low temperature annealing of heavily prestained specimens.

It is known that both brass[52,53,54] and Cu-Al[55,56] produce substantial SRO if annealed for the correct times and temperatures. Therefore, a situation arises where strain-ageing of the alloys produces SRO and also produces transient increases in flow stress, but it has not been proven that the two effects are causally related.

Haasen[57], working with Cu-Al single crystals, found from his own work and that done by Koppenaal and Fine[58], that the flow stress did not appear to be determined by SRO at all. He found good evidence to support his theory that it is the yield point that is effected by the destruction of order along a slip plane. He quotes the work of Koppenaal and Fine[58] on neutron-irradiated Cu-Al alloys. They found that irradiation, known to alter the SRO substantially, did not alter the flow stress of the alloy but did affect the yield point. Haasen concluded that the flow stress is determined by other factors such as solute-dislocation interactions arising from atomic misfit and from changes in the shear modules of the solution[57]. Given these results, the second interpretation involving SRO is accepted as the better of the two rival interpretations of strain-ageing but solute segregation to stacking faults has not been discarded[35].

2.4 ELECTRICAL RESISTIVITY OF METALS AND ALLOYS

The recording of resistivity with increasing temperature is a simple and effective method of investigating any changes or transformations that occur in a metal[59].

2.4.1 *SCATTERING MECHANISMS*

When an electric field is applied to a solid, free or conducting electrons are accelerated and move through the crystal lattice. Electrons may move through an ideal crystal without resistance, but in real metals scattering of free electrons will occur in the presence of an electric field, resulting in electrical resistivity. The scattering is a consequence of the departure of the lattice from perfect periodicity and the result of thermal vibration of atoms. At 0K a perfectly periodic lattice will have a zero resistivity as there will be no effect due to an imperfect lattice or thermal vibrations[60].

Assuming the scattering from different types of deviations from periodicity to be additive, the total resistivity ρ may be expressed in the following way:

$$\rho = \rho_0 + \rho(T). \qquad \textbf{Equation 2.4}$$

This expression is know as Matthiesen's rule[61] and is true for pure metals and dilute alloys. Matthiesen's rule sums two components of resistivity; residual resistivity ρ_0 due to the presence of structural imperfections and $\rho(T)$, the thermal component or ideal resistivity due to the thermal vibration of atoms. The structural imperfections can be impurities, grain boundaries, vacancies, dislocations or any defect that changes the periodicity of the lattice, resulting in sites for scattering to occur[62].

The residual resistivity due to the lattice defects may be considered to be independent of temperature, provided that the concentration of defects remains constant with temperature. This is assumption is very rarely true as the concentration of certain

defects do exhibit some temperature dependence. Concentration of vacancies change with temperature by vacancy diffusion and annihilation processes while grain boundaries and dislocations change in concentration through recovery and recrystallisation processes. The temperature dependent or ideal resistivity ρ_0 arises from the thermal vibration of atoms with the magnitude of the temperature dependence arising from the electronic structure of the metal[63].

An additional contribution to structural defects which can have a significant effect on the residual resistivity is the addition of alloying elements or solute elements. These impurity solute elements result in deviations from perfect periodicity in the crystal lattice and will result in electron scattering and hence increase the resistivity of the metal. The concentration of the alloying element may not vary with time, but the atomic configuration may exhibit a temperature dependence due to a decrease or an increase in structural order in the lattice. Any change in atomic configuration from that of the random state will result in a change of ρ_0.

The effect of the addition of an alloying element depends on the concentration of the solute atoms. In a dilute alloy, one in which the solute atoms are in sufficiently small concentrations that they have no effect on the electronic structure or phonon spectrum of the bulk alloy, the impurity atoms will act as independent scattering centres[63]. The scattering of the conducting electrons at these centres has the effect that scattering of N impurity atoms is just N times that of a single impurity. This will only happen if the solute atoms are randomly distributed with no direct or indirect interaction between them. In real terms this implies the alloy concentration can only be of the magnitude of 1 or 2%, or in some systems up to about 5%. If these low concentrations can be maintained then the ideal resistivity of the alloy will be similar to that of a pure metal. At higher concentrations, however, the electronic structure of the alloy will change depending on the solute concentration, the electronic structure of the solute addition and the atomic configuration of the alloy[64].

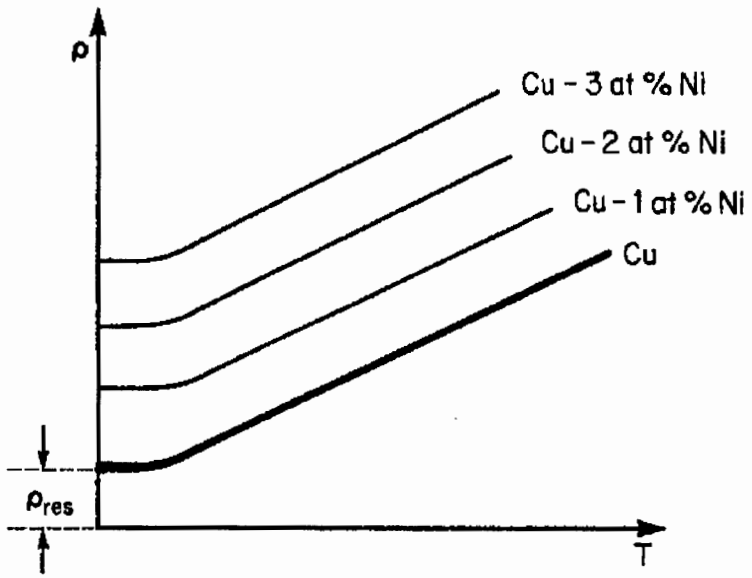

Figure 2.4.1 Schematic representation of the temperature dependence of the resistivity of copper and various copper-nickel alloys. ρ_{res} is the residual resistivity (after Hummel[62]).

Figure 2.4.1 shows how the resistivity of a copper-nickel alloy changes with increasing amount of solute content. Small additions of solute cause a linear shift of the ρ versus T curves to higher resistivity values in accordance with Mathiessen's rule. The slopes of the individual ρ versus T curves however remain essentially constant[62]. This would indicate that the temperature independent part of the resistivity, residual resistivity, is changing as indicated by the linear shift. The temperature dependent part of the resistivity, the ideal resistivity, is not changing which is indicated by no changes in slope on the ρ versus T curves. Various solute elements affect the resistivity of the metal as a whole to different degrees and this is shown in Figure 2.4.2 below. It has been shown that the resistivity of dilute single phase alloys increases with the square of the valence difference between solute and solvent constituents; this is know as Linde's rule (Figure 2.4.2 b.)[62]. It can be seen from these experimental results that the electron concentration of the solute element, i.e. the number of additional electrons the solute contributes, plays a vital role in the resistance increase.

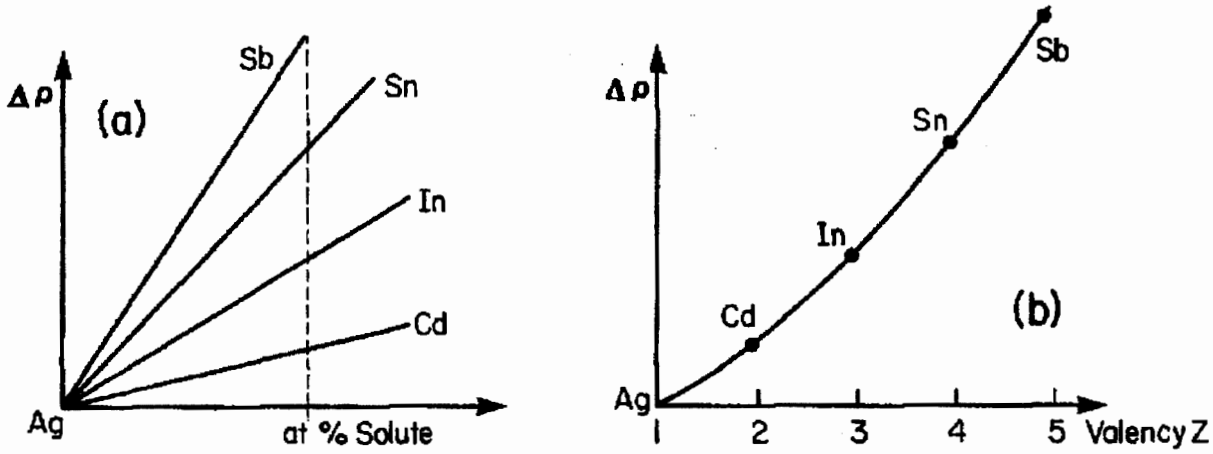

Figure 2.4.2 Resistivity change of various dilute silver alloys (schematic). Solvent and solute are all from the fifth period. a) Resistivity change versus atomic % solute and b) resistivity change due to 1 at% of solute (after Hummel[62]).

The simple-metal models discussed allow a qualitative understanding of the processes which determine electrical resistivity in simple metals. These models require that simplifying assumptions, such as s-s electron scattering, free or nearly free electrons and the Born approximation, have to been made and they are therefore inappropriate for complex metals and alloys such as the transition metals.

2.4.2 *RESISTIVITY OF TRANSITION METALS AND ALLOYS*

The theory discussed above applies predominantly to simple metals characterised by a single conduction band derived from atomic states of s- and p- character. The Fermi surface is then spherical and the conduction electrons are essentially free with the wavefunctions of these electrons being plane waves. In the electronic structure of a simple metal such as copper, there is no interaction between the core states and the valence or conduction electrons[63]. Transition metals on the other hand are not simple metals as there is an overlapping of the partially filled, core d- bands and the conduction electrons in the s- band. There is therefore a significant density of states at the Fermi surface that do not have an s-like character (See Figure 2.4.3). Therefore, the spherical Fermi surface model, free electron behaviour and weak scattering approximations used successfully for simple metals can not be used for transition

metals and alloys. The Fermi surface may be quite irregular and have some parts that are s-like and others that are d-like[64]. The complications introduced by these factors lead to considerable increases in the complexity of the calculations of resistivity for transition metals and sophisticated methods of analysis are involved, all of which are beyond the scope of this project.

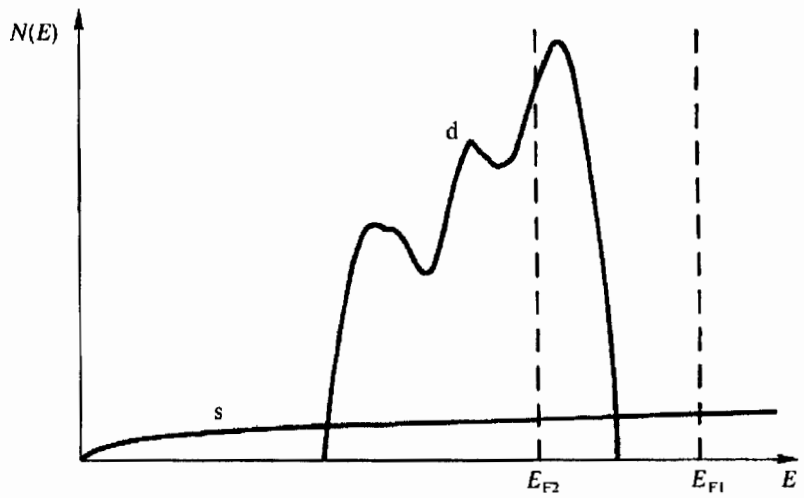

Figure 2.4.3 Density of states of a hypothetical solid containing both s and d electrons. The Fermi level occurs at E_{F1} in a simple metal and E_{F2} in a non-simple metal (after Rossiter[64]).

The single band approximation of resistivity used in Mathiessen's rule cannot always be made and sometimes it is possible to use a multiband approximation. In doing so, there is an assumption that there are a set of bands of electrons which carry current in parallel. The total resistivity would then be

$$\rho = 1/\Sigma\sigma_b = 1/\Sigma(1/\rho_b), \qquad \textbf{Equation 2.5}$$

where σ_b is the conductivity of an individual band, and then in general the resistivity of each band is a sum over different types of scattering:

$$\rho_b = \Sigma_s \rho^s_{b.} \qquad \textbf{Equation 2.6}$$

This multiband approximation has been used mostly to explain the resistivity of spin-up and spin-down electrons in magnetic materials and in transition metals composed of overlapping sp- and d- bands[59].

The participation of the d- band in conduction, not only increases the number of current carriers, but also results in a new s-d scattering. The scattering is due to the interband movement of conduction electrons. Mott[65] found that the density of states in the d- band is much higher than in the s- band. There is, therefore, a higher density of final states for s- electrons scattering into electron d- states and this type of scattering should predominate over conventional s- electrons scattering into another s-state. The s- electron is scattered by either absorbing or emitting a phonon into the low Fermi velocity d- band where it is assumed to have been taken out of the conduction process. The d- band can be considered to act as a scattering trap. Since electrons scattered into the d- band make little further contribution to conduction, this interband scattering offers an explanation for the high resistivities of transition metals. In order to conserve the number of electrons in each band, electrons are also scattered randomly from the d- band to the s- band[59].

2.4.3 RESISTIVITY OF ORDERED ALLOYS

The residual resistivity of an alloy was first analysed by Nordheim[66] in 1931 but strictly speaking, only works for a few selected binary systems. Nordeim's rule does not take the change in density of states with composition into account and this is particularly true for alloys containing a transition metal[62]. He postulated that, considering only random binary solid solutions of elements of similar atomic number, an alloy can be treated as an ordered periodic structure with a potential equal to the mean potential of the constituent atoms. The mean potential is repeated at every lattice site and gives the underlying potential of the alloy. As a result of the mean potential at each lattice site, a conducting electron will be scattered due to the difference in potential between the mean potential and the actual potential of the atom at that site. The total probability of scattering is obtained by summing the

probabilities of scattering from each atom calculated using Fermi's golden rule and the change in potential associated with each constituent atom species[63].
Assuming that the wavefunction over the Fermi surface does not change with composition and that the density of states is unchanged with composition and also remembering that the number of conducting electrons also does not change, the residual resistivity ρ_0 is given by:

$$\rho_0 \propto x(1-x) \qquad \textbf{Equation 2.7}$$

where x is the fractional atomic composition. However, due to the simplifying assumptions made, the expression for residual resistivity cannot be expected to be widely applicable but the dependence has been found to represent the experimental findings in a few alloy series reasonably well[63].

Nordheim's theory does not take one other aspect into account, the effect on the residual resistivity of deviations from a random atomic configuration, such as the presence of long or short-range order or clustering of like atoms. It has been discussed (Section 2.4.1) that disorder in a lattice produces scattering which results in electrical resistivity. Thus when the constituents of an alloy take up an ordered arrangement there should be an effect on the residual resistivity. The effect that ordering has on the residual resistivity of an alloy system can be quite pronounced as shown by the Cu-Au system shown in Figure 2.4.4. The alloy shows local minima in resistivity at compositions corresponding to the ordered structures Cu_3Au and CuAu.

It is important to note that the components of the alloy should form a true solid solution. If not, the alloy could consist of small crystals with different compositions or even a mixture of crystals of two pure components. In these cases the resistivity would be some average of the two separate components and would be different to that of the disordered solid solution.

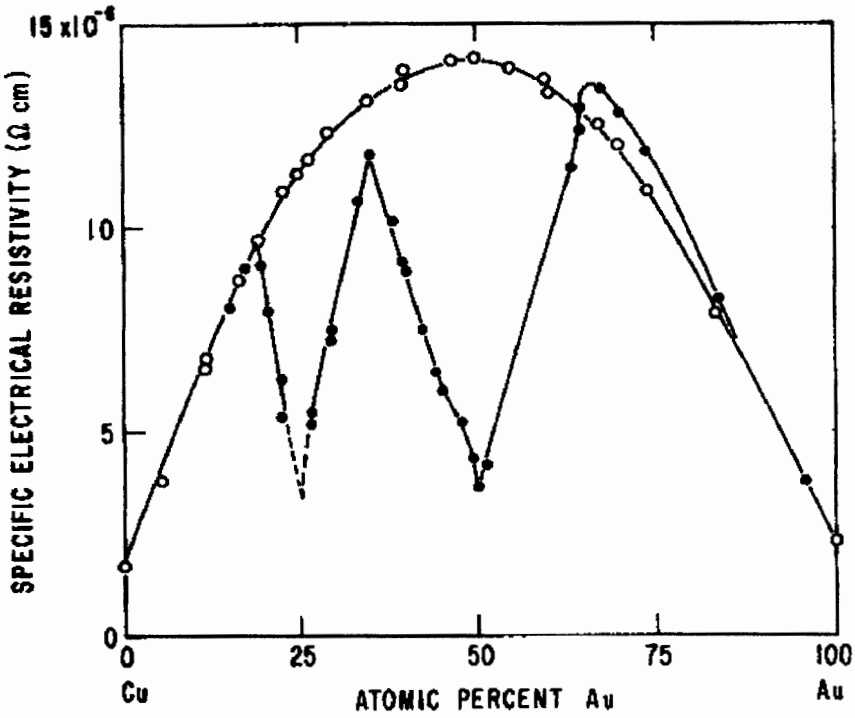

Figure 2.4.4 Electrical resistivity of Cu-Au alloys. •, annealed at 200°C (ordered) and o, quenched from 650°C (disordered) (after Fisk and Webb[59]).

2.5 X-RAY DIFFRACTION OF ORDERED ALLOYS

The process of ordering affects many different properties of materials such as specific heat, electrical resistivity and chemical behaviour. Since all these changes involve atomic rearrangement, x-ray diffraction techniques can show what is occurring during ordering. The section that follows will discuss XRD and how it relates to the study of ordered alloys. It will not, however, discuss general theory on diffraction or XRD techniques.

When an alloy changes from a disordered to an ordered structure it is possible that either the unit cell changes symmetry, or that symmetry is maintained through the ordering process, as was discussed in Section 2.2.3. The Au-Cu system is a well understood and a well researched system and exhibits an ordered composition that changes symmetry (AuCu) and one that maintains symmetry ($AuCu_3$)[67]. To explain what differences exist between diffraction patterns of ordered and random systems, $AuCu_3$ will be used as an illustration.

Since there is only a slight change in the size of the unit cell on ordering of $AuCu_3$, and no change in its shape, there will be practically no change in the positions of the diffraction peaks[67]. The change in the positions of the atoms, however, must cause a change in the intensity of the peaks due to the difference in scattering power of the two atoms. The disordered alloy, therefore, produces a diffraction pattern similar to that of any f.c.c. metal such as pure copper or gold. On ordering, an extra set of diffraction peaks, other than the fundamental peaks, occurs as a result of the formation of the superlattice and are termed superlattice peaks. The physical reason for the formation of the superlattice lines can be deduced from an examination of Figure 2.5.1. In the disordered structure, an incident beam of wavelength λ and angle of incidence θ with the (100) planes will be one whole wavelength out of phase with the waves scattered from adjacent (100) planes. However, there is also a plane halfway between these two adjacent (100) planes, containing, on average, exactly the same distribution of gold and copper atoms. This plane will scatter a wave which is therefore $\lambda/2$ out of phase with the wave scattered by the adjacent (100) plane and of

exactly the same amplitude. There is, therefore, complete cancellation and there is no (100) reflection[67].

The ordered alloy on the other hand, has copper and gold atoms on adjacent (100) plans, but the planes midway contain only copper atoms. The rays scattered by the (100) planes and the midplanes are still exactly out of phase due to no change in shape of the unit cell, but they differ in amplitude due to the difference in scattering power of the gold and copper atoms. The ordered structure will, therefore, produce (100) reflections but they will be weak as the peak produced is the difference of the atomic scattering factors of each atom[67].

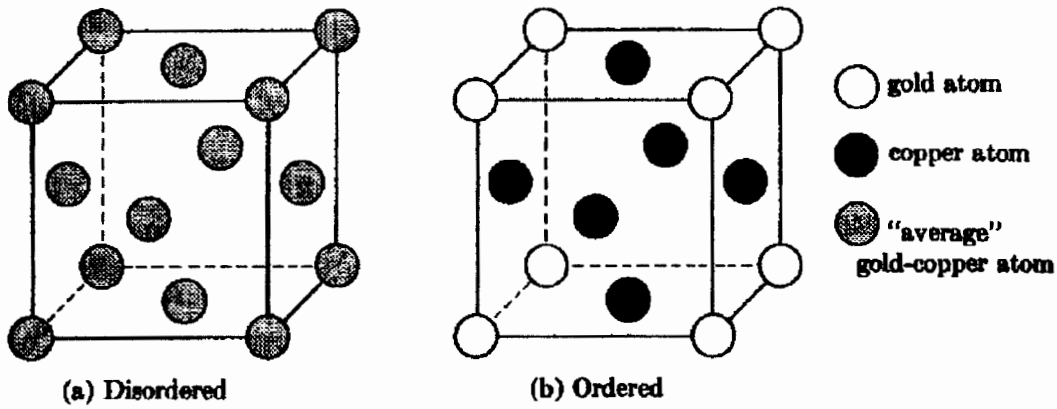

Figure 2.5.1 Unit cell of the disordered and ordered forms of $AuCu_3$ (after Cullity[67]).

Not only are superlattice peaks very weak due to the difference in atomic scattering factors, but the superlattice peaks are made even weaker as the lattice departs from perfect long-range order. The effect of the lattice departing from order is a strong one because the intensity of a superlattice peak is proportional to S^2. As it is only the superlattice peaks, and not the fundamental peaks that are affected by the amount of order, they can become very difficult to see[67].

2.5.1 *X-RAY DIFFRACTION AND SHORT-RANGE ORDER*

Above the critical ordering temperature, T_c, long-range order disappears and the atomic distribution is random, indicated by the loss of the superlattice peaks. It is expected, using the approximate law of the conservation of diffracted energy, that the energy lost from the superlattice peaks should appear in some form in the pattern of a completely disordered alloy, and it does. It takes the form of a weak diffuse background extending over the entire 2θ range and is due to randomness[67]. This is an illustration of the general law that says any departure from perfect periodicity of atom arrangement results in some diffuse scattering at non-Bragg angles. It has also been shown that the intensity of the diffuse scattering, produced if two kinds of atoms A and B are distributed completely at random in a solid solution, is given by

$$I_D = k(f_A - f_B)^2, \qquad \textbf{Equation 2.8}^{67}$$

where k is a constant for any one composition and f_A and f_B are atomic scattering factors. This equation shows that I_D is a maximum at $2\theta = 0$ and decreases as 2θ increases, because both f_A and f_B decrease as $(\sin\theta)/\lambda$ increases and so does their difference. This diffuse scattering is very difficult to measure as it is very weak and is superimposed on other forms of diffuse scattering such as Compton modified scattering and temperature-diffuse scattering[67].

Even though order disappears above T_c, and along with it the superlattice peaks, careful analysis of the diffuse scattering which forms the background on the diffraction pattern will show that perfect randomness is not present. The general nature of SRO can be seen in Figure 2.5.2 where the SRO curve was calculated on the basis of one additional unlike neighbour over the random configuration. In the figure, the intensity of the diffuse scattering is not plotted against 2θ, but against a function of $\sin\theta$ and the position of the fundamental peaks is indicated on the abscissa. If atomic distribution above T_c is perfectly random the diffuse scattering intensity would gradually decrease as 2θ or $\sin\theta$ increases from 0. In the alloy systems where SRO does exist, the scattering at low angles becomes less intense and low broad maxima occur in the scattering curve. These maxima usually occur at the same angle as the

superlattice peaks formed during LRO. These SRO diffuse effects are however very weak and are often hidden by the other diffuse scattering effects and as a result the details shown in Figure 2.5.2 are not seen in normal diffraction patterns made with filtered radiation. To investigate SRO through XRD techniques, strictly monochromatic radiation must be used, and allowances must be made for other forms of scattering[67].

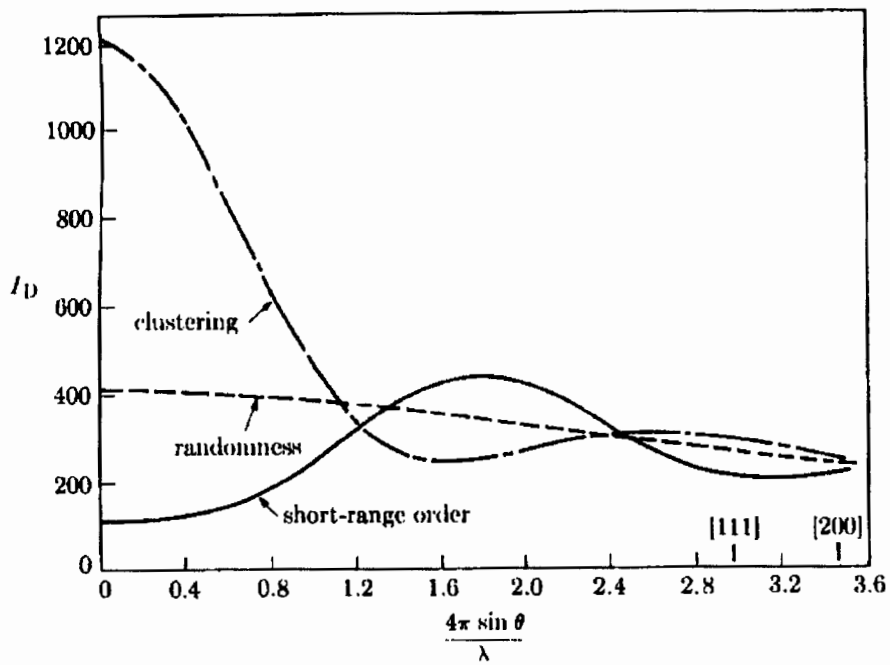

Figure 2.5.2 Calculated intensity I_D of diffuse scattering in powder patterns of solid solutions (here, the f.c.c. alloy Ni_4Au) which exhibit complete randomness, SRO and clustering (after Cullity[67]).

2.5.2 X-RAY DIFFRACTION IN THE Pt-Cu ALLOY SYSTEM

The PtCu superlattice consists of alternating layers of copper and platinum atoms and changes from a cubic unit cell in the disordered state to rhombohedral in the ordered state with an interaxial angle of ≈91°; the side of the unit cell doubles on ordering. As a consequence of the change in symmetry and Bravais lattice upon ordering, certain fundamental XRD peaks, such as the (111) peak, split into two components having an ideal intensity ratio of 3:1. The disordered and ordered XRD pattern can be seen in Figure 2.5.3 which came from a stoichiometric alloy containing equal amounts of copper and platinum[6].

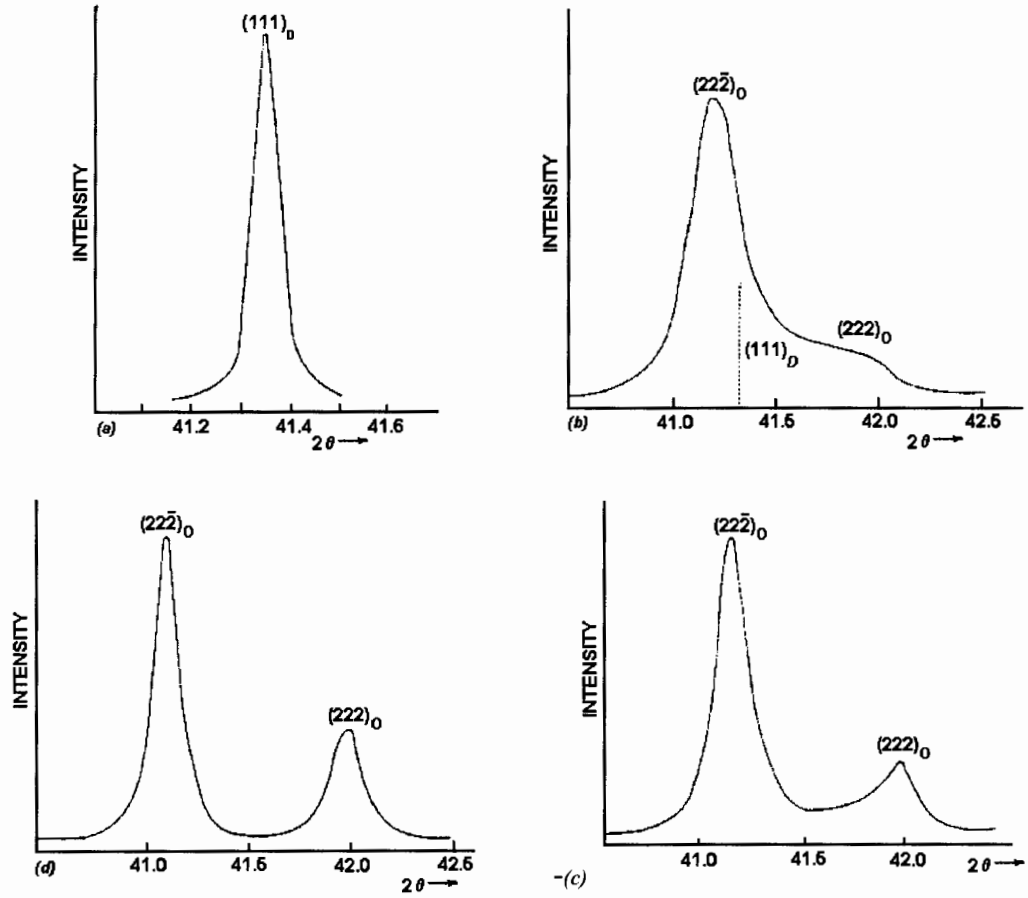

Figure 2.5.3 X-ray diffraction line profiles of stoichiometric PtCu, taken with monochromatic CuKα_1 radiation. a) Disordered: quenched from 860°C. b) Ordered 15 min at 665°C. c) Ordered 30 min at 665°C. d) Ordered 4000 min at 665°C (after Irani & Cahn[6]).

The (111) reflection was used to study the changes in ordering as it has the greatest intensity and due to splitting up into the (222)/(222) doublet. This splitting up into the doublet results from the change in Miller indices because the size of the unit cell doubles. The ideal intensity ratio of 3:1 results from the rhombohedral geometry where one of the four body diagonals is structurally different from the other three. The (222) planes are normal to the trigonal axis, have a smaller d-spacing and come at a higher Bragg angle. The (222), (222) and (222) peaks have the same d-spacing as each other but are larger than $d_{(222)}$ and have a lower angle θ, and combine to form the greater intensity peak[6].

The XRD peaks in Figure 2.5.4 show that the angular separation between the (222) and the $(\bar{2}\bar{2}\bar{2})$ components of the ordered phase is smaller than in Figure 2.5.3. This is because of the higher ordering temperature which means the degree of order is less, corresponding to less rhombohedral distortion of the initially cubic unit cell. Another implication of the two figures referred to in this paragraph is that in PtCu, both the ordered phase and the disordered phase can coexist during the ordered reaction. The diffraction peaks of the ordered phase are initially close to the lines of the disordered phase implying that the ordered phase initially has a degree of order much less than the equilibrium degree eventually achieved at that temperature[6]. The results therefore indicate that for all annealing temperatures ordering in stoichiometric PtCu takes place by a Type 1 reaction (see Section 2.2.4)

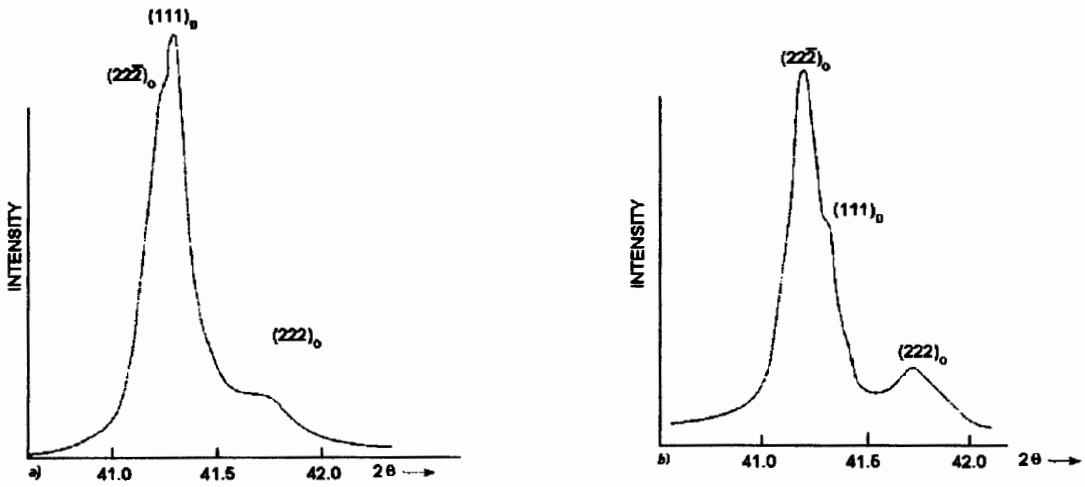

Figure 2.5.4 X-ray diffractometer line profiles of stoichiometeric PtCu, taken with monochromatic CuKα_1 a) Quenched from 860°C and ordered 90 sec at 765°C and b) Ordered 3 min at 765°C (after Irani &Cahn[6]).

The transient ordering mechanism of off-stoichiometric alloys, under equilibrium conditions, was also studied by Irani and Cahn[6]. The results of annealing quenched $Cu_{0.42}Pt_{0.52}$ at 740°C and 770°C can be seen in Figure 2.5.5. A very distinct discontinuity was observed on the $(\bar{2}\bar{2}\bar{2})$ peak at an angle of $2\theta = 41.05$ for an annealing temperature of 740°C. As the annealing temperature increased so did the Bragg angle of the discontinuity, until the discontinuity formed on the $(\bar{2}\bar{2}\bar{2})$ branch of the doublet. The discontinuity, as with stoichiometric alloys, was attributed to the

disordered (111) peak. These results lead Irani and Cahn[6] to draw the conclusion that ordering is always of Type 1, and that a genuine two-phase field comprising ordered and disordered phases exists for non-stoichiometric alloys as shown by the phase diagram in Section 2.1.5.

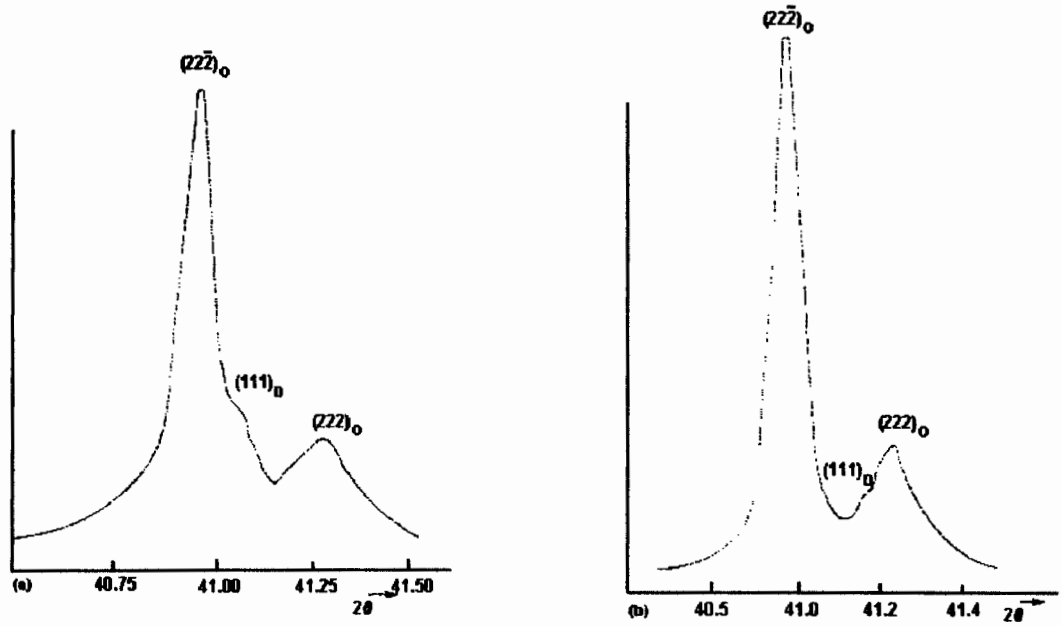

Figure 2.5.5 X-ray diffraction line profiles of $Cu_{0.42}Pt_{0.52}$ taken with monochromatic CuKα_1. a) Quenched from 860°C, annealed to equilibrium at 760°C. b) Quenched from 860°C, annealed to equilibrium at 770°C (after Irani and Cahn[6]).

2.6 DIFFERENTIAL THERMAL ANALYSIS

Differential thermal analysis (DTA) is a thermal analysis technique in which the temperature of a sample is measured and compared with an inert reference as the sample is heated or cooled at a uniform rate. Temperature changes in the sample are due to endothermic or exothermic enthalpic transitions or reactions. Such transitions or reactions can be caused by phase changes, fusion, crystalline structure inversions, sublimation and vaporisation, chemical reactions[68]. The temperature changes during chemical or physical reactions are measured by a differential method. If the sample and reference temperatures are T_s and T_R respectively, then the difference in temperature, $T_s - T_R$ (ΔT), is recorded as a function of the sample, inert material, furnace temperature or even time[68].

2.6.1 *FACTORS AFFECTING DTA MEASUREMENT*

DTA, which is a dynamic temperature technique, has a large number of factors which can affect the resulting experimental curves. If the DTA curve is to be used for qualitative purposes, the shape, position and number of curve peaks is important. By a simple change in heating rate or furnace atmosphere, the positions and possibly the number of peaks can change significantly. For quantitative studies, the area enclosed by the curve peak is of great interest, so the effect of the experimental parameters on the area must be known.

The DTA curve is dependent on two general categories of variables: instrumental factors and sample characteristics. The instrumental factors include variables such as furnace atmosphere, furnace size, sample-holder material and geometry. The sample characteristic variables are factors such as particle size, packing density, amount of sample, thermal conductivity and heat capacity. Of these factors certain, relevant ones have been expanded upon[68]:

HEATING RATE

Heating rates are an important consideration in materials investigations. Slower heating rates will more accurately depict the onset temperature of a transformation and will also diminish the accelerating effects of self-feeding reactions. Additionally, two transformations which are very close in temperature range may be distinctly seen as separate peaks, whereas they may be mistaken for a single transformation under a rapid heating rate. On the other hand, as Figure 2.6.1 shows, slower heating rates make the peaks shorter and broader (in time). Therefore, a transformation with a small thermal effect may result in a peak height no more intense than the thickness of a line under slow heating rates and not be seen[69].

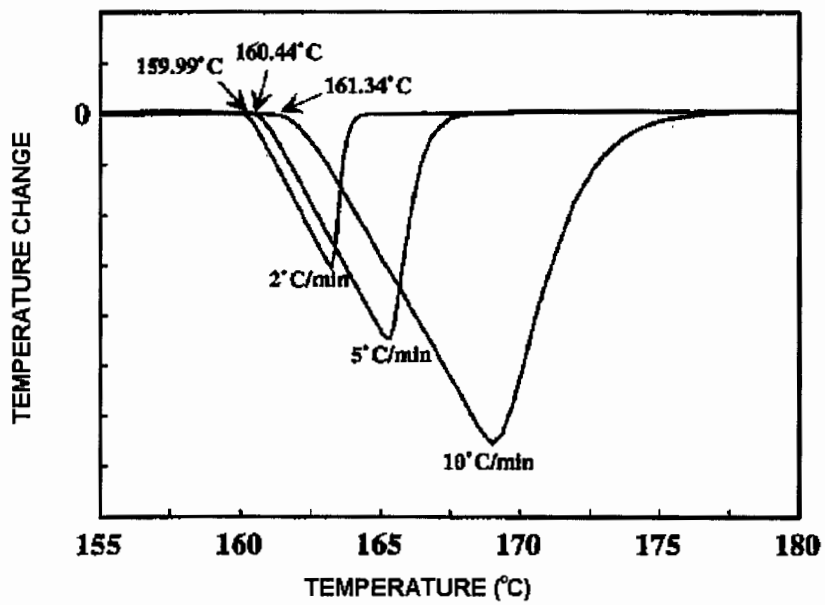

Figure 2.6.1 Effect of heating rate on shape of melting (indium) endotherm (after Speyer[69]).

PARTICLE PACKING, MASS AND DISTRIBUTION

For post-type DTA s, where the thermocouple measures the temperature of the sample crucible, good mechanical contact between the sample and the bottom of the crucible will improve instrument sensitivity to transformations and reactions. Surface contact can be improved by using specimens shaped to match the bottom of the

crucible or using granulated samples, as opposed to odd-shaped chunks. Optimising the mechanical contact will minimise the lag time between when a reaction occurs and when heat propagates to or from the point of temperature measurement, and when the reaction is recorded[69].

For irreversible transformations (Section 2.6.3), the particle size in the sample crucible will affect the rate of reaction. For spherical particles, the surface to volume ratio decreases by 3/r (where r is the radius) with increasing particle size. In the larger particles a time delay in the onset of transformation would result because heat flow from surroundings to the interior would be suppressed. In even larger particles, the heat released from transformations would be insulated from escape and this would further delay detection of the transformation[69].

There is also a risk in having samples with excessive dimensions as a temperature gradient within the sample would result. The temperature gradient could result in different sections of the specimen melting at differing times and acting as heat sinks for heat propagating from the hot zone, motivating an endothermic deviation detected by the differential thermocouple. The onset of the melting endotherm would then be indicated at the sample thermocouple junction at a temperature below the melting point of the sample, resulting in a falsely low melting point[69].

2.6.2 REVERSIBLE TRANSFORMATIONS

MELTING

Reversible transformations such as melting/solidification or the α to β quartz inversion in silica, obey LeChatelier's principle, which dictates, for example, that ice water will stay at 0°C until it fully transforms to ice or fully transforms to water. All the heat added to the system will contribute to the phase change rather than changing the temperature of the specimen. The curve for melting and solidification transformations have a distinct shape in DTA traces (Figure 2.6.2).

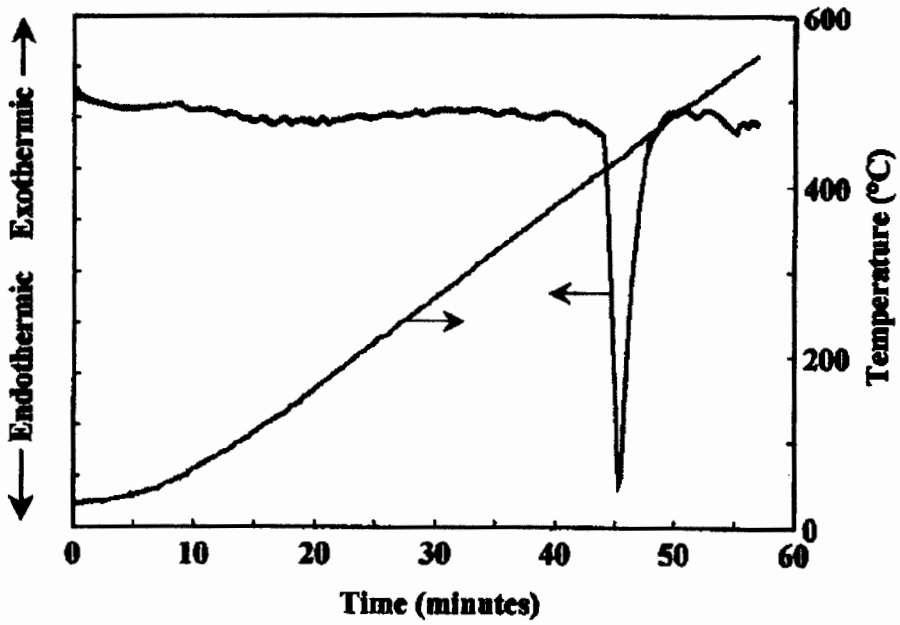

Figure 2.6.2 DTA trace showing the linear rise and exponential decay characteristics of a melting endotherm (Speyer[69]).

A linear deviation from the baseline is seen when ΔT is plotted versus the reference temperature. A DTA will scan at a constant heating rate and the reference material will also increase in temperature at this rate, but the sample temperature remains at the melting temperature until the transformation is complete. The peak of the endotherm represents the temperature at which melting terminates. When the transformation is complete, the sample is at a lower temperature than its surroundings and thus must heat up rapidly to return to the temperature of the surroundings[69].

2.6.3 *IRREVERSIBLE TRANSFORMATIONS*

FIRST AND HIGHER ORDER TRANSITIONS

A phase transition is said to be first order if the Gibbs free energy function is discontinuous at the transformation temperature, and of a higher order if not. Most solid-state polymorphic transformations are first order transitions and are characterised by an activated barrier associated with the breaking of bonds and the diffusion of atoms, and thus occur sluggishly at lower temperatures. The significance

of the kinetic barrier to these transformations is that it permits the metastable presence of the high temperature phases at pressures and temperatures where they are not thermodynamically stable. The latent heats of the first order transitions increase with increasing severity of structural change via the transformation and therefore the peak intensities of the DTA/DSC also increase[69]. Higher order transitions show little or no structural changes and there is no latent heat associated with the transformations.

2.6.4 EXAMPLE OF THE USE OF DIFFERENTIAL THERMAL ANALYSIS IN ORDERED ALLOYS

Mitsui and Mishima[70] have conducted many investigations into the ordering kinetics of platinum and palladium alloys using DTA as one of their main experimental techniques. Figure 2.6.3 is an example of such a tests showing the resultant DTA data. The graph shows that during ordering in Pt-Cu alloys there are two exothermic peaks which correspond to two stages of ordering. Stage I is associated with heterogenous nucleation and growth-type ordering and stage II with homogenous ordering. They found that the relative dominance of stage I and stage II ordering depends on the alloy composition. The third peak is an endothermic peak which occurs due to disordering.

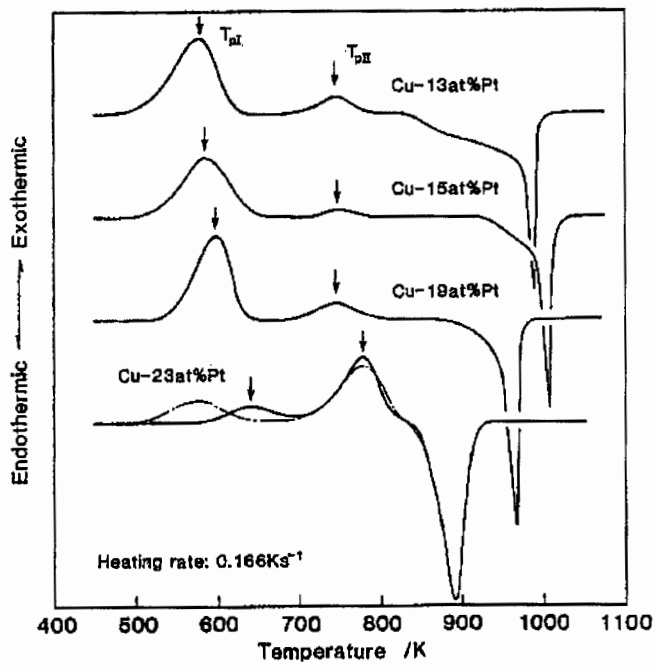

Figure 2.6.3 Sample DTA heating curves of Pt-Cu alloys (after Mitsui et al[70]).

SUMMARY

In summary, two of the alloys, Pt-Ru and Pt-Mo, exhibit single-phase solid solutions at low solute contents with the third, Pt-Cu, exhibiting both an ordered PtCu and $CuPt_7$ phase at similar low solute content compositions. In binary alloys such as these, the atomic species can arrange themselves in a number of different ways but can be broadly classified into ordered or random configurations. Almost all alloys, however, show a type of order, however small, which involves a change from a statistically random arrangement of atoms in the crystal lattice, to that of a regular, ordered structure. In an ordered structure any atomic site is occupied predominately by one or other kind of atom with certain atomic species segregating to designated atomic sites. When this ordered superlattice, as the resulting ordered structure is termed, persists the alloys is said to exhibit long-range order. Even at high temperatures and under certain conditions when this long-range ordered structure breaks down, the atoms can still exhibit an ordered configuration as there is a statistical preference for like or unlike nearest neighbours. This affinity for atoms to prefer unlike nearest neighbours and the resulting atomic structure is termed short-range order. The deformation characteristics of ordered alloys are influenced by the movement of dislocations through the ordered regions of the alloy. In long-range order, dislocations move via a superdislocation process which is similar to a pair of partial dislocations in f.c.c. metals. The first unit dislocation of the superdislocation that travels through an ordered region will disorder the material, the second unit dislocation moving on the same slip plane will, however, reorder the material. The degree of order, coherent stresses, the size of the ordered regions and deviations from stoichiometry all have an influence on the movement of superdislocations and hence the material's deformation characteristics. Short-range ordered regions do not, however, deform through the movement of superlattice dislocation but through normal unit dislocation movement. It is thought, however, that more energy is required to move a unit dislocation through a short-range ordered region than a disordered region because of the reduction in equilibrium short-range order as the dislocation disorders the ordered region, consuming energy as it does so.

3 EXPERIMENTAL PROCEDURE

The aim of the experimental programme was to characterise fully the hardening behaviour of the three experimental alloys. This was carried out through a systematic series of heat treatments, using the annealing temperatures and times established through research and preliminary testing. To aid in the understanding of the hardening mechanisms additional techniques were employed such as differential thermal analysis (DTA), electrical resistivity, x-ray diffraction (XRD) and microscopy. The procedure of preparing the specimens for experimentation required careful control due to the low availability and high cost of the experimental material. The sequence of testing was carefully planned so that previous testing would not affect the subsequent results negatively. The initial aim was to prepare one specimen of each particular heat treatment that could be used for XRD, optical microscopy, scanning electron microscopy (SEM) and finally transmission electron microscopy (TEM). An additional specimen for resistivity testing and small off-cuts for DTA and microhardness testing were also prepared

The preparation of the cast buttons to their final experimental condition is described in detail in Section 3.2. A range of specimens was produced for microhardness measurements, by a systematic series of annealing heat treatments described in Section 3.3. These specimens were specially mounted owing to their thinness after rolling. Microhardness testing was followed by metallographic techniques which could be used to analyse the microstructure of the material. The metallography is covered in Section 3.2.2. Using properly prepared specimens it was possible to assess the effect of heat treatment on mechanical properties and microstructure/property relationships.

3.1 MATERIAL SELECTION

The three experimental alloys under investigation are:

Platinum 5 wt% copper,

Platinum 5 wt% ruthenium and

Platinum 2.5 wt% molybdenum (platinum 5 at% molybdenum).

The first two alloys are commonly used platinum jewellery alloys with the copper alloy being the most well used alloy in South Africa. The specific weight percentage of alloying element should not be increased above 5 wt% because jewellery must contain at least 95% platinum to be considered platinum or given the 950 Fineness hallmark. The molybdenum alloy is a novel alloy and was chosen on the basis of work conducted by Lang[2] on palladium-molybdenum.

3.2 SPECIMEN PREPARATION

Alloys were made by arc-melting the constituent elements (generally 99.99%) under argon on a water-cooled copper hearth. Minimal loses were observed and contamination is unlikely as the alloys are melted under an argon atmosphere which is purged several times. Samples were received in the form of arc melted buttons of approximately 5 mm thickness and 8 mm diameter, weighing approximately 5 g. The cast buttons were cold-rolled to a 50% reduction in thickness to deform the cast structure. They were then homogenised in vacuum at 1000° for 6 hours and subsequently quenched in water.

Optical microscopy performed on the buttons, after the heat treatment, showed incomplete homogenisation with a coarse dendritic cast structure as shown in Figure 3.2.1. The 6 hour, 1000°C heat treatment was carried out again and the microstructure reassessed. Optical micrographs and Energy Dispersive Spectroscopy (EDS) then showed the specimen to be sufficiently homogenised for experimentation to continue. The homogenised buttons were cold-rolled into sheet form in a Dinkel laboratory rolling mill, prior to final specimen preparation. No inter-anneal was used and the specimens could be reduced in steps of up to 0.5 μm from their initial cast thickness of 5 mm to their final thickness of approximately 100 μm. No blistering or cracking occurred other than a slight serration of the edge which was deemed to be acceptable. The rough edges, up to about 500 μm width , were removed before specimens were made from the sheet.

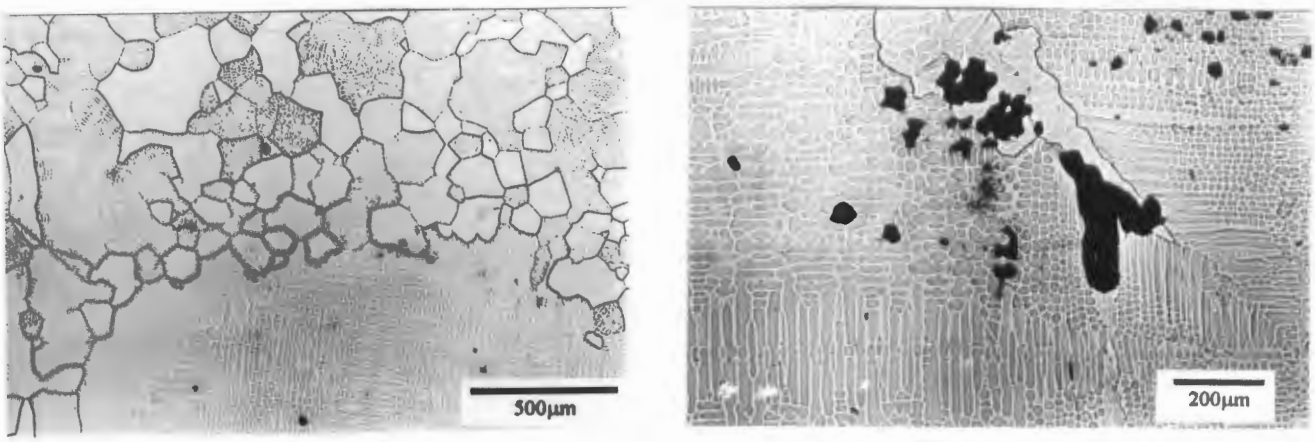

a) b)

Figure 3.2.1 Optical micrographs of Pt 5 at% Mo; (a) showing dendritic cast structure and (b) extensive porosity.

3.2.1 MICROHARDNESS SPECIMENS

Conventional hot or cold mounting techniques proved inadequate for mounting the very thinly rolled specimens. The specimens tended to peel out from the surface of the mount or the centre of the specimen would pull away from the plastic resin and result in erroneous microhardness tests. The specimens were, therefore, mounted at an oblique angle in Struers Epofix Kit resin in order to prevent them from breaking free.

The procedure involved embedding the specimens at an angle in the resin and grinding away excess resin until a tapered section of the specimen was exposed. The first step, as seen in Figure 3.2.2, involved placing the specimen on an angled base inside a conventional mould which is then partially filled with resin. Once the resin had hardened the mounted specimen was inverted in the mould and the mould filled with resin. The specimen was thus encased at an angle in the resin which was exposed by subsequent grinding. The base and surface of the resin mount were then parallel and a small section of the specimen could be worked on without the specimen breaking free.

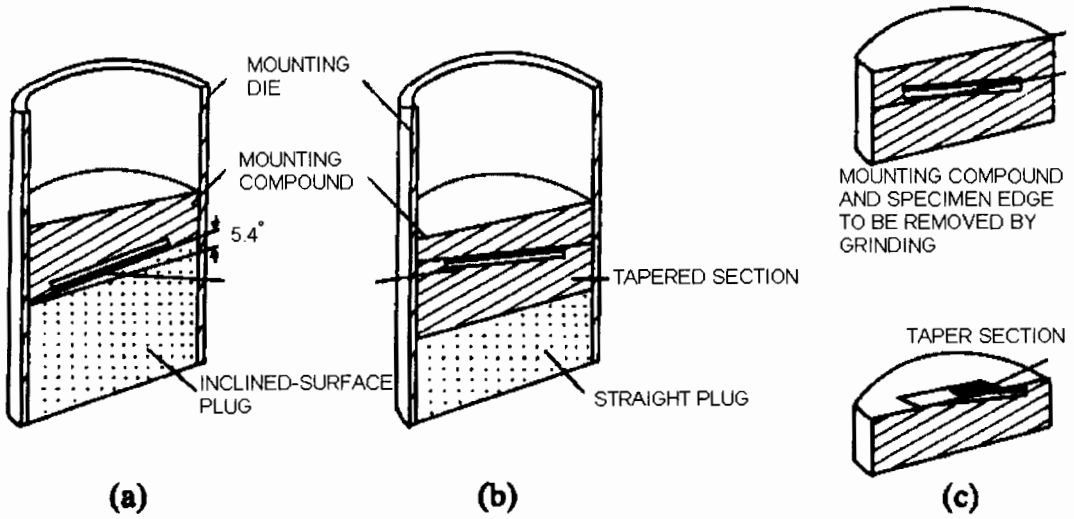

Figure 3.2.2 Procedure for oblique mounting of specimens (by Lang[2]).

The hardness specimens were not polished to a finish required for optical microscopy as different specimens were mounted for optical purposes. The relatively soft nature of platinum resulted in only 1200 grit grinding paper being used in the grinding stage of the polishing procedure. This step removed all scratches from previous working in a short period of time. Mechanical polishing commenced with 3 μm diamond paste until all scratches from the 1200 grit had been removed. The final step was a quick polish with 0.25 μm diamond paste until a relatively scratch free surface was achieved.

3.2.2 METALLOGRAPHY

Finding a suitable method to polish and etch thin platinum specimens proved to be very difficult as conventional techniques could not be used. The final procedure adopted was to glue the specimens onto a polymeric disc of approximately 3 cm in diameter and 1.5 cm thick with methlymethacralate. A short period of time on the 1200 grit grinding pad proved to be satisfactory for the initial grinding stages. The mechanical polishing was then continued with 3.0 μm diamond paste on a polishing pad. It was essential that the disc remained uncontaminated and thus cleaning of the specimen during polishing was important, especially as diamond grit tended to collect between the specimen and the polymeric base. After the initial work on the first 3 μm polishing pad, the specimen was repolished on another 3 μm diamond paste polishing

pad but under a light load and for a short period of time. After both the 3 μm polishing stages were completed, the specimen was polished on a 0.25 μm diamond paste disc until no scratches could be seen with the naked eye. The final step was to polish again on another 0.25 μm diamond paste disc, but very quickly with little pressure. If the polish was not satisfactory (usually with the softer alloys) a light etch was made and then the specimens re-polished on a third 0.25 μm diamond paste disc. This cycle was continued until a good finish was achieved. All specimen preparation was done by hand.

3.2.3 TRANSMISSION ELECTRON MICROSCOPY FOILS

The specimens used for transmission electron microscopy (TEM) were supplied by Dr. Mike Witcomb as stated in the acknowledgements.

3.2.4 ELECTRICAL RESISTIVITY SPECIMENS

Using the van der Pauw[71] method in determining the resistivity of a material requires careful control of the specimen size and thickness. The specimens were cut into small sheets of 12 mm x 12 mm and then rolled again down to a gauge of 90 μm, then recut to the original dimensions. This procedure was necessary as it was found that the thickness of the large rolled sheets was very varied, but rerolling with the small specimens produced a thickness with little variation. Although the thickness of the specimens could not be controlled precisely, the van der Pauw equation does take specimen thickness into account.

3.2.5 X-RAY DIFFRACTION

The same specimens (with the polymer backing) that were prepared for optical microscopy were also used for XRD. The specimens were tested in the polished condition with no chemical surface preparation used to electropolish the specimen surface. Chemical or electropolishing of platinum and high platinum content alloys is very difficult due to the very noble nature of the metal. It was though that the mechanical damage to the specimen would be minimal due the care taken in specimen

preparation and the specimen surface condition would be acceptable for the type of measurements to be made on the x-ray diffractometer.

3.2.6 DIFFERENTIAL THERMAL ANALYSIS

The only specimen preparation that was necessary for DTA was to cut small pieces of material from the rolled strips, with a total mass of approximately 100 mg. The specimens were cleaned to remove any contamination on their surface.

3.3 ANNEALING EXPERIMENTS

The initial conditions under which the specimens were annealed were selected on the basis of researched literature and preliminary testing. Preliminary testing of platinum-molybdenum and platinum-ruthenium alloys showed very similar results to previous research and the initial testing was carried out using the annealing temperatures and times documented by Lang[2]. Lang showed that for the palladium-molybdenum alloys, the maximum change in microhardness occurred after one hour with a slight increase in microhardness up to six hours. Beyond six hours there was very little response in microhardness to annealing time. The annealing time of three hours consistently produced a significant increase in microhardness and was therefore chosen as a standard annealing time for all initial annealing testing. Additional annealing times were introduced as the project continued so as to gain an insight into the response of hardness to a wide range of annealing times.

The optimal annealing times proved to be very specific to the particular alloy with the platinum-copper alloys subjected to a wider range of times and temperatures than the platinum-ruthenium and platinum-molybdenum alloys. An extensive low temperature annealing regime was implemented for the platinum-copper alloy with annealing times between 0 hours to 10 hours and annealing temperatures from 100°C up to 700°C. Additional testing was also carried out at higher temperatures for 3 hours in order to compare results with those found for the other two experimental alloys.

Two different annealing furnaces were used to anneal the specimens. Annealing of the ruthenium and molybdenum specimens up to temperatures of 1300°C were carried out in a vertically supported platinum-rhodium winding furnace capable of annealing in a vacuum or inert atmosphere. The furnace tube was pumped down to a vacuum of 10^{-5} Torr subsequent to which argon was bled into the tube to achieve a partial pressure of 10^{-3} Torr. The heating rate was set to 500°C/hour up to 1000°C after which the heating rate was lowered for temperatures from 1000°C up to 1300°C so as to avoid thermal shock in the alumina tube. Annealing times were started when the temperature control reached the required temperature and stopped when the furnace was turned off. Specimens were left to cool in the furnace with argon still present. Only once the furnace had reached room temperature were the specimens removed. The vacuum furnace also had drop quench capabilities and these were made use of to produce high temperature quench specimens. The quench specimens were dropped from test temperature into distilled water at room temperature.

The platinum copper alloys were annealed in a horizontal, quartz tube furnace in a partial argon atmosphere. The heating cycle was slightly different to that of the vacuum furnace due to a different temperature controller. The specimens were heated up to temperature in one hour, left to dwell for a specific period of time then cooled down to room temperature in one hour. The annealing time was considered to be the time at which the furnace was at the set temperature between the cooling and heating steps. The specimens did not oxidise for most of the testing, but when testing was carried out at over 500°C for long periods of time a thin oxide layer did build up on the surface. The layer was easily removed by grinding on 1200 grit grinding paper and did not appear to influence the results of the annealing experiments. Any of the testing carried out at temperatures over 1300°C was done outside of the department and therefore the control over the annealing times and heating rates could not be verified. This must be considered when interpreting the final results.

3.4 MICROHARDNESS TESTING

Microhardness tests were carried out on a Shimadzu microhardness tester in order to determine the effect of the annealing experiments on mechanical properties. A

standard Vickers diamond indentor was used at varying loads. A load of 100 gf was used for all the alloys in both the cold-worked and annealed conditions. Tests on pure platinum had to be carried out at a lower load of 25 gf due to the softness of the metal. The dwell time for the indentation was set at 10 seconds.

3.5 MICROSCOPY

3.5.1 OPTICAL MICROSCOPY

The polished specimens were examined under a light microscope in order to document the changes in microstructure and to describe the microstructure/property relationship. The etchant used to etch the platinum and platinum alloys was an electrolytic etchant listed below:

- 20 ml HCl
- 25 g NaCl
- 65 ml distilled water.

An alternating current was used at a potential of 10 V for a time period of 50 to 60 seconds using a graphite electrode. A stainless steel clamp was used to make contact with the specimens, hence the need for the polymer bases for the specimens. It was imperative that the clamp should not make contact with the solution, as it would then corrode preferentially, leaving the platinum unetched. This method proved successful, but did leave an unetched area where the clamp had been attached.

The etched samples were examined and photographed on a Reichert MeF2 Metallograph in bright-field mode.

3.5.2 SCANNING ELECTRON MICROSCOPY

A Leica 440S analytical scanning electron microscope with energy dispersive spectroscopy (E.D.S.) facilities, at the Electron Microscope Unit in the University of Cape Town, was used to assess chemical homogeneity of the platinum alloys. The instrument was used in rastor mode to detect any variation in distribution of each

alloying element. The Philips 420 and a Cambridge S200 scanning electron microscope, in secondary and back scattered mode, were used to check for stable second phases in the specimens not visible by optical microscopy.

3.5.3 TRANSMISSION ELECTRON MICROSCOPY

Samples were stored in a vacuum desiccator prior to viewing in a Philips CM200 TEM at the Electron Microscope Unit in the University of the Witwatersrand. The TEM utilised a LaB6 (lanthanium hexaboride) filament at 200kV. Parallel illumination was obtained by using a very spread beam and selected area diffraction patterns taken utilising exposure times of up to 1500 seconds, but more typically up to 500 seconds. Additional bright and dark field images were also taken.

3.6 RESISTIVITY MEASUREMENTS

The resistivity tests were carried out in a purpose designed experimental apparatus. The system used the simple four point connection method described by van der Pauw[71]. The resistivity of the specimen could be measured both at room temperature and as a function of temperature up to 1000°C.

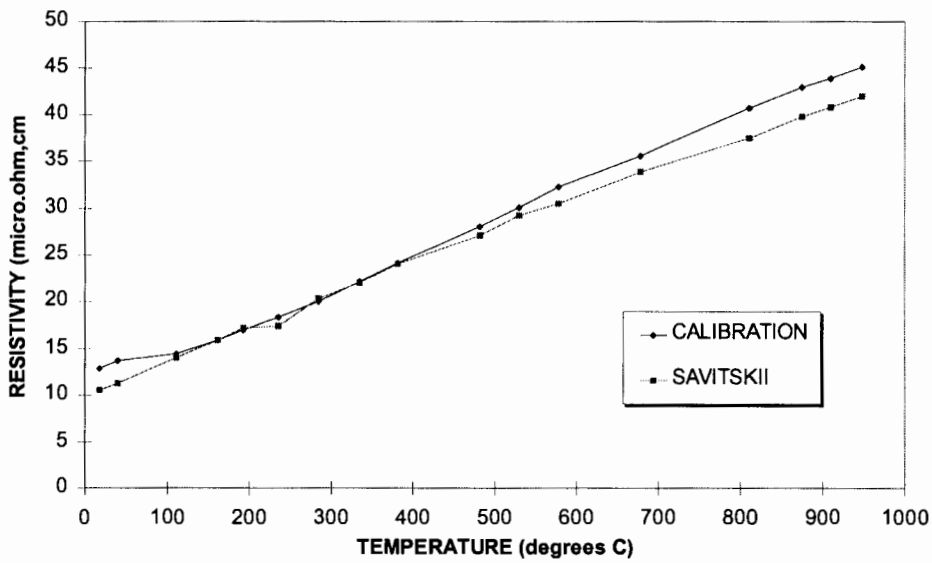

Figure 3.6.1 Calibration graph showing resistivity vs. temperature for platinum tested on the experimental rig and data obtained from literature.

Three tests were carried out in order to determine what effect annealing had on the specimen. The first test was carrried out on the cold-worked specimen; the specimen was then retested (retest 1) then tested for a third time (retest 2).

Figure 3.6.1 shows that results of resistivity vs. temperature obtained for pure platinum on the experimental rig are similar those reported by Savitskii. There is a slight variation in results at the higher temperature with the experimental platinum results slightly higher than those of the literature values.

3.7 X-RAY DIFFRACTION

XRD was carried out using a Philips X-ray diffractometer controlled by a Philips 3710 mpd controller. The specimens were mounted on either one of two types of polymeric bases before being placed into the diffractometer. The specimens were subjected to a XRD scan from 2θ angles of 5° to 95° using a copper radiation source as this was the range considered by Irani and Cahn[6] when investigating Pt-Cu alloys. The XRD was set to scan at 0.01° increments with a x-ray capture time of 3 seconds. This resulted in very long scan times but was necessary for good resolution and high signal to noise ratio. The results of the scan were stored by the instrument as a binary file and could be manipulated by Microsoft Excel.

3.8 DIFFERENTIAL THERMAL ANALYSIS

DTA testing was carried out in a computer controlled NETSCH STA409C which was capable of heating up to 1400°C at varying heating and cooling rates. The reference used was an alumina crucible the same as that used to hold the test sample. Before testing was carried out, each crucible was "burnt in" to remove any contamination that would affect the results negatively. In addition a baseline test was carried out which has been subtracted from the DTA graphs displayed in this investigation. This ensures that only effects due to the test specimen are reflected in the final DTA results.

3.8.1 EFFECT OF DIFFERENT HEATING RATES ON THE DTA RESULTS

The effect that different heating rates had on the DTA results was investigated, an example of which can be seen in Figure 3.8.1 for Pt 5 wt% Cu heated at 1 K/min, 4 K/min and 15 K/min. Three tests were carried out at each heating rate to determine the reproducibility of the results, Figure 3.8.2 is an example of such a test for Pt 5 wt% Cu. The graph shows a large variation in results which was common to all the different heating rates used. As no one heating rate produced more information or showed more reproducibility of results than any other, 4 K/min was selected as the heating rate with which further testing was carried out. Due to an equipment error of unknown nature, many of the DTA tests show electrical "noise" spikes at temperatures above 900°C as well as gradient irregularities at temperatures below 200°C

3.8.2 CALIBRATION AND SENSITIVITY OF THE DTA

In order to check the calibration and sensitivity of the DTA instrument pure gold specimens were also tested, the results of which can be seen in Figure 3.8.3 and Figure 3.8.4. In Figure 3.8.3 the only information of any significance are the melting and solidification peaks at just over 1000°C. The curve above and below these peaks appears to be essentially featureless offering no information regarding transformations or transitions of any kind. However, if the gold specimen is only heated up to 1000°C, which is below the melting point for gold, the DTA results below 1000°C now produce large spikes which could be significant.

3.8.3 RELIABILITY AND REPRODUCIBILTY OF DTA RESULTS

Given the information in Sections 3.8.1 and 3.8.2, the confidence that can be placed in the DTA results is questionable. Firstly, testing of identical specimens under identical conditions produces different results as Figure 3.8.2 shows. Not only do the positions of the peaks change but they appear and reappear during testing for seemingly no reason. Secondly, the value placed on the DTA data must be placed into context due to the gold graphs shown in Figure 3.8.3 and Figure 3.8.4. If the platinum or platinum alloy specimens could be taken to melting, it appears from the information gained by the gold tests, that all the gradient changes and peaks could become insignificant.

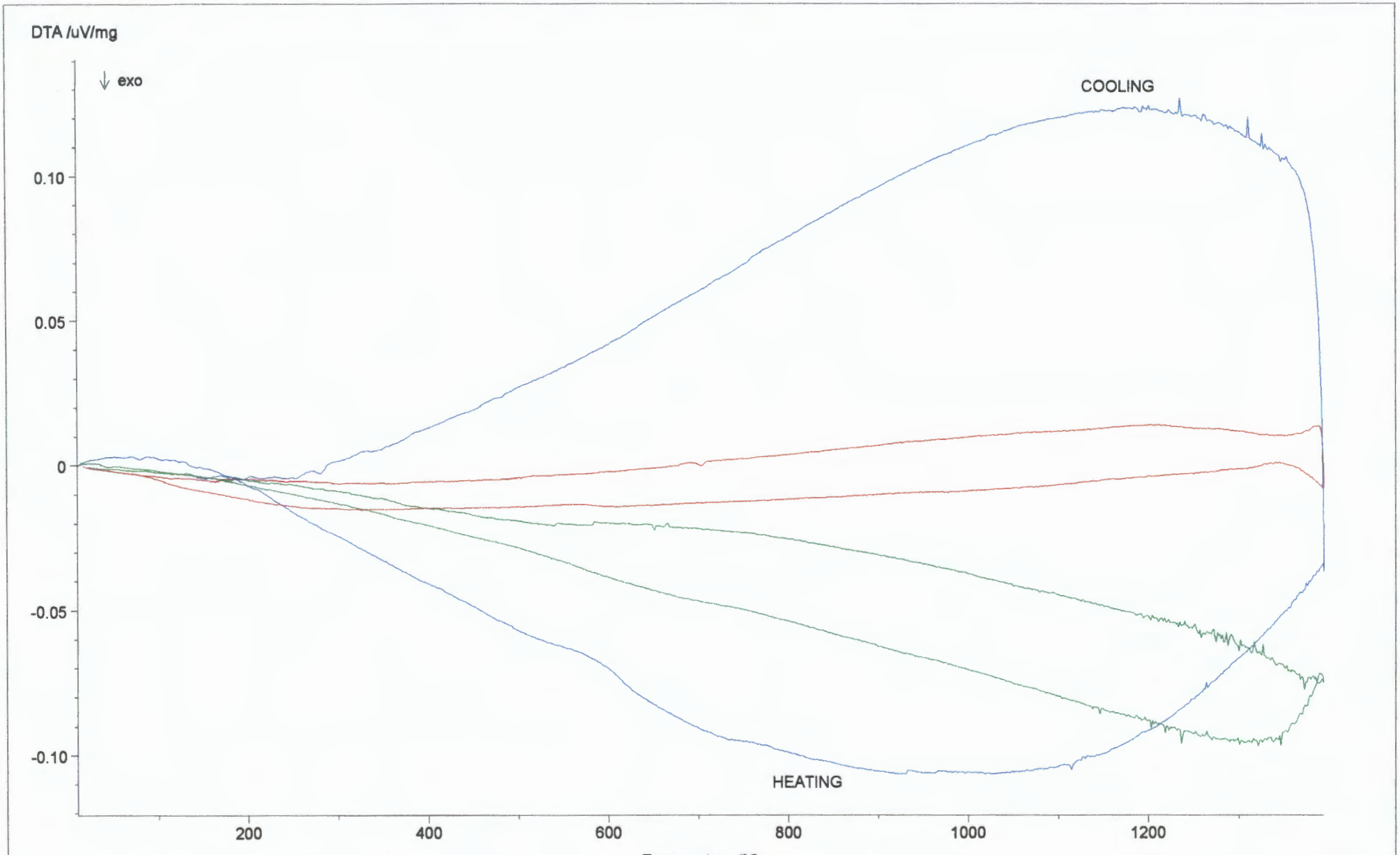

#-INSTRUMENT	FILE	IDENTITY	SAMPLE	DATE	MASS	SEGM.	RANGE	ATMOS.	CORR
1 - STA 409C	COPP_1.DSS	copper 1 k/min first	1400 heating and cooling	09.11.1998	178.690 mg	1-2/2	20 °C/1.0(K/min)/1400 °C/1.0(K/min)/20 °C/	Argon/100	020
2 - STA 409C	COPP1_4.DSS	PtCu 4 k/min test	1400 heating and cooling	12.01.1999	170.890 mg	1-2/2	20 °C/4.0(K/min)/1400 °C/4.0(K/min)/20 °C/	Argon/100	020
3 - STA 409C	COPP_15.DSS	copper fast	1400 heating and cooling	20.11.1998	117.580 mg	1-2/2	20 °C/15.0(K/min)/1400 °C/15.0(K/min)/20 °C/	Argon/100	020

Figure 3.8.1 DTA curves obtained from testing Pt 5 wt% Cu at different heating and cooling rates.

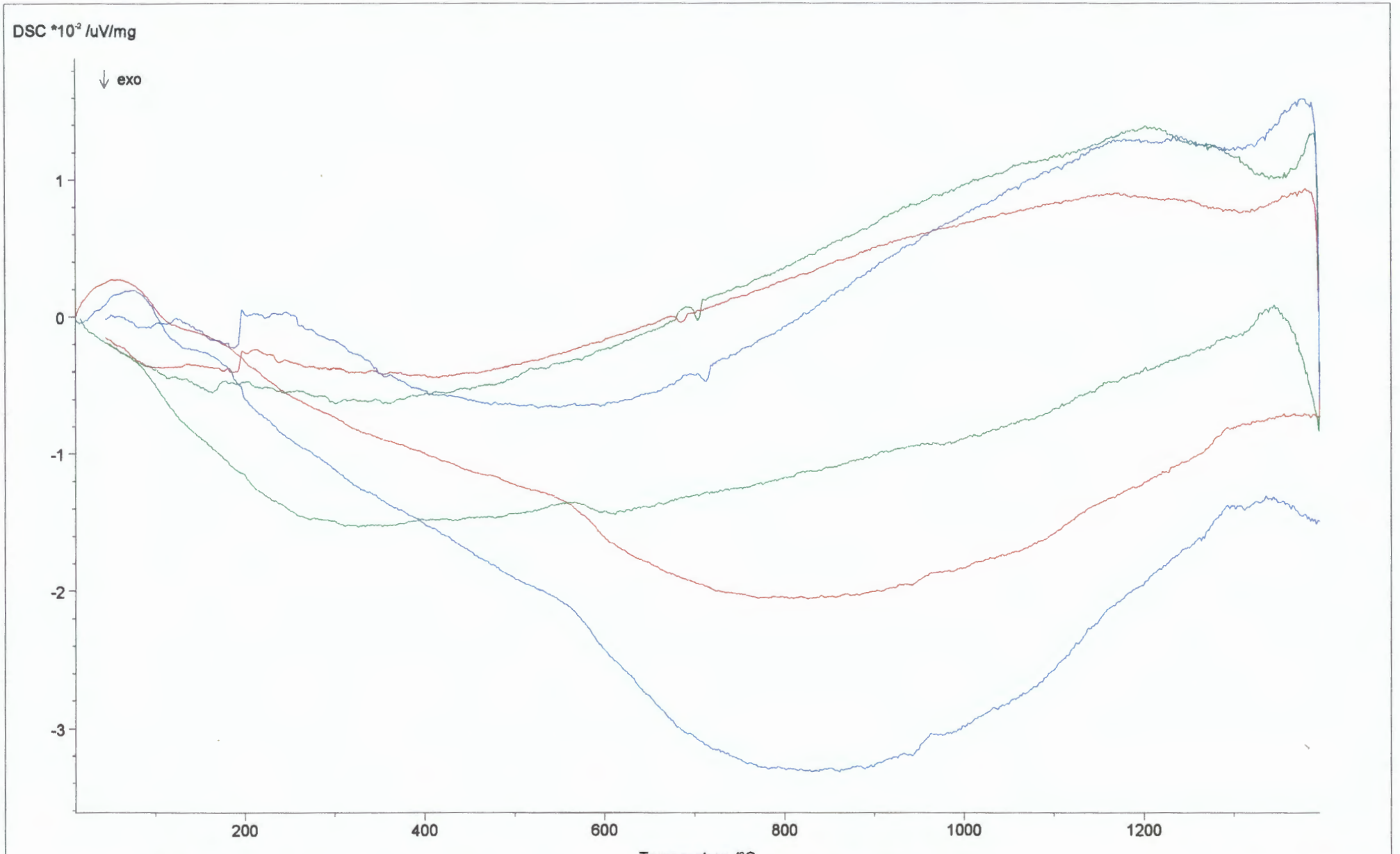

#-INSTRUMENT	FILE	IDENTITY	SAMPLE	DATE	MASS	SEGM.	RANGE	ATMOS.	CORR
1 - STA 409C	COPP1_4.DSS	PtCu 4 k/min test	1400 heating and cooling	12.01.1999	170.890 mg	1-2/2	20 °C/4.0(K/min)/1400 °C/4.0(K/min)/20 °C/	Argon/100	020
2 - STA 409C	COPP3_4.DSS	copper repeat whole test	1400 heating and cooling	17.01.1999	262.120 mg	1-2/2	20 °C/4.0(K/min)/1400 °C/4.0(K/min)/20 °C/	Argon/100	020
3 - STA 409C	COPP5_4.DSS	third time for cu at k k/min	1400 heating and cooling	19.01.1999	146.045 mg	1-2/2	20 °C/4.0(K/min)/1400 °C/4.0(K/min)/20 °C/	Argon/100	020

Figure 3.8.2 Graph showing the variation in DTA results obtained from testing identical specimens of Pt 5 wt% Cu.

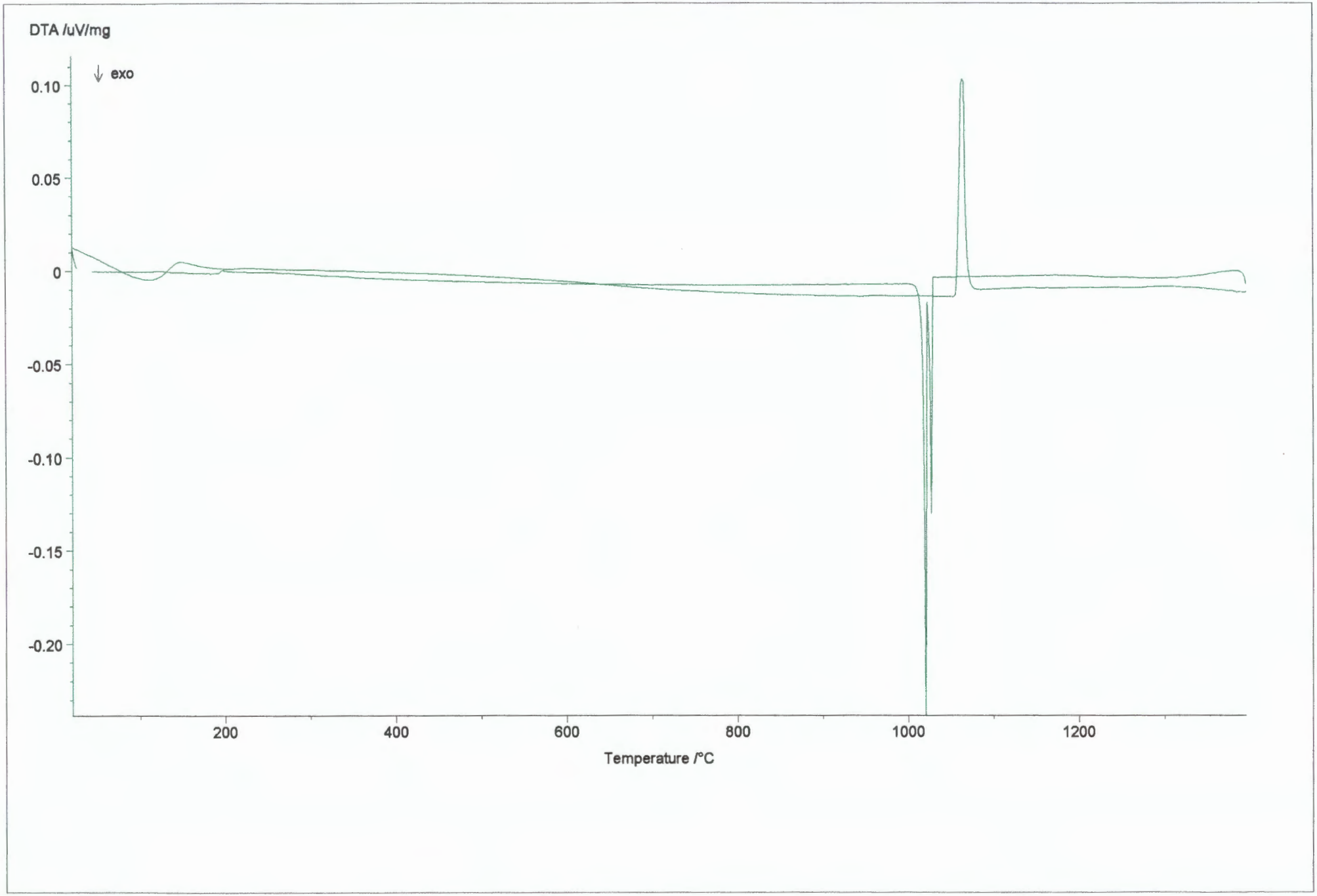

Figure 3.8.3 DTA graph of pure gold heated at 4 K/min up to 1400°C.

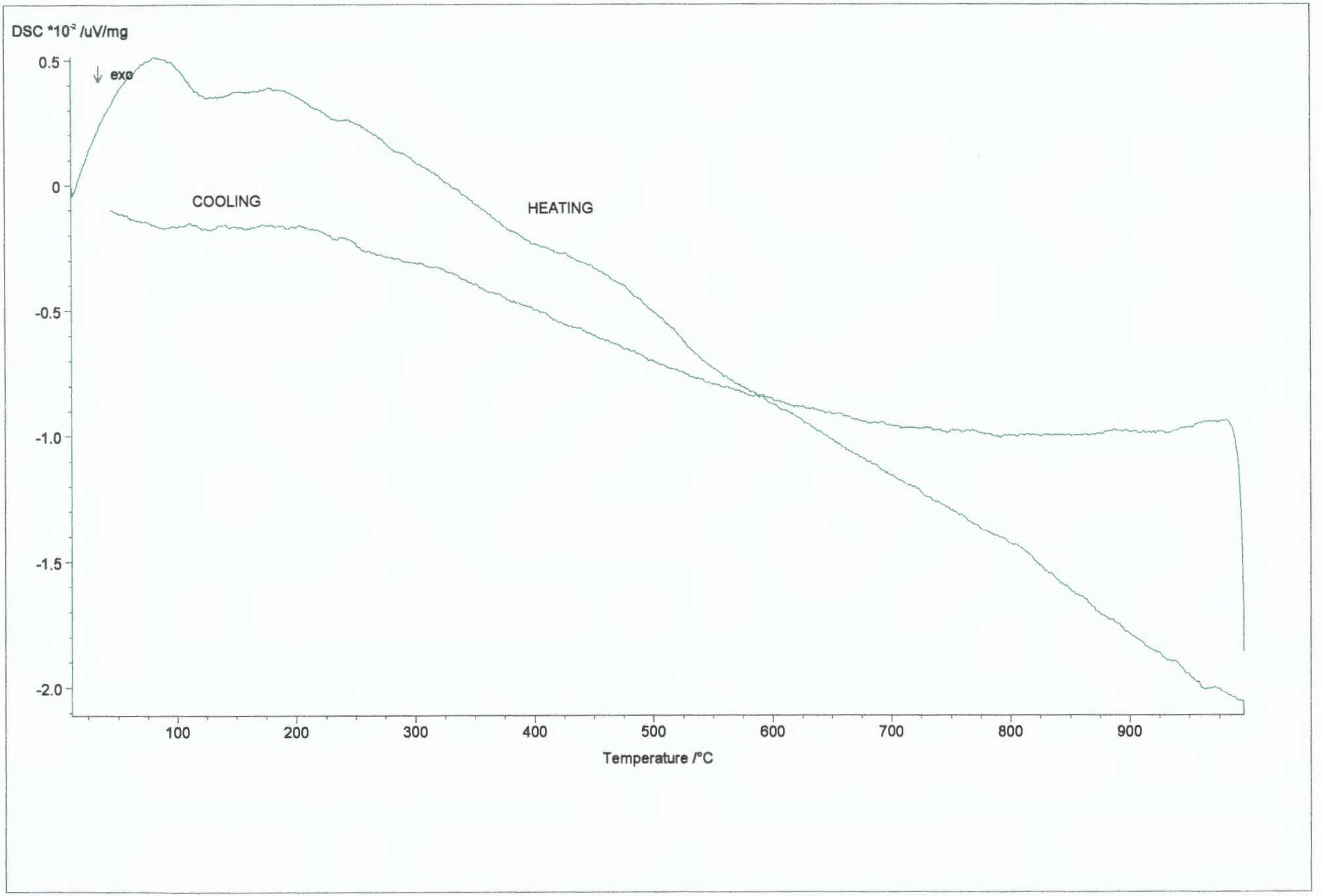

Figure 3.8.4 DTA graph of pure gold heated at 4 K/min up to 1000°C

4 RESULTS

The aim of the experimental programme was to establish the effect that changes in microstructure have on the absolute hardness and the hardening behaviour of the three platinum alloys. The first section, Section 4.1, details the microhardness results obtained for pure platinum and the three experimental alloys, initially in the slow cooled condition and later in the quenched condition. The hardness results for pure platinum and for quench testing are not as comprehensive as the results found during slow cooling. Only selected annealing times and temperatures were isolated from the slow cooled results, Sections 4.1.2, 4.1.3 and 4.1.4, for further testing. The exact annealing times and temperatures selected for quench testing and pure platinum hardness testing are included in the relevant sections. The three sections that follow detail microscopy, with optical microscopy in Section 4.2, and then scanning electron microscopy and transmission electron microscopy in Sections 4.3 and 4.4 respectively. As with the platinum hardness tests and quench hardness tests, only selected annealing times and temperatures were used for microscopy purposes. Following the microhardness and microscopy sections, the results for resistivity are presented in Section 4.5, x-ray diffraction in Section 4.6 and differential thermal analysis in Section 4.7.

4.1 MICROHARDNESS

The section that follows shows the changes in microhardness that result from annealing the three experimental alloys at different times and temperatures. The points on the graphs represent the mean value of eight microhardness measurements but due to limited material some specimens could not accommodate eight indents. The exact number of microhardness indents, when microhardness is referred to in the text, appears in the brackets following the value. The bracketed information also includes the load with which the indent was made and the range of microhardness values obtained during testing of that one specimen.

Section 4.1.2 and Section 4.1.3 contain isochronal heat treatment results on the platinum-molybdenum and platinum-ruthenium alloys respectively. The most comprehensive results were obtained for the 3 hour heat treatment. 0.5 hour and 6 hour heat treatments are also included so as to gain an understanding of the effects of annealing time on microhardness. From these results, 4 specific annealing times and temperatures (for each alloy) were isolated for further investigation: the cold-worked condition and annealing at 700°C, 1000°C and 1300°C for 3 hours. Similarly, 5 specific heat treatment conditions for the platinum-copper alloy were isolated for further investigation: the cold-worked condition, annealing at 300°C for 0.5 hours and 10 hours, and annealing at 700°C for 0.5 hours and 10 hours. Microhardness results for pure platinum specimens annealed for similar times and temperatures to the selected specimens have been included in Section 4.1.1. The final section of the microhardness results, Section 4.1.5, documents the results obtained from testing the selected alloys in the quenched condition, rather than slow cooled as in the former four microhardness sections.

Section 4.1.4, which investigates the hardening behaviour of platinum-copper, includes both microhardness vs. temperature annealing graphs (isochronal) and microhardness vs. time annealing graphs (isothermal). The sections detailing microhardness in the platinum-molybdenum and platinum-ruthenium alloys contain only isochronal annealing graphs. Therefore, isochronal graphs for platinum-copper

allow comparison between the alloys. The isothermal graphs, which are only presented for the platinum-copper alloy, allow comparison with the available literature on order hardening in platinum-copper.

Where only one series of results is plotted on a set of axes, error bars have been included to show the spread of results. The upper and lower error bars represent the highest and lowest microhardness value obtained from the specimen respectively. Error bars indicate the variation in reading the microhardness value from one specimen and do not take into account the error that could occur from one specimen to another. Inhomogeneity in the cast button will result in variation when reading the microhardness of specimens cut from different areas of the rolled sheet. To allow for this variation, many specimens would have to be annealed under the same conditions and their mean hardness averaged. This procedure would have been very expensive and could not be carried out. Additional errors that can not be accounted for could originate from the sample preparation procedure and the microhardness tester. For completeness, an x-axis error bar should also be included in the graphs as there will be errors in both timing the heat treatments and controlling the annealing temperatures.

4.1.1 *PLATINUM*

ANNEALED FOR 0.5 HOURS

The microhardness results obtained from annealing platinum specimens at selected temperatures for 0.5 hours are shown in Figure 4.1.1. The microhardness value for the cold-worked specimen is indicated on the graph by CW and is in the 0°C annealing temperature position. The graph shows that annealing for 0.5 hours at 300°C has little effect on the microhardness of platinum as there is no substantial microhardness change between the cold-worked specimen and the specimen annealed at 300°C. Annealing at 700°C however, has a significant effect on the microhardness as the microhardness value falls from HV 97 (25g, n=8, range 94-103) to HV 49 (25g, n=8, range 44-52).

ANNEALED FOR 3 HOURS

The graph obtained from plotting the microhardness results of platinum annealed for 3 hours at temperatures of 700°C, 1000°C and 1300°C can be seen in Figure 4.1.2. Annealing at 700°C produces a significant decrease in microhardness from HV 97 (25g, n=8, range 94-103) in the cold-worked condition to HV 45 (25g, n=8, range 43-47) at 700°C. Annealing at temperatures greater than 700°C appears to produce very little further change in microhardness with the 1000°C and 1300°C producing values of HV 50 (25g, n=8, range 44-53) and HV 45 (25g, n=8, range 44-47) respectively.

ANNEALED FOR 10 HOURS

The results obtained from annealing platinum for 10 hours at different temperatures can be seen in Figure 4.1.3. Annealing at 300°C produces a slight decrease in microhardness from HV 97 (25g, n=8, range 94-103) in the cold-worked specimen to HV 92 (25g, n=8, 87-97) at 300°C. A more significant decrease in microhardness is obtained by annealing at 700°C as the microhardness drops to HV 45 (25g, n=8, range 43–46).

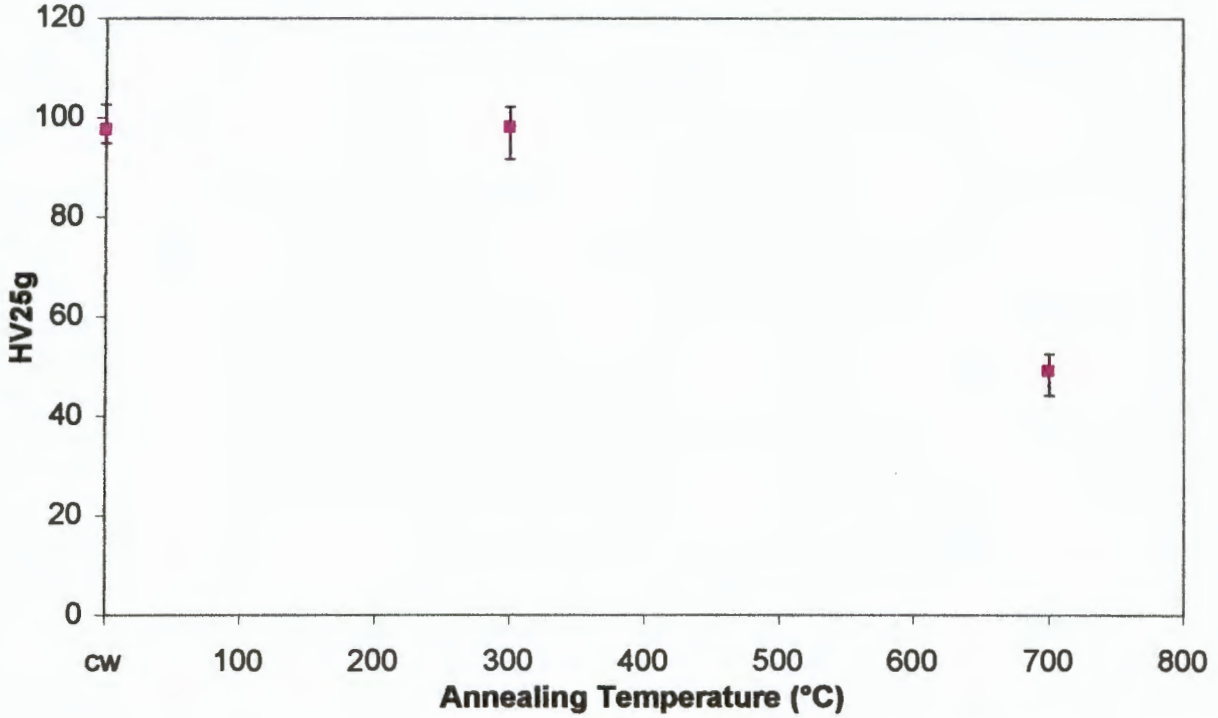

Figure 4.1.1 Graph of microhardness vs. annealing temperature for platinum annealed for 0.5 hours.

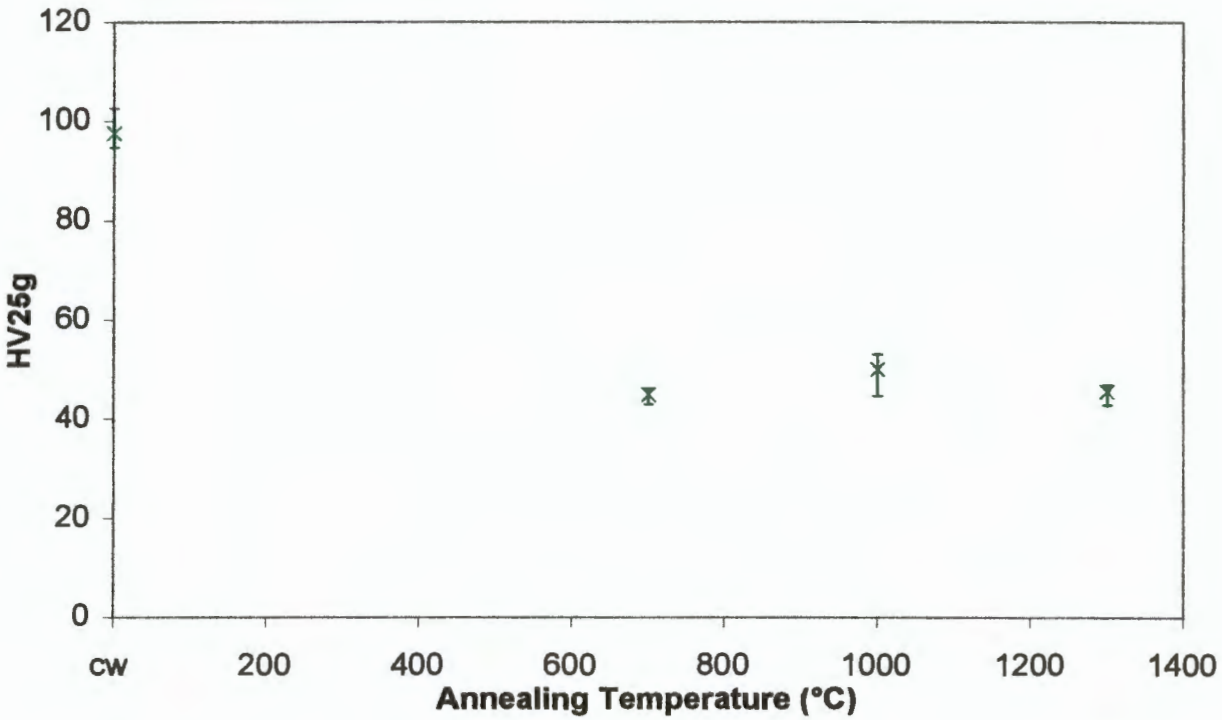

Figure 4.1.2 Graph of microhardness vs. annealing temperature for platinum annealed for 3 hours.

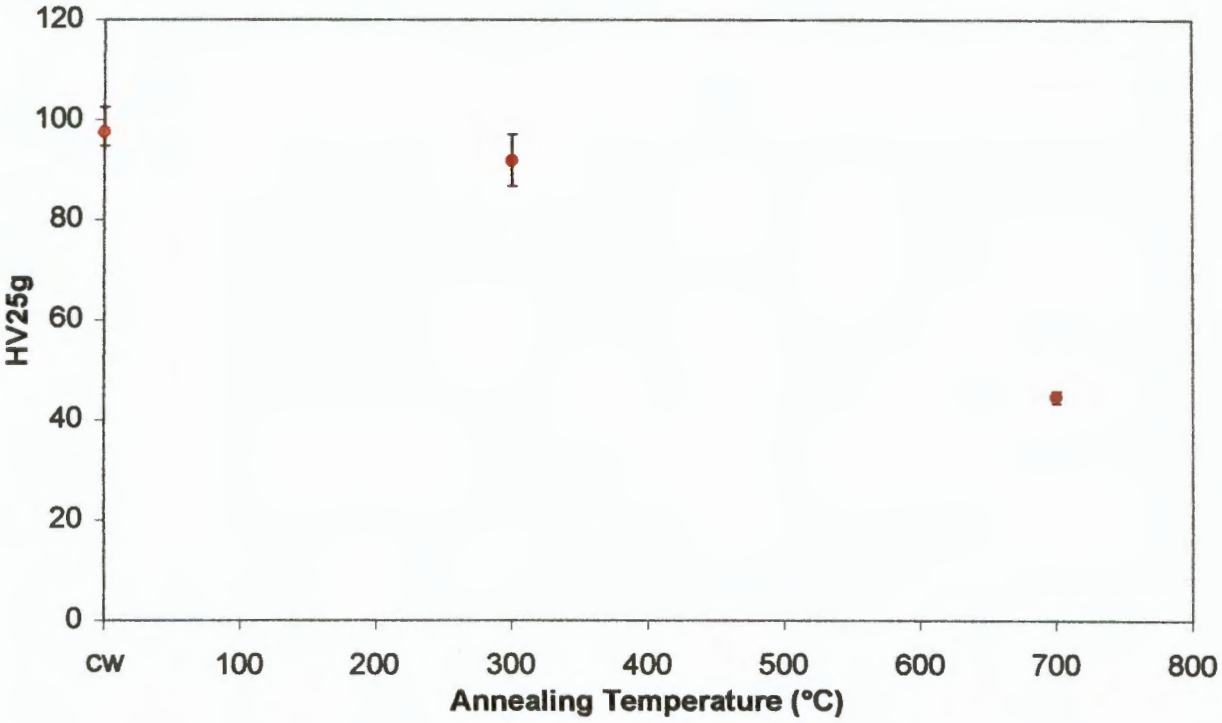

Figure 4.1.3 Graph of microhardness vs. annealing temperature for platinum annealed for 10 hours.

4.1.2 *PLATINUM-MOLYBDENUM*

ANNEALED FOR 0.5 HOURS

The microhardness results obtained from annealing the Pt 5 at% Mo alloy for 0.5 hours in the temperature range 400°C to 1300°C are shown in Figure 4.1.4. The graph shows that annealing at 400°C produces no substantial change in microhardness if compared to the initial cold-worked microhardness of HV 288 (100g, n=8, range 283 - 296). At annealing temperatures above 400°C there is a gradual decrease in microhardness with a minimum value of HV 155 (100g, n=4, range 153 – 157) at an annealing temperature of 1000°C. A microhardness plateau with a slight increase, of values between HV 155 (100g, n=4, range 153 – 157) and HV 169 (100g, n=8, range 165 – 176), is established when the specimen is annealed in the 1000°C to 1275°C temperature range. Annealing at higher temperatures produces a marked increase in microhardness with a final value of HV 286 (100g, n=8, range 269 - 293) achieved by annealing at 1300°C. This value is approximately the same as the initial cold-worked microhardness.

ANNEALED FOR 3 HOURS

The microhardness of Pt 5 at% Mo, found after a comprehensive series of heat treatments between 300°C and 1400°C, is shown in Figure 4.1.5. There is very little change in microhardness after annealing for three hours in the temperature range 300°C - 500°C. Annealing at temperatures above 500°C however, produces a gradual decrease in microhardness reaching a minimum plateau between 1000°C and 1250°C.

The graph shows microhardness values for two specimens annealed at 1250°C, one having a value of HV 155 (100g, n=8, range 150 – 169) and the other HV 252 (100g, n=8, range 227 – 282). Both values have been included to show variations in microhardness produced during heat treatments. The maximum microhardness, of HV 294 (100g, n=8, range 278 – 310), is obtained by annealing at 1300°C. Annealing at higher temperatures results in a decrease in microhardness, with

annealing at 1400°C and 1500°C producing nearly the same microhardness as annealing at 800°C.

ANNEALED FOR 6 HOURS

The microhardness of Pt 5 at% Mo annealed for 6 hours, Figure 4.1.6, shows very little change from the cold-worked microhardness after annealing at a temperature of 400°C. Annealing in the temperature range 400°C to 1000°C results in a gradual decrease in microhardness reaching a minimum value of HV 171 (100g, n=8, range 166 – 177) at 1000°C. As with annealing for 0.5 hours and 3 hours, there is an area of almost constant microhardness between 1000°C and 1200°C with an approximate value of HV 175. Annealing at temperatures higher than 1200°C produces a small increase in hardness reaching a maximum of HV 204 (100g, n=8, range 187 – 246) at 1300°C. There is no sharp microhardness increase as is seen previously for the annealing times of 0.5 hours and 3 hours.

COMBINED PLOT

Figure 4.1.7 shows a combined plot of the three graphs discussed above but only showing their mean microhardness values. The graph shows that for all three annealing times the only major difference in microhardness occurs at annealing temperatures over 1250°C. All three sets of points show a relatively constant microhardness when the specimens are annealed at temperatures under 400°C; they then all decrease to a minimum value in the temperature range between 1000°C and 1250°C. This temperature range also produces a region in which all three alloys show a plateau in microhardness values. Once the annealing temperatures are greater than 1250°C the specimens annealed for 0.5 and 3 hours increase rapidly to microhardness values of HV 286 (100g, n=8, range 269 – 293) and HV 294 (100g, n=8, range 278 – 310) respectively. Annealing the specimens at 1300°C for 6 hours produces a slight increase in hardness, but not to the same extent as seen for the other two annealing times.

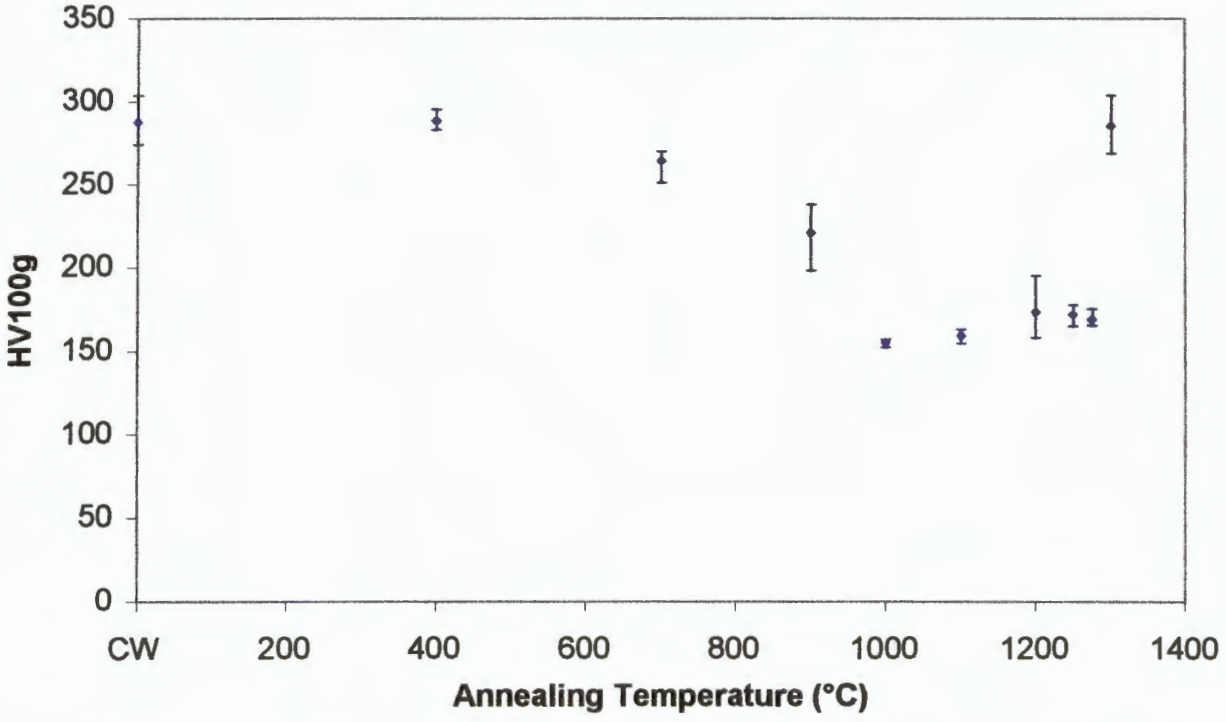

Figure 4.1.4 Graph of microhardness vs. annealing temperature for Pt 5 at% Mo annealed for 0.5 hours.

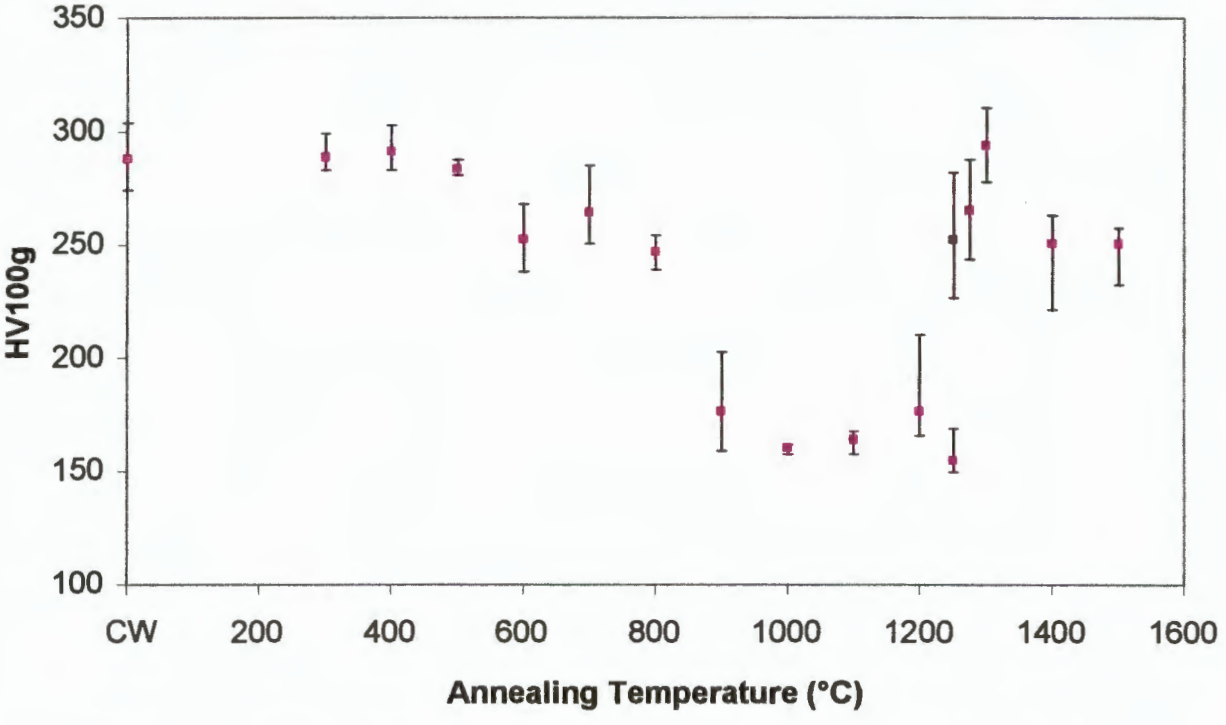

Figure 4.1.5 Graph of microhardness vs. annealing temperature for Pt 5 at% Mo annealed for 3 hours.

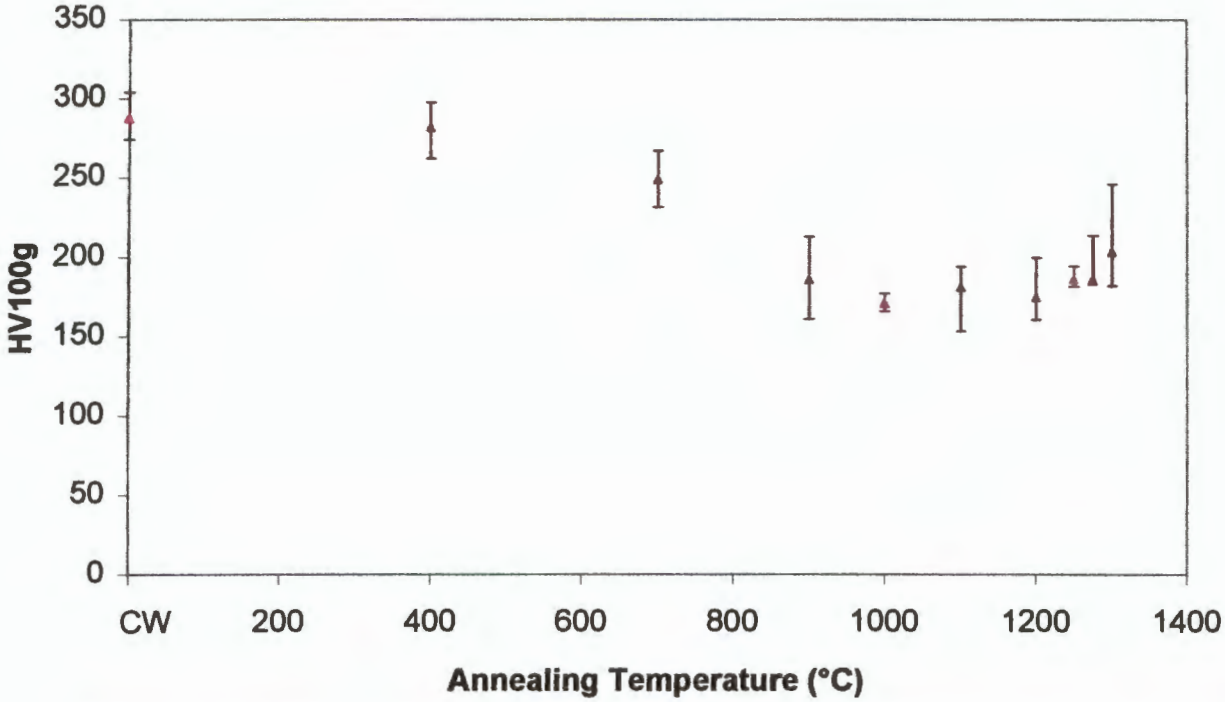

Figure 4.1.6 Graph of microhardness vs. annealing temperature for Pt 5 at% Mo annealed for 6 hours.

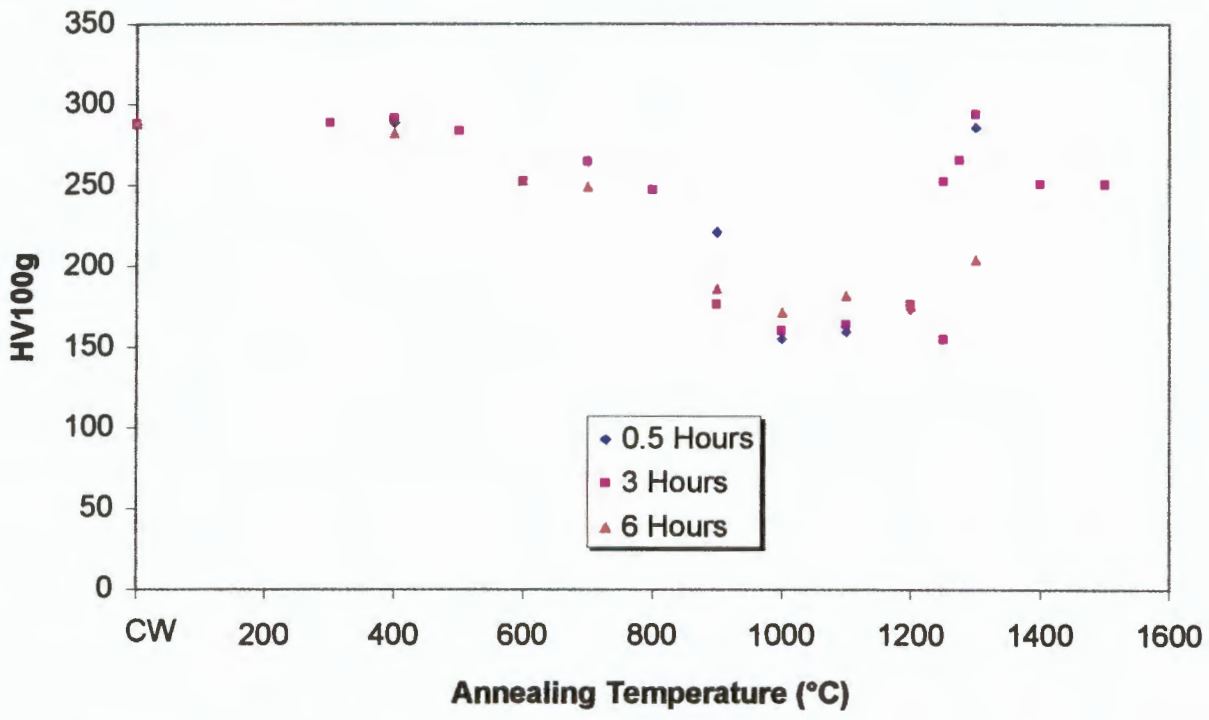

Figure 4.1.7 Graph of microhardness vs. annealing temperature for Pt 5 at% Mo annealed for times of 0.5, 3 and 6 hours.

4.1.3 *PLATINUM-RUTHENIUM*

ANNEALED FOR 0.5 HOURS

Figure 4.1.8 shows the graph of microhardness versus annealing temperature for Pt 5 wt% Ru annealed for 0.5 hours. The graph shows that annealing at a temperature of 400°C does not produce a significant change in microhardness from the value found for the initial cold-worked microhardness. Annealing at 700°C produces a small decrease in microhardness while annealing at 900°C results in a marked decrease in microhardness to HV 173 (100g, n=6, range 168 – 178). A microhardness plateau results from annealing at temperatures between 900°C and 1275°C, with the lowest value of HV 155 (100g, n=6, range 152 – 159) at 1275°C. All the values are, however, within a relatively small range of HV 155 (100g, n=6, range 152 –159) to HV 182 (100g, n=4, range 163 – 190). Annealing at a temperature of 1300°C results in a marked increase in microhardness producing a final value of HV 264 (100g, n=6, range 232 – 272) which is only slightly lower than the initial cold worked hardness of HV 271 (100g, n=8, range 265 – 279).

ANNEALED FOR 3 HOURS

The microhardness of Pt 5 wt% Ru after annealing in the temperature range 300°C to 1400°C for 3 hours is shown in Figure 4.1.9. Annealing in the temperature range 300°C to 500°C does not appear significantly to change the microhardness from the value of the initial cold-worked hardness. Annealing temperatures of 600°C, 700°C and 800°C, produce a steady decrease in the microhardness after which there is a sharp drop to a microhardness of HV 176 (100g, n=8, range 156 – 210) when annealing the specimen at 900°C. A microhardness plateau is seen between annealing temperatures of 900°C and 1250°C, after which there is a sudden and large increase in microhardness with a maximum value of HV 279 (100g, n=7, range 267 – 287) reached on annealing at 1275°C. Annealing at 1300°C also produces a high hardness but once the annealing temperature is greater than 1300°C the microhardness starts to

fall again as indicated by the HV 261 (100g, n=5, range 250 – 272) microhardness value at 1400°C.

ANNEALED FOR 6 HOURS

The microhardness of Pt 5 wt% Ru, shown in Figure 4.1.10, shows little change after annealing at 400°C for 6 hours. Annealing between 400°C and 1000°C produces a steady decrease in microhardness which reaches a minimum value of HV 152 (100g, n=7, range 143 – 164) at 1000°C. At temperatures higher than 1000°C the microhardness shows a steady increase with a final value of HV 223 (100g, n=8, range 208 – 250) after the full series of heat treatments.

COMBINED PLOT

The graph in Figure 4.1.11 shows a combined plot of mean microhardness versus annealing temperature for Pt 5 wt% Ru at annealing times of 0.5, 3 and 6 hours. All three sets of microhardness values follow a trend of an initially constant microhardness followed by decrease to a minimum value at approximately 1000°C. The graph shows that the specimen annealed for 6 hours reaches a lower microhardness value in the 900°C to 1100°C range than do the ones annealed for 0.5 and 3 hours. Annealing the specimens for 6 hours also differs from the other two times, in that the 1300°C microhardness value does not reach a value close to that of the initial cold-worked microhardness. The final microhardness value for the 6 hour anneal is HV 223 (100g, n=8, range 208 – 250), approximately 40 microhardness below that of the 0.5 and 3 hour anneal.

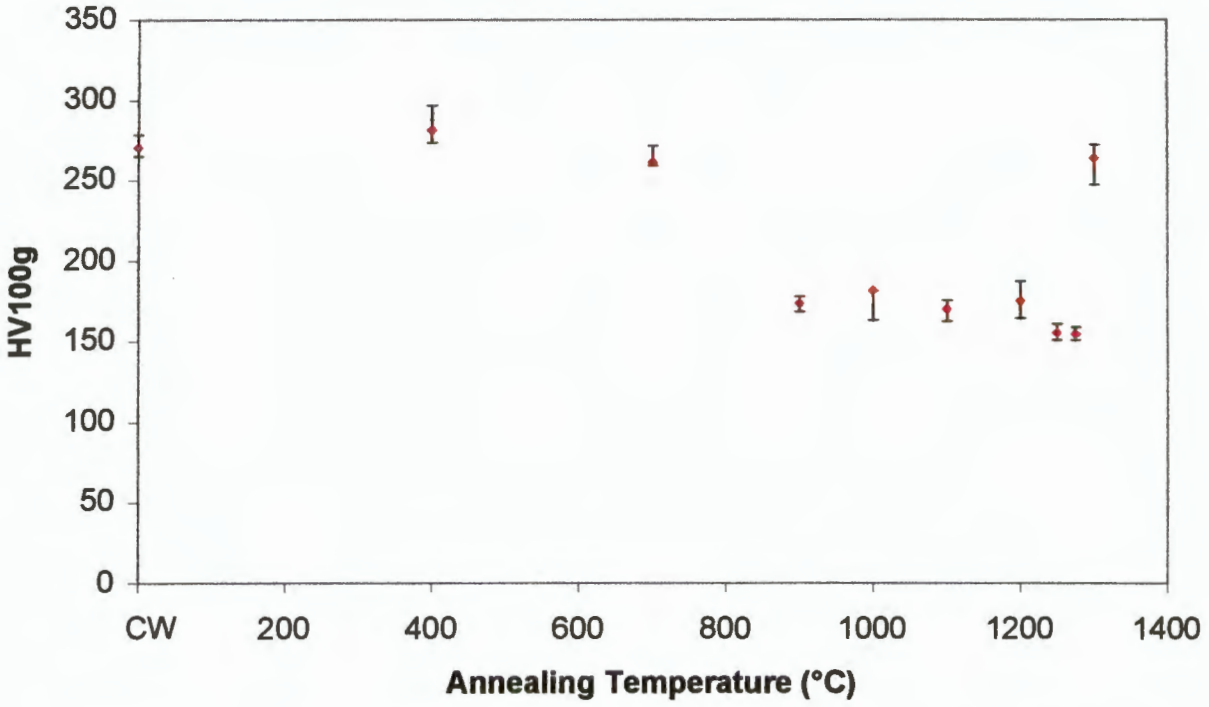

Figure 4.1.8 Graph of microhardness vs. annealing temperature for Pt 5 wt% Ru annealed for 0.5 hours.

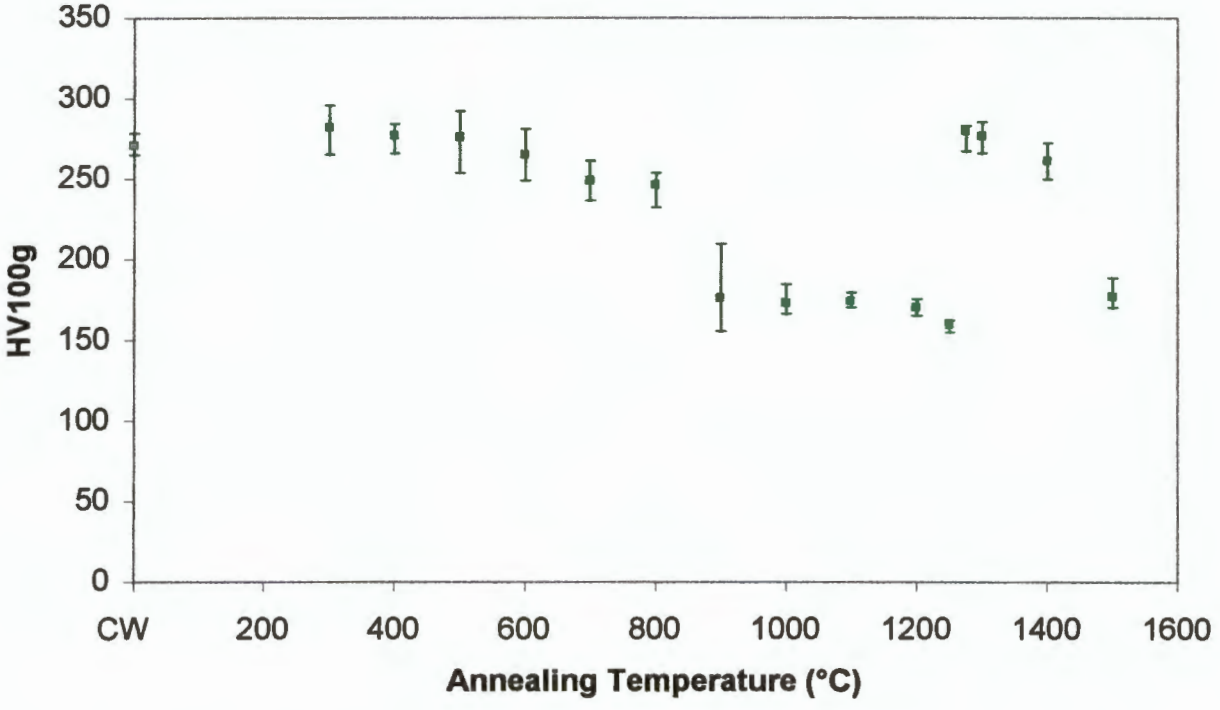

Figure 4.1.9 Graph of microhardness vs. annealing temperature for Pt 5 wt% Ru annealed for 3 hours.

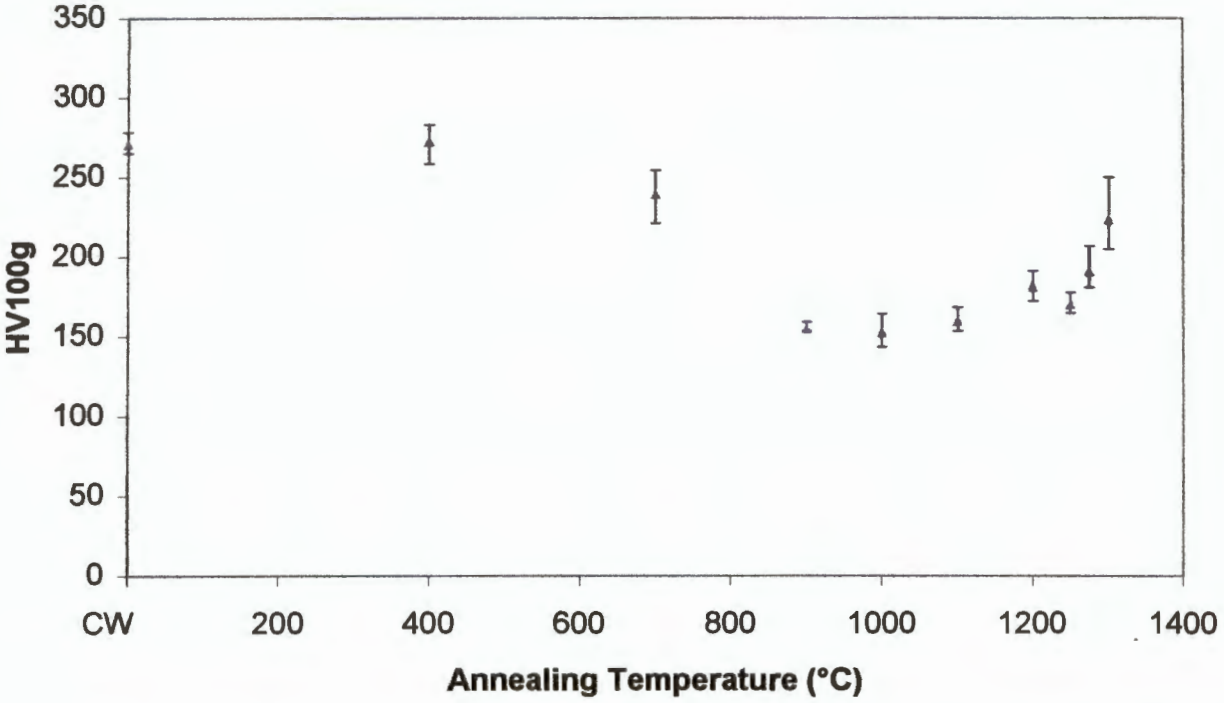

Figure 4.1.10 Graph of microhardness vs. annealing temperature for Pt 5 wt% Ru annealed for 6 hours

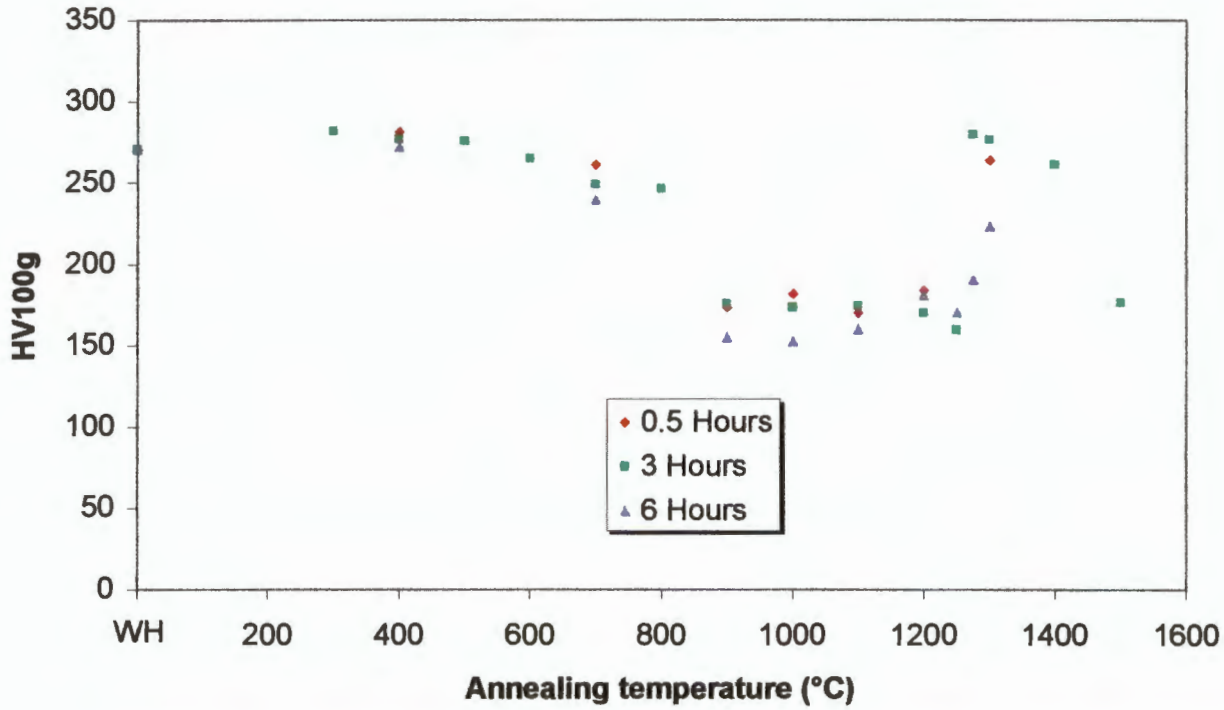

Figure 4.1.11 Graph of microhardness vs. annealing temperature for Pt 5 wt% Ru annealed for 0.5, 3 and 6 hours

4.1.4 PLATINUM-COPPER

Figure 4.1.12 shows the individual graphs of microhardness versus annealing time for Pt 5 wt% Cu annealed in the temperature range 100°C to 700°C. The graphs, unlike in the preceding sections, are microhardness vs. time graphs as this particular format shows interesting trends and this is the format used by all the available literature on the platinum-copper alloy system. Isochronal graphs using the same data follow in Figure 4.1.14 and Figure 4.1.15. The graphs in Figure 4.1.12 and in Figure 4.1.14 have been summarised in Figure 4.1.13 and in Figure 4.1.15 respectively, so that a comparison of trends can be made between all seven different annealing temperatures. The lines joining the points in Figure 4.1.13 are to help the eye follow any trends that might develop from the microhardness results. They do indicate experimental hardness results between individual points. The CW that is indicated on the x-axes of the graphs in Figure 4.1.12, Figure 4.1.13, Figure 4.1.14 and Figure 4.1.15 indicates the initial cold-worked microhardness of the unannealed specimens.

ISOTHERMAL ANNEALING OF Pt 5 wt% Cu AT TEMPERATURES FROM 100°C -700°C.

ANNEALING AT 100°C

Graph a) in Figure 4.1.12 shows the results of annealing Pt 5 wt% Cu at 100°C for between zero and 10 hours. The microhardness results show no consistent trend that would indicate a slow rise or fall of microhardness with increasing annealing time. The microhardness results do, however, all show a value above that of the cold-worked microhardness of HV 280 (100g, n=8, range 306 – 327). The maximum microhardness for the 100°C tests is produced by annealing for 6 hours and corresponds to a microhardness of HV 333 (100g, n=8, range 330 – 340). The 0 hour anneal corresponds to the test specimens which were heated to the test temperature and left to dwell for zero hours before cooling of the specimen.

ANNEALING AT 200°C

Annealing Pt 5 wt% Cu at 200°C for increasing times, shown in graph b) of Figure 4.1.12, produces an initial increase in microhardness up to three hours, after which a constant value of approximately HV 330 is reached. The maximum microhardness attainable by annealing at 200°C occurs at a time of 3 hours and has a value of HV 349 (100g, n=8, range 327 – 376).

ANNEALING AT 300°C

The annealing of Pt 5 wt% Cu shown in graph c) produced a similar trend to graph b) except that after the initial increase in microhardness with increasing time there is a slight decrease in microhardness. The microhardness drops from HV 366 (100g, n=8, range 346 – 389) upon annealing for 0.5 hours, to HV 338 (100g, n=8, range 314 – 348) after annealing for 1 hour. Graph c) shows that this hardness is recovered when annealing times are extended to times greater than 3 hours and a constant value of approximately HV 375 is obtained.

ANNEALING AT 400°C

Graph d) in Figure 4.1.12 shows the microhardness of Pt 5 wt% Cu vs. annealing time for annealing temperature of 400°C. An initial rapid increase in microhardness is produced with a maximum value of HV 366 (100g, n=8, range 354 – 383) obtained after annealing at 400°C for 0.5 hours. The microhardness value decreases slightly when annealing times are increased to 1 hour, but a constant value of approximately HV 350 is obtained for annealing times of 6 hours and longer.

ANNEALING AT 500°C

Annealing the Pt 5 wt% Cu alloy specimens at 500°C for increasing times produces an initial rapid increase in microhardness to a value of HV 330 (100g, n=8, range 319 – 363). This microhardness decreases to HV 315 (100g, n=8, range 289 – 329) when annealing times are increased to 0.5 hours. A maximum microhardness value of HV

348 (100g, n=8, range 329 – 365) is achieved by annealing for 1 hour after which the microhardness levels out at values slightly lower the maximum value.

ANNEALING AT 600°C

When Pt 5 wt% Cu is annealed at 600°C for times of zero and 0.5 hours there is no substantial change in microhardness as graph f) of Figure 4.1.12 shows. The maximum microhardness is achieved after a 0.5 hour anneal but it is not significantly higher than the initial cold-worked microhardness of HV 280 (100g, n=8, range 260 – 300). The graph shows that for annealing times between 1 hour and 3 hours there is a slight decrease in microhardness followed by a constant microhardness value of approximately HV 250.

ANNEALING AT 700°C

Graph g) in Figure 4.1.12 shows the microhardness of Pt 5 wt% Cu versus annealing time for a 700°C anneal. There is a decrease in microhardness from the cold-worked microhardness of HV 280 (100g, n=8, range 306 – 327) to HV 147 (100g, n=8, range 138 – 151) when annealing times are less than 3 hours. For annealing times longer than 3 hours the hardness reaches a constant level of just below HV 150.

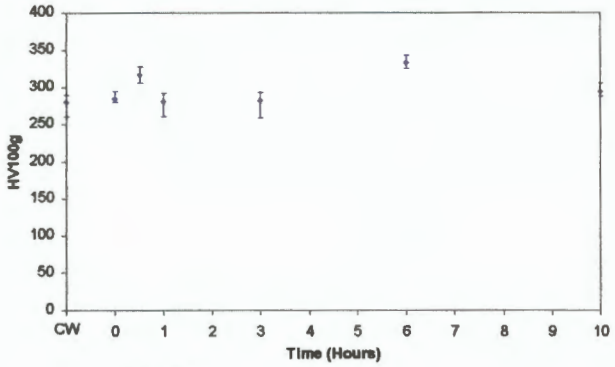

a) 100°C

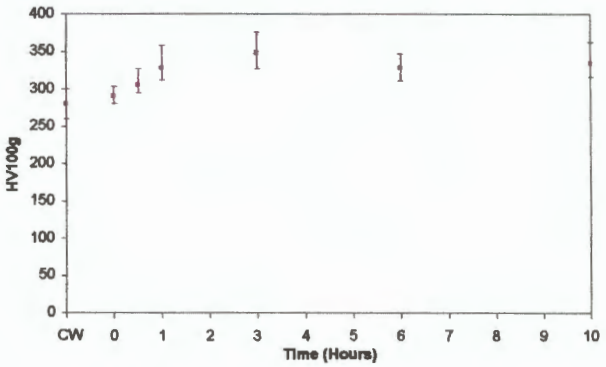

b) 200°C

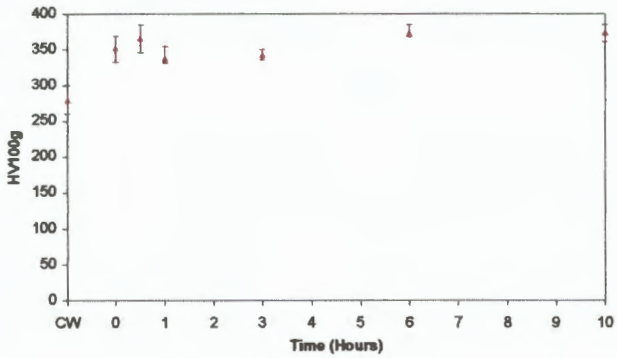

c) 300°C

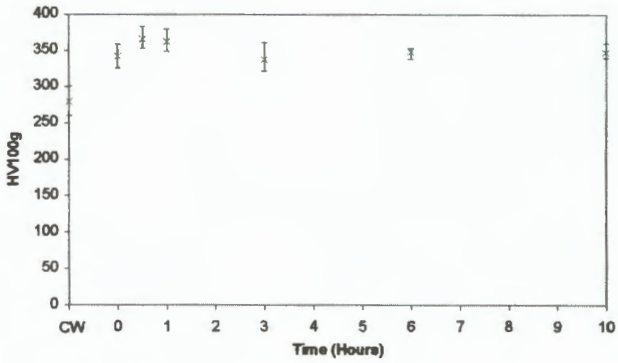

d) 400°C

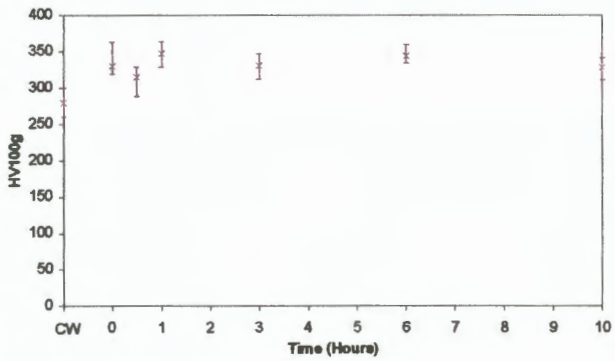

e) 500°C

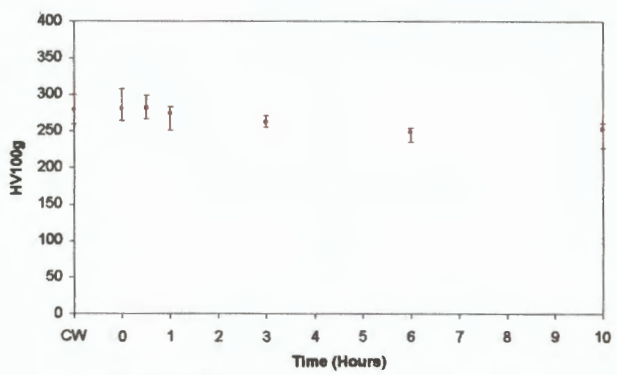

f) 600°C

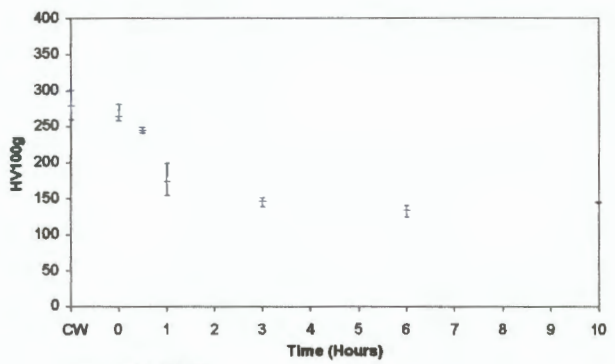

g) 700°C

Figure 4.1.12 Graphs of microhardness vs. annealing time for Pt 5 wt % Cu at temperatures ranging from 100°C to 700°C.

COMBINED GRAPH

Figure 4.1.13 shows the seven graphs of Figure 4.1.12 plotted on one set of axes so that a comparison of trends can be made between different annealing temperatures. There are three different trends developing from the set of microhardness results. Annealing the specimens at 100°C produces a relatively constant microhardness with the values oscillating randomly above and below the HV 300 microhardness level. Annealing specimens at increasing times at temperatures between 200°C and 500°C all produce microhardness values above the HV 300 level. These specimens show an initial increase in microhardness, with the amount of increase depending on the specific annealing temperature. Once past this initial increase the microhardness levels off at a constant level slightly below the maximum microhardness. The third general trend that develops occurs in the specimens annealed at 600°C and 700°C. At these two annealing temperatures, the microhardness decreases and is never higher than the HV 300 microhardness level.

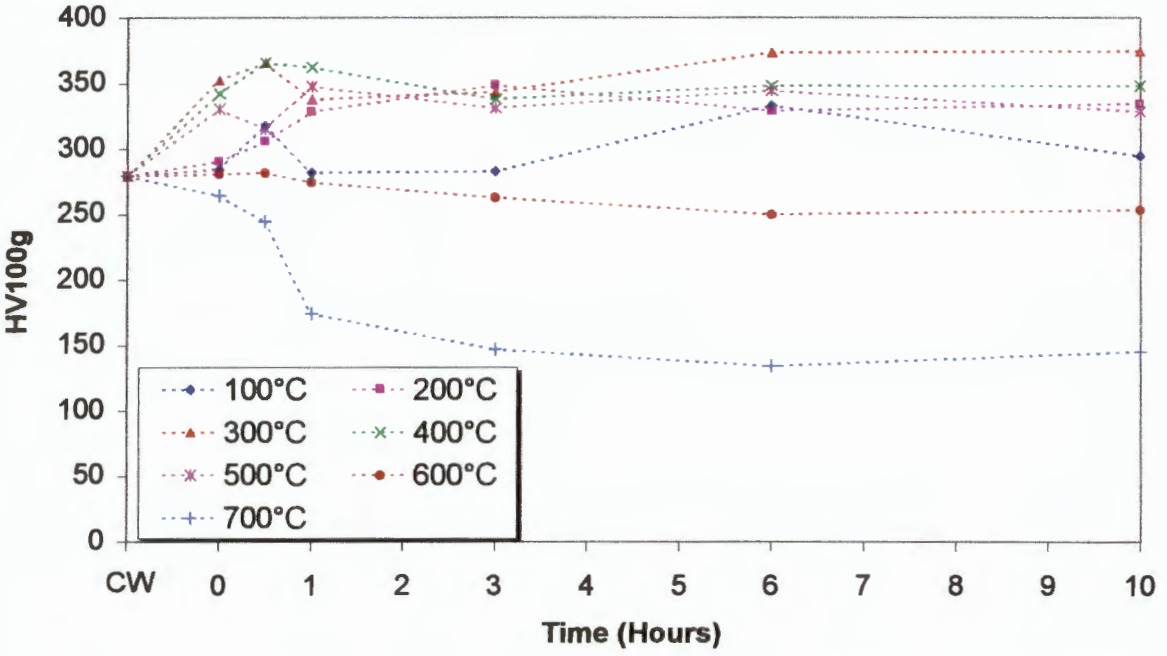

Figure 4.1.13 Combined graph of microhardness vs. annealing temperature for Pt 5 wt.% Cu for annealing temperatures ranging from 100°C to 700°C.

ISOCHRONAL ANNEALING OF Pt 5 wt% Cu AT TEMPERATURES BETWEEN 100°C AND 700°C.

ANNEALED FOR 0 HOURS

Graph a) in Figure 4.1.14 shows the results of heating Pt 5 wt% Cu to temperatures between 100°C - 700°C and cooling directly after the target temperatures had been reached. The graph shows that heating the specimens at temperatures up to 200°C produces a gradual increase in microhardness from the initial cold-worked hardness of HV 280 (100g, n=8, range 260 – 300). Heating up to 300°C produces a peak microhardness of HV 353 (100g, n=8, range 333 – 370), but once past 300°C there is a slow decrease. A minimum microhardness of HV 265 (100g, n=8, range 255 – 282) is obtained upon heating up to 700°C.

ANNEALED FOR 0.5 HOURS

The microhardness versus annealing temperature graph of Pt 5 wt% Cu annealed for 0.5 hours is shown in graph b) of Figure 4.1.14. An initial steady increase in microhardness is produced with a maximum of HV 366 (100g, n=8, range 346 – 385) occurring at an annealing temperature of 300°C. Annealing the specimen at 200°C produces a slight fall in microhardness below the value of the microhardness at 100°C, but the general trend between the cold-worked specimens and the specimen annealed at 300°C is an increasing microhardness. Annealing at 400°C produces a microhardness value of HV 366 (100g, n=8, range 354 – 383) which is very similar to annealing at 300°C. Once the annealing temperature is higher than 400°C a more significant decrease in microhardness occurs with a final value of HV 245 (100g, n=8, range 242 – 249) at 700°C.

ANNEALED FOR 1 HOUR

As with the two previous graphs, graph c) shows that annealing Pt 5 wt% Cu for 1 hour produces an initial increase in microhardness up to a maximum value of HV 362 (100g, n=8, 349 – 368) at 400°C. Annealing at temperatures higher than 400°C

shows a decrease in microhardness reaching a value of HV 174 (100g, n=8, range 155 – 199) at 700°C.

ANNEALED FOR 3 HOURS

Graph d), showing the resulting microhardness after annealing at temperatures between 100°C and 700°C is very similar to the graph in c). A maximum microhardness of HV 349 (100g, n=8, range 327 – 373) is achieved at an annealing temperature of 200°C, this is followed by a slow decrease in microhardness to an annealing temperature of 500°C. At temperatures higher than 500°C there is a rapid decrease in microhardness to a minimum value of HV 147 (100g, n=8, 138 – 151) at 700°C.

ANNEALED FOR 6 HOURS

As in graph b) of Figure 4.1.14, there is a general increasing trend of microhardness as the annealing temperature is increased, but the heat treatment at 200°C also producing a slight decrease in microhardness as compared to the one at 100°C. Annealing Pt 5 wt% Cu for 6 hours at 300°C produces the maximum hardness of HV 373 (100g, n=8, range 355 – 385). A small decrease in microhardness occurs when annealing at 400°C and 500°C. This is followed by a rapid decrease at 600°C and 700°C, reaching a final value of HV 134 (100g, n=8, 125 – 140).

ANNEALED FOR 10 HOURS

Annealing Pt 5 wt% Cu for 10 hours produces a very similar trend to the other 5 annealing times. There is an initial increase in microhardness reaching a maximum of HV 374 (100g, n=8, range 361 – 385) at 300°C followed by an initially slow then rapid decrease in microhardness. As with all the annealing times the 700°C temperature anneal yields the lowest hardness of HV 145 (100g, n=8, range 144 – 147).

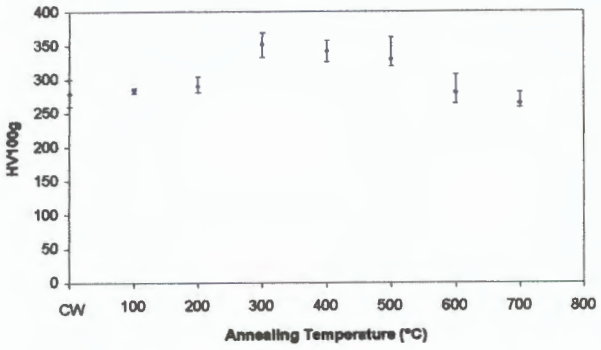

a) 0 Hours

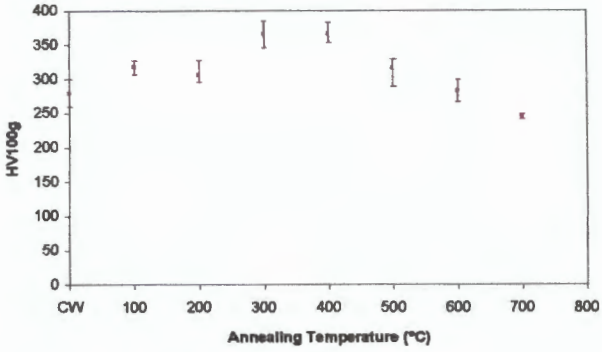

b) 0.5 Hour

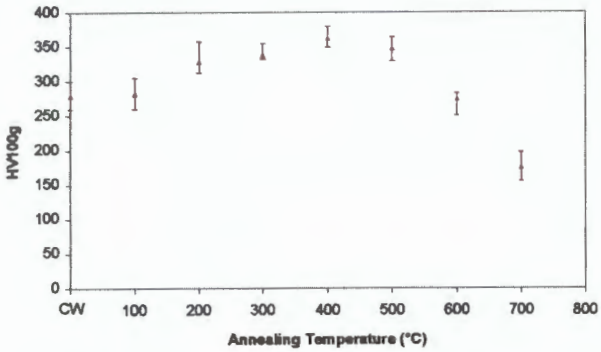

c) 1 Hour

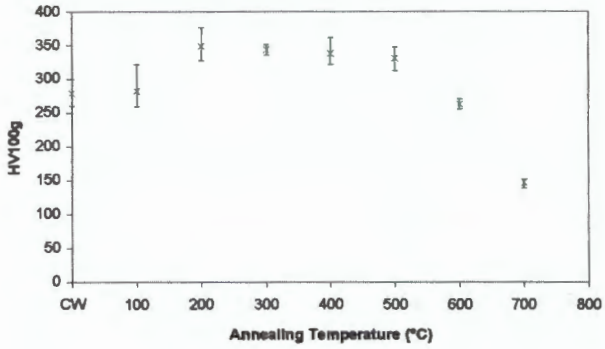

d) 3 Hours

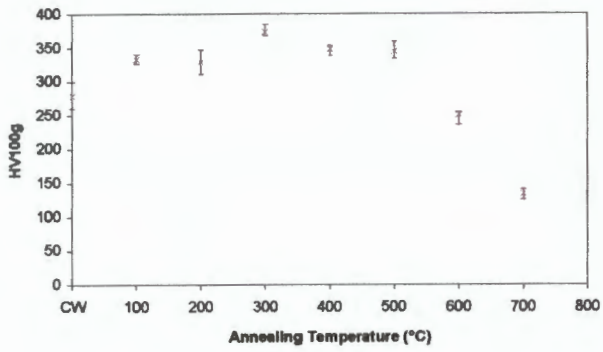

e) 6 Hours

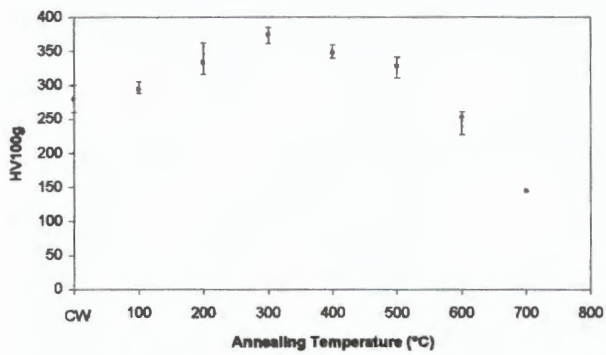

f) 10 Hours

Figure 4.1.14 Graphs of microhardness vs. annealing temperature for Pt 5 wt.% Cu annealed for times between 0 hours and 10 hours.

COMBINED GRAPH

The combined graph of microhardness versus annealing temperature for annealing times between 0 and 10 hours is shown in Figure 4.1.15. All of the annealing times show a similar hardening profile which increases from the cold-worked microhardness of HV 280 (100g, n=8, range 260 – 300), reaching a maximum between 200°C and 400°C. Once past the maximum, there is a decrease in microhardness with the heat treatment for 10 hours producing the lowest microhardness value. The only significant difference that can be seen from the results is in the final minimum value obtained at 700°C. When the alloy is annealed for times of 0 hours and 0.5 hours, significantly higher microhardness values are obtained than for annealing periods of 1 hour and greater. The 0 hour and 0.5 hour annealing times produce microhardness values of approximately HV 250 while the one hour to 10 hour annealing times only produce a maximum microhardness of HV 174 (100g, n=8, range 155 – 199).

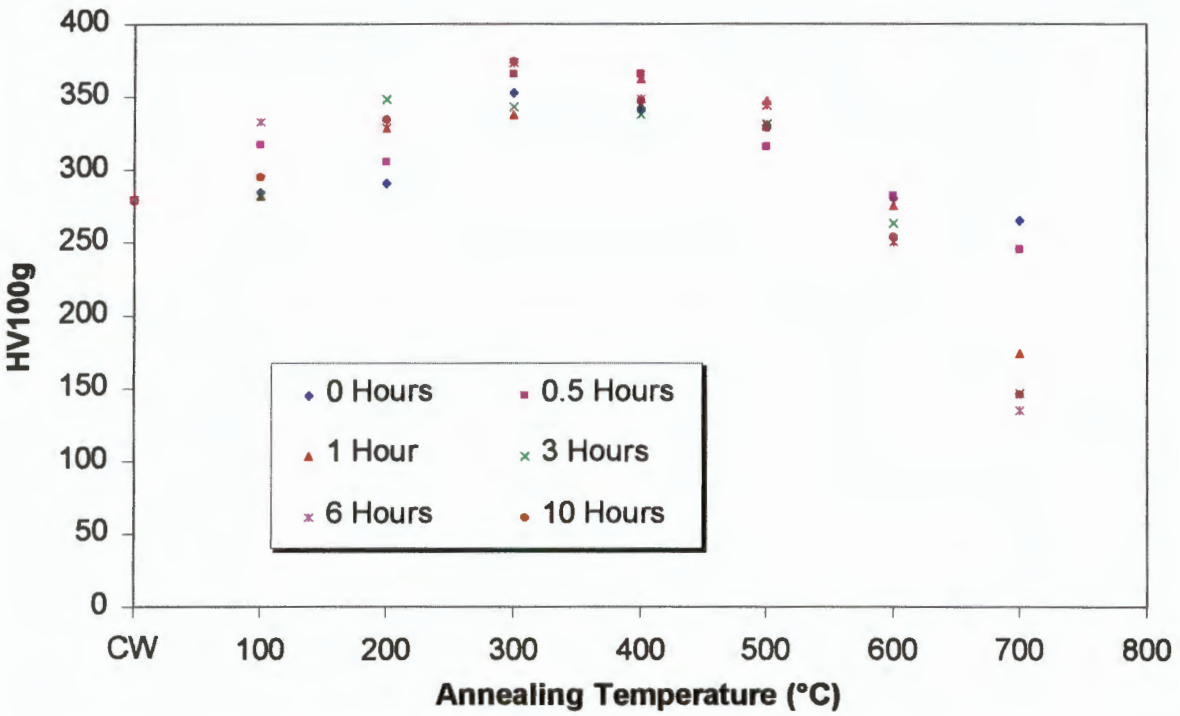

Figure 4.1.15 Combined graph of microhardness vs. annealing temperature for Pt 5 wt.% Cu annealed for times between 0 hours and 10 hours.

4.1.5 *COMBINED ISOCHRONAL ANNEALING OF THE THREE ALLOYS*

The maximum annealing temperature of the isochronal graphs of platinum-copper in Section 4.1.4 was only 700°C. Figure 4.1.16 shows the only graph in which Pt 5 wt% Cu has been annealed over 700°C. It shows, other than its hardness increase at low annealing temperatures discussed previously, an additional hardening at annealing temperatures above 1200°C. This hardness increase is very similar to what has been seen in Pt 5 at% Mo and Pt 5 wt% Ru but the degree of hardening is not as great. In addition, the Pt 5 wt% Cu alloy has an ultimate hardness of just below HV 350 at an annealing temperature of 400°C. Pt 5 at% Mo and Pt 5 wt% Ru achieve their peak hardness of approximately HV 275 at 1300°C and 1275°C respectively.

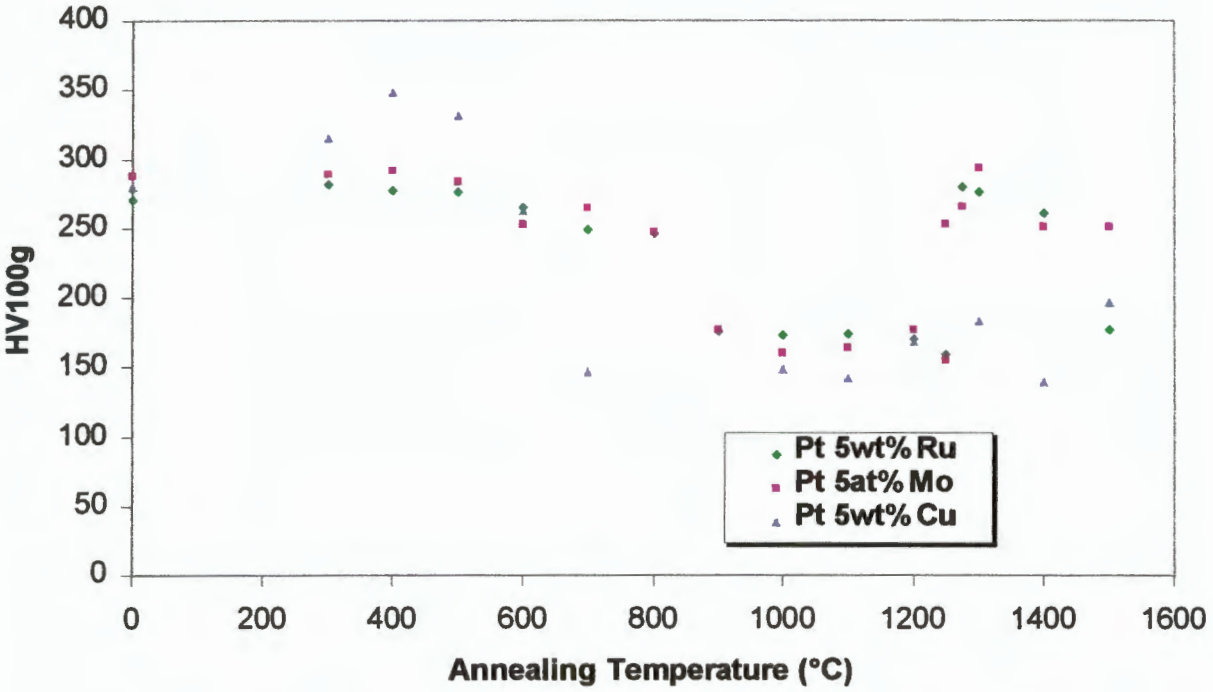

Figure 4.1.16 Combined graph of Pt 5 at% Mo, Pt 5 wt% Ru and Pt 5 wt% Cu annealed for 3 hours.

4.1.6 *EFFECT OF COOLING RATE ON MICROHARDNESS*

The preceding five sections of microhardness results are for specimens allowed to slow cool in the furnace to room temperature, after annealing. The microhardness results in this section are for selected specimens which were quenched directly into water and not allowed to cool slowly once annealing was complete. The corresponding microhardness value for the slow cooled tests have been included on the graphs that follow and are identified by a black circle with no error bars.

PLATINUM 5 at% MOLYBDENUM

Figure 4.1.17 shows the graph of microhardness vs. annealing temperature for test temperatures of 700°C, 1000°C and 1300°C followed by quenching. Annealing at 700°C shows a slight decrease in microhardness from that of the cold-worked specimen. A substantial change in microhardness is produced by annealing at 1000°C as the microhardness drops from HV 266 (100g, n=6, range 257-275) to HV 178 (100g, n=6, range 172-187). Annealing at 1300°C does not produce a significant change in microhardness from that seen in the 1000°C annealed condition.

When comparing quenched and slow cooled specimens it can be seen that the microhardness values for 700°C and 1000°C are very similar. It is only on annealing at 1300°C that a substantial difference can be seen. Slow cooling from 1300°C produces a microhardness of HV 294 (100g, n=8, range 278-310) whereas quenching produces a value of only HV 180 (100g, n=6, range 158-185).

PLATINUM 5 wt% RUTHENIUM

Figure 4.1.18 shows a graph of microhardness vs. annealing temperature for Pt 5 wt% Ru specimens that have been quenched from their annealing temperature. Annealing at 700°C does not produce a microhardness value that is very different from that of the cold-worked value. Annealing at 1000°C does however produce a large change in microhardness, as it decreases from HV 264 (100g, n=6, range 254-273) to HV 174 (100g, n=6, range 158-205). There is an additional slight decrease in microhardness after increasing the annealing temperature to 1300°C.

Comparing data for slow cooled specimens and quenched specimens, shows that the only major effect of changing the cooling rate occurs at 1300°C. Slow cooling Pt 5 w% Ru from 1300°C produces a high microhardness value of HV 276 (100g, n=6, range 266-285) while quenching only produces a value of HV 161.2 (100g, n=6, range 157-168).

PLATINUM 5 wt% COPPER ANNEALED FOR 0.5 HOURS

The graph in Figure 4.1.19 shows the effect of annealing for 0.5 hours then quenching the test specimen to room temperature. The microhardness value for the specimen annealed at 300°C is substantially higher than that of the cold-worked microhardness, peaking at HV 366 (100g, n=6, range 346-385). There is then a large decrease to a value of HV 245 (100g, n=6, range 242-249) at 700°C.

A comparison between quenched and slow cooled microhardness values at 300°C, show that they are very similar. The microhardness at 700°C is, however, slightly different with the slow cooled specimen producing a microhardness of HV 245 (100g, n=5, range 242-2249) and the quenched specimen HV 262 (100g, n=6, range 260-269).

PLATINUM 5 wt% COPPER ANNEALED FOR 10 HOURS

The graph in Figure 4.1.20 is very similar to 0.5 hours and shows the values of microhardness vs. annealing temperature for Pt 5 wt% Cu after quenching from temperature after annealing for 10 hours. The microhardness increases to a value of HV 374 (100g, n=6, range 361-385) at 300°C then falls sharply to a low value of only HV 145 (100g, n=6 range 144-146) at 700°C.

Comparison of the data shows a very similar trend with the microhardness values being nearly identical. After annealing at 300°C for 10 hours a specimen with a microhardness of HV 376 (100g, n=8, range 368-388) is produced for a slow cooled specimen and HV 374 (100g, n=6, range 361-385) for the quenched specimen. Annealing at 700°C produces a microhardness of HV 145 (100g,n=5, range 144-147) and HV 145 (100g,n=6, range 142-160) for the slow cooled and quenched specimens respectively.

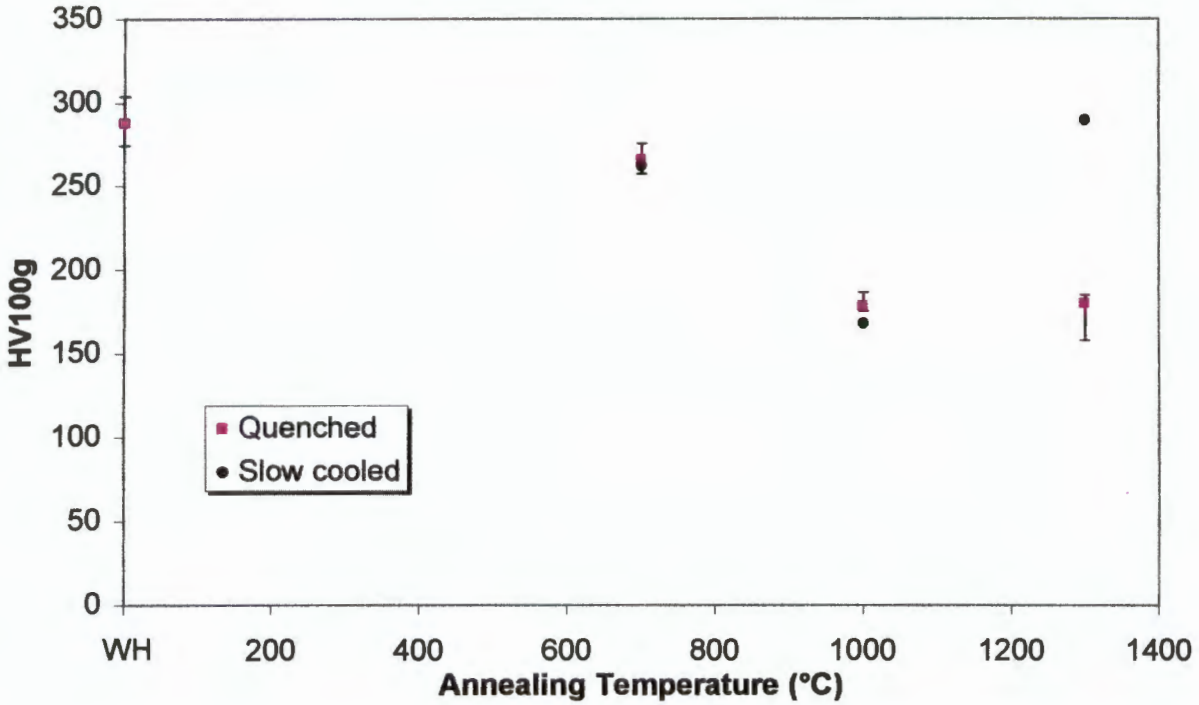

Figure 4.1.17 Graph of microhardness vs. annealing temperature for Pt 5 at% Mo annealed for 3 hours then quenched.

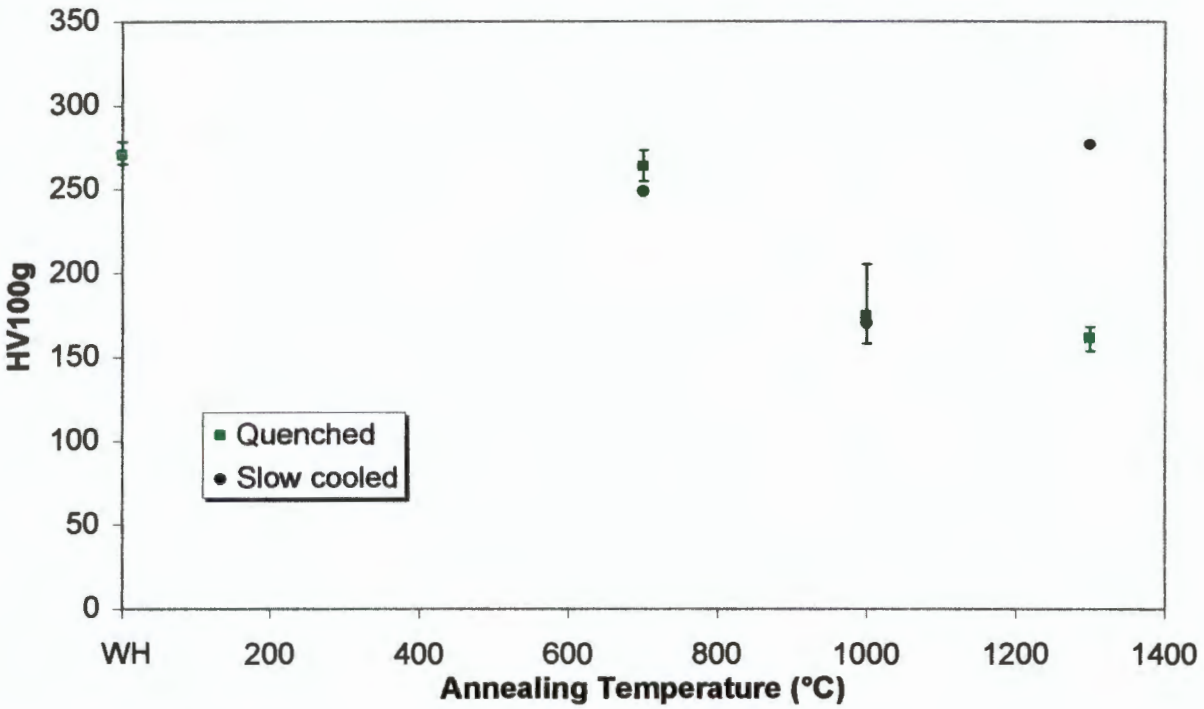

Figure 4.1.18 Graph of microhardness vs. annealing temperature for Pt 5 at% Ru annealed for 3 hours then quenched.

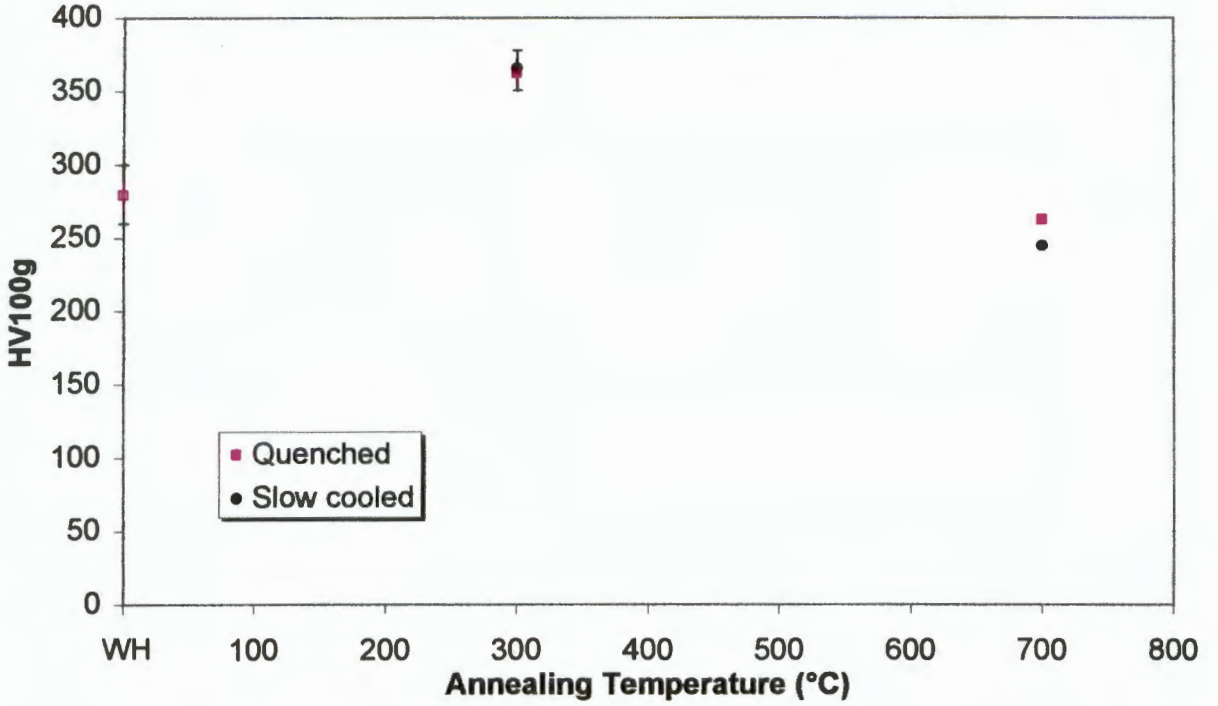

Figure 4.1.19 Graph of microhardness vs. annealing temperature for Pt 5 wt% Cu annealed at for 0.5 hours then quenched.

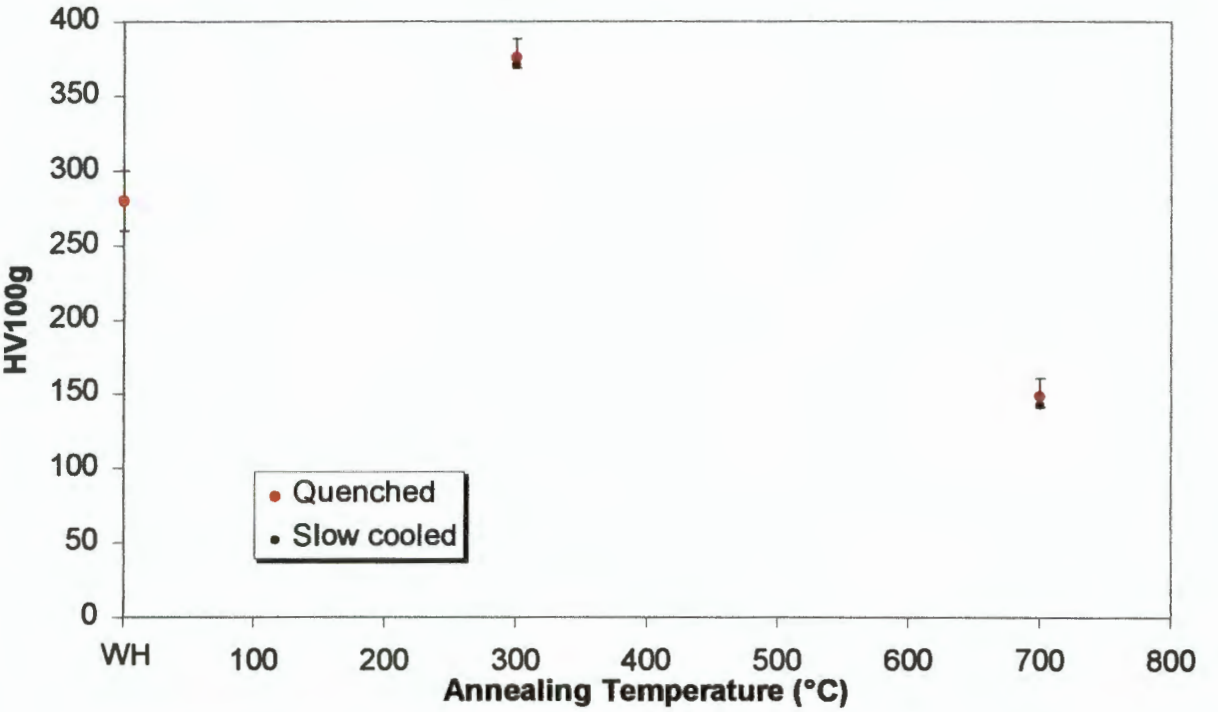

Figure 4.1.20 Graph of microhardness vs. annealing temperature for Pt 5 wt% Cu annealed for 10 hours then quenched.

4.2 OPTICAL MICROSCOPY

In order to assess the effect that heat treatment has on microstructure, optical microscopy techniques were employed. In the previous section, once the comprehensive annealing sequence had been completed, certain annealing conditions were selected for further quench testing and for annealing of pure platinum specimens. These same annealing conditions, in addition to the cold-worked condition, have been selected for optical microscopy purposes. The optical micrographs of Pt 5 at% Mo, Pt 5 wt% Ru and Pt 5 wt% Cu appear in Sections 4.2.1, 4.2.2 and 4.2.3 respectively.

4.2.1 PLATINUM 5 at% MOLYBDENUM

The microstructure of Pt 5 at% Mo in the cold worked condition can be seen in Figure 4.2.1, which shows heavily deformed grains with no clearly defined grain boundaries. The grains that can be distinguished are elongated and very large, of the order of millimeter size. If the same alloy is annealed at 700°C for 3 hours the microstructure changes to that seen in Figure 4.2.2. The micrographs show alternating light and dark areas which are similar to the internal structure of what appear to be grains in Figure 4.2.1, or could be highly deformed and elongated grains although all the specimens were deformed to the same degree.

Increasing the annealing temperature to 1000°C produces the microstructure seen in Figure 4.2.3. It consists of recrystallised grains but there is still evidence of the cold-worked structure in the top right of the micrograph. Annealing at 1300°C for 3 hours (Figure 4.2.4), produces a specimen containing only large, equiaxed, recrystallised grains with high angle grain boundaries. The grain size increases substantially when the annealing time was increased from 1000°C to 1300°C.

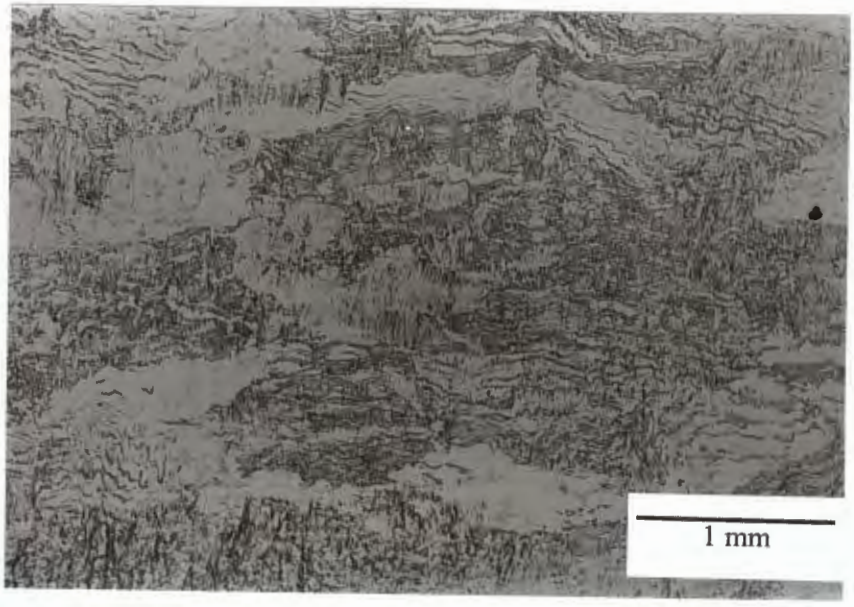

Figure 4.2.1 Optical micrographs of Pt 5 at% Mo in the cold-worked condition.

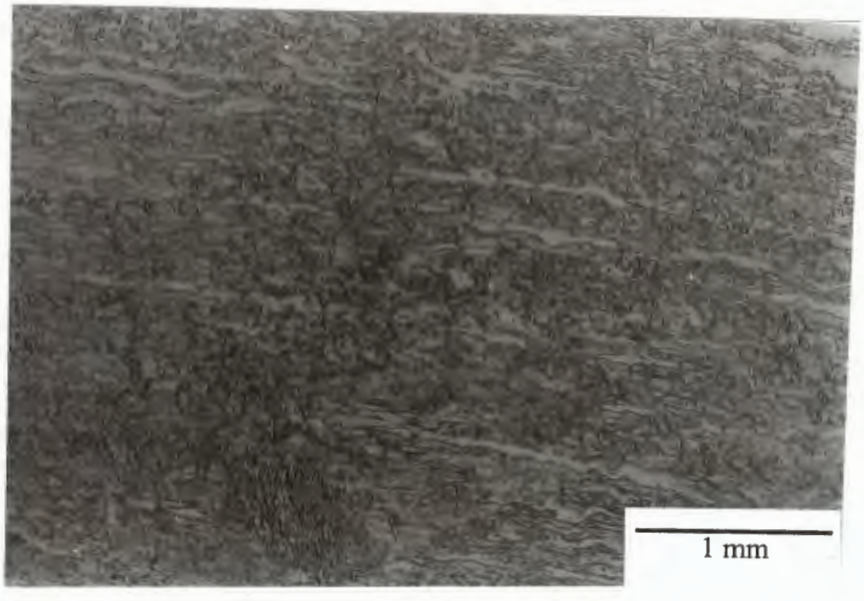

Figure 4.2.2 Optical micrograph of Pt 5 at% Mo annealed at 700°C for 3 hours.

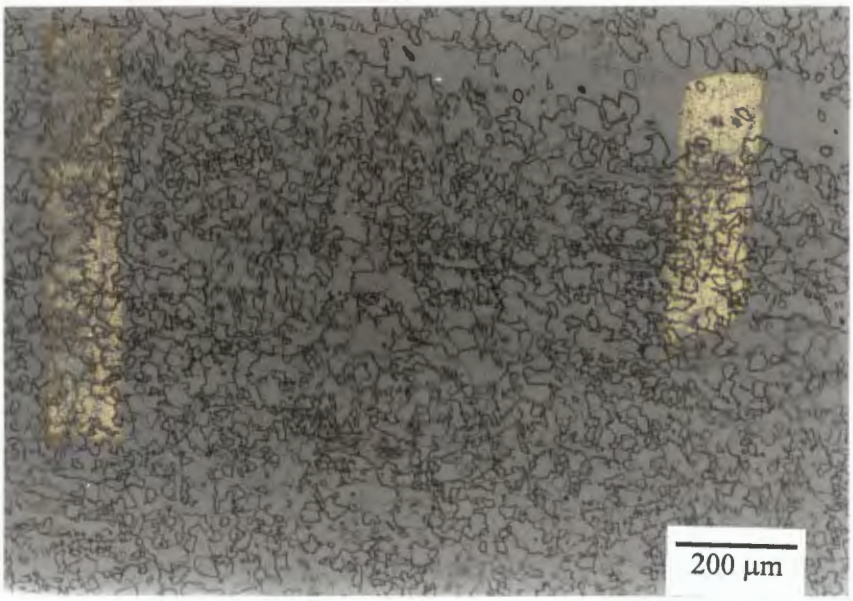

Figure 4.2.3 Optical micrograph of Pt 5 at% Mo annealed at 1000°C for 3 hours.

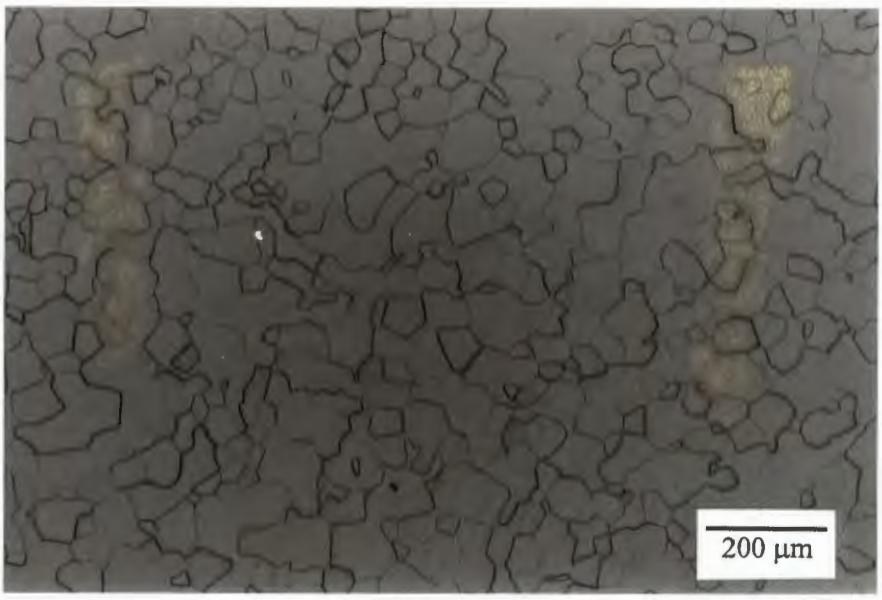

Figure 4.2.4 Optical micrograph of Pt 5 at% Mo annealed at 1300°C for 3 hours.

4.2.2 PLATINUM 5 wt% RUTHENIUM

The microstructure of cold-worked Pt 5 wt% Ru shown in Figure 4.2.5 is very similar to the microstructure of Pt 5 at% Mo shown in Figure 4.2.1. There are what appear to be large, elongated grains due to the cold-rolling but the grain boundaries are again very unclear. Figure 4.2.6 is a micrograph of Pt 5 wt% Ru after annealing for 3 hours at 700°C. There are certain areas of the image, (upper right-hand corner) that show a microstructure very similar to that seen in Figure 4.2.2 which consists of alternating light and dark bands. The surface of the specimen has more defined grain boundaries which are either very light in shading or dark. There are still, however, certain areas where the grains are difficult to differentiate.

Increasing the annealing temperature to 1000°C produces angular, irregular shaped recrystallised grains (Figure 4.2.7). The etch does not reveal all the grain boundaries but there is no evidence of the cold-worked grains seen in Pt 5 at% Mo (Figure 4.2.3). After annealing at 1300°C the microstructure consists entirely of equiaxed, recrystallised grains which have increased in size from annealing at 1000°C, but are still very angular with high angle grain boundaries.

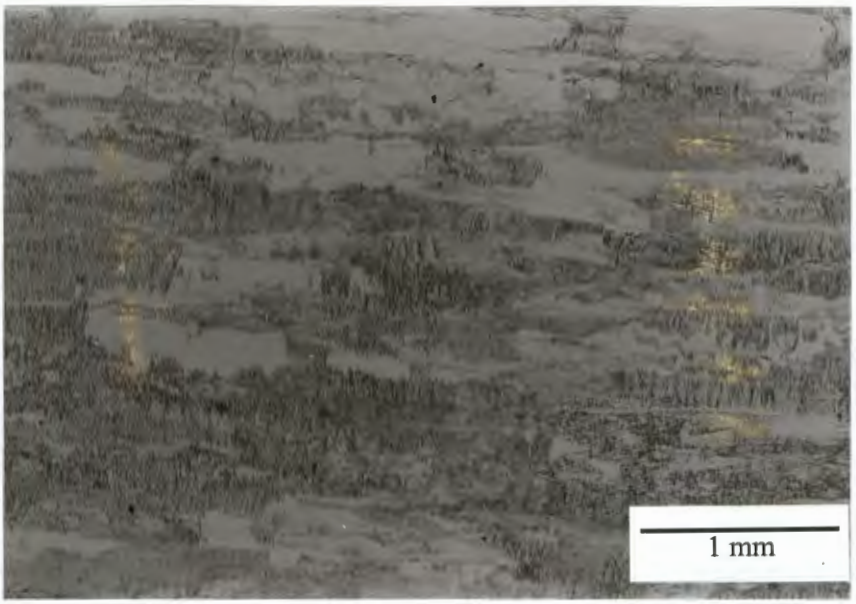

Figure 4.2.5 Optical micrograph of Pt 5 wt% Ru in the cold-worked condition.

Figure 4.2.6 Optical micrograph of Pt 5 wt% Ru annealed at 700°C for 3 hours.

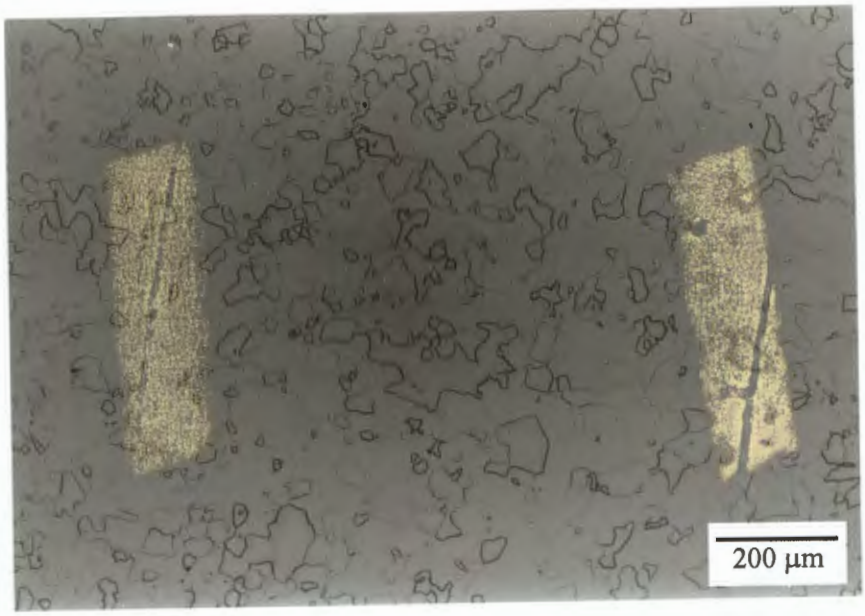

Figure 4.2.7 Optical micrograph of Pt 5 wt% Ru annealed at 1000°C for 3 hours.

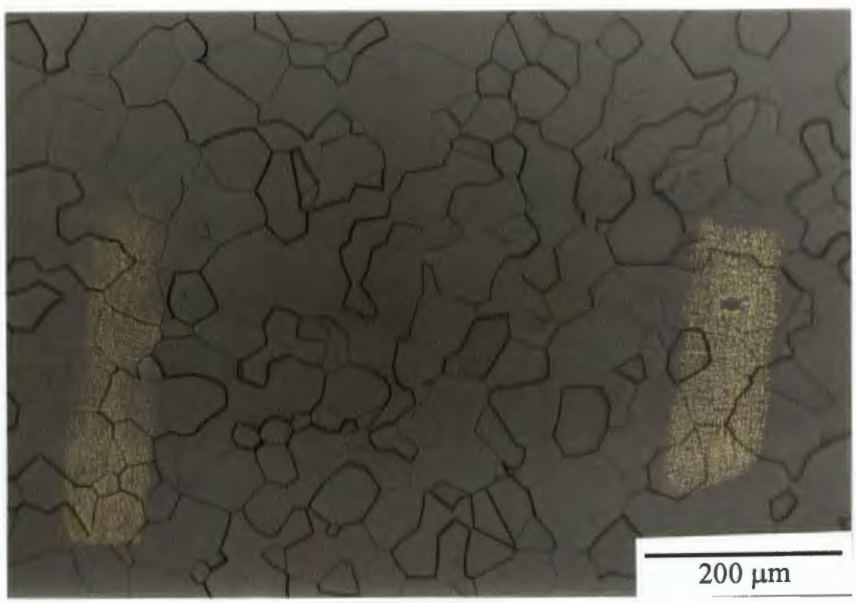

Figure 4.2.8 Optical micrograph of Pt 5 wt% Ru annealed at 1300°C for 3 hours.

4.2.3 PLATINUM 5 wt% COPPER

Pt 5 wt% Cu in the cold worked condition (Figure 4.2.9) is very similar to the cold-worked specimens of Pt 5 at% Mo and Pt 5 wt% Ru. There are light areas with no internal features and darker areas with a textured surface running perpendicular to the direction of grain elongation. Figure 4.2.10 shows Pt 5 wt% Cu annealed at 300°C for 0.5 hours and is very similar to Figure 4.2.9. Figure 4.2.11 is a micrograph of Pt 5 wt% Cu annealed at 300°C for 10 hours and also shows very large, elongated grains. The grain boundaries are, however, more difficult to differentiate.

If the annealing temperature is increased to 700°C the specimen undergoes partial recrystallisation. Figure 4.2.12, which shows a micrograph of Pt 5 wt% Cu annealed at 700°C for 0.5 hours shows a partially recrystallised microstructure with equiaxed recystallised grains growing in what is still a predominately cold-worked structure. The new grains are nucleating predominately in the formally darker cold worked grains. Increasing the annealing time to 10 hours (Figure 4.2.13) produces a microstructure consisting entirely of recrystallised grains with irregular angular shapes. There is no evidence of the cold worked structure but unetched areas are visible creating a mottled appearance on the specimen surface.

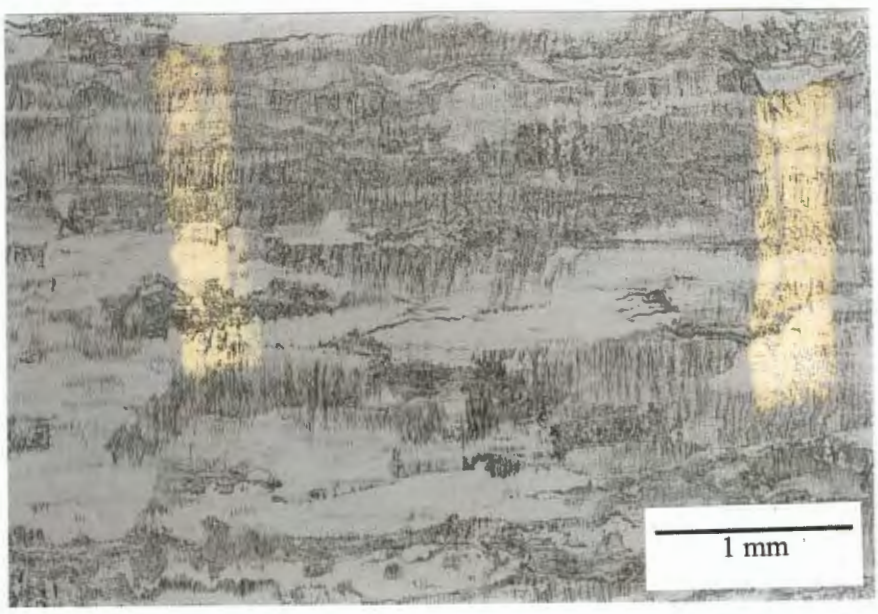

Figure 4.2.9 Optical micrograph of Pt 5 wt% Cu in the cold worked condition.

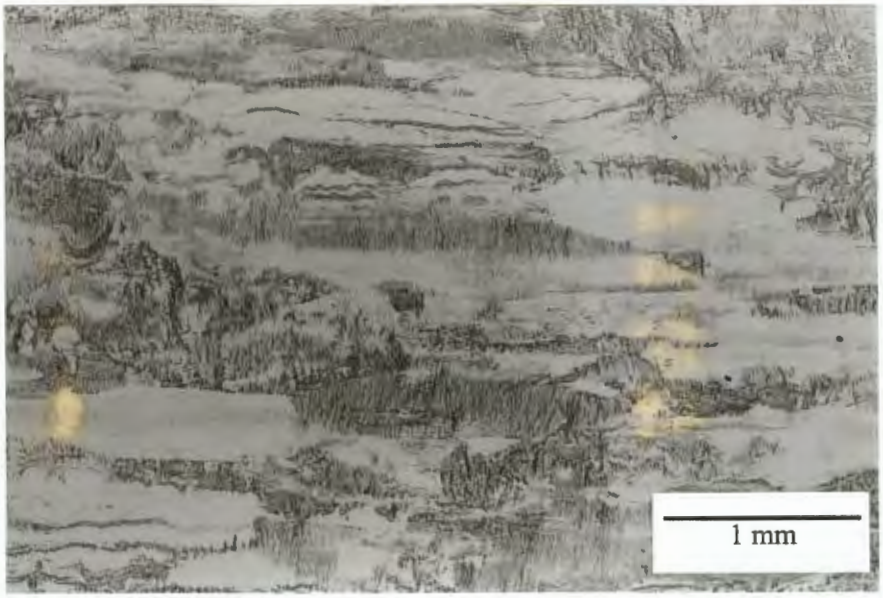

Figure 4.2.10 Optical micrograph of Pt 5 wt% Cu annealed at 300°C for 0.5 hours.

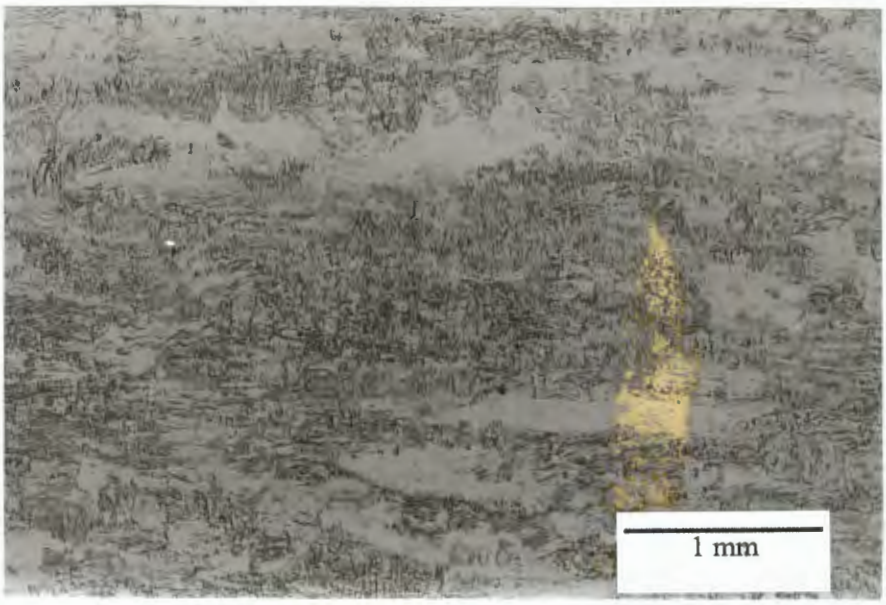

Figure 4.2.11 Optical micrograph of Pt 5 wt% Cu annealed at 300°C for 10 hours.

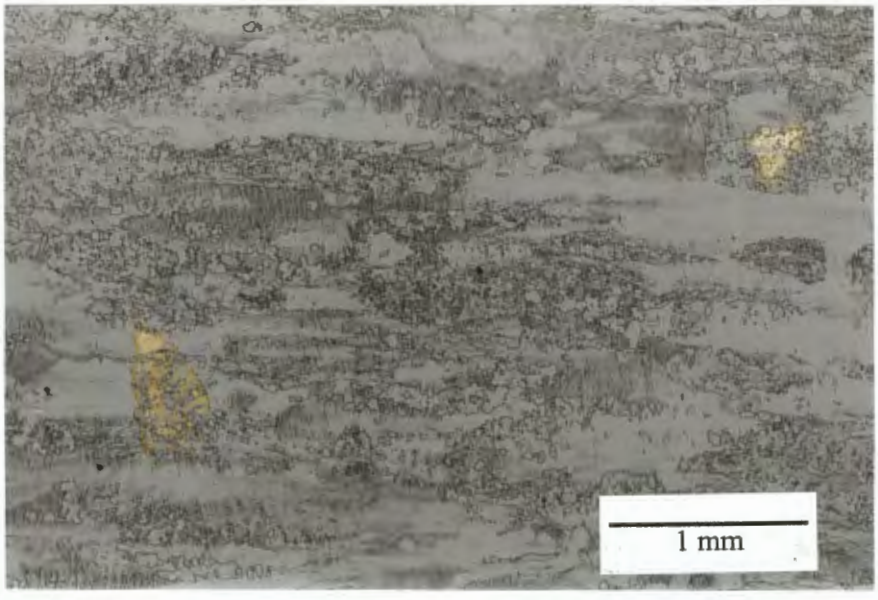

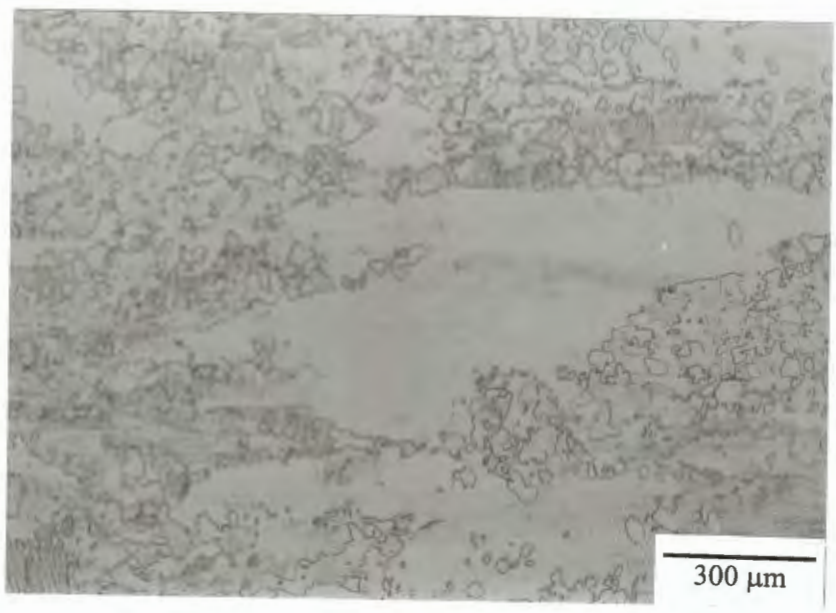

Figure 4.2.12 Optical micrographs of Pt 5 wt% Cu annealed at 700°C for 0.5 hours.

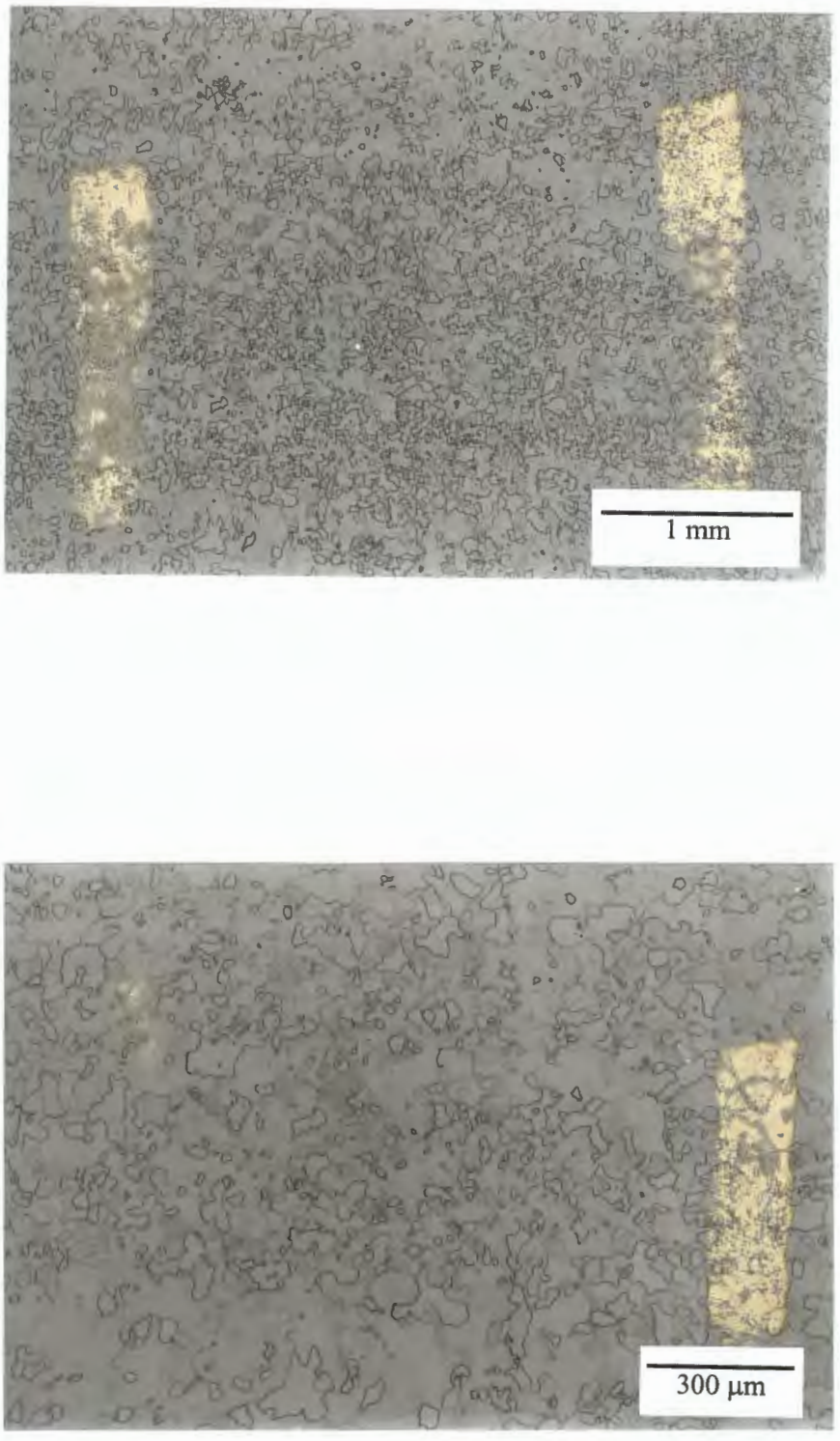

Figure 4.2.13 Optical micrographs of Pt 5 wt% Cu annealed at 700°C for 10 hours.

4.3 SCANNING ELECTRON MICROSCOPY

Specimens for scanning electron microscopy were prepared by annealing specimens of the platinum-molybdenum and platinum-ruthenium alloys at 1300°C for 3 hours and the platinum-copper alloy at 300°C for 0.5 hours and 10 hours. These are the annealing conditions that produced specimens with an increased hardness. The specimens were viewed in the scanning electron microscope using both the secondary electron and backscattered imaging mode, to look for any stable precipitates that might not be resolved using the optical microscope.

4.3.1 PLATINUM 5 at% MOLYBDENUM AND PLATINUM 5 wt% RUTHENIUM ANNEALED AT 1300°C FOR 3 HOURS.

The experimental alloys containing 5 at% Mo and 5 wt% Ru showed very similar images. The secondary electron images shown in Figure 4.3.1 and Figure 4.3.2 show very straight grain boundaries with very angular intersections, which have been revealed by the etchant. There is no clear evidence of precipitate formation on the grain boundaries or within the grains. The grains that have been preferentially etched do, however, show a textured surface but this could be an artefact of the specimen preparation.

The backscattered images again show very defined grains revealed by crystallographic differences from one grain to another. In addition, the Pt 5 at% Mo specimen shows some evidence of grain boundary separation which has been indicated by the arrows in Figure 4.3.3 and Figure 4.3.4. Other than the porosity resulting from this separation, there is no evidence of any other stable structure on the grain boundaries or in the grain interiors. Figure 4.3.5, a backscattered image of Pt 5 wt% Ru annealed for 3 hours at 1300°C, also shows the same well defined grain structure seen in Pt 5 at% Mo (Figure 4.3.3 and Figure 4.3.4). It does not, however, show any evidence of grain boundary separation.

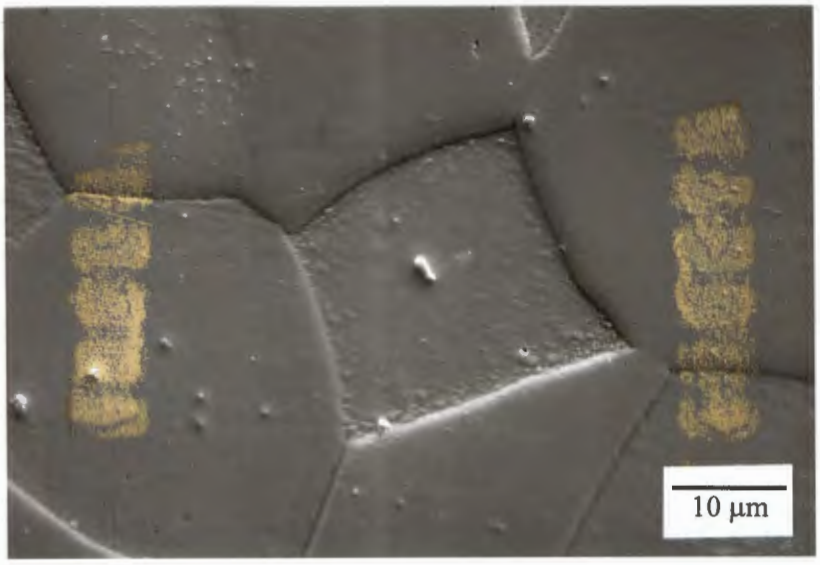

Figure 4.3.1 Secondary electron image of Pt 5 at% Mo annealed at 1300°C for 3 hours showing straight grain boundaries with angular interceptions.

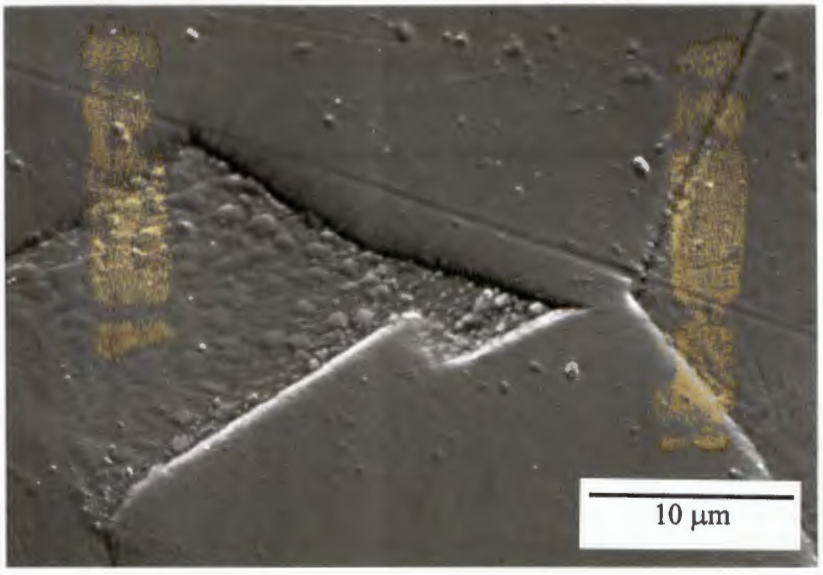

Figure 4.3.2 Secondary electron image of Pt 5 at% Mo annealed at 1300°C for 3 hours showing evidence of a textured surface.

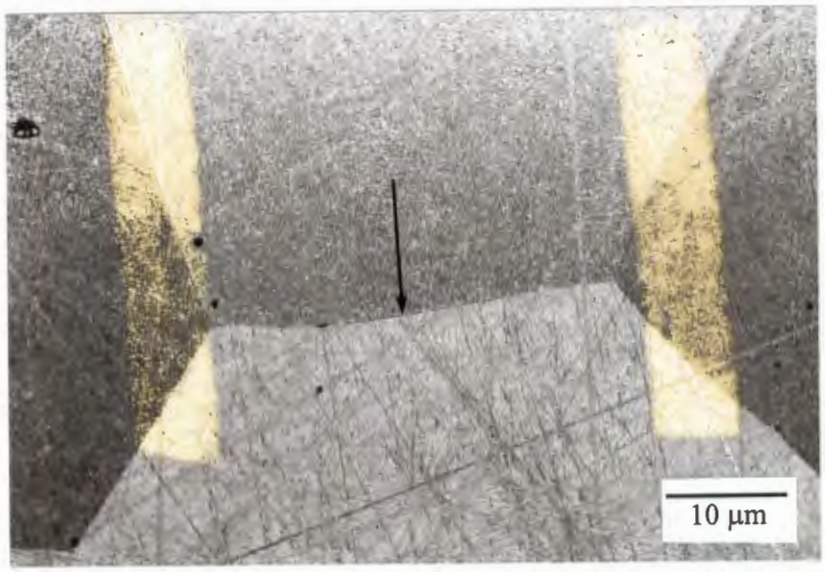

Figure 4.3.3 Backscattered image of Pt 5 at% Mo annealed at 1300°C for 3 hours showing evidence of grain boundary separation but no precipitation along grain boundaries is visible.

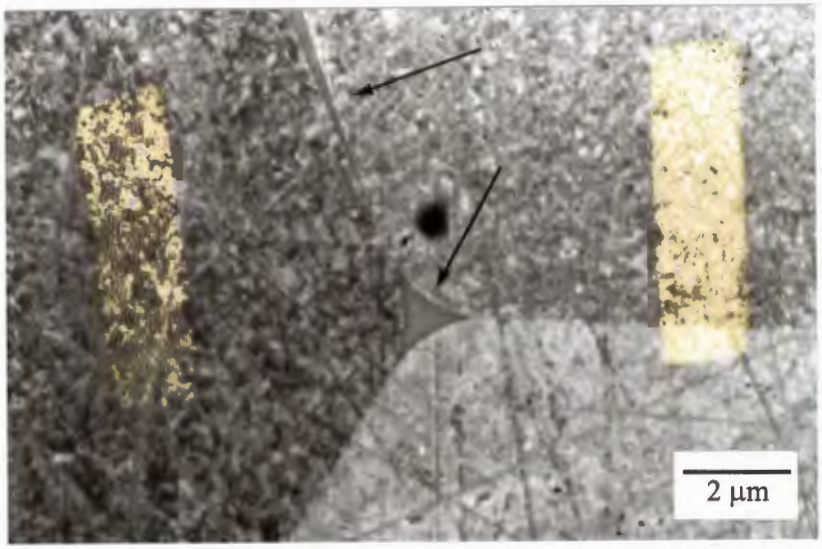

Figure 4.3.4 High magnification backscattered image of the grain boundary separation in Pt 5 at% Mo.

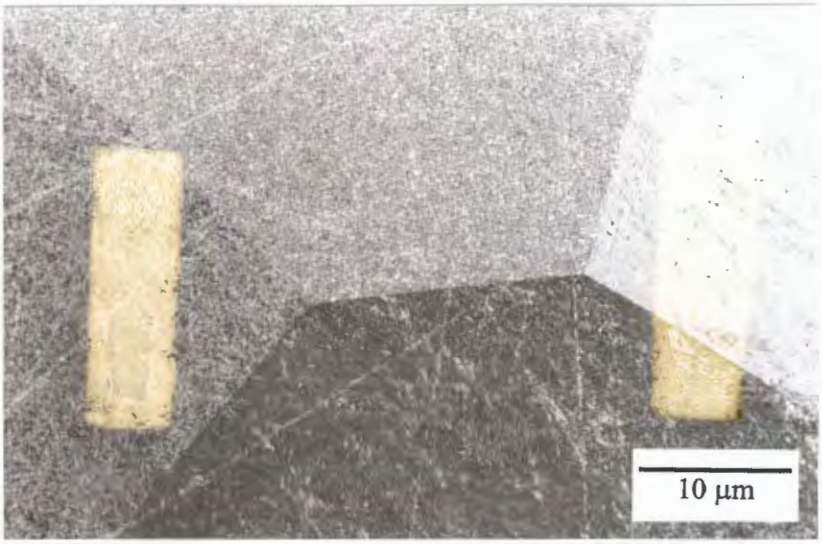

Figure 4.3.5 Backscattered image of Pt 5 wt% Ru showing sharply defined grains but no grain boundary separation or precipitation.

4.3.2 *PLATINUM 5 wt% COPPER ANNEALED AT 300°C FOR 0.5 AND 10 HOURS*

The Pt 5 wt % Cu specimens annealed at 300°C for differing time periods showed very similar microstructures. The secondary electron images shown in Figure 4.3.6 and Figure 4.3.7 do not show clearly defined grain boundaries as was seen in the SEM micrographs for the platinum-molybdenum and platinum-ruthenium alloys. There is also no evidence of any stable precipitation. This is also true of the backscattered images seen in Figure 4.3.8. The backscattered images do, however, show elongated grain boundaries running from top to bottom of the micrograph. Figure 4.3.7 shows evidence of the textured surface seen in the optical micrographs in Figure 4.2.9 and Figure 4.2.10.

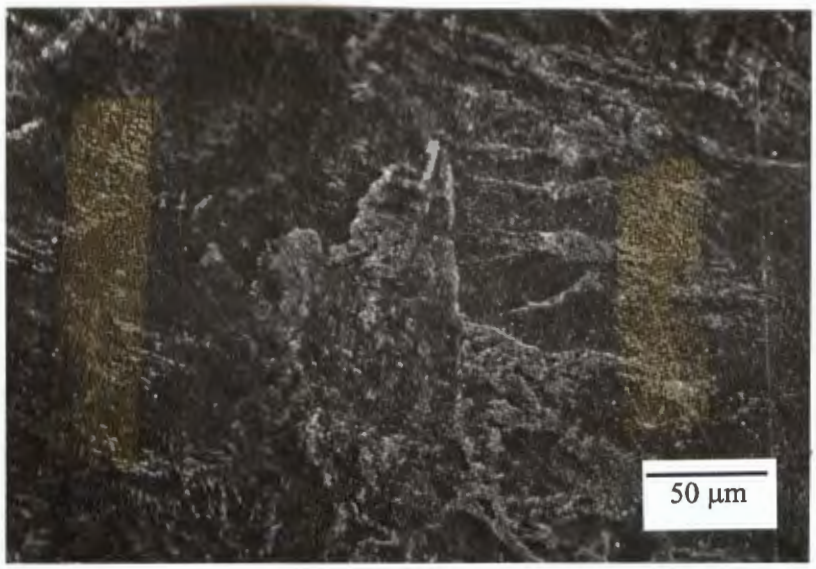

Figure 4.3.6 Secondary electron image of Pt 5 wt% Cu annealed at 300°C for 0.5 hours showing poorly defined grain boundaries and no evidence of precipitation.

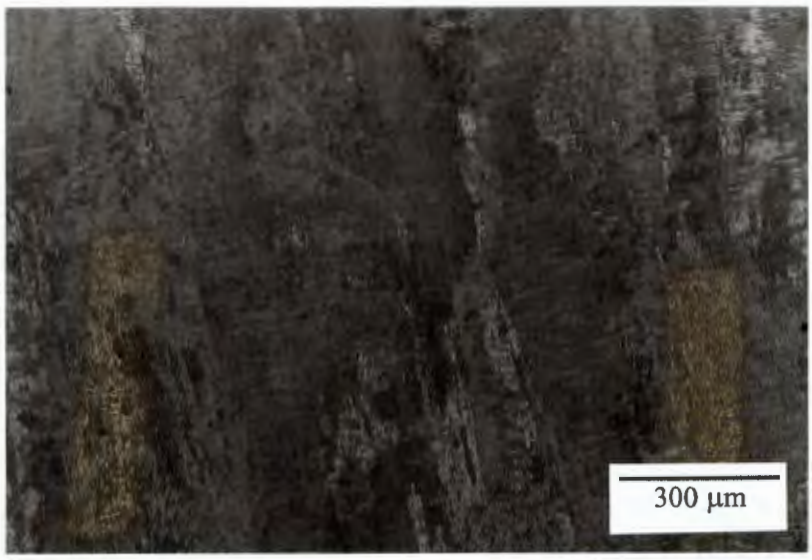

Figure 4.3.7 Backscattered images of Pt 5 wt% Cu annealed at 300°C for 0.5 hours showing grain elongation as well as the textured surface effect running perpendicular to the grain elongation.

Figure 4.3.8 High magnification backscattered images of Pt 5 wt% Cu annealed at 300°C for 0.5 hours showing grain elongation.

4.4 TRANSMISSION ELECTRON MICROSCOPY

The section that follows on transmission electron microscopy represents a preliminary investigation to aid any further research that might be carried out on these or similar types of alloys. Only the platinum-molybdenum and platinum-ruthenium alloys were investigated using TEM due to time and equipment constraints.

4.4.1 CRYSTAL STRUCTURE

Selected area zone-axis electron diffraction patterns from the Pt 5 at% Mo and Pt 5 wt% Ru specimens, annealed at 1300°C for 3 hours were investigated. Electron diffraction patterns of the high symmetry [001] and [112] zone axes were taken from the Pt 5 wt% Ru specimen and [001], [112] and [111] zone axes for Pt 5 at% Mo.

Figure 4.4.1 and Figure 4.4.2 show zone axis diffraction patterns from Pt 5 at% Mo after annealing at 1300°C for 3 hours. Additional reflections can be seen in all three zone axes diffraction patterns. Additional diffuse scattering can be seen in the [111] zone axis diffraction pattern at 1/3242-type positions. There are also additional sharper reflections associated with the reflections at 1/3242-type positions as well as a ring around the transmitted beam. The additional reflections seen in the diffraction pattern for the [112] zone axis are at 1/2220-type positions. The reflections are not singular but consist of a group of two or more. The extra reflections in the [001] zone axis are not very clear but a clustering of two extra reflections can just be seen at 1/2220-type positions. The intensity of the transmitted beam is overexposed, but this is necessary to reveal the very faint extra reflections.

Bright and dark-field images have been recorded from the additional reflections by placing the objective aperture over the centered additional reflection. This has been done in order to determine the microstructural features from which these additional reflections arise. The bright-field images are shown in Figure 4.4.3 and contain a precipitate-like structure. A close examination of the precipitate-like structure reveals a streaking effect which is more predominant on the outer edge.

Figure 4.4.4 shows a bright-field (a) and dark-field (b) image obtained by using the 1/2220-type reflection. Both images show the distribution of the fine precipitate-like structure seen in Figure 4.4.3

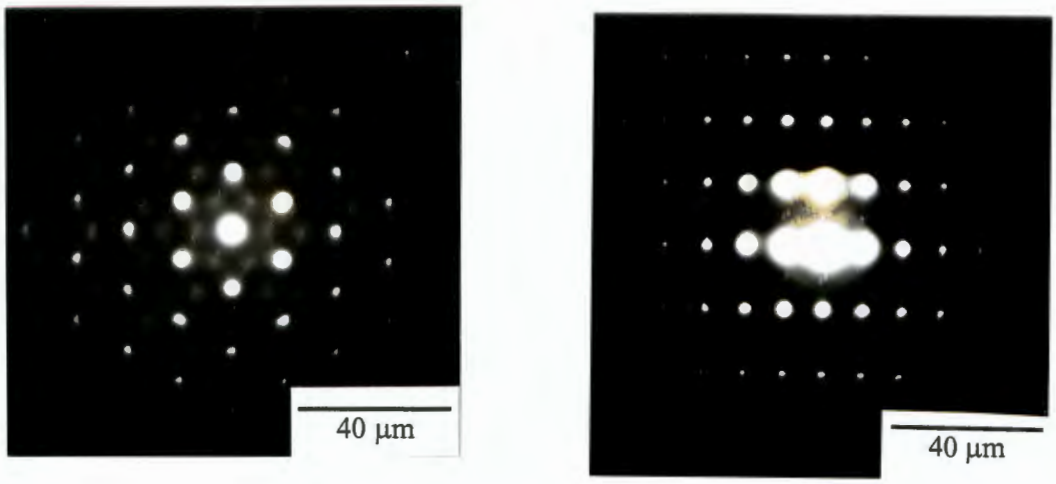

Figure 4.4.1 Electron diffraction patterns from Pt 5 at% Mo annealed at 1300°C for 3 hours: (a) [111] zone axis showing additional reflections at 1/3242-type positions (b) [112] zone axis showing additional reflections at the 1/2220-type positions.

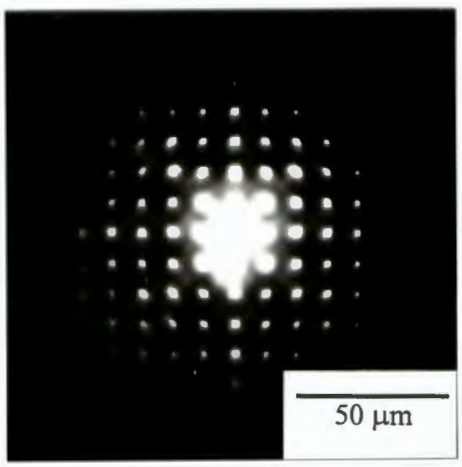

Figure 4.4.2 Electron diffraction pattern from Pt 5 at% Mo annealed at 1300°C for 3 hours: (a) [001] zone axis showing additional reflections at 1/2220-type positions.

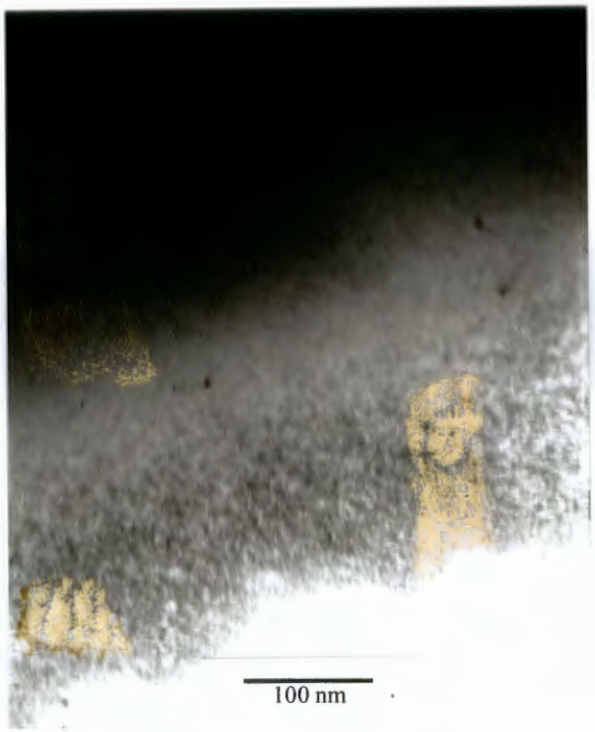

Figure 4.4.3 Pt 5 at% Mo after annealing at 1300°C: Bright-field images showing precipitate-type structure.

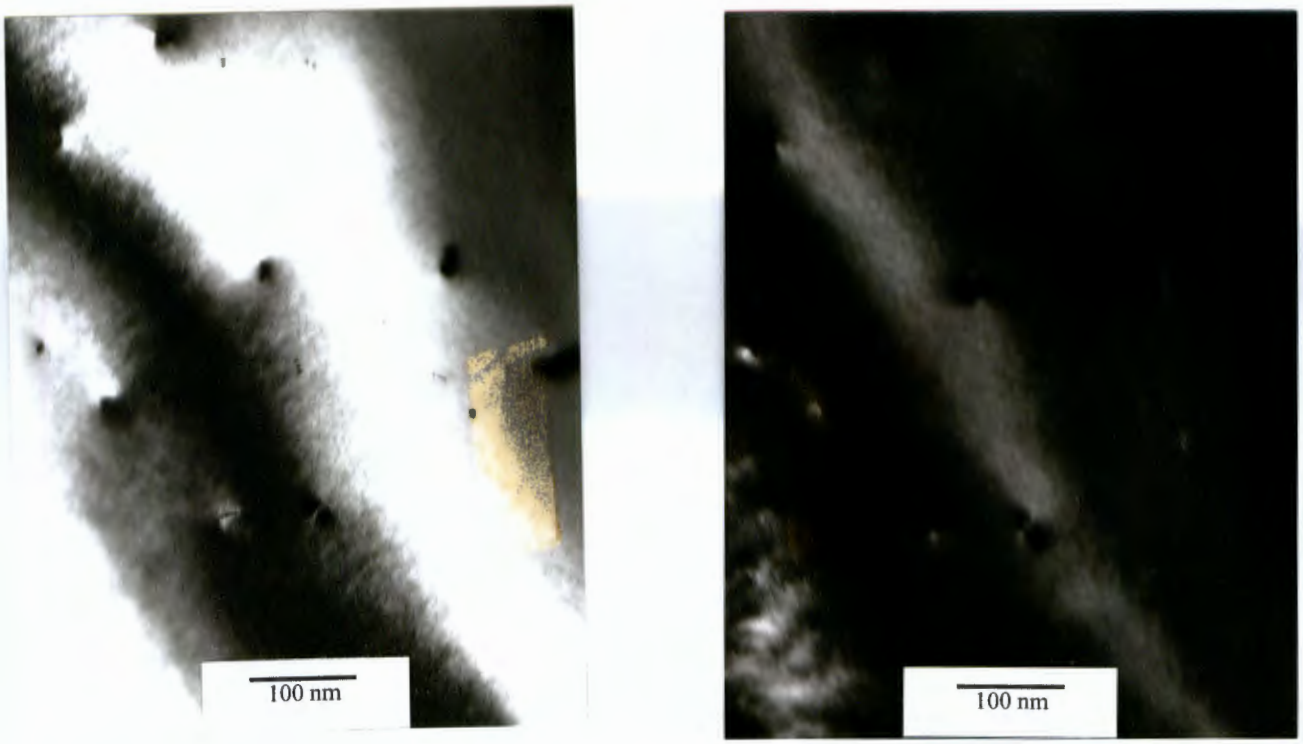

Figure 4.4.4 Pt 5 at% Mo after annealing at 1300°C: (a) bright-field image (b) dark-field image using 1/2220-type reflection showing distribution of precipitate-type structure.

Figure 4.4.5 shows a zone axis diffraction patterns from Pt 5 wt% Ru annealed at 1300°C for three hours. Additional reflections are observed in the 1/2131-type position in the [112] zone axis diffraction pattern. The extra reflection are again not sharp single spots but consist of a diffuse centre region flanked by two other, additional reflections on opposite sides.

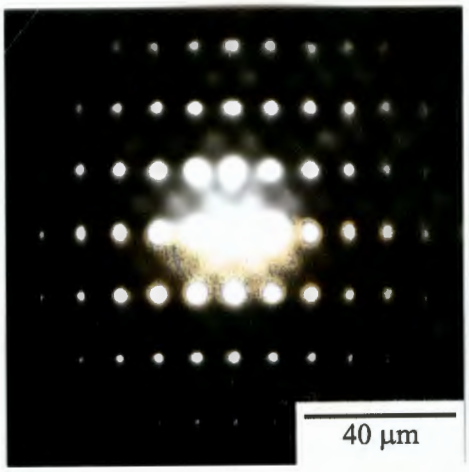

Figure 4.4.5 Electron diffraction patterns from Pt 5 at% Ru annealed at 1300°C for 3 hours: [112] zone axis showing additional reflections at the 1/2131-type positions.

4.5 RESISTIVITY

Resistivity is the sum of both residual and ideal resistivity components. Residual resistivity changes shift the curve in the y-direction while ideal resistivity changes will effect the gradient of the curve. Both y-shift and gradient changes should be monitored for possible transformations. Only one specimen from each alloy was tested but each specimen was tested three times. The first test was on the cold-worked specimen, which, once cooled back to room temperature was retested in an identical manner to the first. This twice tested specimen, was restested for a third time. This was done in order to assess the effect that annealing has on resistivity. Representative graphs are presented here; the full results can be found in Appendix A.

4.5.1 *RESISTIVITY TEST ON INITIALY COLD-WORKED SPECIMENS*

Figure 4.5.1 shows a resistivity vs. temperature graph of Pt 5 at% Mo tested in the cold-worked condition. This graph has been selected from the resistivity testing found in Appendix A, and is also typical of what was seen for Pt 5 wt% Ru and Pt 5 wt% Cu. The first tests, on the specimens in the cold-worked condition, show an almost linear relationship between resistivity and temperature with little variation in gradient, similar to the pure platinum graph in Figure 3.6.1. The graph in Figure 4.5.1 does, however, show a slight gradient change at approximately 600°C but this is not observed in Pt 5 wt% Ru or Pt 5 wt% Cu.

4.5.2 *RESISTIVITY TESTS ON RETESTED SPECIMENS*

Figure 4.5.2 and Figure 4.5.3 are of Pt 5 at% Mo and Pt 5 wt% Cu restested once respectively. They do not show the near linear relationship between resistivity and temperature seen in the cold-worked specimens. Pt 5 at% Mo in Figure 4.5.2 shows large resistivity variation with the largest occurring at 550°C. Pt 5 wt% Cu in Figure 4.5.3 shows a similar, but larger resistivity change at 600°C. These changes in

resistivity are common to the specimens that have been retested for resistivity vs temperature, with these two graphs isolated from the rest seen in Appendix A.

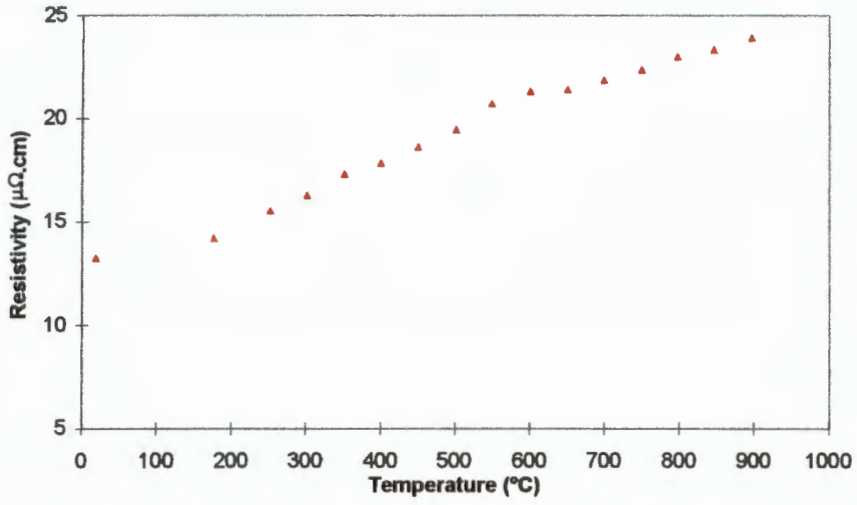

Figure 4.5.1 Resistivity vs. temperature graph for cold-worked Pt 5 at% Mo.

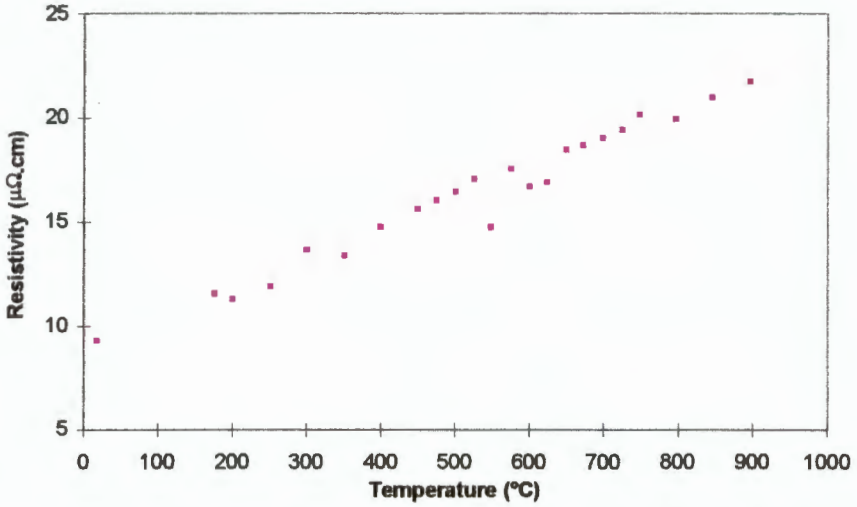

Figure 4.5.2 Resistivity vs. temperature graph for Pt 5 at% Mo retested once.

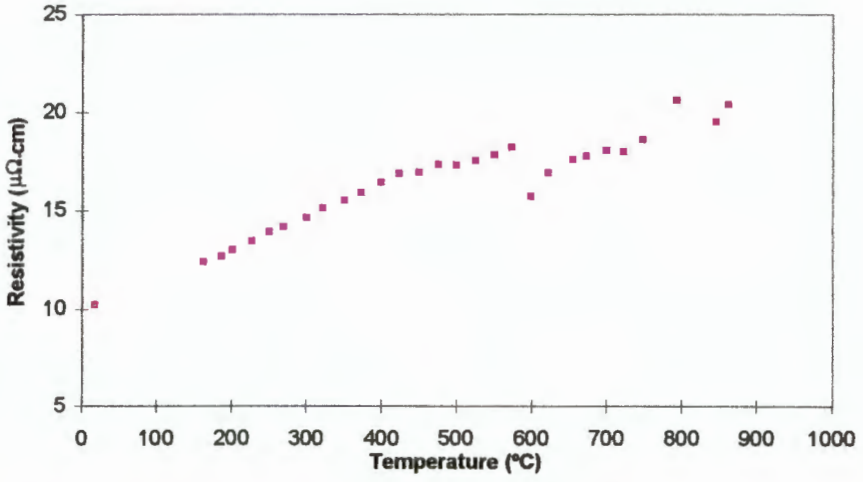

Figure 4.5.3 Resistivity vs. temperature graph for Pt 5 wt% Cu retested once.

4.6 X-RAY DIFFRACTION

The same specimens that were selected for optical microscopy purposes were also used for XRD. In addition, pure platinum specimens in the cold-worked and the annealed condition were tested. Selected, representative spectra of pure platinum and the three experimental alloys are displayed and reported on in this section but the majority of the XRD spectra can be found in Appendix B. The XRD results for Pt 5 wt% Cu are in Section 4.6.2 which is separate to Section 4.6.1 containing the results for pure platinum, Pt 5 at% Mo and Pt 5 wt% Ru. It should be noted that certain spectra have been influenced by the polymeric backing used to support the specimen during XRD testing.

4.6.1 *X-RAY DIFFRACTION SPECTRA OBTAINED FROM PURE PLATINUM, PLATINUM-MOLYBDENUM AND PLATINUM-RUTHENIUM.*

The XRD spectra obtained from pure platinum, Pt 5 at% Mo and Pt 5 wt% Ru in the annealed and cold-worked condition are all very similar and are typical of those shown in Figure 4.6.1 and Figure 4.6.2. XRD spectra of additional specimens can be found in Appendix B.

Comparison of Figure 4.6.1 and Figure 4.6.2 shows that a noticeable sub-peak has formed on the major peak at a 2θ angle of 81°. This peak corresponds to a d-spacing of 1.18 Angstroms which is the {311} family of planes. This type of sub-peak could be seen on all the Pt 5 at% Mo alloy specimens annealed over 700°C.

Table 4.2, Table 4.3 and Table 4.4 summarise the major peaks obtained from the systematic series of XRD testing on pure platinum, Pt 5 at% Mo and Pt 5 wt% Ru respectively. In addition to the peaks summarised in the tables, some XRD spectra showed many additional peaks not seen previously in any XRD spectra of platinum or platinum alloy, or stated in the Powder Diffraction File[73]. Figure 4.6.1 and Figure 4.6.2 show one of the unexpected peaks at a 2θ angle of approximately 20°. This very

broad peak is suspected to be due to the polymeric resin used to support the specimens during testing. An XRD spectra of the polymeric resin can be seen in Appendix C1. A second polymeric base was also used to support some of the specimens and produces the XRD spectra seen in Appendix C2.

Table 4.1 Table of d-spacings for pure platinum.

	(111)	(311)	(200)	(220)	(222)
Cold-worked	Y	N	N	N	N
700°C 3 hours	Y	Y	Y	Y	Y
1000°C 3 hours	Y	Y	Y	Y	N
1300°C 3 hours	Y	Y	Y	Y	Y
300°C 0.5 hours	Y	Y	N	Y	Y
300°C 10 hours	Y	Y	Y	Y	N
700°C 0.5 hours	Y	Y	Y	Y	Y
700°C 10 hours	Y	Y	Y	Y	Y

Table 4.2 Table of d-spacings for Pt 5 at% Mo.

	(111)	(311)	(200)	(220)	(222)
Cold-worked	Y	Y	Y	Y	N
700°C 3 hours	Y	Y	Y	Y	N
1000°C 3 hours	N	Y	Y	Y	N
1300°C 3 hours	N	Y	Y	Y	Y

Table 4.3 Table of d-spacings for Pt 5 wt% Ru.

	(111)	(311)	(200)	(220)	(222)
Cold-worked	Y	Y	Y	Y	N
700°C 3 hours	Y	Y	Y	Y	N
1000°C 3 hours	Y	Y	Y	Y	N
1300°C 3 hours	N	Y	Y	Y	N

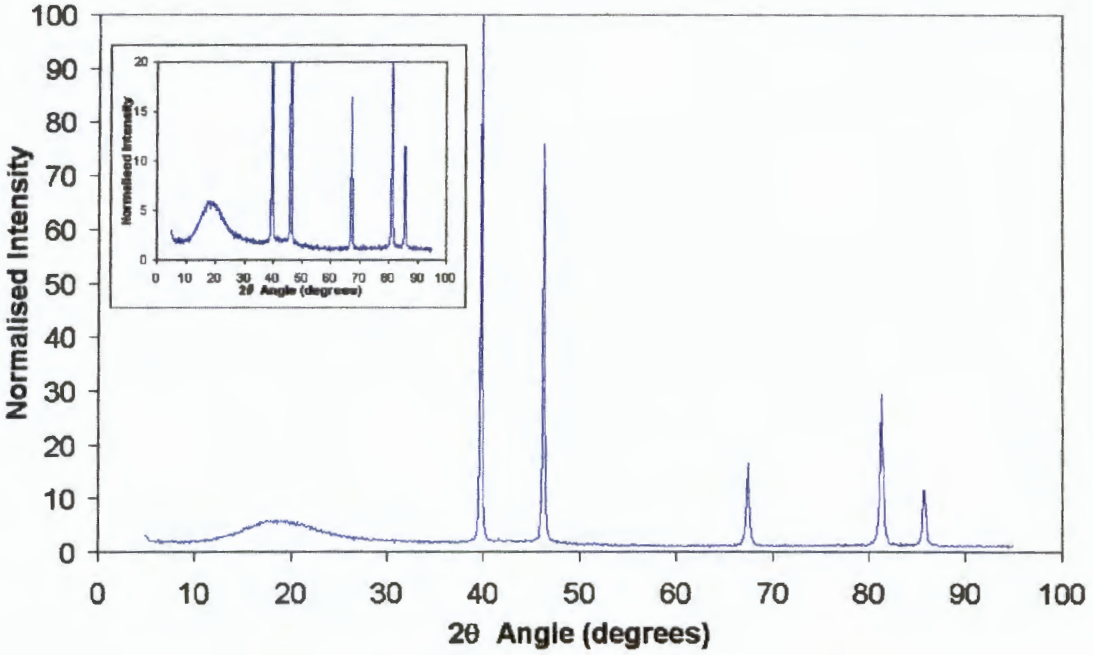

Figure 4.6.1 Typical x-ray diffraction spectra of pure platinum (pure platinum annealed at 700°C for 3 hours).

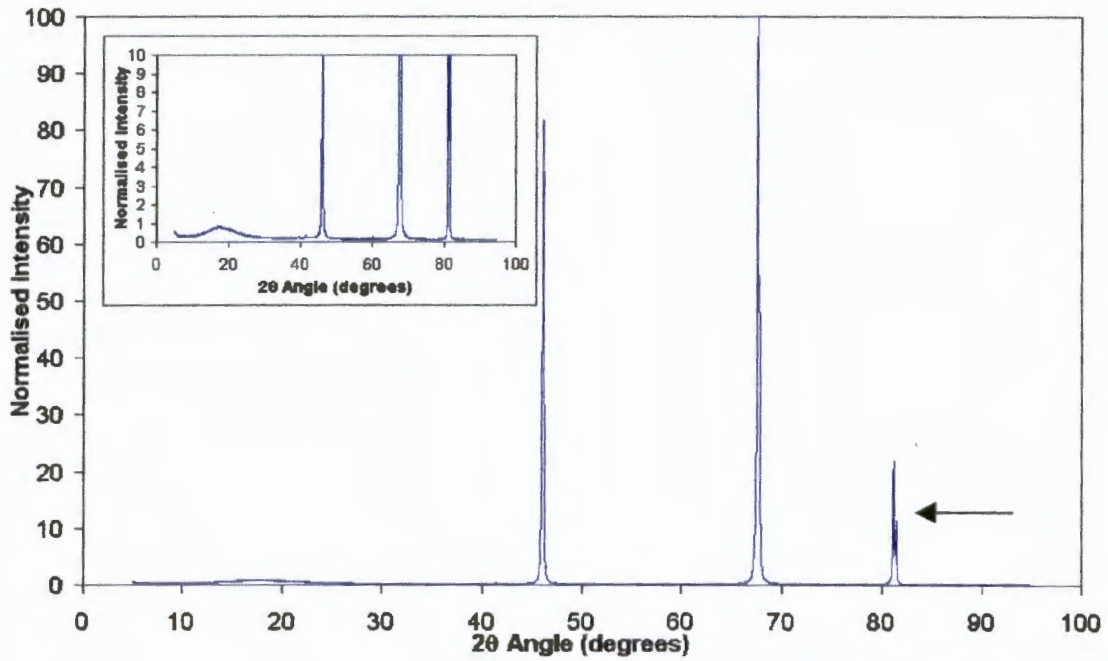

Figure 4.6.2 Typical x-ray diffraction spectra of pure platinum showing sub-peak (Pt 5 at% Mo annealed at 1000°C for 3 hours).

4.6.2 *X-RAY DIFFRACTION OF PLATINUM-COPPER*

The major peaks obtained from XRD testing of the cold-worked and annealed Pt 5 wt% Cu specimens have been summarised in Table 4.4. Typical XRD spectra of Pt 5 wt% Cu specimens, which have been annealed at 300°C for 10 hours and 700°C for 10 hours, can be seen in Figure 4.6.3 and Figure 4.6.5 respectively. The positions of the major peaks are similar except for the peak at approximately 70° which changes its position on annealing at 700°C. This particular peak has moved from 70.4° in Figure 4.6.4 c) to 68.4° in Figure 4.6.6 c). Noticeable changes in the peak shape can be observed if they are isolated as in Figure 4.6.4 and Figure 4.6.6, for the 300°C and 700°C heat treatments respectively. The specimen annealed at 700°C develops extra sub-peaks at both higher and lower 2θ angles as shown in Figure 4.6.6 b), c) and d).

There are many additional peaks seen in Figure 4.6.5 that are not listed in the Powder Diffraction File[73] for pure platinum or seen in the XRD spectra tested during the current investigation. They are most likely due to the polymeric base that was used to support the specimen as they match the 2θ angles seen in Appendix C2.

Table 4.4 Table of d-spacings for Pt 5 wt% Cu.

	(111)	(311)	(200)	(220)	(222)
Cold-worked	N	Y	Y	Y	N
300°C 0.5 hours	Y	Y	Y	Y	N
300°C 0.5 hours	Y	Y	Y	Y	N
700°C 3 hours	Y	Y	Y	Y	N
700°C 3 hours	Y	Y	Y	Y	N

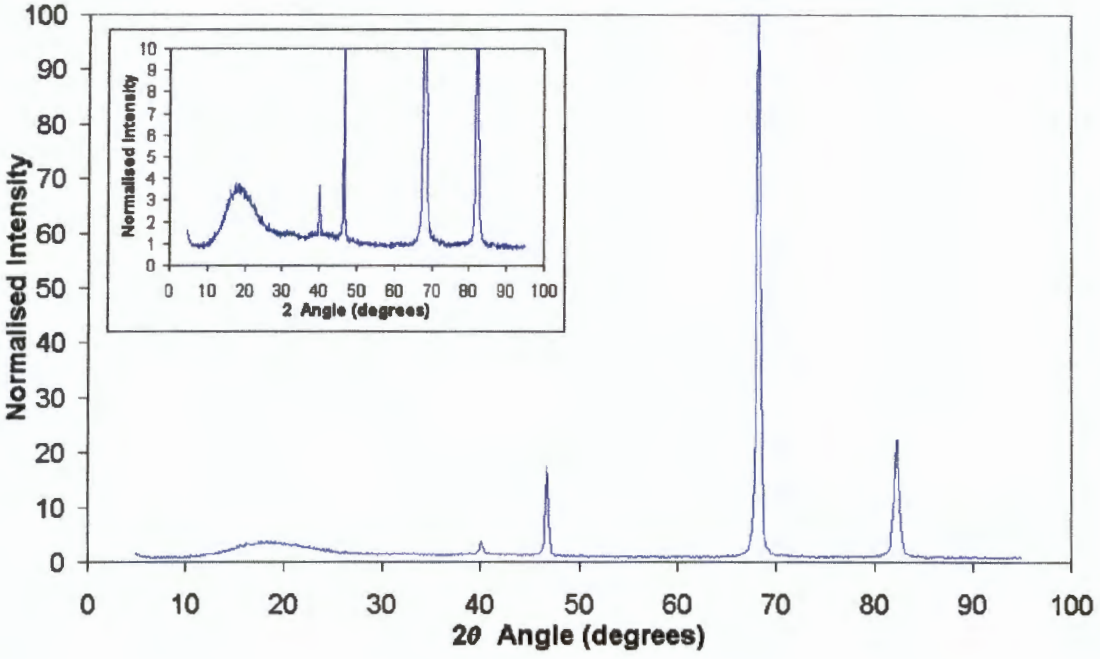

Figure 4.6.3 X-ray diffraction profile of Pt 5 wt% Cu annealed at 300°C for 10 hours.

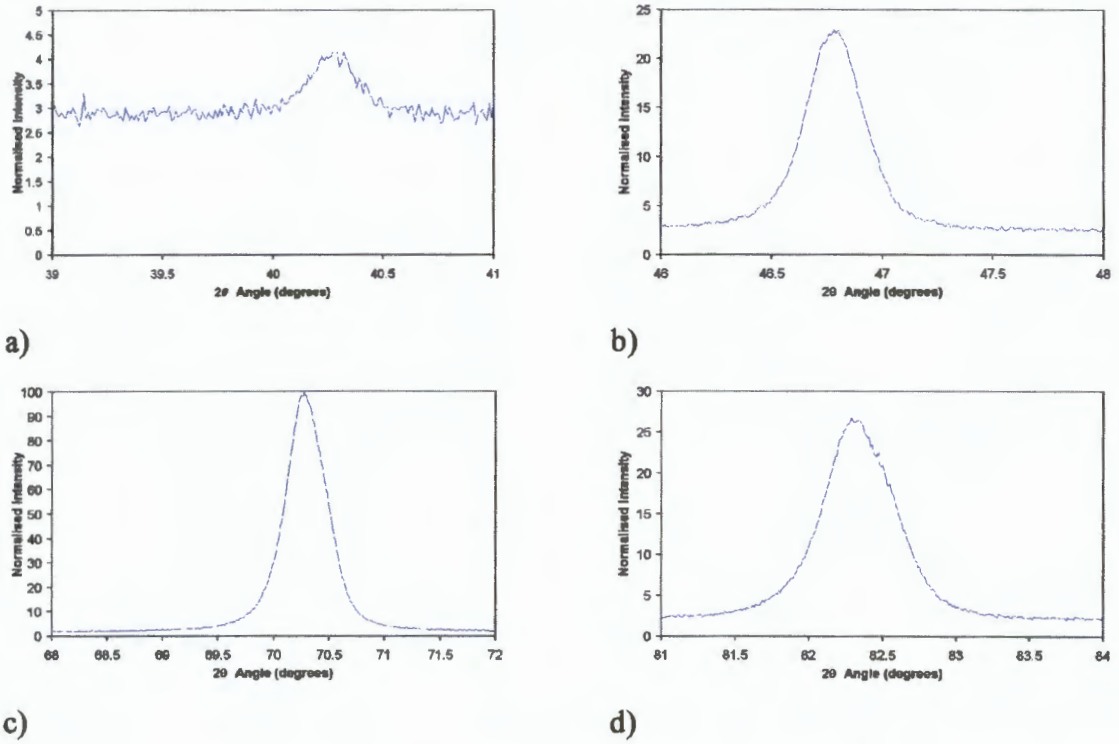

Figure 4.6.4 Isolated peaks from Figure 4.6.3 a) 39°-41° b) 46°-48°, c) 68°-72° and d) 81°-84°.

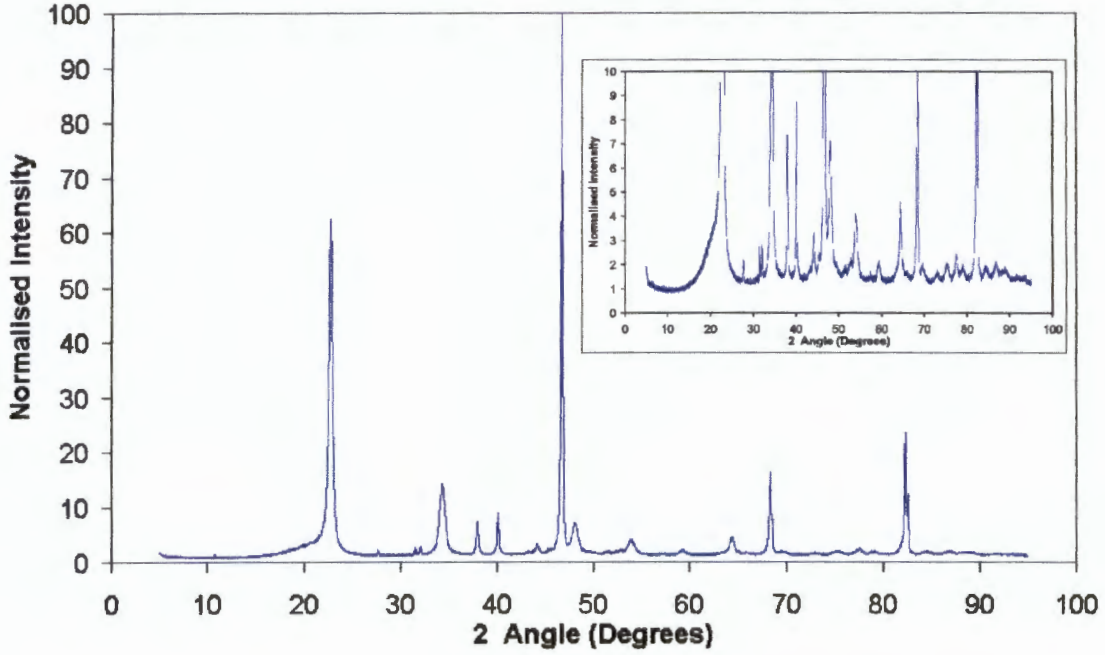

Figure 4.6.5 X-ray diffraction profile of Pt 5 wt% Cu annealed at 700°C for 10 hours.

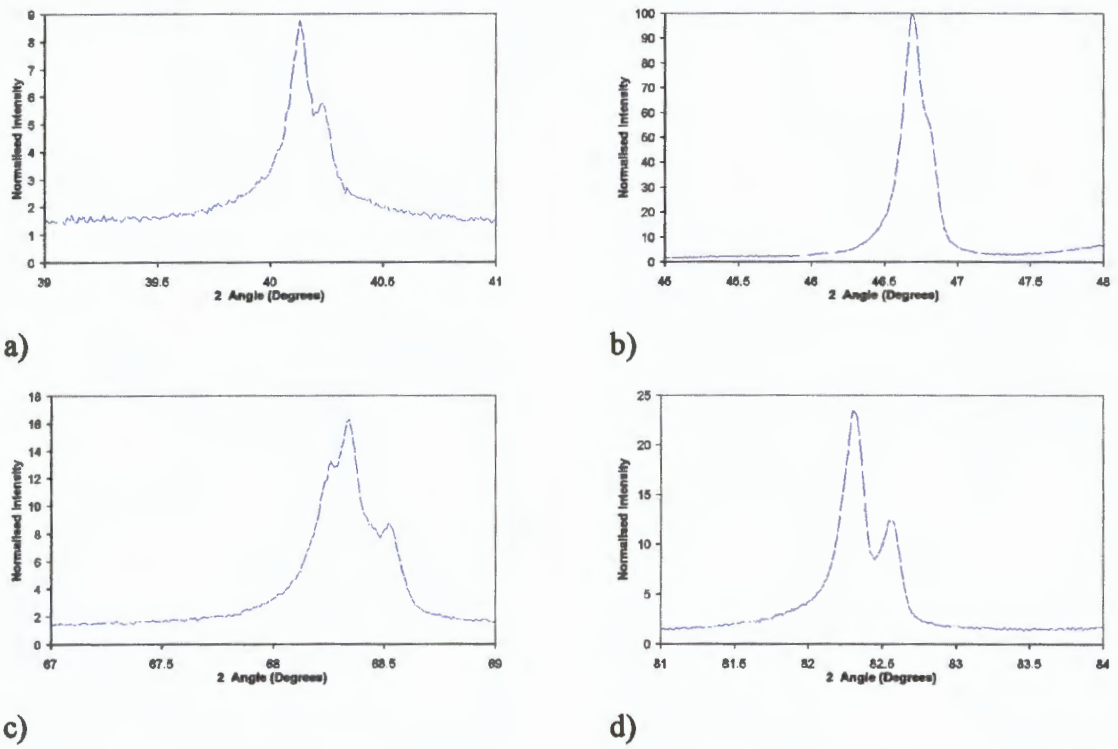

Figure 4.6.6 Isolated peaks from Figure 4.6.5 a) 39°-41° b) 45°-48°, c) 67°-69° and d) 81°-84°.

4.7 DIFFERENTIAL THERMAL ANALYSIS

The experimental methods section discussed the possible inaccuracies and lack of reproducibility in results for DTA testing. However, certain curve irregularities did appear at similar temperatures to the unexpected changes in microhardness discussed in Section 4.1. This section briefly discusses what was found during testing but the majority of the results appear in Appendix D for further reference.

Figure 4.7.1 shows a DTA heating and cooling graph for Pt 5 wt% Ru. The green curve is for testing of the Pt 5 wt% Ru specimen in the cold-worked condition and the red curve for re-testing of the previously cold-worked specimen in an identical manner to the first. Testing of pure platinum, Pt 5 at% Mo and Pt 5 wt% Cu all revealed very similar profiles to Pt 5 wt% Ru and can be seen in Appendix D. There are two features in the figure that could be caused by a specimen transformation or transition. The first, is the broad minimum seen on the heating segment of both curves. These minima occur on all the DTA plots for platinum and platinum alloys, usually at temperatures between 600°C and 1000°C. Secondly, the local minimum seen on the green curve during the cooling segment at 1300°C occurs on certain DTA plots, but with unfortunately no consistency. Not only do these cooling minima not appear all the time but, when they do, their shape, size and position vary considerably.

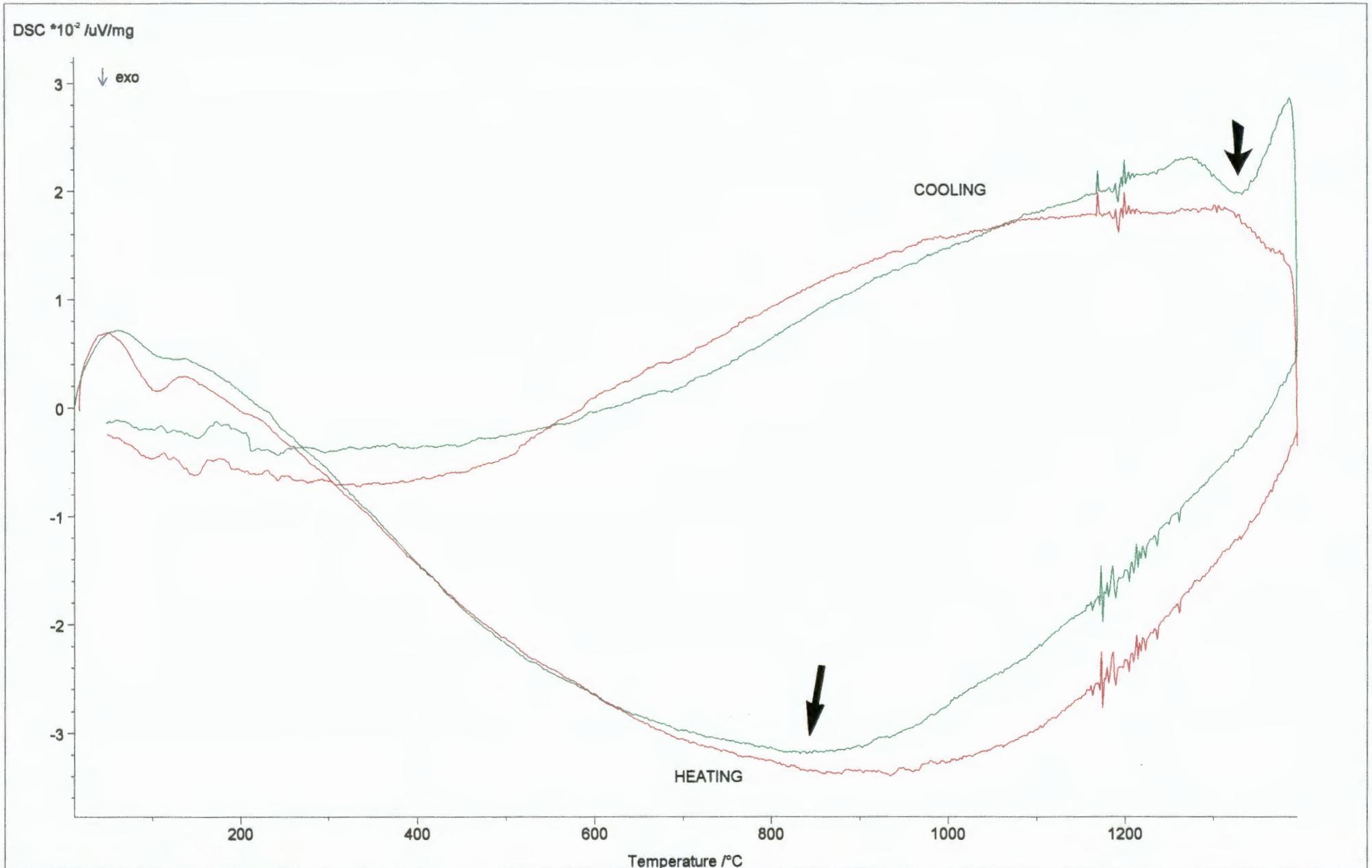

#-INSTRUMENT	FILE	IDENTITY	SAMPLE	DATE	MASS	SEGM.	RANGE	ATMOS.	CORR
1 - STA 409C	RUTH1_4.DSS	ptru 4 k/min first	1400 heating and cooling	08.01.1999	129.350 mg	1-2/2	20 °C/4.0(K/min)/1400 °C/4.0(K/min)/20 °C/	Argon/100	020
2 - STA 409C	RUTH2_4.DSS	ptru 4 k/min repeat	1400 heating and cooling	09.01.1999	129.350 mg	1-2/2	20 °C/4.0(K/min)/1400 °C/4.0(K/min)/20 °C/	Argon/100	020

Figure 4.7.1 DTA graph showing curves of cold-worked and retested Pt 5 wt% Ru heated and cooled at 4 K/min.

5 DISCUSSION

The results of the systematic series of heat treatments show that the three cold-worked, experimental alloys exhibit unexpected changes in hardness as a result of annealing. There is, however, a distinct difference in the hardening behaviour of the platinum-copper alloy relative to that of the platinum-molybdenum and platinum-ruthenium alloys. The discussion on the latter two alloys will show that the most likely hardening mechanism is the development of short-range order at annealing temperatures higher than the recrystallisation temperature, similar to that seen by Lang[2] in palladium alloys. This is in contrast to the platinum-copper alloy which shows increased hardening at temperatures lower than the recrystallisation temperature with an isothermal hardening profile very similar to that of age-hardening. The hardening mechanism in platinum-copper is thought to be due to the development of long-range order, the type of order depending on annealing temperature and alloy composition[21,22].

There are two sections in the discussion on the hardness results, the first of which, Section 5.1 and only discusses the shape and characteristics of the hardening curves. Section 5.3 also discusses the hardness results, but in reference to the phase equilibria in Section 5.2. Possible interpretations are offered regarding mechanisms whereby alloys could harden. Sections 5.4, 5.5 and 5.6 are an interpretation of the resistivity, XRD and DTA results respectively and include a discussion of the errors that were involved with using each technique.

5.1 MICROHARDNESS TESTING

When a previously cold-worked specimen is heated it is expected that restoration processes such as recovery and recrystallisation may occur, depending on the annealing temperature and time and the extent of prior plastic deformation. These restoration processes result in a decreased hardness with increased annealing temperature and time due to a decrease in dislocation density.

5.1.1 MICROHARDNESS OF PLATINUM-MOLYBDENUM AND PLATINUM-RUTHENIUM

The Pt 5 at% Mo and the Pt 5 wt% Ru alloys show very similar microhardness trends with respect to annealing temperature as can be seen in Figures 4.1.1 to 4.1.11. The initial decrease in microhardness is expected due to normal recovery and recrystallisation processes and is consistent with the micrographs seen in Figures 4.2.1 to 4.2.4 for Pt 5 at% Mo and 4.2.5 to 4.2.8 for Pt 5 wt% Ru. From the cold-worked hardness the slight decrease in microhardness up to annealing temperatures of 700°C can be attributed to recovery processes with the onset of recrystallisation accounting for the more drastic decrease in microhardness at higher temperatures. The microhardness results and optical micrographs show that recrystallisation is complete at a temperature of 1000°C or just above. Once recrystallisation is complete, further annealing only produces a large increase in grain size which can be seen in Figures 4.23 and 4.24 for the platinum-molybdenum alloy and in Figures 4.2.7 and 4.2.8 for the platinum-ruthenium alloy. Grain growth processes, which occur above the recrystallisation temperature, are expected to produce a decrease in specimen hardness but microhardness testing shows an unexpected increase. As no dramatic changes in dislocation density are expected once recrystallisation is complete, the measured increase in microhardness must be due to some other form of hardening mechanism which occurs in these experimental alloys upon annealing.

5.1.2 MICROHARDNESS OF PLATINUM-COPPER

Although the Pt 5 wt% Cu alloy does not follow the same characteristic hardening trend as the other two alloys under investigation, it also exhibits unexpected changes in hardness on annealing. For example, the microhardness graph in Figure 4.1.12 c) and the optical micrographs in Figures 4.2.9 to 4.2.11 show that even though the visible microstructure has changed very little upon annealing at 300°C, there is a significant increase in microhardness. The isothermal annealing graphs in Figure 4.1.12 show that for annealing temperatures less than 500°C a hardness increase is seen with a peak hardness produced upon annealing in the 200°C to 400°C temperature range. There is, therefore, some form of hardening mechanism resulting in an increased specimen hardness upon annealing of Pt 5 at% Cu. This hardening mechanism is either only prevalent at low annealing temperatures, or recovery and recrystallization processes outweigh hardening effects at temperatures above 500°C.

5.2 PHASE EQUILIBRIA IN THE EXPERIMENTAL ALLOYS

An increase in hardness can occur through many different hardening mechanisms; cold-work, precipitation of second phases, solute strengthening, displacive transformations, ordering and others. However, the specimens under investigation in the present work have been cold-worked prior to testing and annealing can only produce a decrease in dislocation density, not an increase. Therefore, cold-work is clearly not a possibility. For precipitation or age-hardening to be the cause of the hardening, precipitates should be evident, but microscopy of the experimental alloys showed no evidence of precipitates or second phases of any kind. Solute strengthening does not change significantly during annealing and microscopy does not reveal any evidence of a displacive transformation. There is, however, another possible mechanism: order hardening, whereby some alloys show an increased hardness due to changes in structural order upon annealing under certain conditions. In order to establish whether order hardening is possible in the three experimental alloys, their respective phase equilibrium diagrams must be examined for evidence of ordering.

5.2.1 STRUCTURAL ORDER IN PLATINUM-MOLYBDENUM AND PLATINUM-RUTHENIUM

Examination of the equilibrium phase diagrams of Pt-Mo and Pt-Ru reveals that a single-phase terminal solid solution exists from 0 – 20 at% Mo[3] and from 0 – 60 at% Ru[14] for the Pt-Mo and Pt-Ru respectively. Therefore, the experimental alloy compositions of Pt 5 at% Mo and Pt 5 wt% Ru should both exhibit, according to the phase diagrams, a single-phase solid solution up to very high temperatures. This is borne out by the microscopy reported in Sections 4.2, 4.3 and 4.4. Light microscopy, secondary and backscattered SEM and bright field TEM reveal a simple, single-phase microstructure with no evidence of precipitation on grain boundaries or within the grains themselves.

A change in structural order has not been documented before at these very low alloy compositions but the Pt-Mo alloy is very well known for the formation of ordered phases and intermetallic compounds at higher platinum compositions. In addition, palladium 5 at% molybdenum, which has been shown to exhibit short-range order[74] shows a very similar hardening behaviour to that seen in Pt 5 at% Mo[2]. Although this is not conclusive evidence that the same short-range ordering effects seen in palladium should be seen in platinum, platinum and palladium are known to have very similar physical and chemical properties and are often found to behave in a similar manner.

Many authors[75,76,77,78] have shown that the presence of short-range order may be detected by electron diffraction investigations such as the ones discussed in Section 5.2.2 that follows. Although the additional reflections seen in the diffraction patterns of Figure 4.1.1, Figure 4.1.2 and Figure 4.1.5 are not direct evidence of short-range order, the presence of additional scattering in electron diffraction patterns may result from short-range order.

Indirect evidence for the presence of order can be obtained from published research on lattice parameter measurements on the Pt-Mo alloy system[7]. Figure 2.1.2 shows an unusual dependence of lattice parameter on concentration for annealed alloys. It is expected that in a Pt-Mo random solid solution, the lattice parameter should increase with increasing solute content showing molybdenum is slightly oversized in the platinum lattice. A deviation from randomness is the probable reason why the curve shows an initial decrease in lattice parameter with solute content, reaching a minimum at 10 at%. The alloy concentration in question, Pt 5 at% Mo, is within this lattice parameter irregularity and may, therefore, exhibit a non-random atomic configuration.

A non-random atomic configuration in a solid solution may take the form of clustering (a localised preference for like nearest neighbours) or short-range order (a preference for unlike nearest neighbours), both of which could bring about a decrease in lattice parameter relative to the disordered alloy. It is unlikely, however, that clustering of the oversized molybdenum atom would bring about a decrease in lattice

parameter. It is more likely that the presence of short-range order may influence the lattice parameter to the degree shown in Figure 2.1.2. It might also be expected that the composition 10 at% Mo, where the lattice parameter is a minimum, could be the composition at which the degree of short-range order is greatest.

5.2.2 ELECTRON DIFFRACTION INVESTIGATIONS OF PLATINUM-MOLYBDENUM AND PLATINUM-RUTHENIUM

A change in structural order can be investigated by selected area diffraction techniques using representative thinned foils of the experimental specimen. The change in structural order, either short-range or long-range order, may result in additional scattering in the electron diffraction patterns. The nature of this scattering is dependent on the type of order from which it arises, with the intensity of the reflections increasing with increasing solute content and degree of order[75].

The purpose of the electron diffraction experiments was to investigate the presence of structural order in annealed Pt 5 at% Mo and Pt 5 wt% Ru, by means of a systematic investigation of high-symmetry zone-axis electron diffraction patterns. Only the specimens annealed for 3 hours at 1300°C were investigated. Other than the expected fundamental f.c.c. reflections, the electron diffraction results also showed additional reflections. The additional reflections were observed in representative specimens of both the alloys but not in all the investigated zone-axis diffraction patterns.

The intensity of the additional reflections were very weak and only with long exposure times and over-exposing the film could they be observed. In addition to being very weak, the additional reflections did not consist of single intense spots, as the diffraction patterns in Figures 4.4.1, 4.4.2 and 4.4.5 show. The [111] zone axis in Pt 5 at% Mo shows two types of additional reflections, the first of which are diffuse reflections at 1/3242-type positions. The [111] zone axis also shows sharper reflections, in close proximity to the diffuse reflections, but not following the same symmetrical arrangement. Both the [112] and [001] zone axis diffraction patterns

show a clustering of extra reflections at 1/2220-type positions while in Pt 5 wt% Ru the extra reflections are at 1/2131-type positions in the [121] zone axis.

In order to identify the features which give rise to these additional reflections, dark-field and bright-field images were recorded. The micrographs in Figures 4.4.3 and Figure 4.4.4 show a mottled texture which appears to be a fine distribution of precipitate-like structures. This type of structure is common to alloys showing short-range and long-range order and has been attributed to microdomains[75,76,77,78]. These consist of very small, highly ordered regions that can be as small as one unit cell and have been referred to as the precursor to long-range ordered domains.

There is the possibility that the additional reflections could be an artefact such as a surface film due to the polishing or cleaning solution used. The concentric rings around some of the fundamental reflections suggest that this is possible, but the rings are not observed in all the diffraction patterns and previous use of this preparation technique did not reveal similar effects.

The preliminary TEM investigation did not provide any conclusive evidence of ordering, but, the TEM micrographs and the electron diffraction investigation suggest a strong possibility of ordering in Pt-Mo and Pt-Ru. Further TEM investigation is necessary to test the ordering hypothesis and to establish if the additional reflections are due to ordering and if the hardness increases are a result of ordering.

5.2.3 STRUCTURAL ORDER IN PLATINUM-COPPER

The equilibrium phase diagram of the Pt-Cu system at around 5 wt% Cu is more complicated than that of the Pt-Mo and the Pt-Ru systems. The equilibrium phase diagram indicates that Pt-Cu consists of a continuous solid solution with numerous, low temperature ordered phases. Of interest to this alloy, Pt 5 wt% Cu (14 at% Cu), is the large equiatomic phase PtCu which extends from approximately 70 at% Cu to very low copper contents, and also the low temperature $CuPt_3$ and $CuPt_7$ ordered

phases. Unfortunately, Miida et al[16] , who mentioned the latter two phases, did not investigate them in any great detail and no additional literature could be found. Therefore, given the characteristic shape of the ordered phase field found in this and similar systems (Figure 2.1.5, 2.1.6 and 2.2.9), $CuPt_3$, $CuPt_7$ and the extensive PtCu phase could all have an influence on what equilibrium phases exist at 5 wt% Cu and at what temperature they exist. The extent of their influence, however, is not known as the temperature and composition range over which the phases are stable has not been fully investigated.

The above mentioned ordered phases are of the Kurnakov compound type. These Kurnakov compounds, as they are known, are not compounds in the true sense but are ordered phases that take on compound type atomic arrangements at stoichiometric compositions. The ordered phases are disordered above a certain critical temperature, T_c, and as they cool they take on an ordered arrangement with atoms segregating to specific lattice sites which is termed long-range order.

5.3 EFFECT OF STRUCTURAL ORDER ON MICROHARDNESS

The previous section has shown that there is a strong possibility of ordering in the experimental alloys under investigation in this project. It is also known that structural order, both short-range and long-range order, can influence the hardness of a material. It is, therefore, likely that these ordering effects are causing the increase in hardness seen in the results. The following section discusses the various order hardening mechanisms and theories and will show that ordering, both short-range and long-range order, may be used to change the hardness of single phase materials.

It has previously been noted that when a cold-worked specimen is heated it is expected that recovery and recrystallisation may occur, depending on the annealing temperature and time and the extent of prior plastic deformation. At the same time as these restoration processes are occurring, alloys which exhibit ordering may undergo a change in their atomic configuration. The hardness of the annealed specimen will, therefore, be dependant on both of these processes. A decrease in dislocation density due to recovery and recrystallisation is expected to decrease the hardness of the specimen, while ordering has been shown to increase the hardness of certain alloy systems[2,24,25,79]. The concern of this section is to correlate the evolution and development of these two processes, restoration and ordering, and to determine what their influence is on the mechanical properties of the three alloys under investigation.

5.3.1 PLATINUM-MOLYBDENUM AND PLATINUM-RUTHENIUM

Fisher[34] was the first to suggest that short-range order must influence the flow stress of a solid solution by increasing the frictional drag on the dislocation. His assumption was simply that more energy is required to move a unit dislocation through a short-range ordered region than a disordered region. This increase in energy is provided by an increased stress to move the unit dislocation, which is then manifested as an increased flow stress in the test material. This has been seen before by many authors in specimens quenched from above T_C then annealed, but is most prominent in disordered materials that have been strained prior to annealing[33]. The development of

short-range order in the prestrained specimens upon annealing has been given the name strain-ageing or order hardening. This strain-ageing develops in alloys that exhibit ordering at annealing temperatures below the recrystallisation temperature. This is, however, not consistent with the results for Pt-Mo and Pt-Ru which show an increase in hardness at annealing temperatures above the recrystallisation temperature. This hardening at annealing temperatures above the recrystallisation temperature has been observed by Lang[2] in Pd-Mo and Pd-W alloys, and was also attributed to short-range order that had developed at high annealing temperatures.

It has been argued above that an increase in the degree of order will increase the microhardness of the specimens under investigation; whereas microhardness will be decreased by a decrease in dislocation density during recrystallisation and further decreased by grain growth. There are accordingly, two possible competitive processes influencing hardness which could produce the characteristic microhardness vs. temperature profiles seen in the results.

Firstly, microhardness could be an outcome of the competition between the processes of ordering and recovery/recrystallisation. If ordering occurs over a wide temperature range it appears that a consistent decrease in microhardness due to decreasing dislocation density outweighs any contribution from structural order effects, as an increase in microhardness is only observed when the dislocation density is constant after recrystallisation is complete. A similar idea was argued by Lang[2] for Pd-Mo and Pd-W alloys which showed a hardness increase directly after recrystallisation was complete.

The microhardness graphs for Pt-Mo and Pt-Ru are, however, slightly different in that the hardness increase is not seen directly after recrystallisation is complete but at temperatures approximately 250°C higher. This could imply that the hardness increase due to short-range order only occurs once recrystallisation is complete and that there is no competitive effect between ordering and recovery/recrystallisation. Once these restoration processes are complete, an increase in grain size can still produce a hardness decrease. The profile of the microhardness curves and the optical

micrographs suggest that a competitive process between grain growth and short-range order is taking place not recovery/recrystallisation and ordering. It appears from the results, however, that the decrease in microhardness due to grain growth is not that significant and will only have a very small effect on the overall hardness of the specimen. The microhardness, between when the alloys have recrystallised and just before they harden, shows a constant microhardness plateau, but Figures 4.2.3 and 4.2.4 and Figures 4.2.7 and 4.2.8 show a large increase in grain size. The most probable reason for this discrepancy is that microhardness testing is a poor method of detecting hardness changes due to grain growth when the grain size is very large.

Three more aspects of the hardening behaviour of Pt-Mo and Pt-Ru have to be considered: the effect that the cooling rates, annealing time and annealing temperature have on the ultimate hardness of the alloys. Firstly, the cooling rates show that slow cooled specimens harden, whereas the quenched specimens show the expected hardness decrease and have a more expected type of annealing profile. It is assumed, therefore, that ordering of the specimen does not occur on heating, or during the constant temperature annealing segment but only upon cooling. This is assuming that that if order does develop in the former two stages of the heat treatment, quenching would "trap" in the ordered high temperature structure. This would imply that heating the specimen to 1300°C and directly cooling, with no isothermal anneal, would produce a specimen of maximum hardness, as grain growth would be minimised, and with an increased hardness due to the development of order on slow cooling. This hypothesis could be verified by further heat treatments.

Secondly, considering the annealing times, Figure 4.1.7 and 4.1.11 show that the annealing times of 0.5 hours and 3 hours produce microhardness values of approximately the same value but annealing for 6 hours produces a much lower hardness at 1300°C. Using the microdomain model discussed in Section 5.2.2 it is possible that a process similar to "overageing" in precipitation hardened alloys or long-range ordered alloys could produce this hardness decrease at long annealing times. Overageing would, however, occur during the isothermal anneal at 1300°C, but it has just been stated that hardening occurs during the cooling cycle not during

annealing at constant temperature. It must be assumed, therefore, that the isothermal anneal at 1300°C has some influence on the hardening behaviour during cooling.

Thirdly, Figures 4.1.5 and 4.1.9 show that at annealing temperatures above 1300°C there is a decrease in microhardness. This might indicate a critical short-range ordering temperature, T_c, similar to that seen in long-range ordered alloys. For the same reason that the long-range ordered superlattice is destroyed by thermal vibration above a critical temperature, short-range order could also be destroyed at very high annealing temperatures. All the specimens annealed at temperatures above 1300°C were heat treated in different furnaces and under slightly different conditions. As there was no direct control of such factors as furnace cooling rate, these tests should be repeated under more controlled conditions.

As a final comment on the microhardness and microscopy of the Pt-Mo alloy an explanation for the porosity and grain separation seen in the backscattered SEM images must be given. The porosity can be seen in Figures 4.3.3 and 4.3.4 and is unique to this specific specimen and was not seen in either TEM or optical microscopy performed on similar specimens. The expected reason for this porosity is due to a combination of a very thin specimen and large grain size. The SEM specimen was so thin, that it only consisted of a few grains between the lower and upper surface. There was, therefore, very little mechanical strength in the specimen and the grain boundaries started to separate.

5.3.2 PLATINUM-COPPER

Although the graphs for Pt-Mo and Pt-Ru are very different to those seen for Pt-Cu, given the information on the phases present at 5 wt% Cu, Section 5.2.3, the most likely explanation for the microhardness increase is also due to structural order effects. However, the type of ordering mechanism in this case is probably long-range order and not short-range order. Although alloys that exhibit age-hardening (precipitation hardening) show similar isothermal profiles to those in Figure 4.1.12,

the microscopy performed on the specimens do not show any evidence of precipitates forming in the alloy. It is assumed, therefore, that precipitation or age-hardening cannot be the reason for the hardness increase. Added to this, research by Irani & Cahn[6] and Mitchell et al[43] on PtCu, show similar isothermal graphs to the Pt 5 wt% Cu alloy under investigation. They have attributed this hardness increase to the formation of long-range order. The hardness results of Irani & Cahn[6] and Mitchell et al[43] obtained for PtCu were from annealing of quenched specimens and not cold-worked specimens as in this project. This suggests that the PtCu specimens were disordered or at most contained a small degree of short-range order due to being quenched from temperatures above T_C. The process of cold-work, to which Pt 5 wt% Cu alloy specimens in this work were treated, drastically reduces order which suggests that the specimen prior to testing would be similarly disordered (but heavily cold-worked). Roessler et al[80] and Cohen & Bever[81] have conducted similar experiments using cold-worked Cu_3Au with a similar result to these presented for Pt 5 wt% Cu in the present work. Cu_3Au is a similar type of ordered phase to those found in the Pt-Cu specimens; Cohen & Bever[81] too attributed the hardening to long-range order effects.

An examination of the optical micrographs for Pt 5 wt% Cu in the cold-worked condition and after being annealed for 0.5 hours at 300°C reveal very similar microstructures, with both of them exhibiting a cold-worked structure. However, even though the microstructure of the two specimens has not changed upon annealing, the specimen annealed at 300°C shows a 30% increase in microhardness. This hardness is most likely due to long-range order as has been seen for PtCu[6,43] and Cu_3Au[80,81]. This increase in hardness is superimposed on the strain hardening due to cold-work as the ordering is occurring at temperatures lower than the recrystallisation temperature which appears to be at approximately 700°C. Therefore, as discussed in the last section, there appears to be a competitive effect between recovery/recrystallisation processes and ordering. It is not certain, however, if the decrease in microhardness from 400°C to 700°C is totally due to restoration processes, the fact that the ordered structure is changing or a combination of both. It is known from the optical micrographs in Figures 4.2.9 to 4.2.13, that recrystallisation

is occurring somewhere between 400°C and 700°C. It is also known from the work by Stoloff and Davies[25] that the peak hardness occurs at an intermediate degree of order and from Savitskii[3] that the critical ordering temperature is at approximately 500°C. Therefore, between the peak hardness at either 300°C or 400°C and 500°C, both ordering and recrystallisation processes are influencing the hardness of the annealed specimen. Above 500°C, however, only recrystallisation processes will have an influence on hardness. The large difference in microhardness results produced during annealing at 700°C were due only to recrystallisation effects. Figure 4.2.12 and 4.2.13 show that increasing the annealing time from 0.5 hours to 10 hours has a large impact on the extent of recrystallisation in the annealed specimen and as a result the final hardness.

The most likely phases to influence Pt 5 wt% Cu are the very broad PtCu phase and the low temperature $CuPt_7$ phase mentioned by Miida & Watanabe[16]. Savitkii's[3] phase diagram and the work conducted by Irani & Cahn[6] both advocate that PtCu has a rhombohedral type structure. However, Miida & Watanbe say that at platinum compositions larger than 70 at%, the PtCu phase changes from rhombohedral to cubic (Figure 2.1.8). All that is known about the $CuPt_7$ phase, is that it is cubic and centred at 12 at% Cu with the apex of the phase below T_c (approximately 500°C) for the PtCu ordered phase. As 5 wt% equates to approximately 14 at% Cu, and knowing the characteristic shape of these ordered phases, it is very likely the $CuPt_7$ phase will have some influence on the Pt 5 wt% Cu alloy.

Unfortunately, as a TEM investigation on the Pt 5 wt% Cu alloy was not carried out and the literature available at this particular phase composition is small, only very tentative postulates can be made as to the ordering. What is known, however, if the phase predictions by Miida and Watanabe[16] are correct, is that there will be no hardening due to changes in crystal structure. This is because both the ordered PtCu and $CuPt_3$ are cubic which is the same as the random solid solution above T_c, the critical ordering temperature of approximately 500°C. This would imply that hardening does not occur by lattice misfit stresses created due to differing lattice symmetries. Stoloff and Davies[25] have shown that if hardening does occur by a

change in crystal symmetry, then the peak hardness will be at the critical ordering temperature. The experimental results show this not to be true for Pt 5wt% Cu, as there is a slight decrease in hardness from 400°C to 500°C for all annealing times. This suggests that the peak hardness occurs at some intermediate degree of order.

There are two important hardening mechanisms in ordered alloys which show a peak hardness at an intermediate degree of order; a variation in the degree of order and domain hardening. Both of these mechanisms are similar and involve the transition from unit dislocations to superlattice dislocations. Stoloff and Davies[25] have stated that hardening during isothermal ordering is a consequence of the extra energy to move unit dislocations, and the peak in hardness corresponds to a transition from deformation by unit dislocations to deformation by superlattice dislocations.

The first mechanism, variation in the degree of order, is explained by Section 2.3.2 in the literature review. Although this mechanism applies predominantly to quenched, then aged specimens, it works equally well for cold-worked then aged specimens. Initially, the specimens are cold–worked and ideally contain no order, and as a result all deformation is by unit dislocations. As the degree of order increases due to a rise in annealing temperature, the specimen will harden by the movement of unit dislocations through a partially ordered structure. The unit dislocations require more energy to move through the ordered regions as they produce APD leaving disorder in their wake. As the degree of order increases so does the amount of APD formed by the moving unit dislocations and the specimen hardens even more. But once the degree of order is large, it is energetically more favourable for the dislocations to move in pairs, superlattice dislocations, to minimise the amount of APD formed. Thus, the hardness of the material drops at the transition between dislocation types, which is usually at some intermediate degree of order, at an annealing temperature slightly less than T_c. It should also be noted that the material will never reach perfect order as the composition is not at the stoichiometric composition for either the PtCu or $CuPt_7$ phase.

The second mechanism, that of domain hardening is very similar to that above. The difference is that a domain size change results in the dislocation transition not a change in the degree of order, although they could essentially be viewed as the same thing. When the domain size is small, unit dislocations will dominate deformation, moving easily through disordered regions but with more difficulty through the ordered domains due to the formation of APD. It is very likely that the "disordered" regions between the domains contain short-range order. This short-range order will also improve the hardness by the Fisher[34] mechanism, possibly accounting for most of the early hardness. As the domains start to grow with increasing annealing temperature, they will reach a size where superlattice dislocation movement will dominate deformation and the hardness will start to fall. This is usually at the point when the domains coalesce. The extent of the driving force, depending on how far below T_c the specimen is annealed, will also influence the size and distribution of the domains. Depending on the kinetics, low annealing temperatures will produce a fine distribution of many, small domains, whereas annealing temperatures near 500°C will produce a small number of big domains. The fine distribution of domains will result in a greater hardness due the movement of unit dislocations, whereas the large domains, in which superlattice dislocations will dominate, will result in a softer specimen.

Mention was made of the effect that short range order could have on order hardening in Pt 5 wt% Cu at low annealing temperatures. Vidoz et al[82] and Roessler et al[80] have shown that in cold-worked specimens of Ni_3Fe and Cu_3Au respectively, short-range order is responsible for the initial hardening through the Fisher[34] bond cutting mechanism. This hardening is also termed strain-hardening and is limited to low annealing temperatures. However, the isothermal annealing graphs for Pt 5 wt% Cu show that annealing for short periods of time, at or below 200°C, produces very little change in hardness. This is most likely due to very sluggish ordering kinetics at these comparatively low temperatures, considering that platinum has a very high melting point.

As a final comment on the hardening of Pt 5 wt% Cu it is interesting to note that the alloy shows a slight increase in hardness at annealing temperatures above the recrystallisation temperature. Figure 4.1.16, the only graph to show this effect, shows the increase is at a similar annealing temperature to the hardness increase seen in Pt 5 at% Mo and Pt 5 wt% Ru. Although, the extent of hardening is not to the same degree it is likely that the formation of short-range order is also responsible.

5.4 ELECTRICAL RESISTIVITY

As shown in Section 2.6, the only two processes likely to affect resistivity in the three experimental alloys are structural order effects and changes in dislocation density. However, the effect of dislocation changes on resistivity is very small, leaving only structural order effects to significantly influence the shape of the resistivity vs. temperature graph. Of the three cold-worked alloy resistivity tests, only that for Pt-Mo shows any change in gradient and this in the 500°C to 600°C temperature range. This is, however, a temperature range in which no transformations are known to occur. It is possible, using the microdomain theory, that the critical domain size to cause electron scattering is much smaller than the domain size necessary to be observed through microhardness testing. It is, however, very unlikely that there is an 800°C temperature difference between the critical domain size for resistivity and that for microhardness. What is more probable is that resistivity changes due to short-range ordering will occur above the end test temperature of 900°C. It was not possible to increase the test temperature due to apparatus constraints and the welding of the specimen to the platinum electrodes at high temperatures.

Retesting of the alloy specimens, as shown in Figures 4.5.2 and 4.5.3, did produce a larger change in resistivity than testing of cold-worked specimens but what are real resistivity effects and what are variations due to the test apparatus is unclear. There is a visible resistivity change in the re-tested Pt-Mo specimen (Figure 4.5.2) in the same temperature range as was seen in the cold-worked specimen. It is still unclear as to what is causing this effect.

For the Pt-Cu alloys in Figure 4.5.3, there is evidence of gradient changes and resistivity changes in the 450°C to 650°C temperature range. This is the temperature range in which long-range ordering effects are known to occur[3,6,16] and it is likely that structural order changes are totally or partly responsible for these resistivity changes. Before any certainty is attached to these results, however, reproducibility tests should be performed. There is enough evidence, however, especially for the Pt-Cu alloy, to

suggest that further resistivity testing could be valuable in identifying long-range order changes.

5.5 INTERPRETATION OF X-RAY DIFFRACTION RESULTS

The XRD diffraction investigation did not reveal much information regarding ordering in Pt-Mo and Pt-Ru, but the suspected presence of short-range order in these alloys is known not to influence XRD spectra in a noticeable manner. The changes that did occur in the XRD profiles for Pt-Mo, Pt-Ru as well as pure platinum, were as a result of grain size and strain changes within the test specimens. The grain size of the specimens was very large and become larger during annealing. As a result very few grains were sampled during XRD testing and the predominant crystal orientations sampled, dominated the intensities of the XRD spectra.

Strain in a test sample will produce a broadening of the peaks in XRD spectra, but this broadening cannot always be seen by simple inspection unless some good standard is available for comparison. A feature which can be used to pick up strain in a sample, is the separation of the Kα doublet, one component due to $K\alpha_1$ radiation and the other due to $K\alpha_2$ radiation. An annealed metal will produce a well resolved doublet as increased strain in a sample results in the overlapping of the doublet to such an extent that they appear as one resolved peak. An unresolved Kα doublet can, therefore, be taken as evidence of cold-work, if the same doublet is resolved when the metal is in the annealed condition[67]. This can be seen for example in the Pt 5 at% Mo alloy annealed for 3 hours at 1000°C.

The effect that long-range order has upon an x-ray diffraction profile is usually much larger than short-range order and should as a result be easier to identify. As order increases, the fundamental diffraction lines gradually split and slowly move to positions corresponding to the equilibrium value of the ordered structure for that temperature. These "continuous" sequences result from the increase of the superstructure's lattice parameter which is a function of the degree of order[6]. Such an

effect was not seen in the ordered specimens for the Pt 5 wt% Cu alloy. All the main peaks for the 300°C temperature anneals, which is where ordering should occur, do not reveal the formation of split peaks. This could mean that either ordering is not occurring in the alloy or that the degree of long-range order is not sufficient to cause peak separation. As the two peaks are always very close to one another, peak broadening caused from the strain of cold-work could be masking the peak separation. Optical microscopy has shown that the 300°C specimens are still heavily cold-worked and it is, therefore, quite likely that the different ordered and disordered peaks have merged to form one broader peak.

The peaks of the specimens annealed at 700°C, however, do show some splitting up into sub peaks. It could be that the extra peak is the product of the Kα doublet discussed previously. However, the peak at a 2θ angle of 68.4° in the Pt 5 wt% Cu specimen annealed at 700°C for 10 hours (Figure 4.6.5) does show a third peak at lower diffraction angles not normally associated with the Kα doublet. Although this specimen should be disordered as it is annealed above the critical ordering temperature, the specimens was slow cooled through the ordered region. This slow cooling may not be able to allow equilibrium order to develop, but a small degree of order is very likely and as no strain is present, ordered peaks may be just visible.

5.6 INTERPRETATION OF DIFFERENTIAL THERMAL ANALYSIS RESULTS

Section 3.8 and Section 4.7 have shown that the reproducibility of the DTA results are questionable. Testing of similar specimens under identical conditions produced DTA graphs that varied vastly. In addition, testing of pure gold up to 1400°C and 1000°C showed that results of the DTA testing of pure platinum and the three experimental alloys may not be significant. This would suggest that the gradient changes and maxima and mimima peaks observed in the DTA graphs may not be due to transformations of any kind but due to small instrument and crucible variations.

The reasons for this are twofold: Differential scanning calorimetry (DSC) and not DTA is the preferred thermal analysis technique for the study of metals as it provides a more accurate measurement of certain transformations, one of which is order/disorder transformations. Unlike melting which involves latent heat changes, and can, therefore, be identified by DTA techniques, order/disorder transformations transformation may involve no latent heat. Order/disorder transformations are, therefore, not identified by DTA techniques, whereas, specific heat varies considerably during the transformation which can be easily identified by DSC.

The second factor which may influence the results, is the choice of specimen shape, size and mass. Off-cuts of small size were used for testing with a mass of 0.1 g. The mass is sufficient, but due to the high density of platinum, 0.1 g does not yield a very high volume of material. There may, therefore, be a poor conducting path between the specimen, crucible and thermocouple tip which would severly effect the sensitivity of the instrument and the accuracy of the final results. Due to these two reasons and the lack of consistent results after much testing, no useful conclusions can be drawn from the DTA data.

6 CONCLUSIONS

The current investigation shows that the hardness and hardening behaviour of Pt 5 at% Mo, Pt 5 wt% Ru and Pt 5 wt% Cu can be controlled by a simple process of cold-work and annealing. A cold-worked material is expected to show a decrease in hardness on increasing annealing temperature due to a decrease in dislocation density, during recovery/recrystallisation processes, and subsequent grain growth. The recovery and recrystallisation processes that cause the decrease in hardness are seen in the three experimental alloys, however, the alloys also show unexpected increase in hardness on annealing within specific temperature ranges. Pt 5 wt% Mo and Pt 5 wt% Ru, when annealed at temperatures above the recrystallisation temperature, show a large hardness increase with the final value comparable to the original cold-worked hardness. Pt 5 wt% Cu exhibits only a small increase in hardness at high annealing temperatures, but shows a much larger increase on annealing in the 200°C to 500°C temperature range and can achieve a peak hardness 30% higher than the original cold-worked hardness.

The hardening behaviour in the three experimental alloys is attributed to changes in structural order occurring during annealing of the cold-worked specimens. Pt 5 wt% Cu, which is known to contain ordered phases at low temperatures, has an improved low temperature hardness due to the nucleation and growth of long-range order. The hardness increase seen in all three experimental alloys at annealing temperatures above the recrystallisation temperature is attributed to the formation of short-range order.

To successfully use any alloy in the jewellery industry a thorough knowledge of its annealing and hardening behaviour is needed. The results of the present investigation show that order hardening is a viable method of improving the hardness and hardening behaviour of platinum jewellery alloys.

6.1 FUTURE WORK

Given that this investigation into the hardening of Pt 5 at% Mo, Pt 5 wt% Ru and Pt 5 wt% Cu is a preliminary study, there are many areas that still need clarity and areas where further work is needed:

1) The TEM investigation showed very promising but incomplete results. For a better understanding of the ordering behaviour in these and similar alloys, additional TEM must be undertaken.
2) In the current investigation only one solute content for each alloy was chosen. A better understanding of the hardening could be obtained by testing an array of similar alloys but with differing compositions.
3) Other platinum-transition metal alloys should be investigated as the high temperature hardening effect could be common to many such alloys.
4) A greater understanding of the effect of cooling rate on the final hardness should be obtained.
5) Pt 5 wt% Ru and Pt 5 wt% Cu are alloys used currently in the jewellery industry. In order to see if the hardening effects in Pt 5 at% Mo are of any commercial value, this alloy should also be tested as a platinum jewellery alloy for features such as work-ability, castability, colour, etc.

APPENDIX A

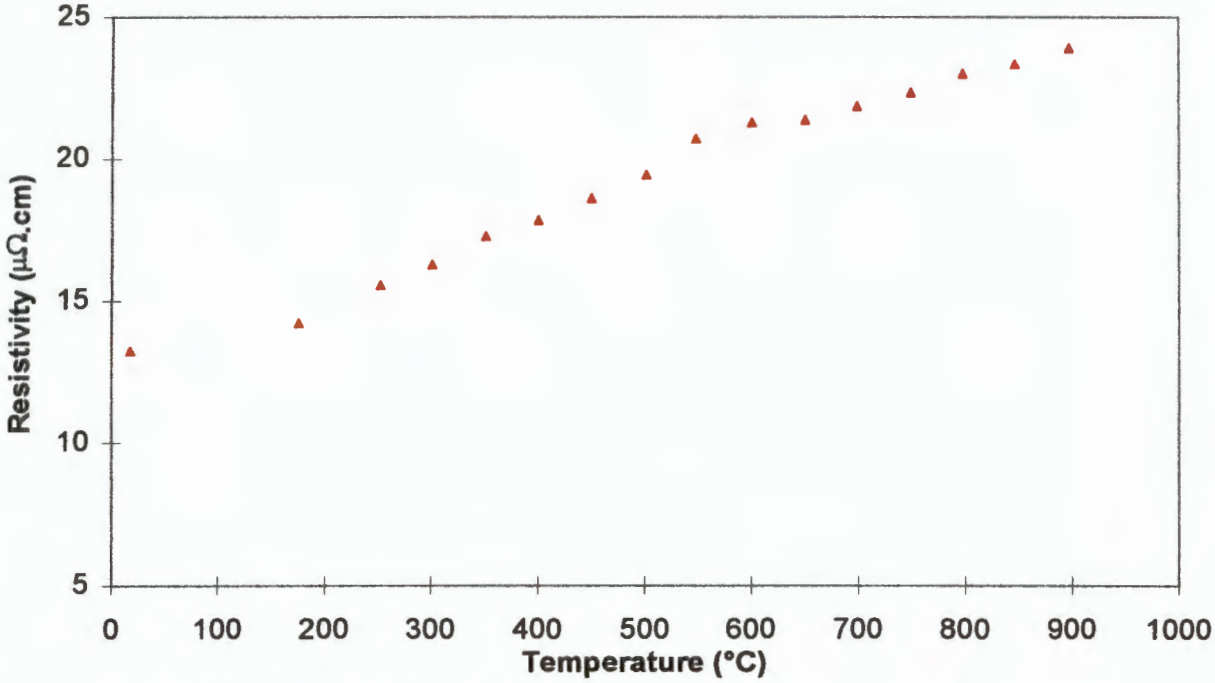

Figure A1 Graph of resistivity vs. temperature for cold-worked Pt 5 wt% Mo.

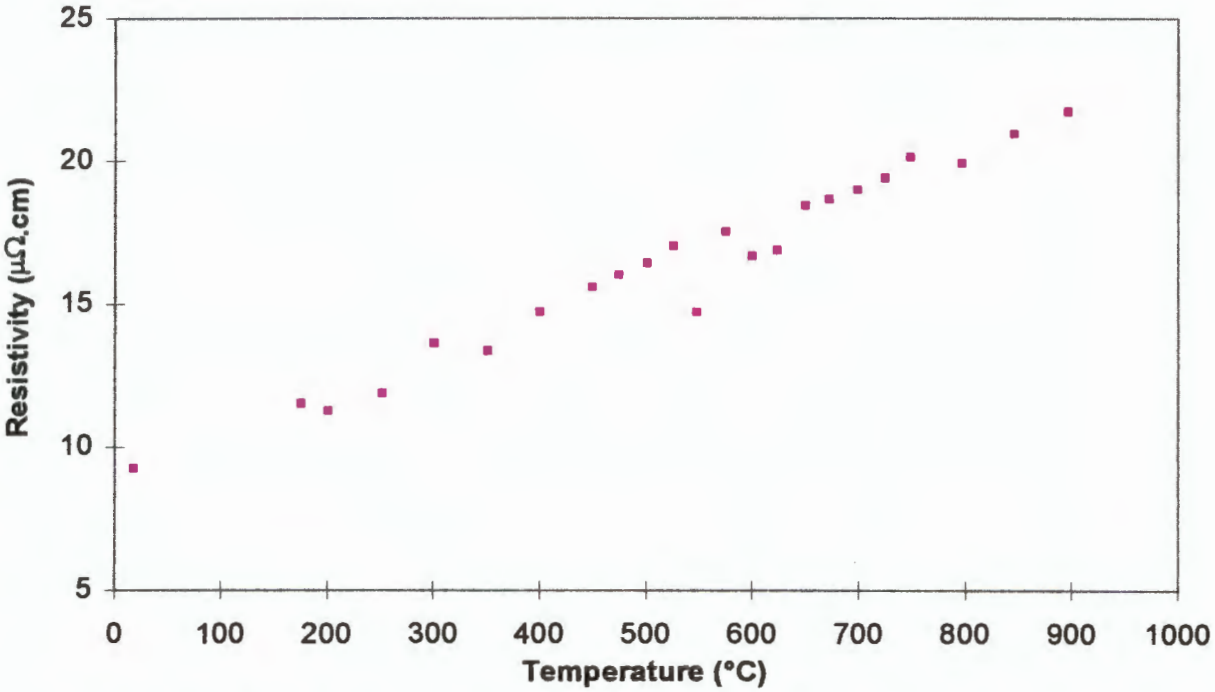

Figure A2 Graph of resistivity vs. temperature for Pt 5 wt% Mo retested once.

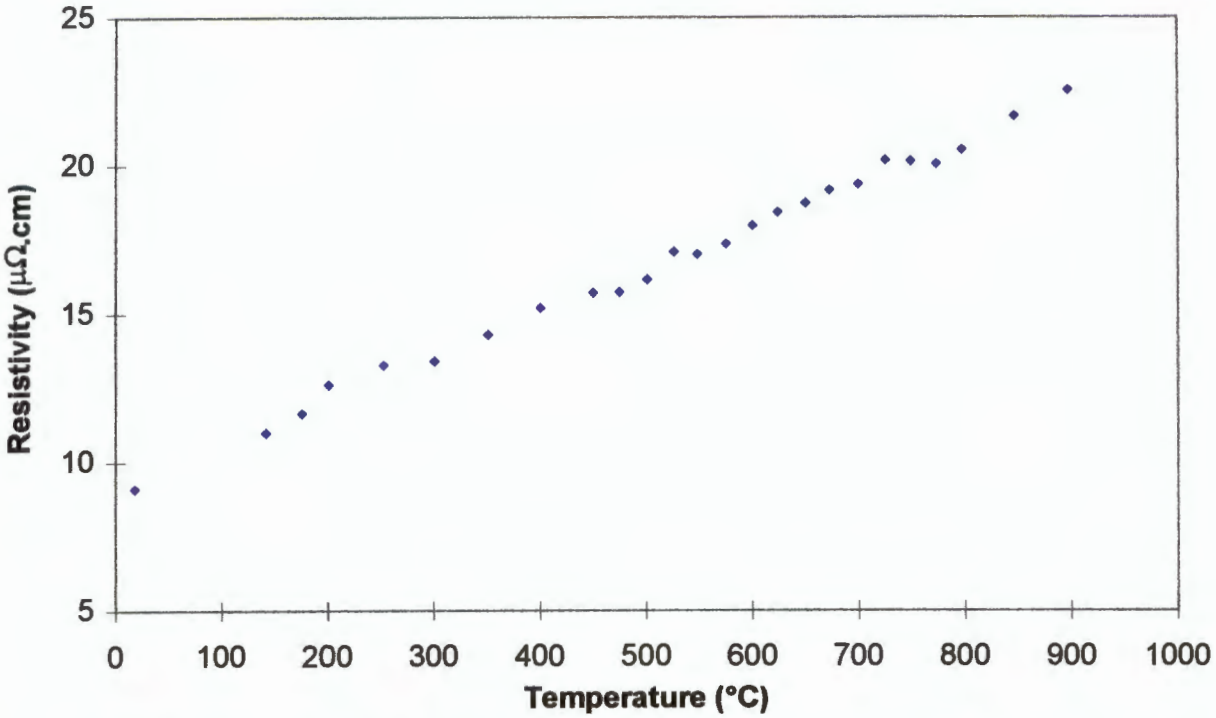

Figure A3 **Graph of resistivity vs. temperature for Pt 5 wt% Mo rested twice.**

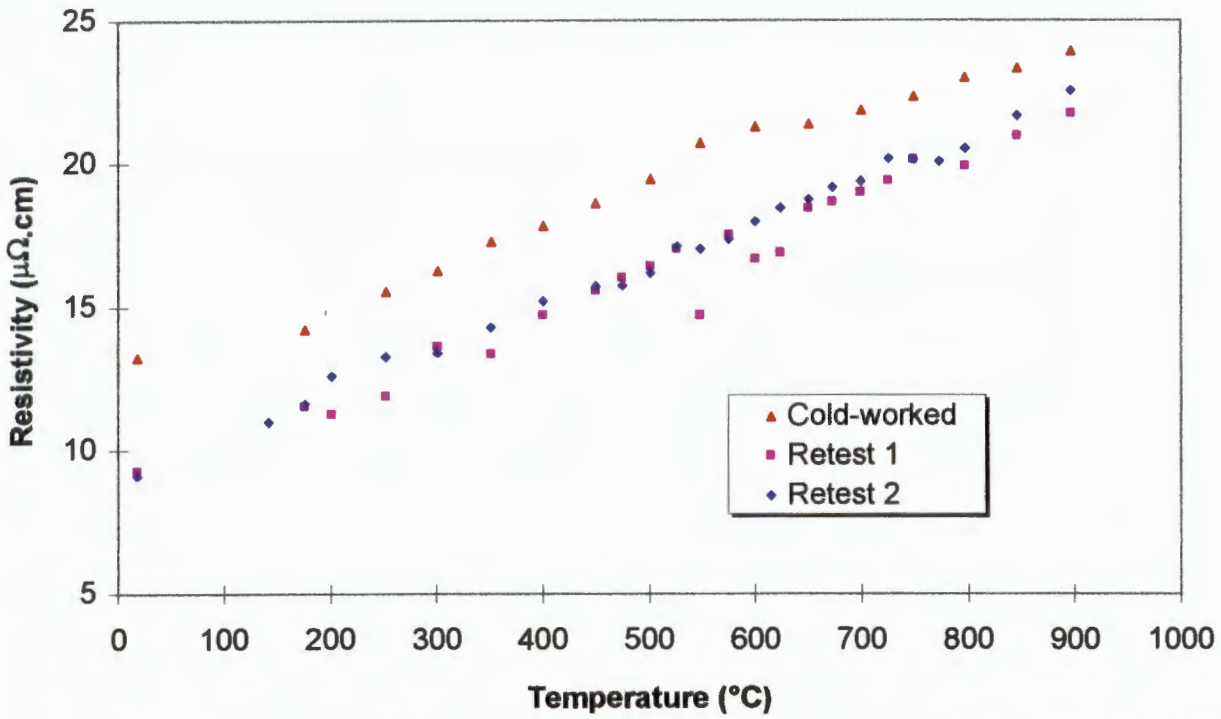

Figure A4 **Combined graph of resistivity vs. temperature for cold-worked Pt 5 at% Mo, rested once and retested twice.**

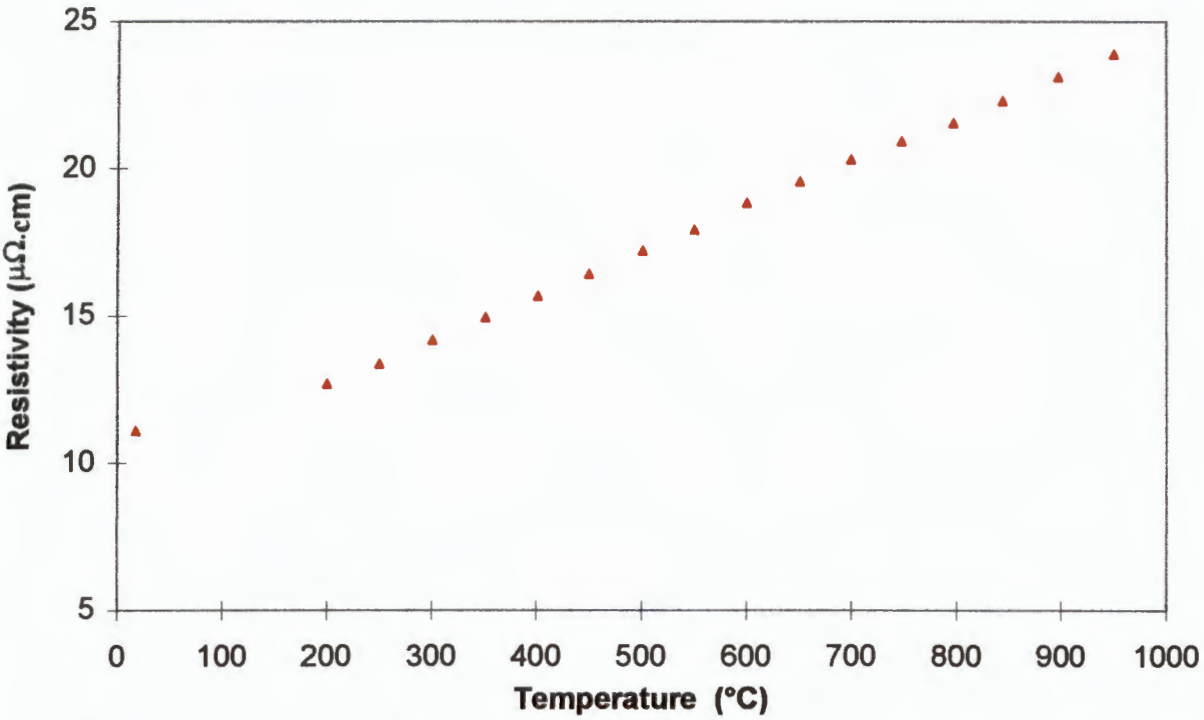

Figure A5 Graph of resistivity vs. temperature for cold-worked Pt 5 wt% Ru.

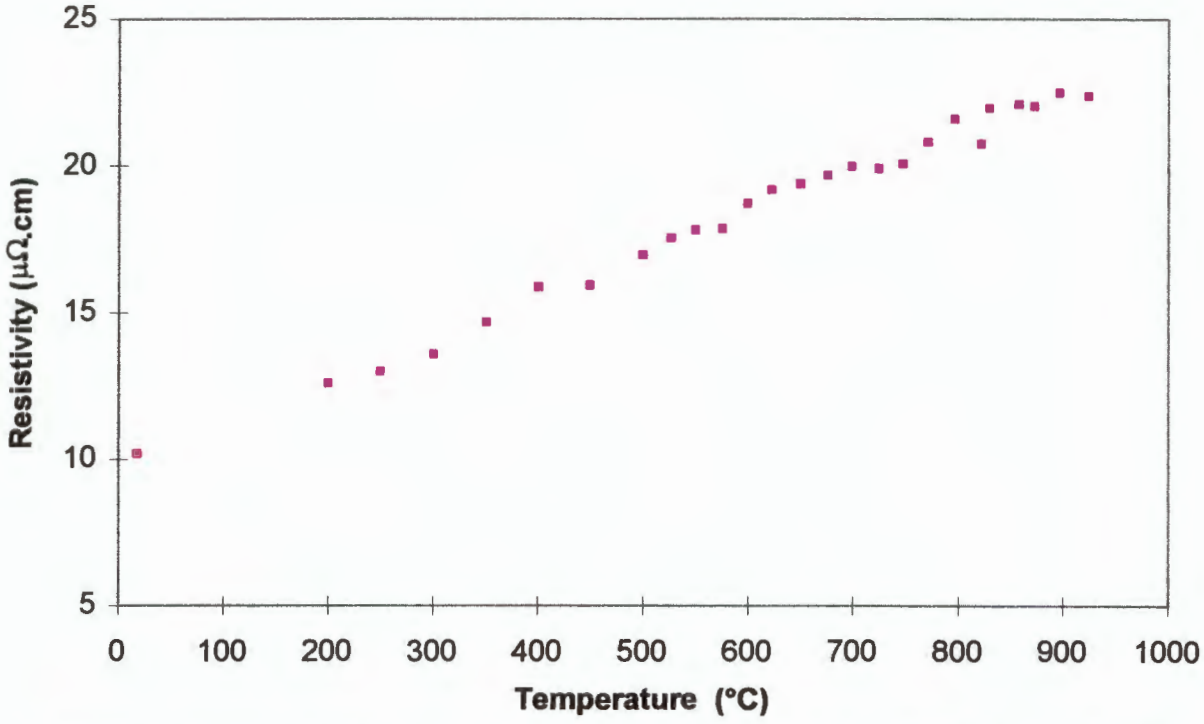

Figure A6 Graph of resistivity vs. temperature for Pt 5 wt% Ru retested once.

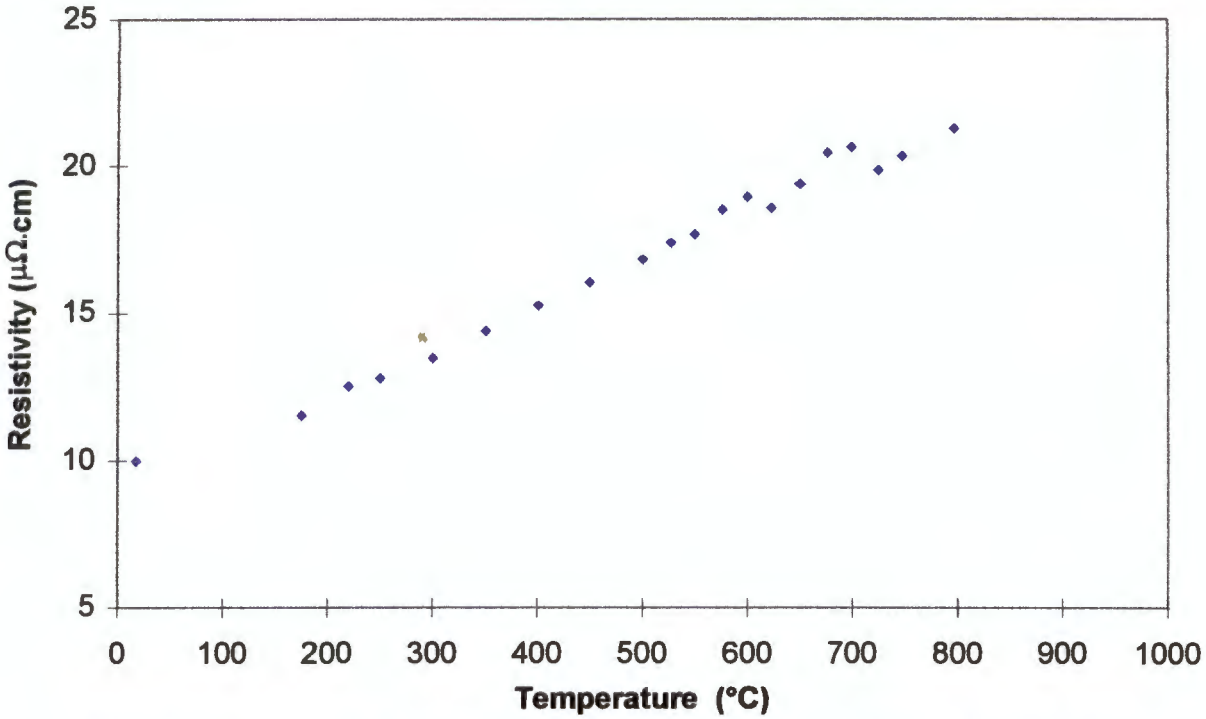

Figure A7 **Graph of resistivity vs. temperature for Pt 5 wt% Ru rested twice**

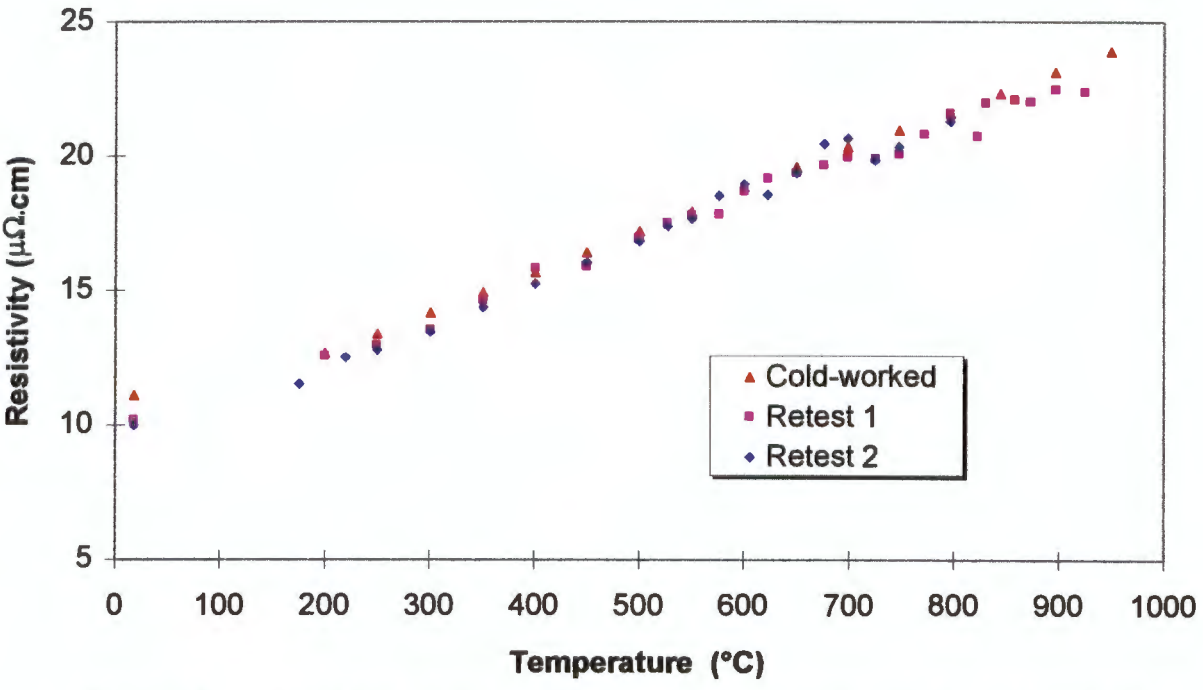

Figure A8 **Combined graph of resistivity vs. temperature for cold-worked Pt 5 wt% Ru, retested once and retested twice.**

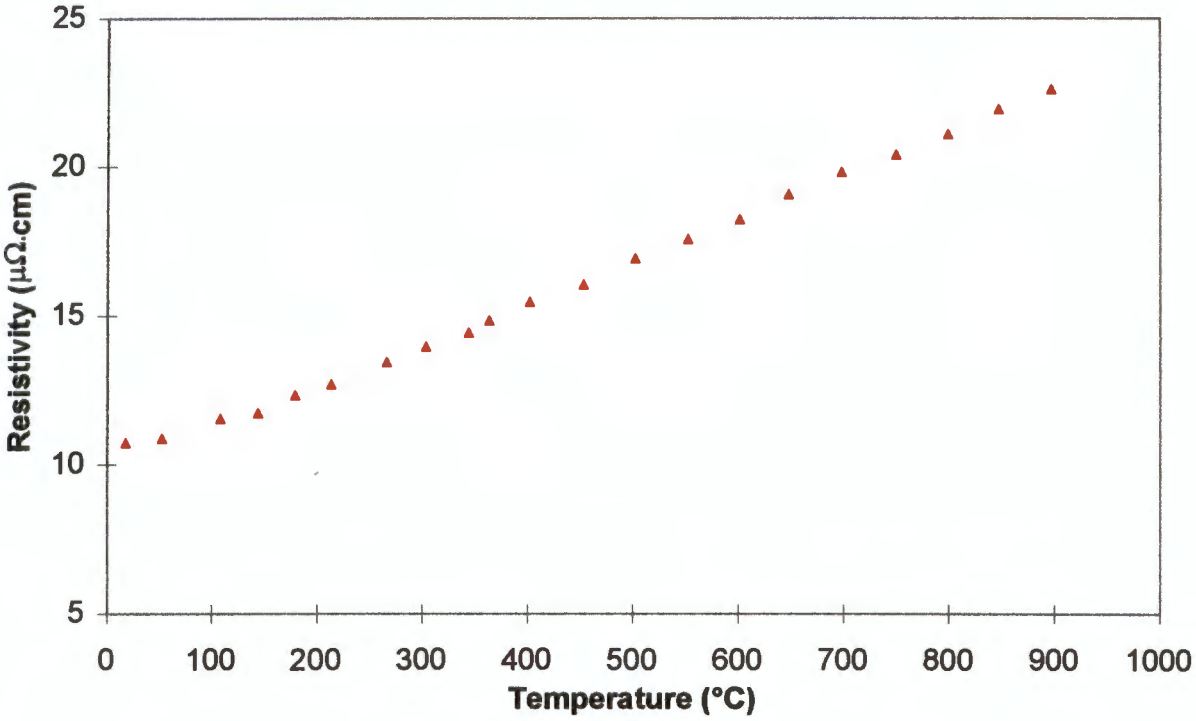

Figure A9 Graph of resistivity vs. temperature for cold-worked Pt 5 wt% Cu.

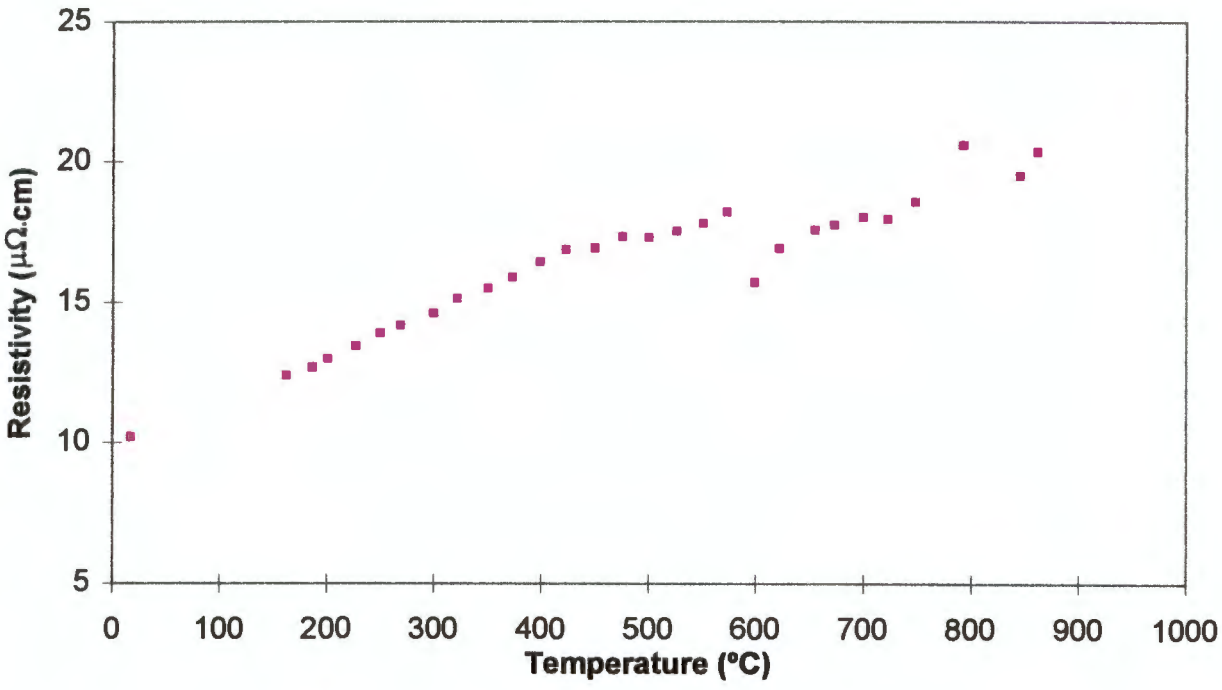

Figure A10 Graph of resistivity vs. temperature for Pt 5 wt% Cu retested once.

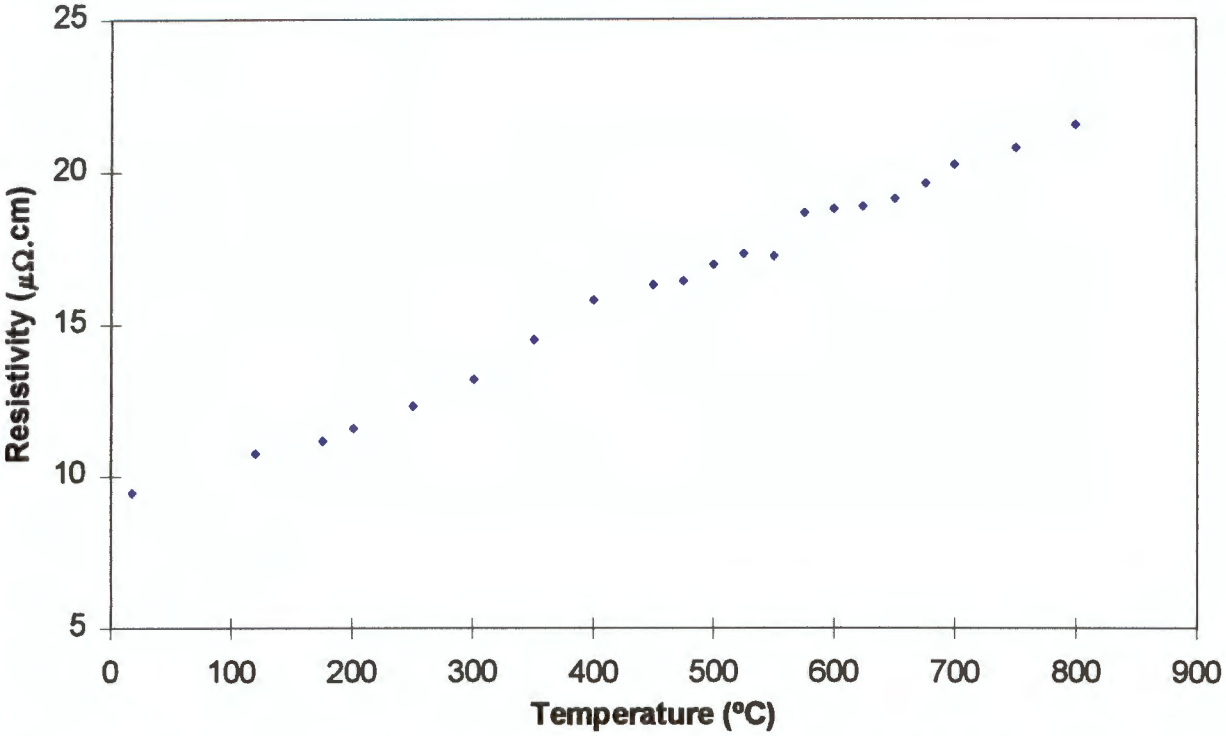

Figure A11 Graph of resistivity vs. temperature for Pt 5 wt% Cu retested twice.

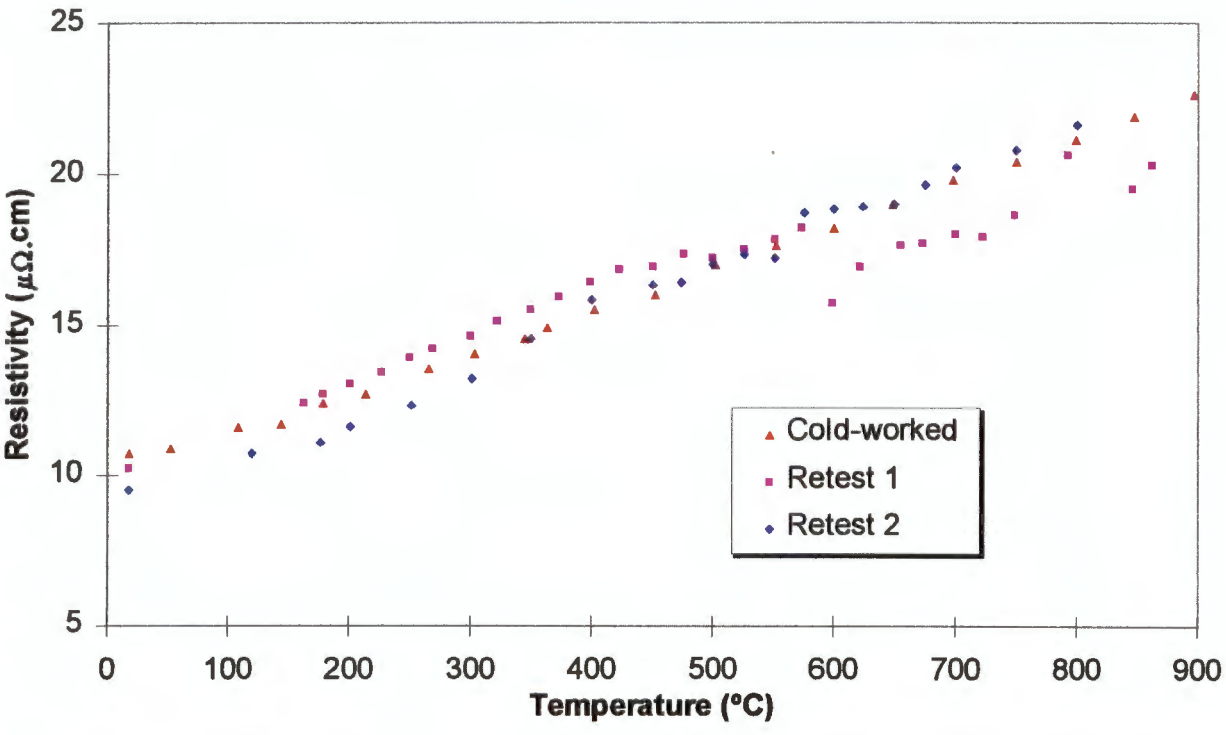

Figure A12 Combined graph of resistivity vs. temperature for cold-worked Pt 5 wt% Cu, retested once and retested twice.

APPENDIX B

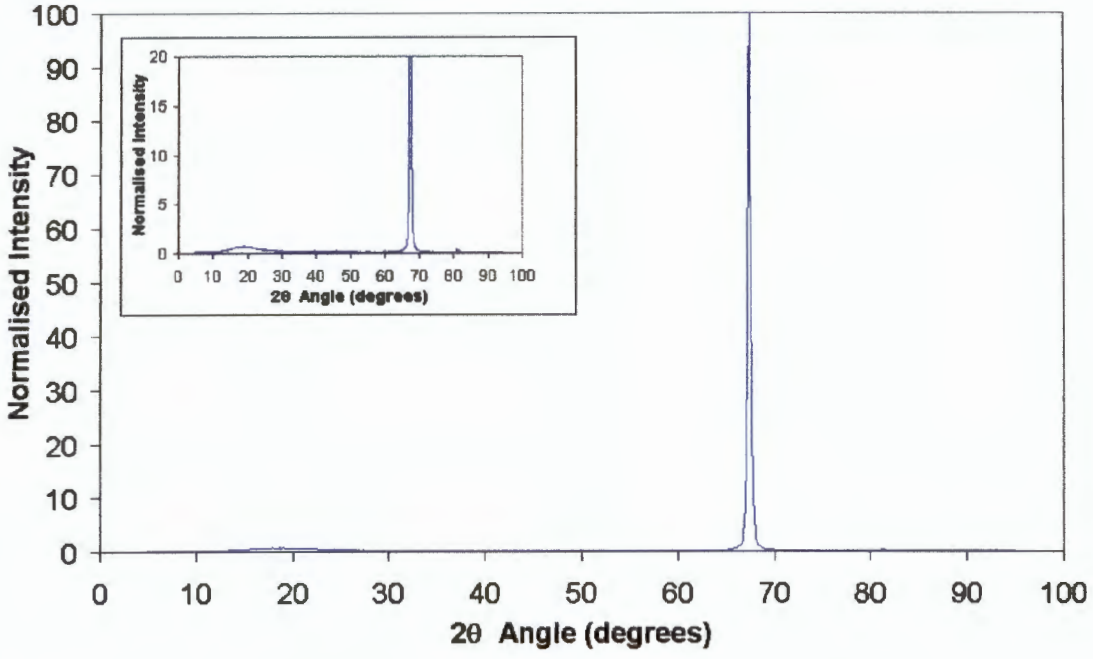

Figure B1 **X-ray diffraction profile of cold-worked platinum.**

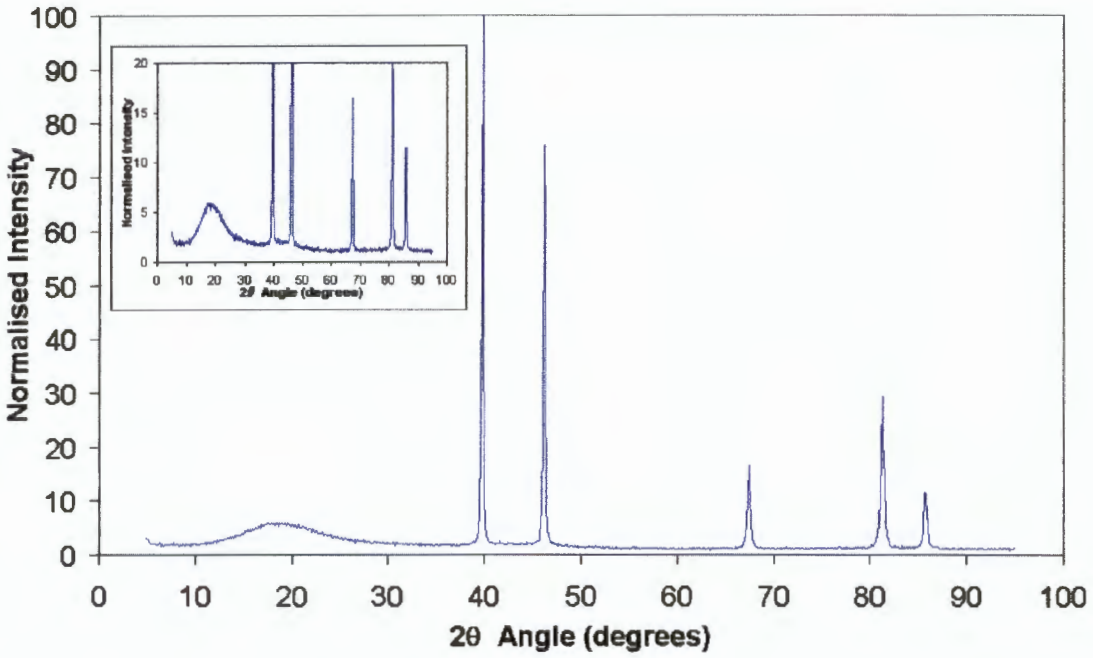

Figure B2 **X-ray diffraction profile of platinum annealed for 3 hours at 700°C.**

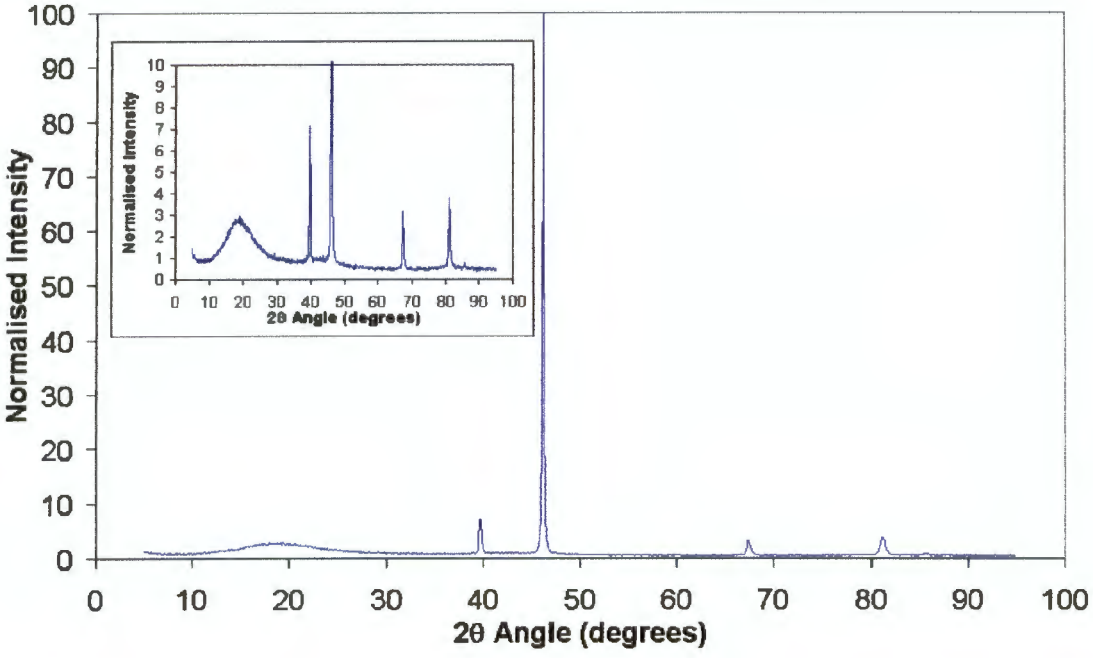

Figure B3 **X-ray diffraction profile of platinum annealed for 3 hours at 1000°C.**

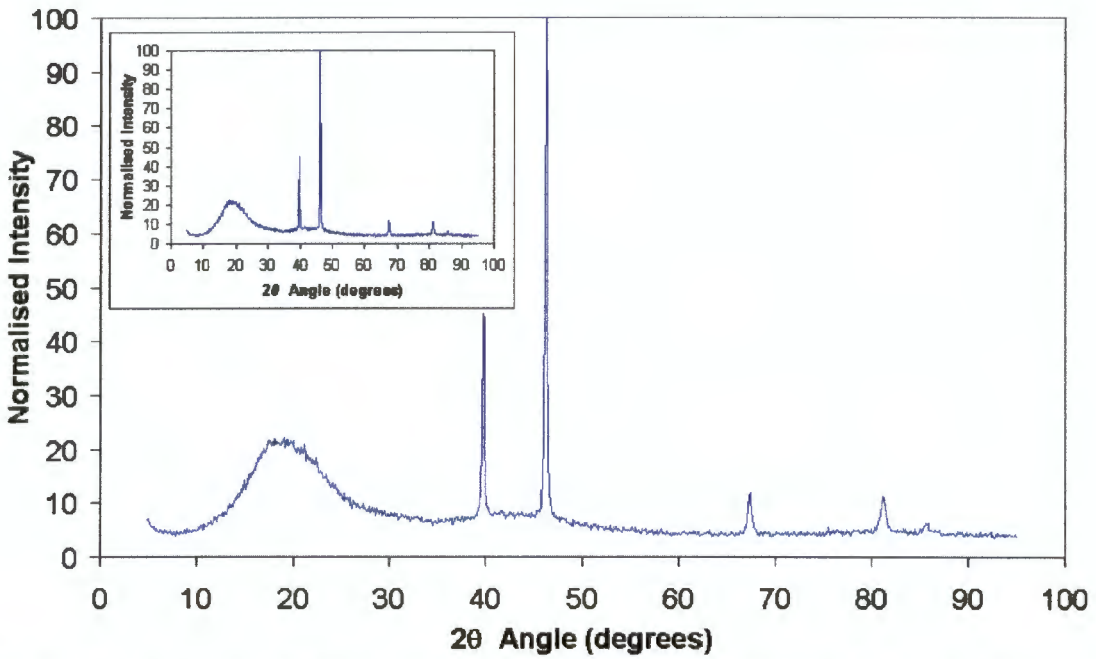

Figure B4 **X-ray diffraction profile of platinum annealed for 3 hours at 1300°C.**

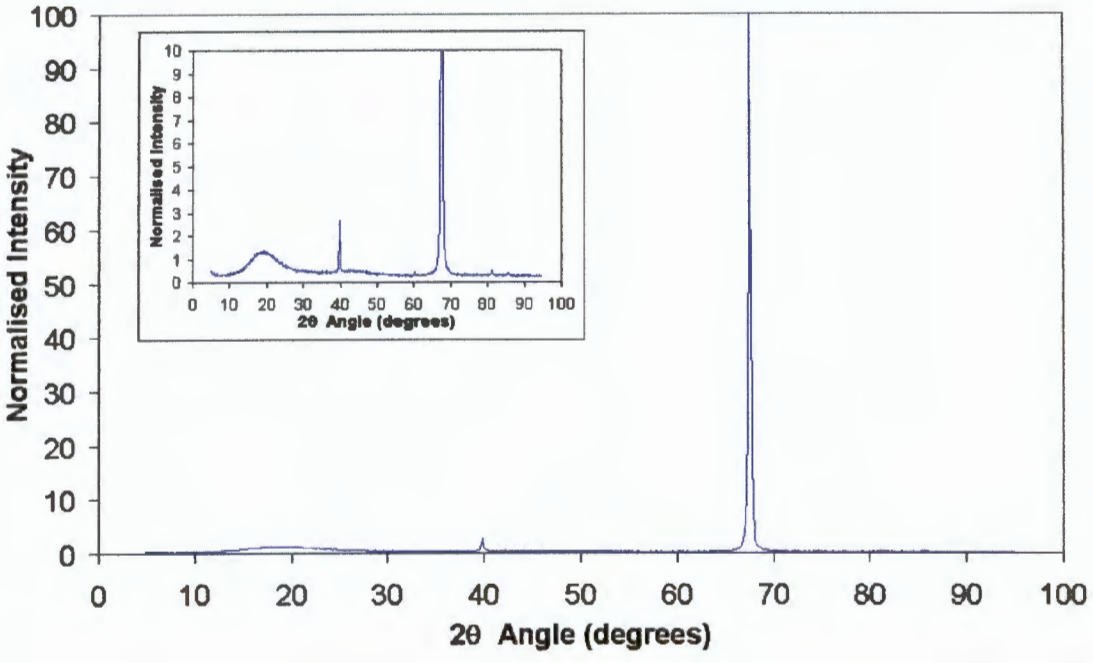

Figure B5 **X-ray diffraction profile of platinum annealed for 0.5 hours at 300°C.**

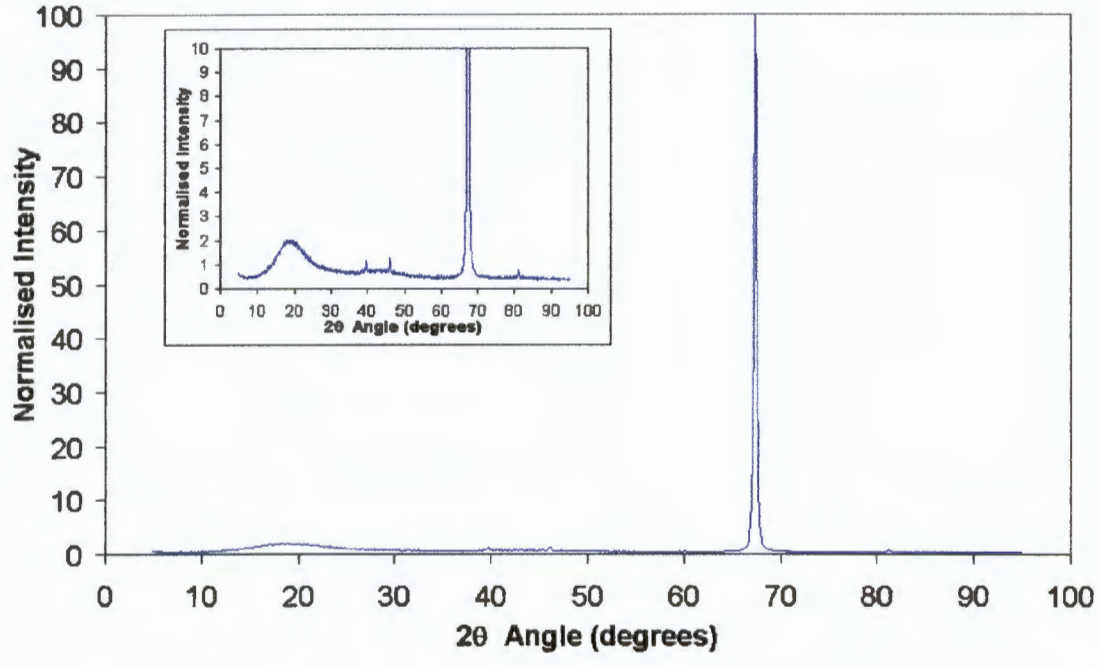

Figure B6 **X-ray diffraction profile of platinum annealed for 10 hours at 300°C.**

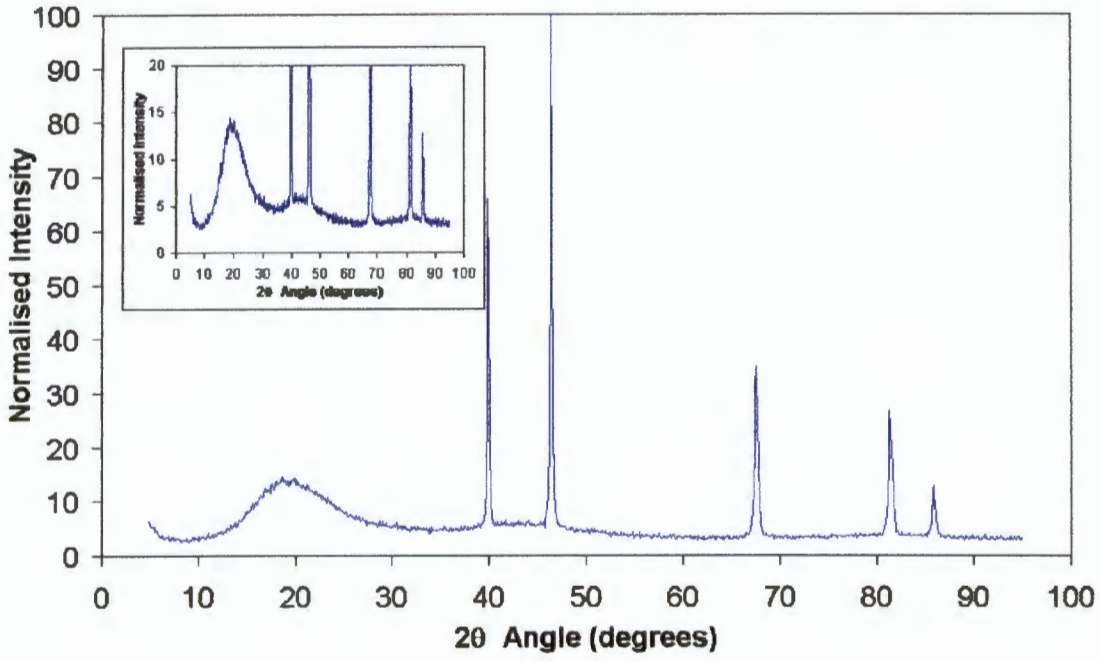

Figure B7 **X-ray diffraction profile of platinum annealed for 0.5 hours at 700°C.**

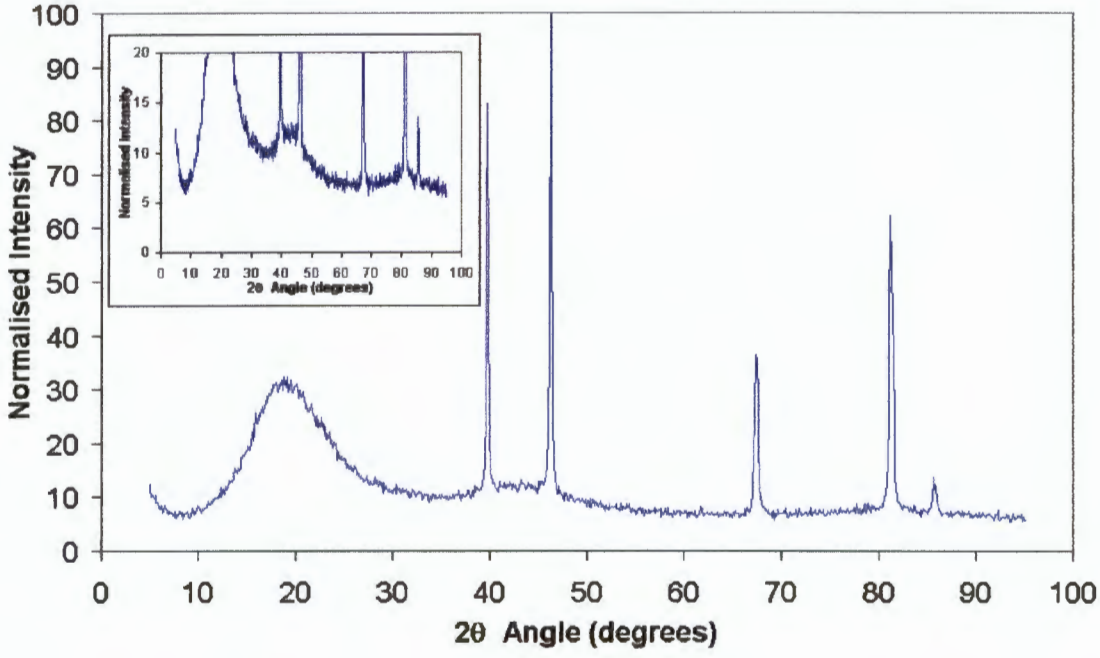

Figure B8 **X-ray diffraction profile of platinum annealed for 10 hours at 700°C.**

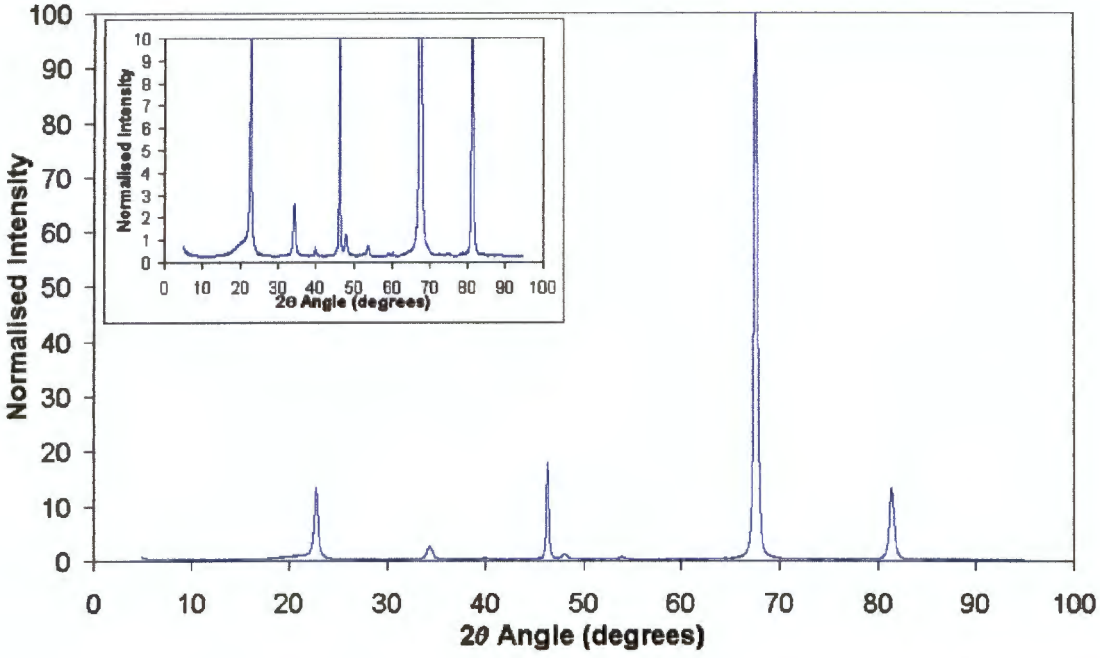

Figure B9 **X-ray diffraction profile of cold-worked Pt 5 at% Mo.**

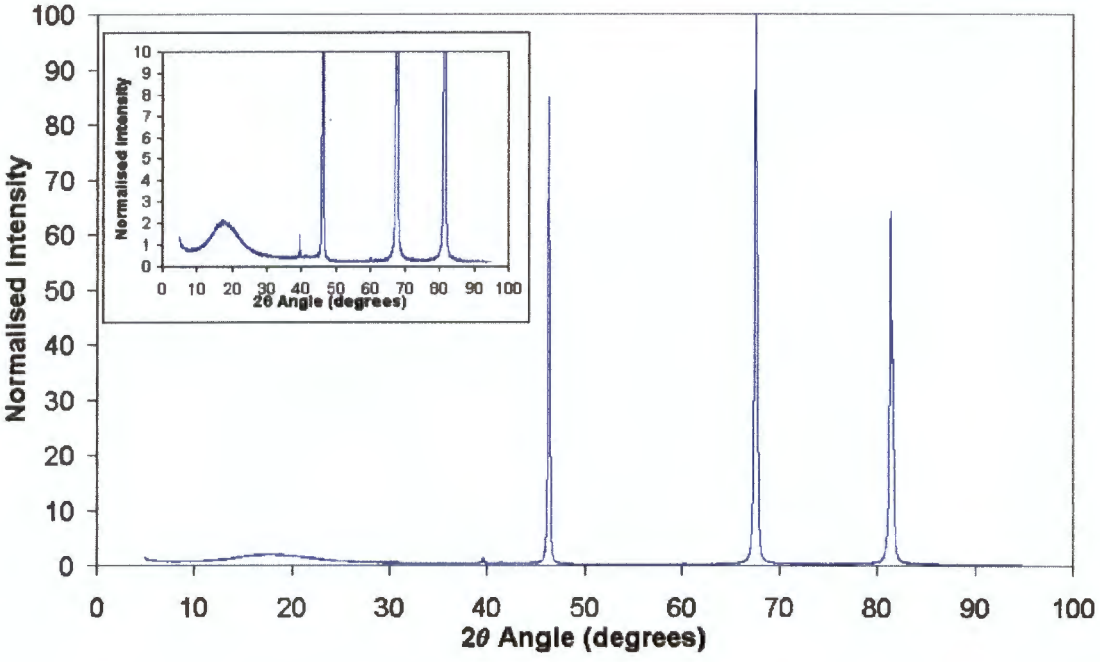

Figure B10 **X-ray diffraction profile of Pt 5 at% Mo annealed for 3 hours at 700°C**

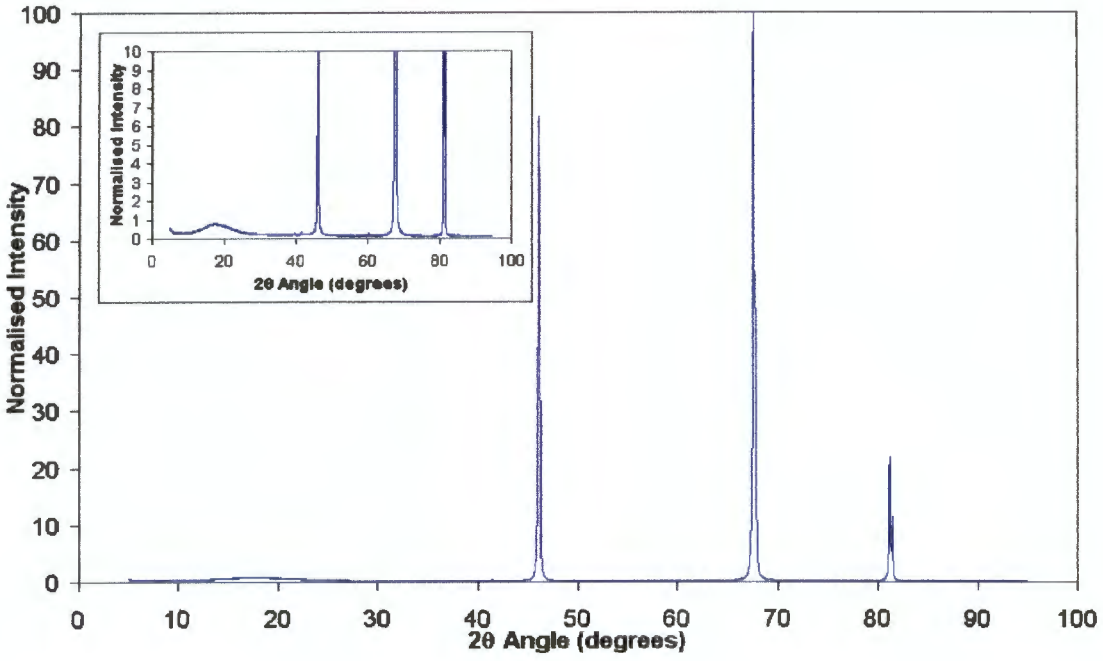

Figure B11 X-ray diffraction profile of Pt 5 at% Mo annealed for 3 hours at 1000°C

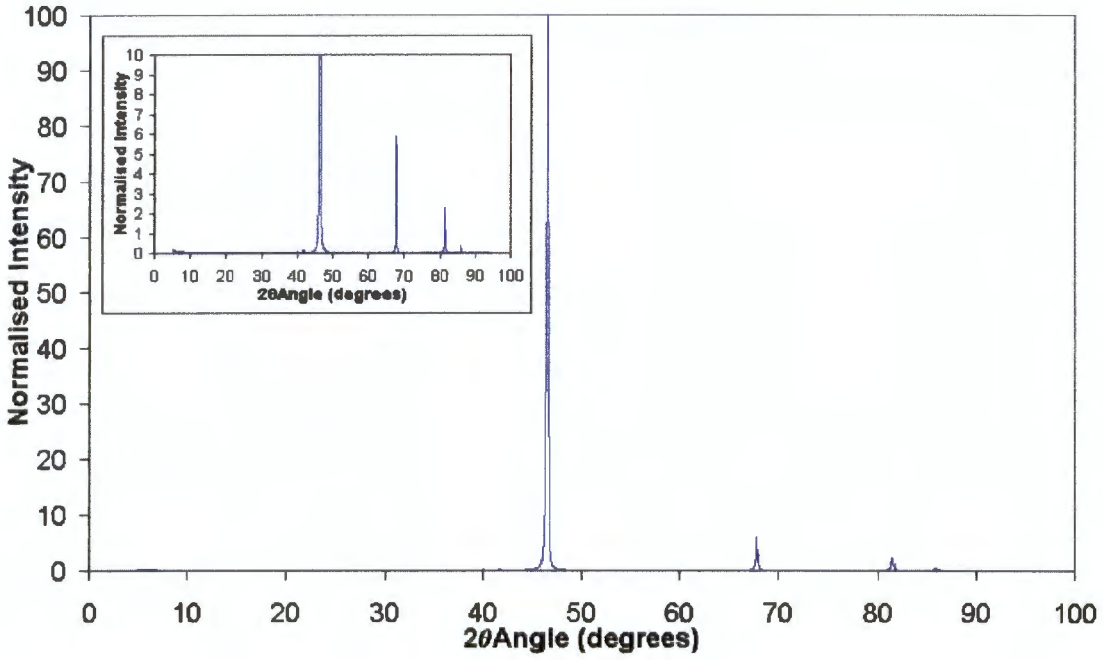

Figure B12 X-ray diffraction profile of Pt 5 at% Mo annealed for 3 hours at 1300°C

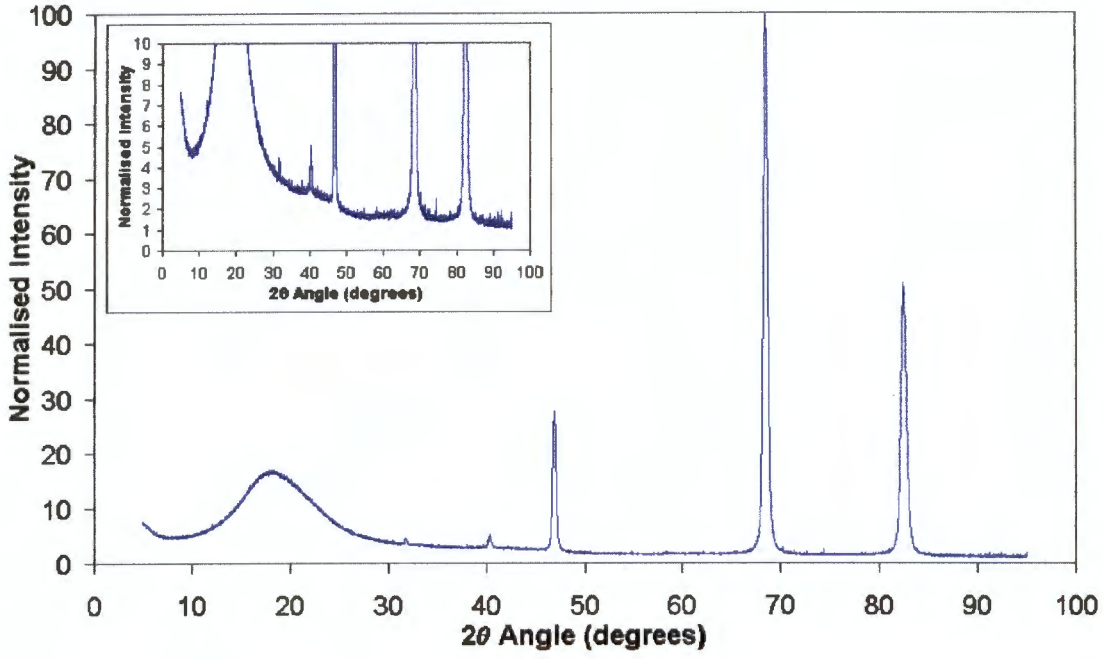

Figure B13 X-ray diffraction profile of cold-worked Pt 5 wt% Ru.

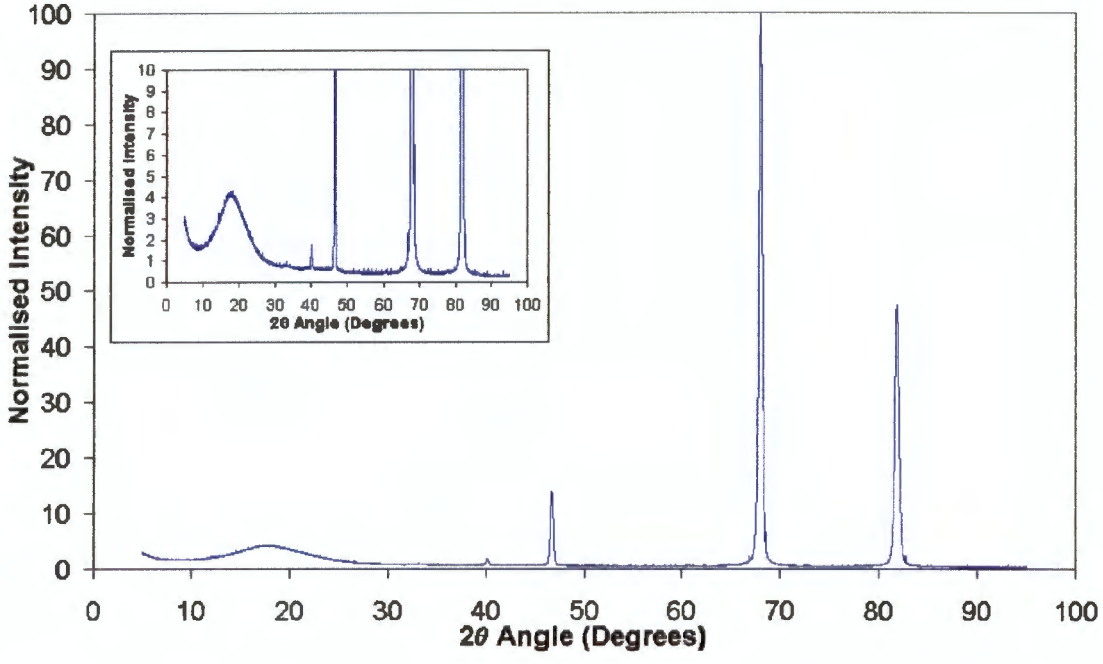

Figure B14 X-ray diffraction profile of Pt 5 wt% Ru annealed for 3 hours at 700°C

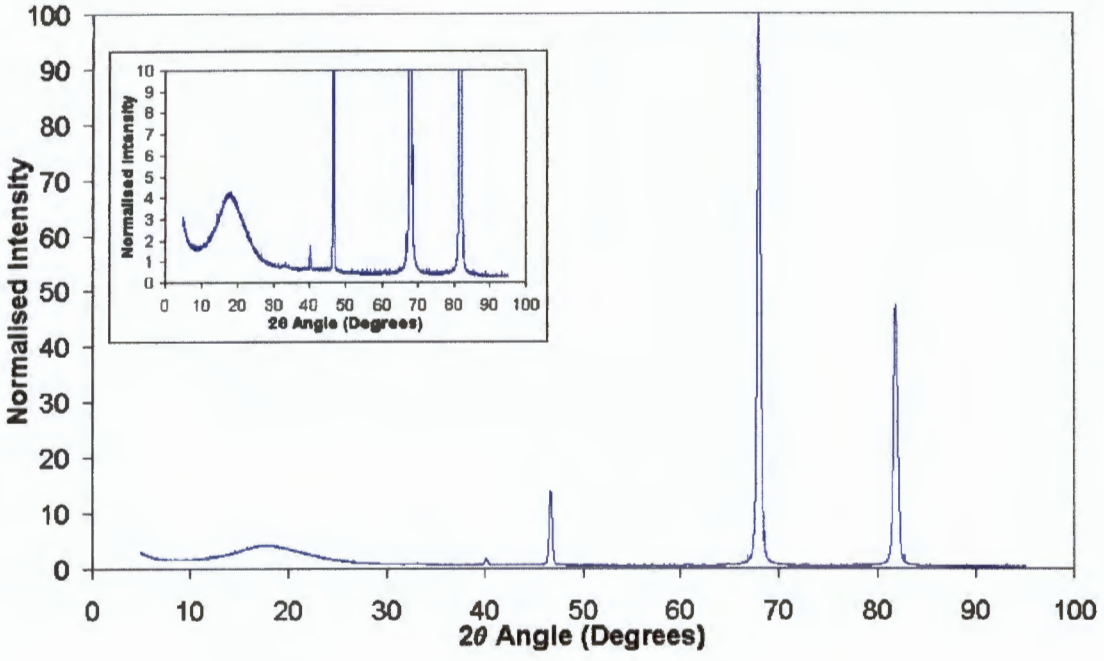

Figure B15 **X-ray diffraction profile of Pt 5 wt% Ru annealed for 3 hours at 1000°C**

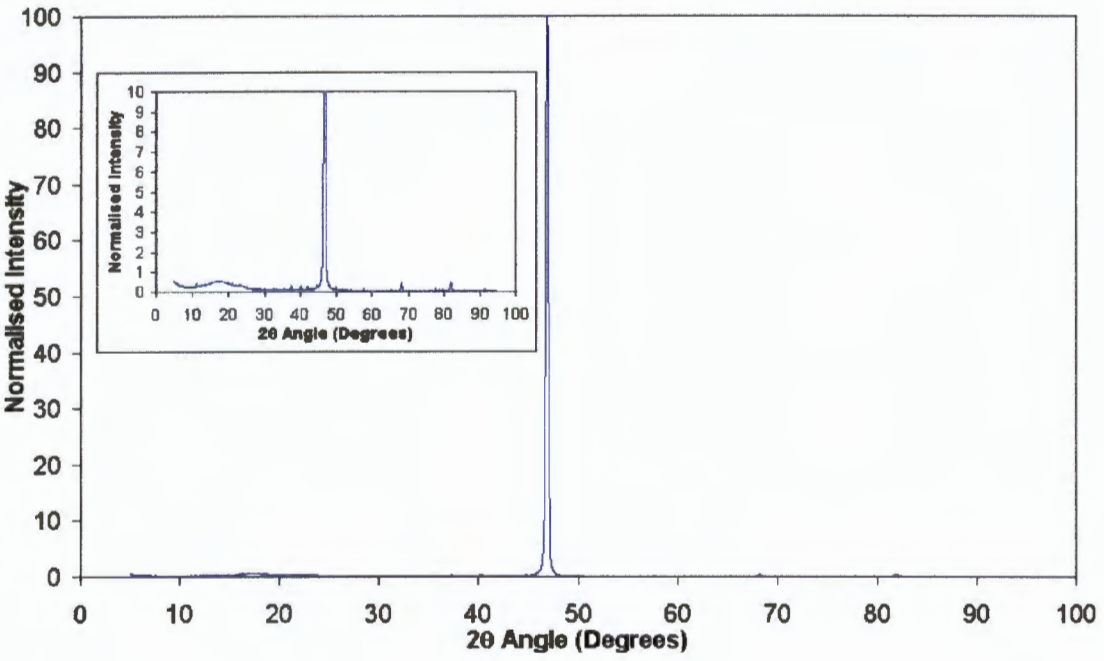

Figure B16 **X-ray diffraction profile of Pt 5 wt% Ru annealed for 3 hours at 1300°C**

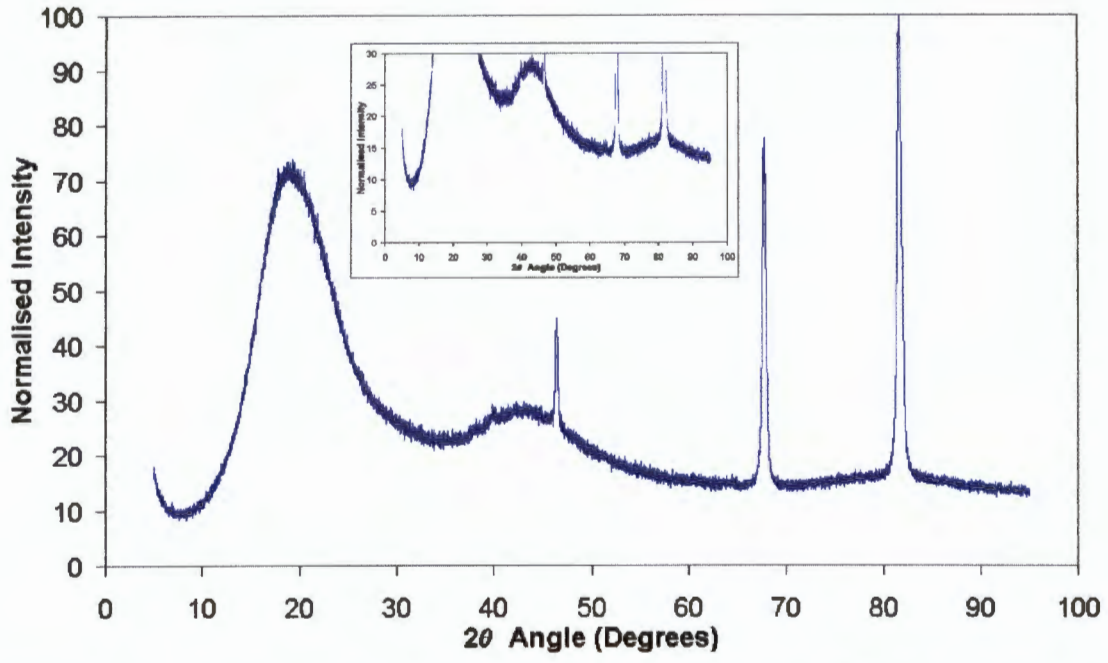

Figure B17 **X-ray diffraction profile of Pt 5 wt% Cu in the cold worked condition.**

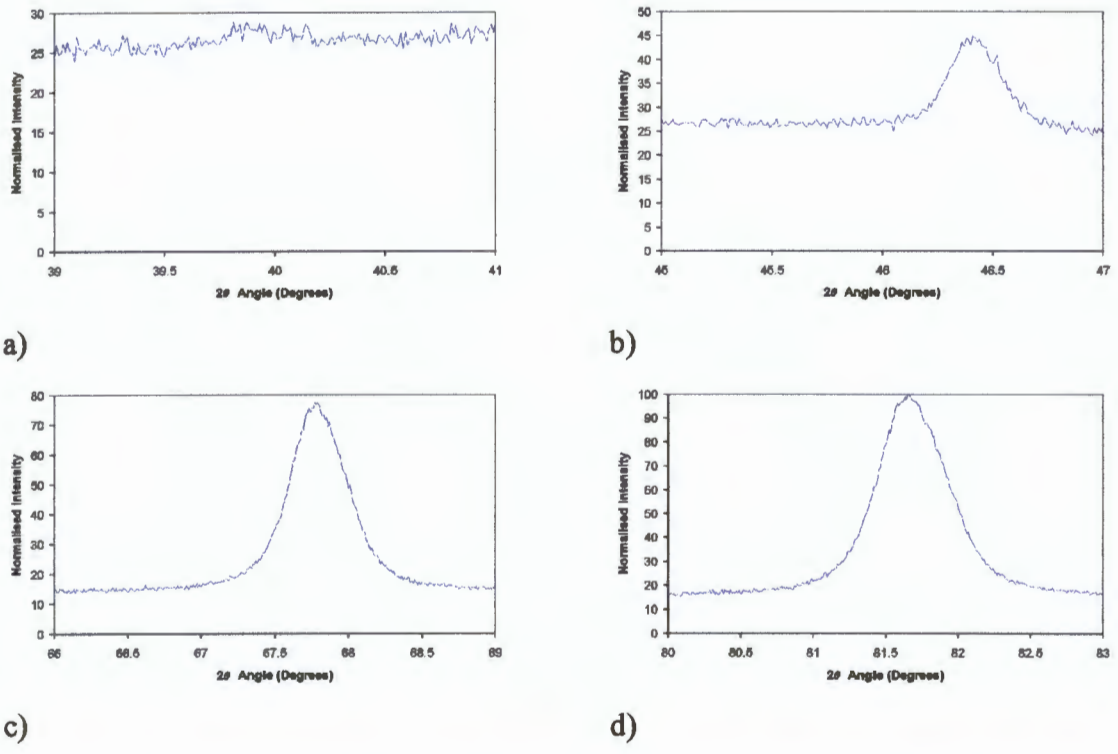

Figure B18 **Isolated peaks from Figure B17: a) 39°-41° b) 45°-47°, c) 66°-79° and d) 80°-83°.**

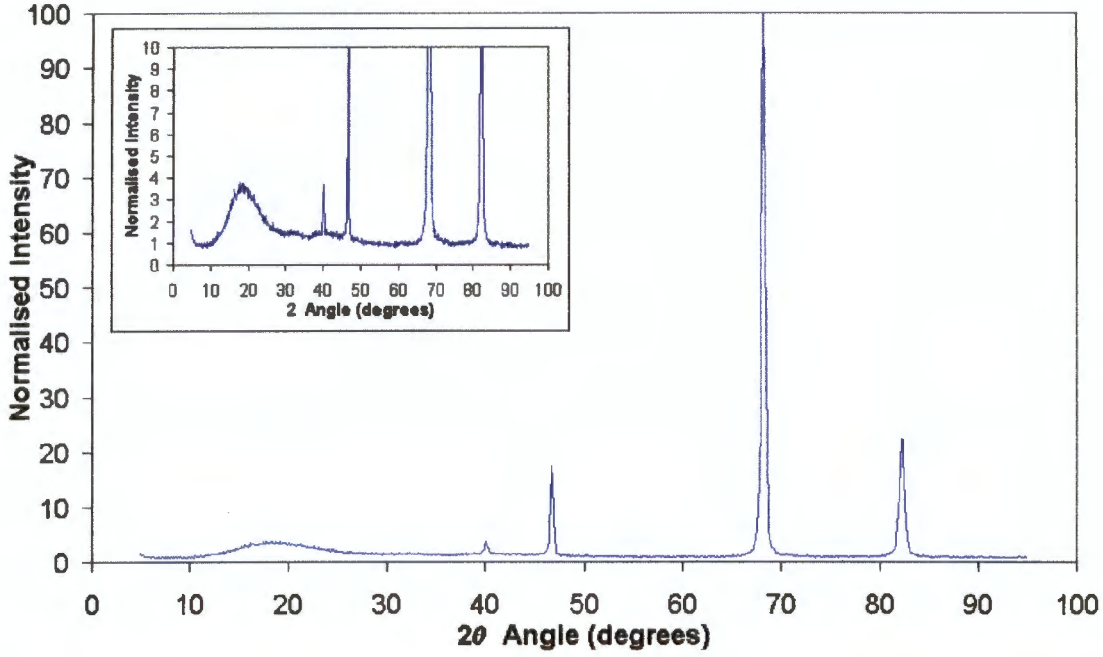

Figure B19 **X-ray diffraction profile of Pt 5 wt% Cu annealed at 300°C for 0.5 hours.**

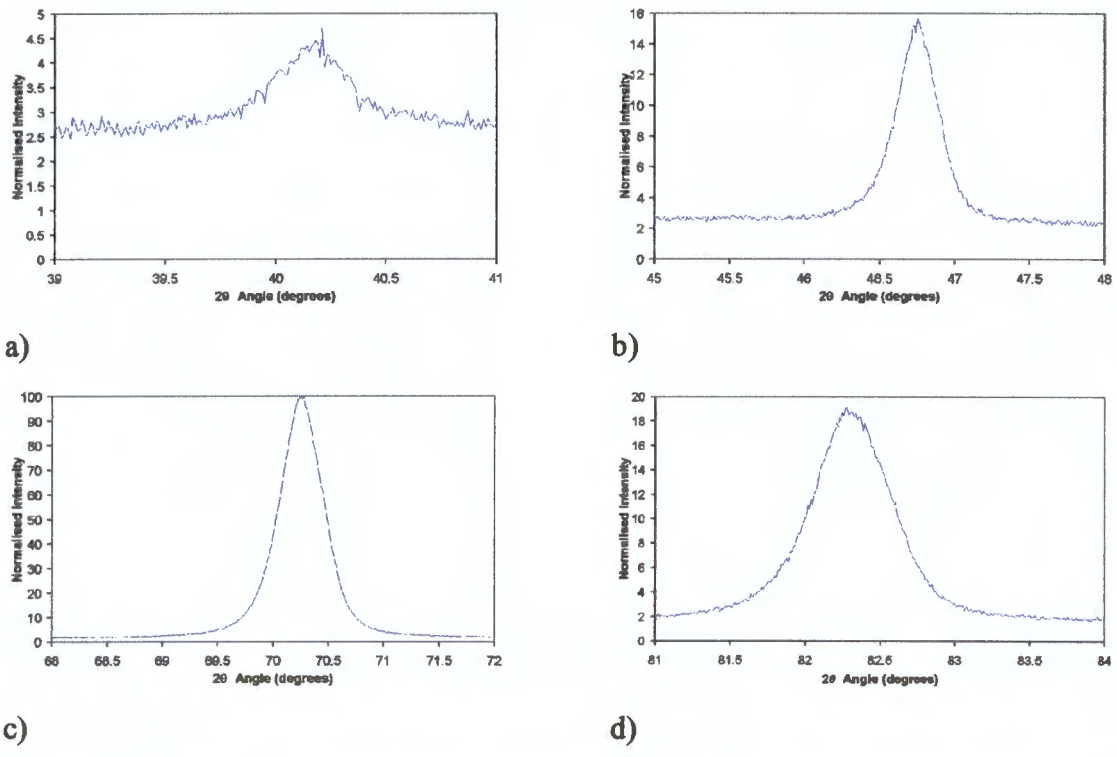

Figure B20 **Isolated peaks from Figure B19: a) 39°-41° b) 46°-48°, c) 68°-72° and d) 81°-84°.**

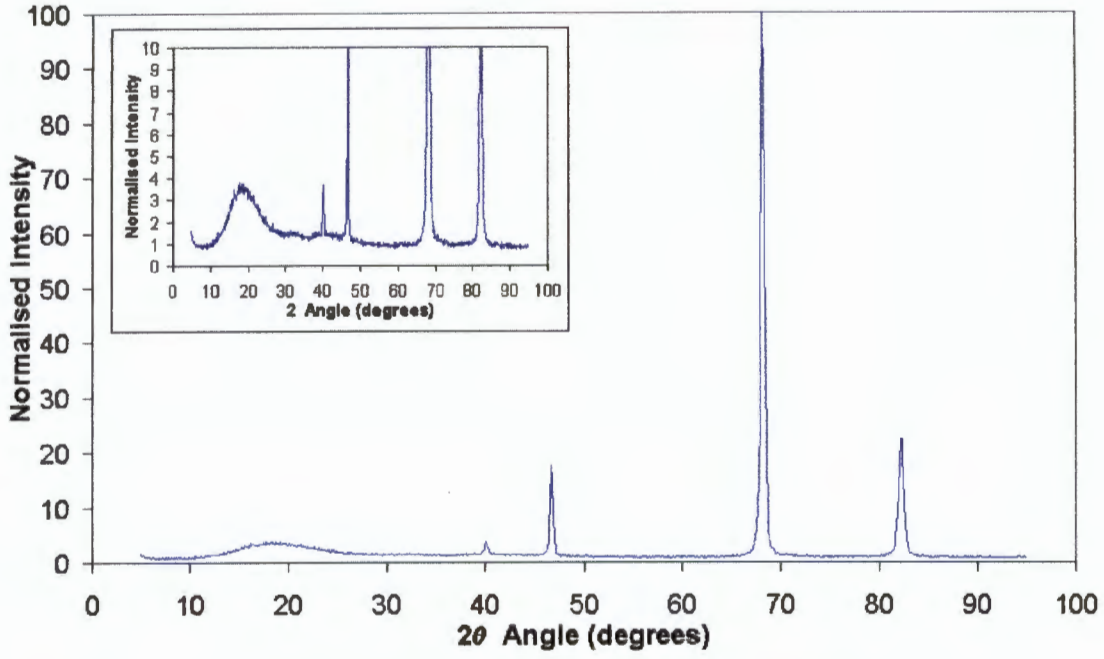

Figure B21 **X-ray diffraction profile of Pt 5 wt% Cu annealed at 300°C for 10 hours.**

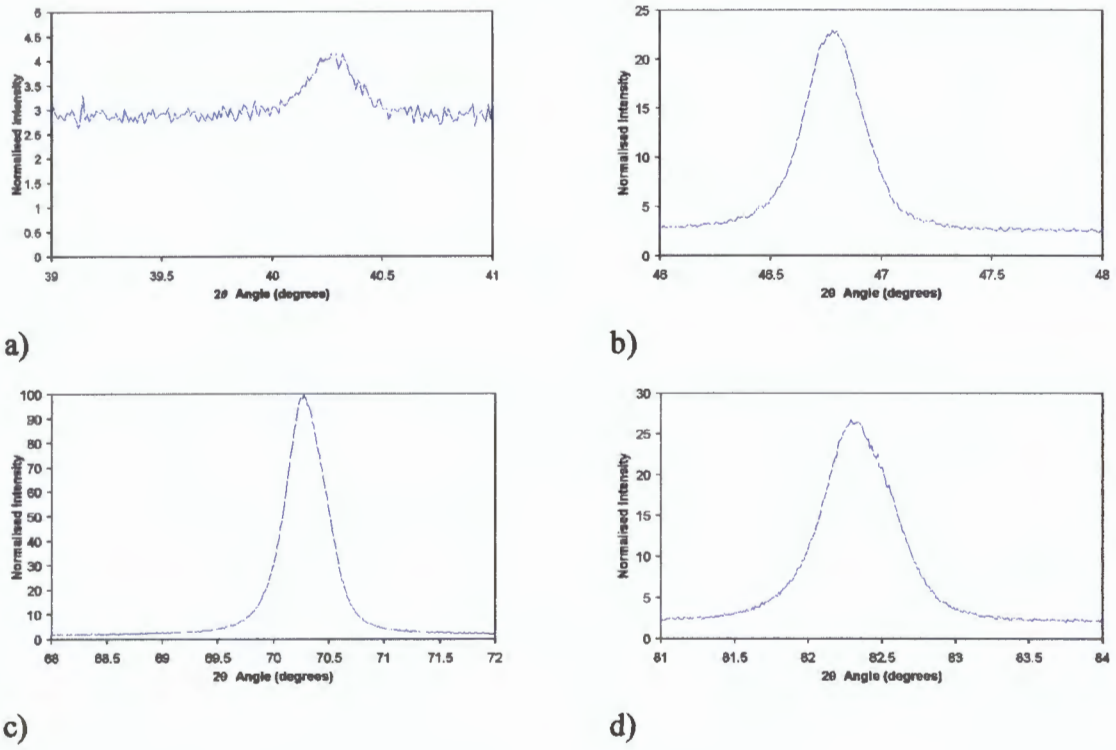

Figure B22 **Isolated peaks from Figure B21 a) 39°-41° b) 46°-48°, c) 68°-72° and d) 81°-84°.**

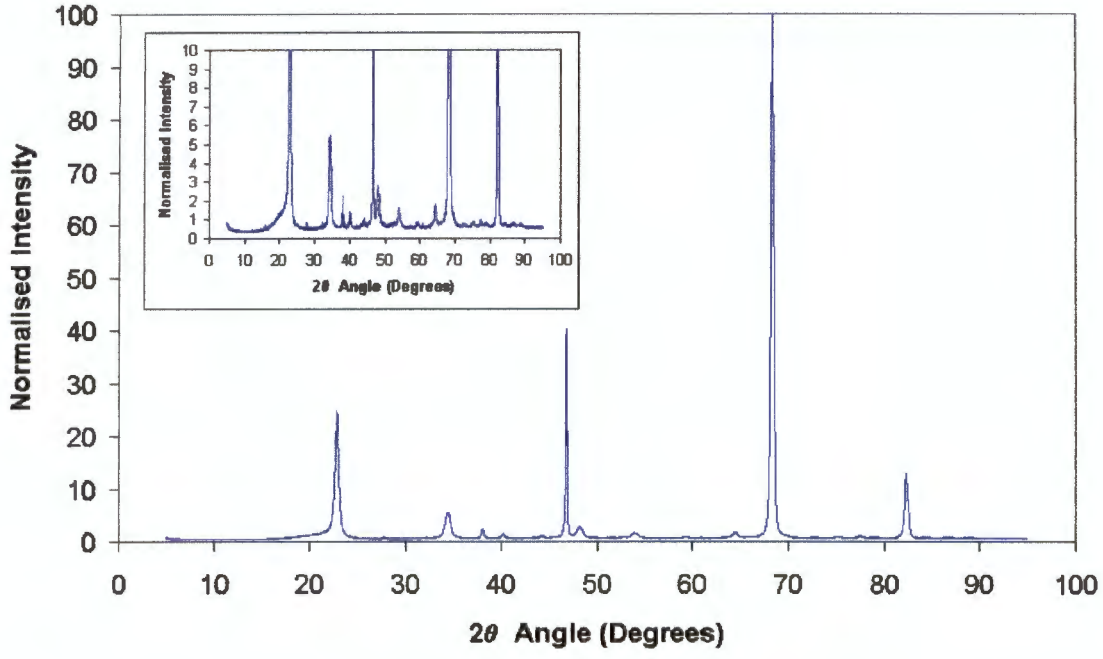

Figure B23 **X-ray diffraction profile of Pt 5 wt% Cu annealed at 700°C for 0.5 hours.**

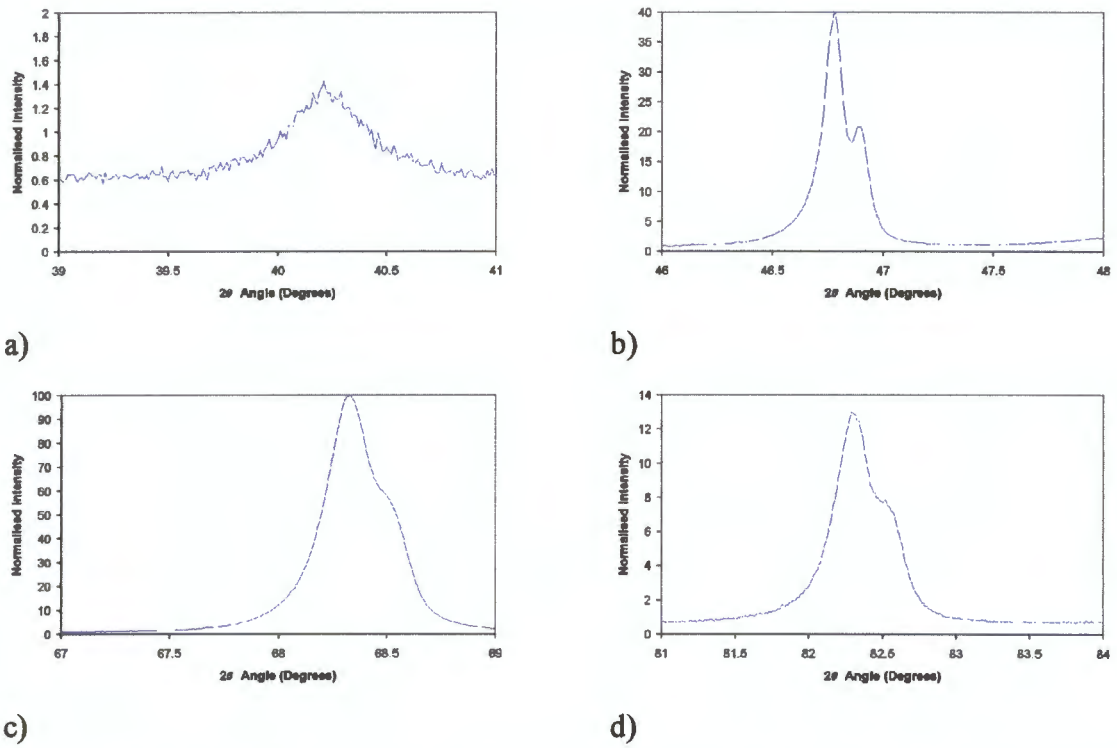

Figure B24 **Isolated peaks from Figure B23: a) 39°-41° b) 46°-48°, c) 67°-79° and d) 81°-84°.**

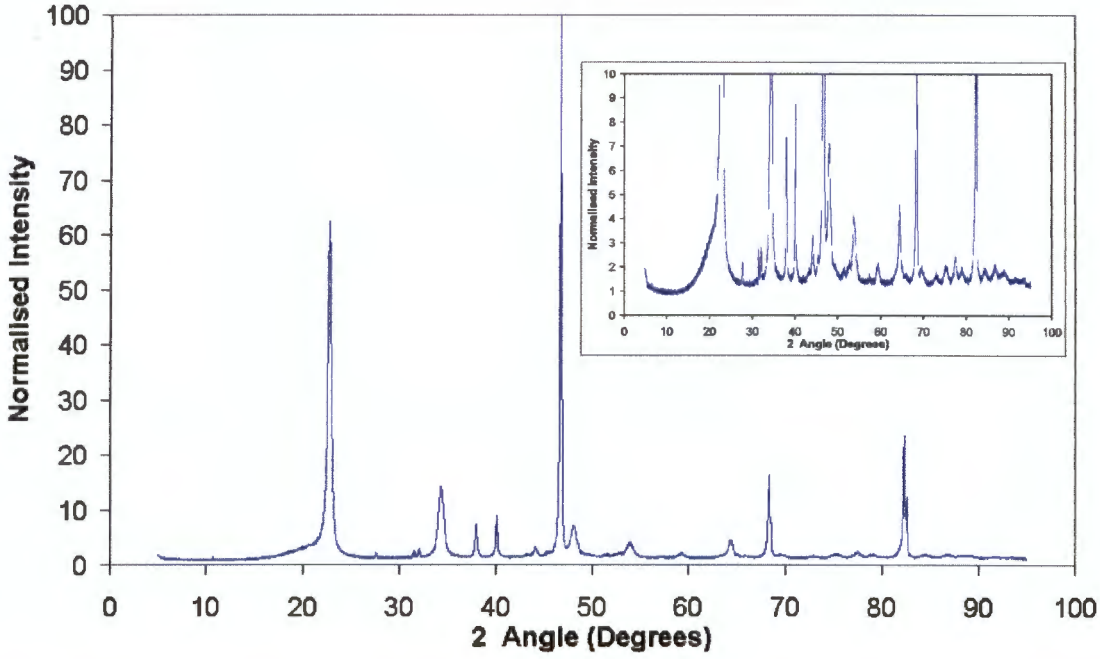

Figure B25 **X-ray diffraction profile of Pt 5 wt% Cu annealed at 700°C for 10 hours.**

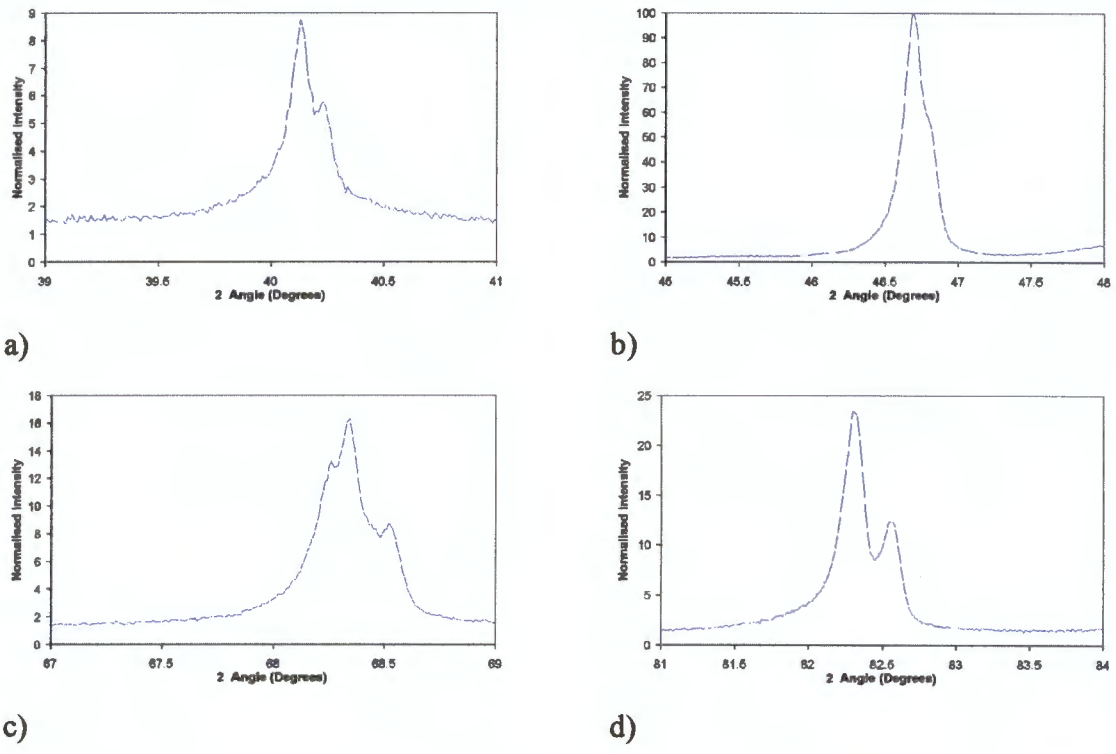

a) b)

c) d)

Figure B26 **Isolated peaks from Figure B25: a) 39°-41° b) 46°-48°, c) 67°-79° and d) 81°-84°.**

APPENDIX C

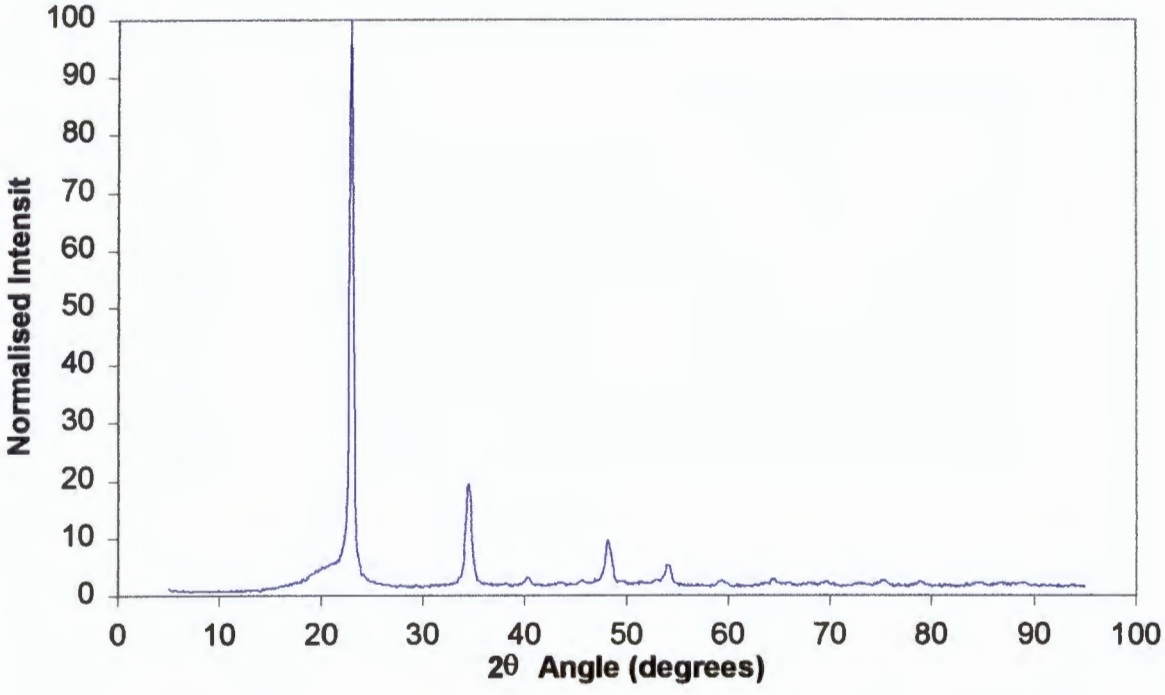

Figure C1 X-ray diffraction pattern of polymeric base – Type 1

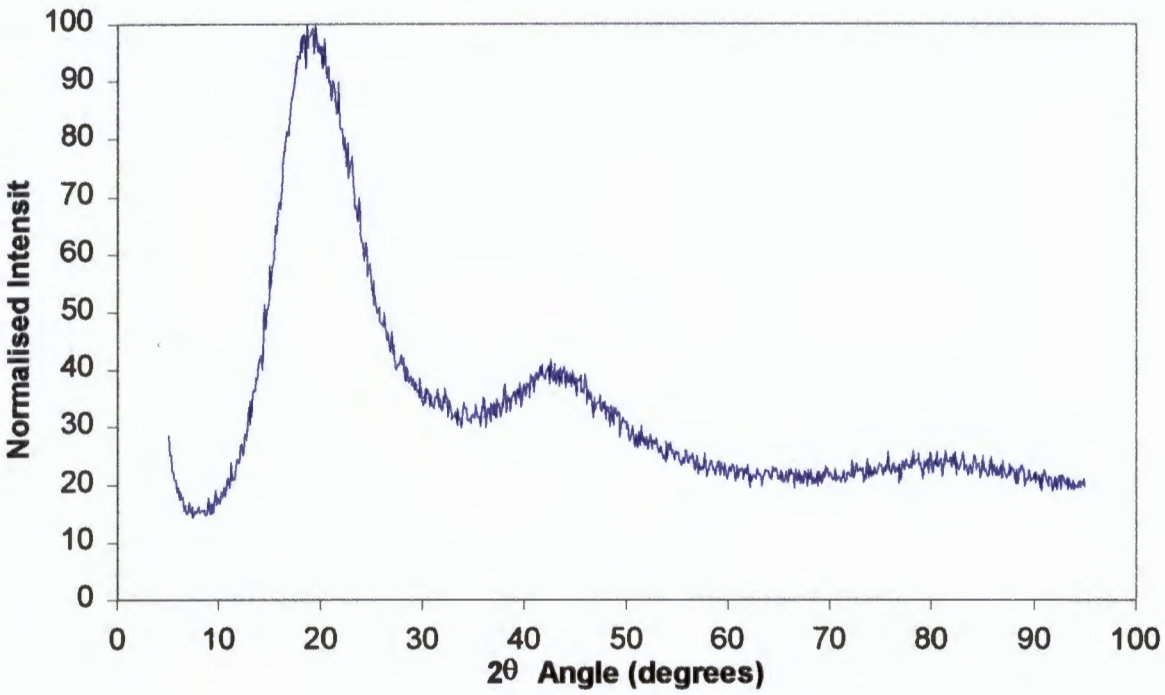

Figure C2 X-ray diffraction pattern of polymeric base – Type 2

APPENDIX D

(DTA curves appear on pages 177-180)

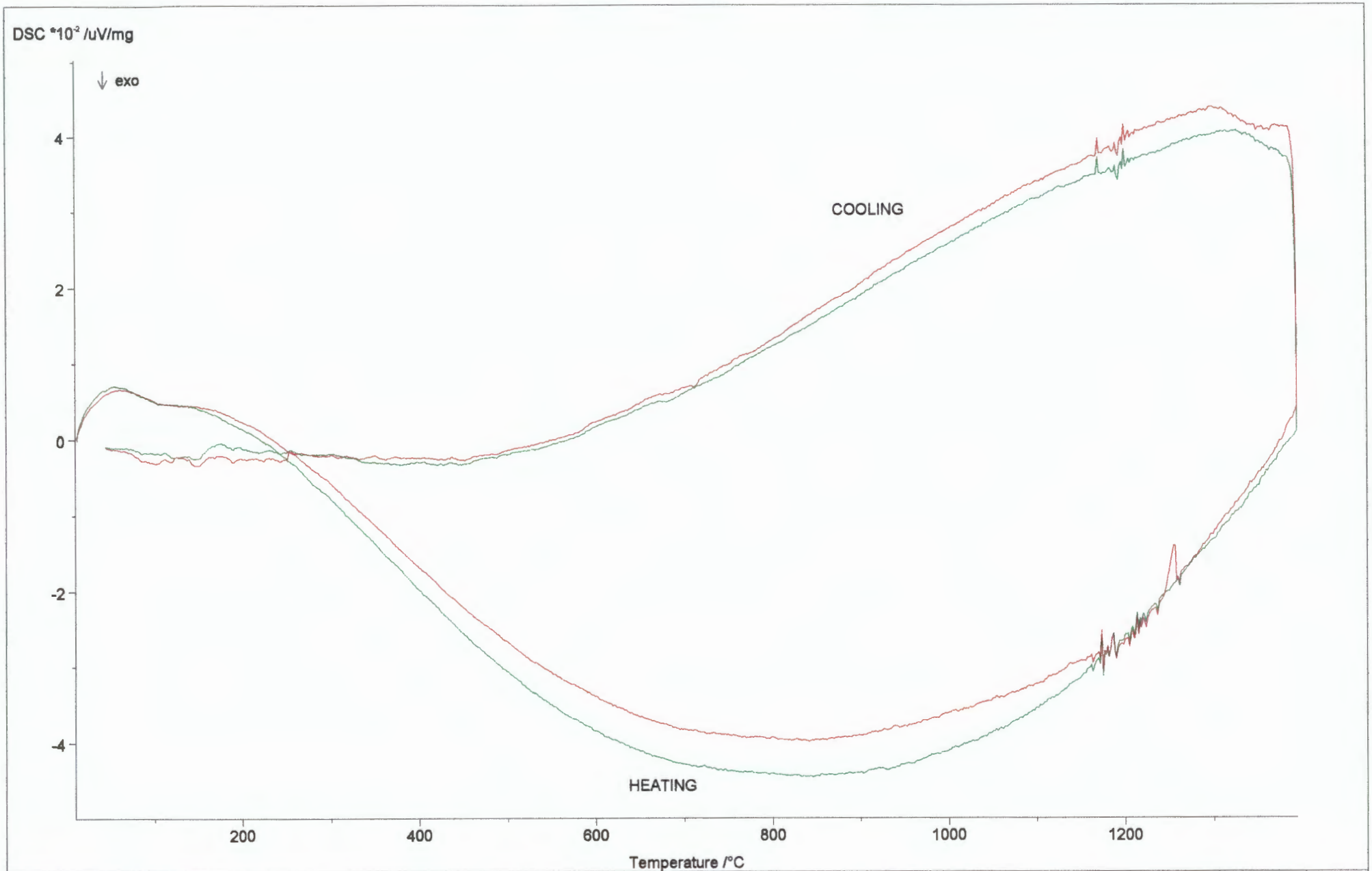

#-INSTRUMENT	FILE	IDENTITY	SAMPLE	DATE	MASS	SEGM.	RANGE	ATMOS.	CORR
1 - STA 409C	PLAT4_1T.DSS	pure pt at 4 k/min	1400 heating and cooling	06.01.1999	122.800 mg	1-2/2	20 °C/4.0(K/min)/1400 °C/4.0(K/min)/20 °C/	Argon/100	020
2 - STA 409C	PLAT4_2T.DSS	pure plat second time at 4	1400 heating and cooling	07.01.1999	122.860 mg	1-2/2	20 °C/4.0(K/min)/1400 °C/4.0(K/min)/20 °C/	Argon/100	020

Figure D1 DTA graph showing curves of cold-worked and retested pure platinum heated and cooled at 4 K/min.

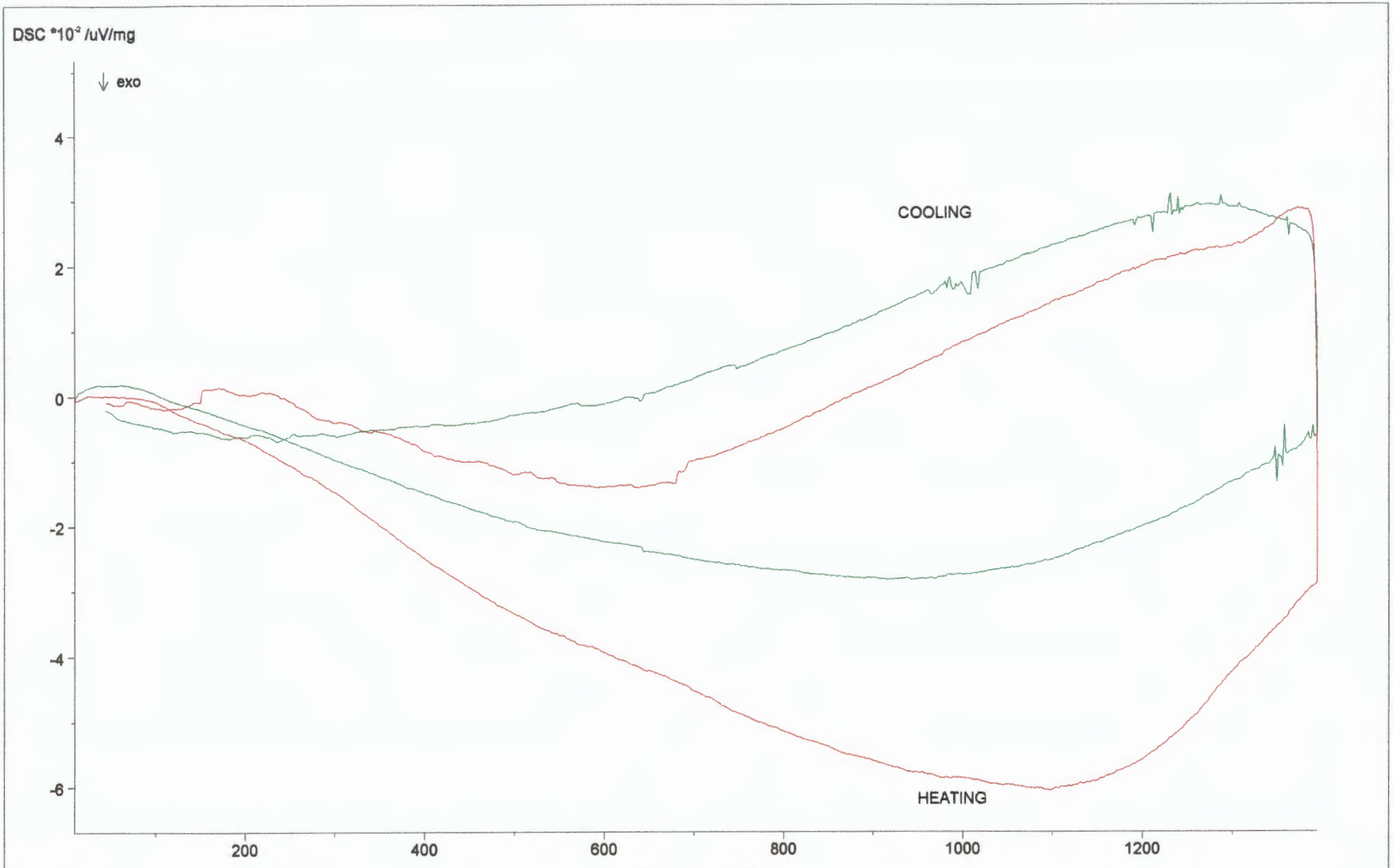

#-INSTRUMENT	FILE	IDENTITY	SAMPLE	DATE	MASS	SEGM.	RANGE	ATMOS.	CORR
1 - STA 409C	MO_4.DSS	moly at 4	1400 heating and cooling	23.11.1998	160.020 mg	1-2/2	20 °C/4.0(K/min)/1400 °C/4.0(K/min)/20 °C/	Argon/100	020
2 - STA 409C	RE3MOLY.DSS	re3moly_4	1400 heating and cooling	22.10.1998	127.820 mg	1-2/2	20 °C/4.0(K/min)/1400 °C/4.0(K/min)/20 °C/	Argon/100	020

Figure D2 DTA graph showing curves of cold-worked and retested Pt 5 at% Mo heated and cooled at 4 K/min.

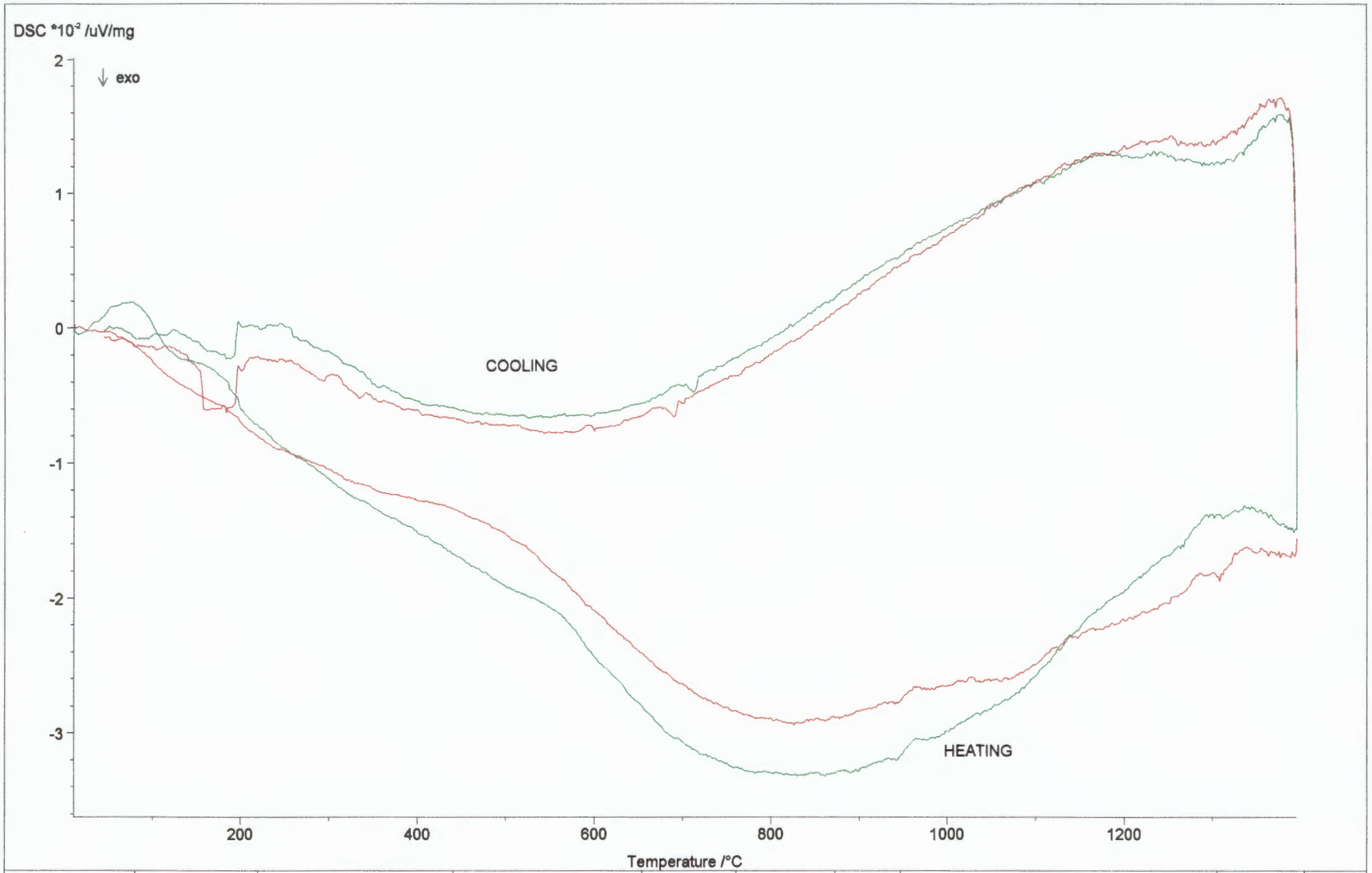

#-INSTRUMENT	FILE	IDENTITY	SAMPLE	DATE	MASS	SEGM.	RANGE	ATMOS.	CORR
1 - STA 409C	COPP5_4.DSS	third time for cu at k k/min	1400 heating and cooling	19.01.1999	146.045 mg	1-2/2	20 °C/4.0(K/min)/1400 °C/4.0(K/min)/20 °C/	Argon/100	020
2 - STA 409C	COPP6_4.DSS	thrid time second test	1400 heating and cooling	20.01.1999	142.960 mg	1-2/2	20 °C/4.0(K/min)/1400 °C/4.0(K/min)/20 °C/	Argon/100	020

Figure D3 DTA graph showing curves of cold-worked and retested Pt 5 wt% Cu heated and cooled at 4 K/min.

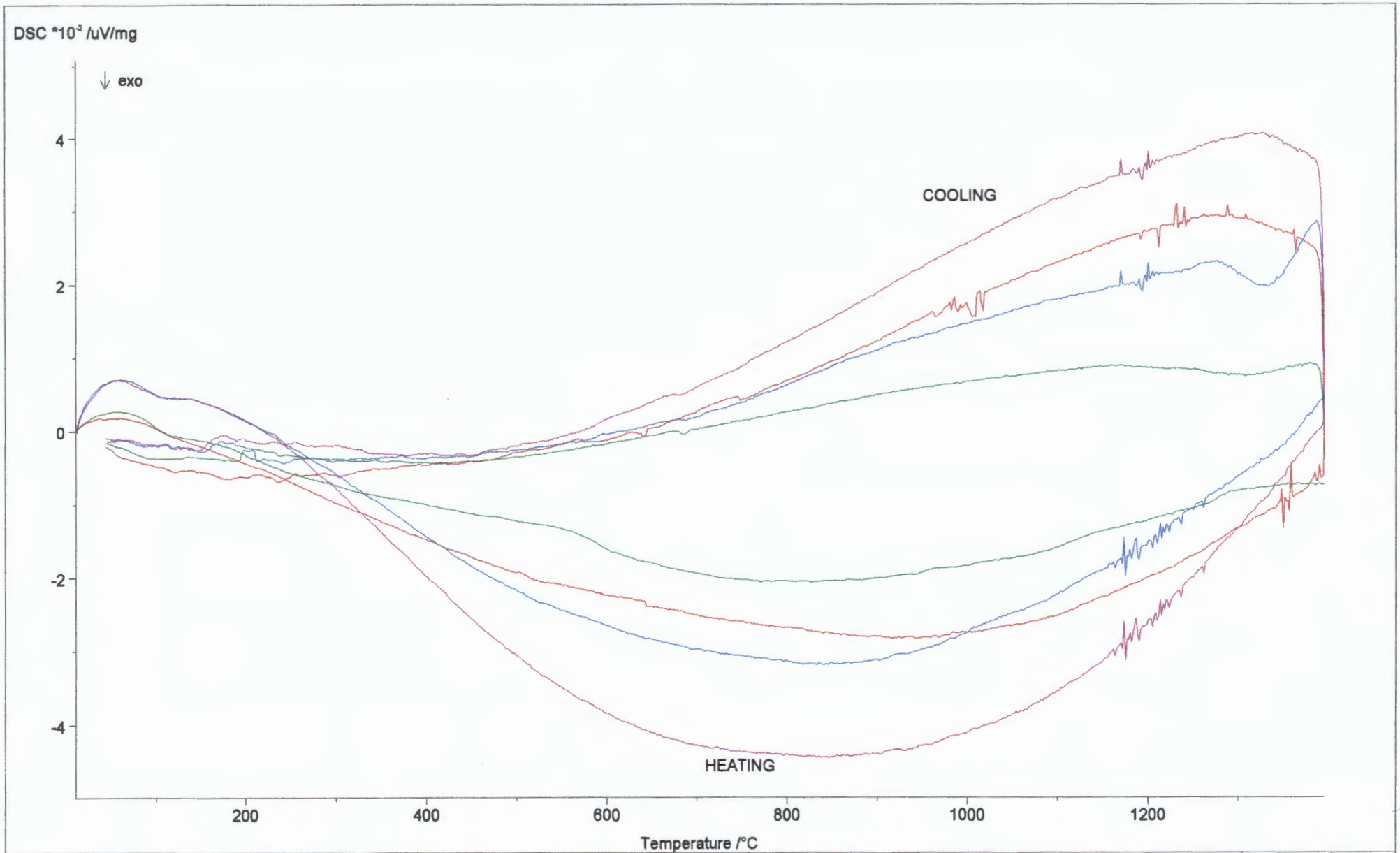

#-INSTRUMENT	FILE	IDENTITY	SAMPLE	DATE	MASS	SEGM.	RANGE	ATMOS.	CORR
1 - STA 409C	COPP3_4.DSS	copper repeat whole test	1400 heating and cooling	17.01.1999	262.120 mg	1-2/2	20 °C/4.0(K/min)/1400 °C/4.0(K/min)/20 °C/	Argon/100	020
2 - STA 409C	MO_4.DSS	moly at 4	1400 heating and cooling	23.11.1998	160.020 mg	1-2/2	20 °C/4.0(K/min)/1400 °C/4.0(K/min)/20 °C/	Argon/100	020
3 - STA 409C	RUTH1_4.DSS	ptru 4 k/min first	1400 heating and cooling	08.01.1999	129.350 mg	1-2/2	20 °C/4.0(K/min)/1400 °C/4.0(K/min)/20 °C/	Argon/100	020
4 - STA 409C	PLAT4_1T.DSS	pure pt at 4 k/min	1400 heating and cooling	06.01.1999	122.800 mg	1-2/2	20 °C/4.0(K/min)/1400 °C/4.0(K/min)/20 °C/	Argon/100	020

Figure D4 DTA graph comparison of cold-worked pure platinum, Pt 5 at% Mo, Pt 5 wt% Ru and Pt 5 wt% Cu heated and cooled at 4 K/min.

APPENDIX E

PUBLICATIONS

1) N.R. Towle, C.I.Lang and D. Miller, Order hardening of platinum 5 wt% copper, Microscopy Society of Southern Africa – Proceedings. **28**, 15 (1998)

PATENTS

1) Provisional Patent no. 9810988, South Africa, Hardening of low-solute content platinum alloys.

REFERENCES

[1] Platinum Guild International, *Platinum Manufacturing Process Volume 1,* Platinum Day Symposium, New York (1995)

[2] C.I. Lang, PhD thesis, (1991)

[3] E Savitskii, V Polyakova, N Gorina & N Roshan, *Physical Metallurgy of Platinum Metals,* Pergamon Press, Oxford (1978)

[4] C.T. Lynch, *Practical Handbook of Materials Science,* CRC Press, U.S.A. (1990)

[5] A.S. Darling, International Metallurgical Review. **18**, 91 (1973)

[6] R.S. Irani & R.W. Cahn, J. Mater. Sci. **8**, 1453 (1973)

[7] E. Raub, J. Less Common Metals. **1**, 3 (1959)

[8] L. Dreibholz, Z. phys. Chem. **108**, 1 (1924)

[9] E. Raub, Z. Metallk. **45**, 23 (1954)

[10] P. Greenfeld & P.A. Beck, Trans AIME. **206**, 265 (1956)

[11] H.P. Rooksby & B. Lewis, J. Less-Common Metals. **6,** 451 (1964)

[12] H. Ocken & J.H.N. van Vucht, J. Less-Common Metals. **13**, 193 (1968)

[13] Ye. M. Savitskii, *Handbook of Precious Metals,* Hemisphere, London (1989)

[14] J.M. Hutchinson, Platinum Metals Rev. **16**, 88 (1972)

[15] C.B Walker, J. of Applied Physics. **23**, no. 1, 118 (1952)

[16] R. Miida and D. Watanabe, J. Appl. Cryst. **7**, 50 (1974)

[17] I.O. Linde, Ann. Phys. **30**, 151 (1937)

[18] A. Schneider & U. Esch. Z. Elektrochem. **50** 290 (1944)

[19] N.C. Wu, H. Iwasaki and S. Ogawa, Trans. Japan Inst. Met. **14**, 309 (1973)

[20] T. Hirone & K. Adachi, Sci. Rep. RITA. **A-7**, 282 (1955)

[21] R.S. Irani & R.W. Cahn, Acta Met. **21**, 575 (1973)

[22] R Mitchel, H.G. Paris and B.G. Le Fevre, Met. Trans. **4**, 833 (1973)

[23] C.S. Barrett & T.B. Massatski, *Structure of Metals*, Pergamon Press, Oxford, 1980

[24] R.S. Irani, Contemparary Physics. **13**, 559 (1972)

[25] N.S. Stoloff & R.G. Davies, Progress in Materials Science, **13**, no. 1, 3 (1966)

[26] K. Mitsui, Y. Mishima and T. Suzuki, Phil. Mag. A. **53**, no. 3, 357 (1986)

[27] C.S. Darken & R.W. Gurry, *Physical Chemistry of Metals,* McGraw-Hill Book Company, U.S.A. (1953)

[28] P.S. Rudman, Ordered Alloys: Structural Application and Physical Metallurgy, Proceedings 3rd Bolton Landing Conference Sept 1969 page 37, Claitor's (1970)

[29] W. Gaudig, P. Okamoto, G. Schanz and G. Thomas, Ordered Alloys: Structural Application and Physical Metallurgy, Proceedings 3rd Bolton Landing Conference Sept 1969 page 347, Claitor's (1970)

[30] R.E. Smallman, *Modern Physical Metallurgy*, Butterworths, U.K. (1985)

[31] C.L. Corey, Ordered Alloys: Structural Application and Physical Metallurgy, Proceedings 3rd Bolton Landing Conference Sept 1969 page 241, Claitor's (1970)

[32] A Kelley & R.B. Nicholson, *Strengthening Methods in Crystals*, Elesevier, Amsterdam (1971) Chapter 4, Intermetallic Compounds and Ordered Phases

[33] R. W. Cahn, Met. Soc. Conferences – Local Atomic Arrangements Studied by X-Ray Diffraction, **36**, 179 (1966)

[34] J.C. Fisher, Acta Met. **2**, 9 (1954)

[35] D. Hull & D.J. Bacon, *Introduction to Dislocations*. Pergamon Press, U.K.. (1984)

[36] J.B. Cohen & M.E. Fine, J. Phys. Radium. **23**, 749 (1962)

[37] N.S. Stoloff & R.G. Davies, Acta. Met. **12**, 473 (1964)

[38] G.W. Ardley, Acta Met. **3**, 525 (1955)

[39] P.S. Rudman, Acta Met. **10**, 253 (1962)

[40] P.A. Flinn, Trans. Amer. Inst. Met. Ingrs. **218**, 145 (1960)

[41] N. Brown. Acta Met. 7, 10 (1959)

[42] M.J. Marcinkowski & D.S. Miller, Phil. Mag. **6**, 871 (1961)

[43] V.S. Arunachalam & R.W. Cahn, J. Mat Sci. **2**, 160 (1967)

[44] R. Mitchell, H.G. Paris and B.G. Le Fevre, Met. Trans. **4**, 833 (1973)

[45] A.H. Geisler J.B. Newkirk, Trans. Amer. Inst. Met. Engrs. **200**, 1076 (1954)

[46] J.B.. Newkirk, A.H. Geisler, D.L. Martin and R. Smoluehowski, Trans. AIME. **188**, 1249 (1950)

[47] M.J. Marcinkowski & D.S. Miller, Phil. Mag. **6,** 871 (1961)

[48] S.M. Copley & B.H. Kear, Trans. AIME. **239,** 984 (1967)

[49] R.R. Hasiguti, J. Japan Inst. Metals. **19**, 103, (1955)

[50] R.G. Davies & R.W. Cahn, Phil. Mag. **5**, 1119 (1959)

[51] H.M. Otte, J. Appl. Phys. **33,** 1436 (1962)

[52] A.C. Damask, J. Appl. Phys. **27**, no. 6, 610 (1956)

[53] J.M. Pelletier, G. Vigier and R. Borrelly, Scripta Met. **16**, 1343 (1982)

[54] D. Trattner, J.Phys. F. **13**, 739 (1983)

[55] T. Doppler, Phys. Stat. Sol a. **140**, 329 (1993)

[56] L. Trieb & G Veith, Acta Met. **26**, 185 (1978)

[57] P. Haasen, Z. Metallkde. **55**, 55 (1964)

[58] T.J. Koppenaal & M.E. Fine, Trans Met Soc. AIME. **221**, 1178 (1961)

[59] Z. Fisk & G.W. Webb, *Treatise on Materials Science and Technology vol. 21, Electronic Structure and Properties*, Edited by F. Y. Fradin, Academic Press, INC., New York (1981)

[60] R. M. Rose, L.A. Shepard & J. Wulff, *Structure and Properties of Materials: Electronic Properties,* John Wiley & Sons INC, NewYork (1966)

[61] E. Savitskii, V. Polyakova, N. Gorina and N. Roshan, *Physical Metallurgy of Platinum Metals,* Pergamon Press, Oxford (1978)

[62] R. E. Hummel, *Electronic Properties of Materials*, Springer-Verlag, Ann Arbor (1993)

[63] J.S. Dugdale, *The Electrical Properties of Metal and Alloys,* Edward Arnold, London (1977)

[64] P.L. Rossiter, *The Electrical Properties of Metal and Alloys*, Cambridge, *1987*

[65] N.F. Mott, Proc. R. Soc. London. **A153**, 699 (1936)

[66] L. Nordheim, Ann. Phys. **9**, 607 (1931)

[67] B.D. Cullity, *Elements of X-Ray Diffraction,* Addison-Wesley Publishing Company, Massachusetts (1956)

[68] W.W. Wendlanndt, *Thermal Analysis*, John Wiley and Sons, Inc., U.S.A. (1986)

[69] R.F. Speyer, *Thermal Analysis of Materials.* Marcel Dekker, Inc, U.S.A. (1994)

[70] K. Mitsui, Y. Mishima and T. Suzuki, Phil. Mag. A. **54**, no. 4, 501 (1986)

[71] M.J. Witcomb. Proc. Electron Microsc, Soc. South Afr. **22**, 39 (1992)

[72] L.J. van der Pauw, Philips Res. Repts. 131 (1958)

[73] International Council for Diffraction Data, *Powder Diffraction File,* I.C.D.D., U.S.A. (1997)

[74] SH. A. Alimov & A.A. Katsnel'son. Fiz. metal. metalloved. **22**, no. 3, 468 (1966)

[75] W. Gaudig, P. Okamoto, G. Schanz, G. Thomas and H. Warlimont, in J.H. Westbrook (Editor), *Mechanical Properties of Intermetallic Compounds,* page 347, John Whiley, New York (1960)

[76] G. Thomas & R Sinclair, Acta Met. **25**, 231 (1977)

[77] P.R. Okamoto & G. Thomas, Acta Met. **19**, 825 (1971)

[78] W.B. Snyder & C.R. Brooks, in J.H. Westbrook (Editor), *Mechanical Properties of Intermetallic Compounds,* page 347, John Whiley, New York (1960)

[79] B. Chakravarti, E.A. Starke JR and G. Lefevre, J. Mater. Sci. **5**, 394 (1970)

[80] B. Roessler, D.T. Novick and M.B. Bever, Trans. Met. Soc. **227**, 985 (1963)

[81] J.B. Cohen & M.B. Bever, Trans. Met. Soc. **218**, 155 (1960)

[82] A.E. Vidiz, D.P Lazerevic' and R.W. Cahn, Acta Met. **11**, 17 (1963)